

**STUDIES ON THE PATHOPHYSIOLOGY OF
CANCER-INDUCED DEPRESSION**

STUDIES ON THE PATHOPHYSIOLOGY OF
CANCER-INDUCED DEPRESSION

BY

MINA G. NASHED, B.Sc. (HONOURS), M.Sc.

A Thesis

Submitted to the School of Graduate Studies

in Partial Fulfillment of the Requirements

for the Degree

Doctor of Philosophy

DOCTOR OF PHILOSOPHY (2016)

McMaster University

(Medical Sciences)

Hamilton, Ontario, Canada

TITLE: Studies on the pathophysiology of cancer-induced depression

AUTHOR: Mina George Nashed, B.Sc. (HONOURS) (*McMaster University*),
 M.Sc. (*McMaster University*)

SUPERVISOR: Professor Gurmit Singh, Ph.D.

NUMBER OF PAGES: xxv, 315

Lay Abstract

Cancer patients are at a high risk of developing depression. In addition to the psychological stress caused by a cancer diagnosis, there is evidence that cancer causes depression through biological pathways. To investigate these pathways, a mouse model of cancer-induced depression (CID) was developed. This model showed comparable behavioural and structural brain deficits to those observed in a stress model of depression. Cancer cells secrete elevated levels of glutamate, a signalling molecule that is involved in depression. In CID mice, inhibiting glutamate release had an antidepressant effect similar to that of fluoxetine, a standard clinical antidepressant. A genetic analysis on brain samples from the CID model revealed significant overlap with the stress model of depression. CID mice had additional changes relevant to learning, memory, and brain cell development that were not detected in the stress model. A better understanding of CID will lead to better treatment strategies developed specifically for cancer patients.

Abstract

Despite the lack of robust clinical response, treatment strategies for cancer-induced depression (CID) are currently limited to those developed for non-cancer-related depression. The work presented in this dissertation conceptualizes CID as a pathophysiologically distinct form of depression. To investigate CID at the most basic level, we first developed a preclinical model that was validated by comparison to an established model of stress-induced depressive-like behaviours. The positive control model was developed by chronically treating female BALB/c mice with oral corticosterone (CORT). The CID model was developed using subcutaneous inoculation with 4T1 mammary carcinoma cells. Anhedonia, behavioural despair, and dendritic atrophy in the medial prefrontal cortex (mPFC) were observed in both models. Similar to many human cancer cell lines, 4T1 cells were shown to secrete significant amounts of glutamate, which was markedly attenuated using the system x_c^- inhibitor sulfasalazine (SSZ). In CID mice, oral treatment with SSZ was at least as effective as fluoxetine, a popular clinical antidepressant, at preventing depressive-like behaviours. This effect was primarily attributable to intact SSZ, rather than its anti-inflammatory metabolite. RNA-sequencing was performed on hippocampal samples from CID and CORT animals. Analysis of differential expressed genes (DEGs) revealed significant overlap between the two models. Kyoto Encyclopedia of Genes and Genomes (KEGG) pathways and biological process gene ontologies (GO:BP) terms related to ion homeostasis and neuronal communication were enriched for both models. CID

was associated with additional DEGs that were not identified in the CORT model. These DEGs were enriched in KEGG pathways and GO:BP terms related to neuronal development, intracellular signalling cascade, learning, and memory. These studies suggest that CID may involve a distinct aetiology, and that glutamate secretion by cancer cells presents a viable target for antidepressant treatment. The development of mechanism-based therapeutics for CID will dramatically improve the quality of life for cancer patients.

Preface

This doctoral dissertation is presented as a *sandwich* thesis, and consists of four manuscripts that were prepared for publication during the author's Ph.D. candidacy. Two manuscripts have been published (Chapters 1 and 2), and two manuscripts have been submitted for publication (Chapters 3 and 4). Each manuscript is presented as a separate chapter and includes a preface detailing each author's contributions, as well as a description of the underlying context for the manuscript. The first manuscript presented in Chapter 1 was prepared as a book chapter for *Oncodynamics: Effects of Cancer Cells on the Body*. This manuscript provides a conceptual overview and comprehensive background information on the pathophysiology of depression, the role of cancer in depression, and related topics. The three chapters that follow (Chapters 2, 3, and 4) detail experiments that were performed during the author's Ph.D. candidacy. A concluding chapter (Chapter 5) summarizes the major findings of this dissertation and discusses future directions to be considered in the study of cancer-induced depression.

Literature cited within each manuscript are independent and consistent with the requirements of their corresponding journal. Literature cited elsewhere use the American Psychological Association (5th edition) style, and appear in a separate *References* section at the end of the dissertation. Appendices are included, which describe relevant optimization experiments and provide details for certain methodologies used in this research.

Acknowledgments

I would like to wholeheartedly thank my supervisor, Dr. Gurmit Singh, for accepting me into his lab and entrusting me with this project. His mentorship and guidance were invaluable in shaping my approach to scientific questions. Above all else, Dr. Singh is an advocate for his students. He has allowed me the freedom to explore my interests, while also challenging me to always think about the broader context. I would also like to thank Dr. Benicio Frey and Dr. Laurie Doering for serving on my supervisory committee. Dr. Frey has provided me with many years of mentorship since first serving on my Master's supervisory committee. I have had the pleasure of collaborating with him on several manuscripts and his insightful clinical input on my translational research has always been incredibly valuable. Dr. Doering has always made himself available to me. His early guidance with the histological aspect of my project was fundamental in establishing my model. I also greatly appreciated his support as my advisor for the comprehensive examination.

I would like to thank the entire Singhlab team for over 4 years of research experience that will be hard to beat. To my on-demand encyclopaedia, Dr. Eric Seidlitz, thank you for always making yourself available and for somehow always replying to my ridiculously long-winded email questions with even longer detailed answers. To the powerhouse mitochondria of the lab, Natalie Zacal, thank you the countless hours you spent troubleshooting with me, as well as guiding me through techniques and training. To the most dedicated scientist I know, Dr. Katja

Linher-Melville, you set the bar for me for what a postdoctoral fellow and scientist should be. I learned more from you than you might realize. My Ph.D. experience would not have been nearly as productive, engaging, and outright fun without my wonderful labmates (current and former). So a big thank you goes to Jennifer Fazzari, Robert Ungard, Tanya Miladinovic, Kimberly Young, Eric Habib, Matthew Balenko, Robert Cowan, Meghan Verschoor, and all the undergraduate students. My appreciation also extends to all of the staff at McMaster's Central Animal Facility. Without their dedication and hard work my research would literally not have been possible.

Special thanks go to all my brilliant, loving, outrageous, loyal, and supportive *out-of-lab* friends—you know who you are. It would take another dissertation to acknowledge each one of you properly. I hope you realize your value in getting me to this point; from grade school games, to undergrad all-nighters, to 303 gatherings, to Nasheid nights, and everything in between. Thank you for being the incredible people you are.

This dissertation, along with everything I have been able to accomplish, would not have been possible without the sacrifices of my incredible parents. George and Soheir, thank you for showing me what hard work looks like. I hope to one day be as inspirational to my children as you have been to me. Thank you for your unwavering love and support. To my big sister Mariam, you were my first role model and my first best friend. Thank you for being the “lab rat”, so to

speaking, and going through all of life's milestones before me. You guided me through everything from my first crush, to the scary world of high school, to the scarier world of university. And now, you are an amazing mom to Bella and I get to learn from you again. Thank you for your friendship and love.

Lastly, and most importantly, I would like to thank my beautiful and brilliant wife, Nancy. I still remember the first time I saw you in the Biology 1A03 lab; that may have been when I subconsciously decided to become a scientist by positive association. You were my friend during undergrad, my girlfriend during my Master's, and my fiancé and wife during my Ph.D. I can't imagine going through any of those milestones without you beside me. You have always encouraged every goal I set for myself, and even agreed to marry me during the peak (or valley) of my grad student poverty. I look forward to raising a family together, growing old together, and eventually retiring in Hawaii. Thank you for being my rock for the past few years. I hope you know how much I love and appreciate you.

Table of Contents

| | |
|--|-------------------------------------|
| Lay Abstract | iii |
| Abstract..... | iv |
| Preface..... | vi |
| Acknowledgments | vii |
| Table of Contents | x |
| List of Diagrams, Figures, and Tables | xvii |
| List of Abbreviations | Error! Bookmark not defined. |
| Declaration of Academic Achievement | xix |
| CHAPTER 1: Oncodynamic Effect of Cancer on Depression | 1 |
| Preface..... | 2 |
| <i>Context and Background Information</i> | <i>2</i> |
| Abstract | 6 |
| Introduction..... | 7 |
| Depression..... | 8 |
| <i>Diagnosis & Classification of Depression.....</i> | <i>8</i> |
| Neurobiology of Depression | 10 |
| <i>The Monoamine Hypothesis of Affective Disorders.....</i> | <i>10</i> |
| <i>Neurotrophins, BDNF, and the Anatomy of Depression</i> | <i>13</i> |
| <i>Stress and Cytokines</i> | <i>15</i> |
| <i>Glutamate</i> | <i>17</i> |
| Antidepressants | 20 |

| | |
|--|-----------|
| <i>Antidepressants in Major Depressive Disorder</i> | 21 |
| <i>Antidepressants in Cancer-Induced Depression</i> | 22 |
| Cancer-Induced Depression | 25 |
| <i>Oncodynamic Effect Through Inflammation</i> | 27 |
| <i>Oncodynamic Effect Through Physiological Stress</i> | 29 |
| <i>Oncodynamic Effect Through Glutamatergic Signalling</i> | 30 |
| Conclusion | 34 |
| References | 36 |
| | |
| CHAPTER 2: Depressive-like behaviours and decreased dendritic branching in the medial prefrontal cortex of mice with tumors: A novel validated model of cancer-induced depression | 58 |
| Preface | 59 |
| <i>Context and Background Information</i> | 60 |
| Abstract | 64 |
| Introduction | 66 |
| Materials and Methods | 69 |
| <i>Mice</i> | 69 |
| <i>Drug treatments</i> | 69 |
| <i>Tumor cell inoculation</i> | 70 |
| <i>Behavioural analyses</i> | 71 |
| <i>Experimental groups</i> | 72 |
| <i>Euthanasia and tissue processing</i> | 73 |

| | |
|---|-----|
| <i>Dendritic analysis</i> | 73 |
| <i>Blood collection and CORT ELISA</i> | 74 |
| <i>Data analysis</i> | 75 |
| Results | 78 |
| <i>Weight and tumor size monitoring</i> | 78 |
| <i>Behavioural analyses</i> | 78 |
| <i>Dendritic analyses</i> | 79 |
| <i>Serum CORT ELISA</i> | 81 |
| Discussion | 83 |
| Conclusion | 89 |
| Acknowledgements | 90 |
| References | 91 |
| Tables & Figures | 103 |

CHAPTER 3: Inhibiting glutamate release with sulfasalazine in a mouse

| | |
|---|------------|
| model of cancer-induced depression | 116 |
| Preface..... | 117 |
| <i>Context and Background Information</i> | 118 |
| Abstract | 121 |
| Introduction..... | 123 |
| Materials and Methods..... | 127 |
| <i>Cell culture</i> | 127 |
| <i>Cell treatment</i> | 127 |

| | |
|--|-----|
| <i>Glutamate release through system x_c^-</i> | 127 |
| <i>Mice</i> | 128 |
| <i>Tumor cell inoculation</i> | 129 |
| <i>Drug treatments</i> | 129 |
| <i>Behavioral analyses</i> | 131 |
| <i>Experimental groups</i> | 132 |
| <i>Euthanasia and tissue harvesting</i> | 132 |
| <i>Brain Metastases</i> | 132 |
| <i>Serum Glutamate</i> | 133 |
| <i>Serum Cytokines</i> | 133 |
| <i>Data Analyses</i> | 133 |
| Results | 136 |
| <i>Glutamate release through system x_c^-</i> | 136 |
| <i>Behavioral analyses</i> | 136 |
| <i>Serum Glutamate</i> | 138 |
| <i>Serum Cytokines</i> | 138 |
| Discussion | 140 |
| Acknowledgements..... | 146 |
| References..... | 147 |
| Figures & Tables..... | 156 |
| Supplemental Materials and Methods..... | 163 |
| <i>Cell Culture</i> | 163 |
| <i>Glutamate release through system x_c^-</i> | 163 |

| | |
|--|-----|
| <i>Mice Weights and Tumor Volume</i> | 164 |
| <i>Brain Metastases</i> | 165 |
| <i>Serum Cytokines</i> | 166 |
| Supplemental Figures | 167 |
| References | 169 |

CHAPTER 4: RNA-sequencing profiles hippocampal gene expression in a validated mouse model of cancer-induced depression 170

| | |
|---|-----|
| Preface | 171 |
| <i>Context and Background Information</i> | 171 |
| Abstract | 175 |
| Introduction | 177 |
| Materials and Methods | 181 |
| <i>Mice</i> | 181 |
| <i>Tissue Collection</i> | 181 |
| <i>RNA Isolation</i> | 182 |
| <i>RNA-Sequencing</i> | 182 |
| <i>Quantitative Real-Time RT-PCR</i> | 183 |
| <i>Data Analyses</i> | 184 |
| Results | 188 |
| <i>RNA-sequencing</i> | 188 |
| <i>Quantitative Real-Time RT-PCR</i> | 189 |
| <i>Enrichment Analyses</i> | 190 |

| | |
|--|------------|
| Discussion | 192 |
| Acknowledgements | 197 |
| References | 198 |
| Figures & Tables | 207 |
| Supplemental Information | 213 |
| CHAPTER 5: Summary and Future Directions | 225 |
| Summary | 226 |
| Future Directions | 234 |
| Conclusions | 239 |
| References | 240 |
| APPENDIX 1: Optimization Data for Establishing Cancer-Induced | |
| Depression Model | 246 |
| Preface | 247 |
| Experiment 1 | 248 |
| <i>Background Information</i> | 248 |
| <i>Experimental Design</i> | 248 |
| <i>Results & Discussion</i> | 250 |
| <i>Figures</i> | 252 |
| Experiment 2 | 254 |
| <i>Background Information</i> | 254 |
| <i>Experimental Design</i> | 254 |
| <i>Results & Discussion</i> | 255 |

| | |
|---|------------|
| <i>Figures</i> | 256 |
| Experiment 3 | 258 |
| <i>Background Information</i> | 258 |
| <i>Experimental Design</i> | 258 |
| <i>Results & Discussion</i> | 262 |
| <i>Figures</i> | 265 |
| Experiment 4 | 269 |
| <i>Background Information</i> | 269 |
| <i>Experimental Design</i> | 270 |
| <i>Results & Discussion</i> | 272 |
| <i>Figures</i> | 275 |
| APPENDIX 2: Details for Methodologies | 279 |
| Preface | 280 |
| Cell Culture Technique | 281 |
| Tail Suspension Test | 282 |
| Forced Swim Test | 285 |
| Dendritic Analysis | 289 |
| ¹⁴ C-Cystine Uptake Assay | 292 |
| Bio-Rad Protein Assay | 294 |
| Quantitative Real-Time RT-PCR | 296 |
| RNA-seq Analysis | 298 |
| APPENDIX 3: Springer Copyright Licence | 309 |

List of Diagrams, Figures, and Tables

| | |
|---|------------|
| CHAPTER 1 | 1 |
| Oncodynamic Effect of Cancer on Depression | |
| Table 1 — Symptoms for major depressive episode | 10 |
| Figure 1 — Schematic summarizing proposed oncodynamic mechanisms of cancer-induced depression | 33 |
| CHAPTER 2 | 58 |
| Depressive-like behaviours and decreased dendritic branching in the medial prefrontal cortex of mice with tumors: A novel validated model of cancer-induced depression | |
| Figure 1 — Timeline of the experiment | 103 |
| Figure 2 — Mean body weight of mice | 104 |
| Figure 3 — Tumor growth in mice | 105 |
| Figure 4 — Behavioural results | 106 |
| Figure 5 — Identification of the mPFC in coronal sections, neuronal impregnation, digital reconstructions of neurons | 108 |
| Figure 6 — Basilar and apical branch lengths | 109 |
| Table 1 — Details of Sholl analyses | 110 |
| Figure 7 — Sholl analyses of basilar and apical dendrites | 112 |
| Table 2 — Endpoint serum levels of corticosterone | 114 |
| Table 3 — Summary of results for behavioural and dendritic analyses | 115 |
| CHAPTER 3 | 116 |
| Inhibiting glutamate release with sulfasalazine in a mouse model of cancer-induced depression | |
| Figure 1 — ¹⁴ C-cystine uptake assay on 4T1 cancer cells and TM40A mammary epithelial cells | 156 |
| Figure 2 — Behavioral results | 157 |
| Figure 3 — Brain metastases regression analyses | 159 |
| Figure 4 — Serum level of glutamate | 160 |

| | |
|--|------------|
| Figure 5 — Serum level of pro-inflammatory cytokines | 161 |
| Table 1 — Summary of results for behavioral and cytokine analyses | 162 |
| Figure S1 — Mean body weight of mice | 167 |
| Figure S2 — Tumor growth in mice | 168 |
| CHAPTER 4 | 170 |
| RNA-sequencing profiles hippocampal gene expression in a validated mouse model of cancer-induced depression | |
| Figure 1 — Visual representation of individual gene data | 207 |
| Figure 2 — Visual summary of differential gene expression patterns | 208 |
| Figure 3 — qRT-PCR fold-changes compared with RNA-seq fold-changes | 209 |
| Figure 4 — Linear regression analysis of qRT-PCR vs. RNA-seq results | 210 |
| Figure 5 — Enrichment analyses of DEGs identified using RNA-seq | 211 |
| Table S1 — Primers utilized for relative qRT-PCR analysis | 213 |
| Table S2 — Housekeeping gene primers for relative qRT-PCR analysis | 214 |
| Table S3 — List of differentially expressed genes and fold changes | 215 |
| APPENDIX 1 | 246 |
| Optimization Data for Establishing Cancer-Induced Depression Model | |
| Figure 1.1 — Saccharin preference curve for BALB/c nu/nu mice | 252 |
| Figure 1.2 — Saccharin preference test | 253 |
| Figure 2.1 — Saccharin preference curve for Fox Chase SCID mice | 256 |
| Figure 2.2 — Behaviour results | 257 |
| Figure 3.1 — Saccharin preference test | 265 |
| Figure 3.2 — Tail suspension test | 266 |
| Figure 3.3 — Forced swim test | 267 |
| Figure 3.4 — CORT ELISA | 268 |
| Figure 4.1 — Sucrose preference test | 275 |
| Figure 4.2 — Tail suspension test (energy of movement) | 276 |
| Figure 4.3 — Forced swim test | 277 |
| Figure 4.4 — CORT ELISA | 278 |

List of Abbreviations

| | |
|----------------|---|
| 5-ASA | 5-aminosalicylic acid |
| 5-HT | 5-hydroxytryptamine |
| 6-TG | 6-thioguanine |
| ACTH | adrenocorticotropic hormone |
| Akt | Protein kinase B |
| AMPA | α -amino-3-hydroxy-5-methyl-4-isoxazolepropionic acid |
| ANOVA | analysis of variance |
| APA | American Psychiatric Association |
| BBB | blood-brain-barrier |
| BDNF | brain-derived neurotrophic factor |
| bp | base pairs |
| CA1 | Cornu Ammonis area 1 |
| CBT | cognitive behavioural therapy |
| cDNA | complementary DNA |
| CID | cancer-induced depression |
| CNS | central nervous system |
| CORT | corticosterone |
| CPM | counts per minute |
| CPPene | midafotel |
| CREB | cAMP response element binding protein |
| CRH | corticotropin-releasing hormone |
| CSF | cerebrospinal fluid |
| C _T | cycle threshold |
| DAVID | Database for Annotation, Visualization and Integrated Discovery |

| | |
|-----------|---|
| DEG | differentially expressed gene |
| DMEM:F12 | Dulbecco's Modified Eagle Medium: Nutrient Mixture F-12 |
| DNA | deoxyribonucleic acid |
| DSM-5 | Diagnostic and Statistical Manual of Mental Disorders |
| EAAT | excitatory amino acid transporter |
| EASE | Expression Analysis Systematic Explorer threshold |
| ECF | extracellular fluid |
| ECM | extracellular matrix |
| ECT | electroconvulsive therapy |
| ELISA | enzyme-linked immunosorbent assay |
| ERK | extracellular signal-regulated kinase |
| FBS | fetal bovine serum |
| FDR | false discovery rate |
| FLX | fluoxetine |
| FPKM | Fragments Per Kilobase of transcript per Million mapped reads |
| FST | forced swim test |
| GABA | γ -Aminobutyric acid |
| Glu | MRS glutamate alone signal |
| glutamate | L-glutamic acid |
| Glx | unresolved MRS glutamate/glutamine signal |
| GnRH | gonadotropin-releasing hormone |
| GO:BP | biological process gene ontologies |
| HAM-D | Hamilton Depression Rating Scale |
| HBSS | Hanks' Balanced Salt Solution |

| | |
|--------------------|---|
| HCl | hydrochloric acid |
| HIP | hippocampus |
| HPA | hypothalamic-pituitary-adrenal axis |
| IL | interleukin |
| IMDM | Iscove's Modified Dulbecco's Media |
| INF- α | interferon alpha |
| KEGG | Kyoto Encyclopedia of Genes and Genomes |
| MAO | monoamine oxidase |
| MAOI | MAO inhibitor |
| MAPK | Mitogen-activated protein kinases |
| Mbases | mega bases |
| MDD | major depressive disorder |
| miRNA | microRNA |
| MK-801 | dizocilpine |
| MMP | matrix metalloproteinase |
| mPFC | medial prefrontal cortex |
| mRNA | messenger RNA |
| MRS | magnetic resonance spectroscopy |
| mTOR | mammalian target of rapamycin |
| NAc | nucleus accumbens |
| NaOH | sodium hydroxide |
| NGS | next-generation sequencing |
| NH ₄ OH | ammonium hydroxide |
| NIMH | National Institute of Mental Health |
| NMDA | N-Methyl-D-aspartate |
| NSAID | non-steroidal anti-inflammatory drug |

| | |
|-----------|--|
| PBS | phosphate buffered saline |
| PDGF | platelet derived growth factor |
| PFC | prefrontal cortex |
| PHG | parahippocampal gyrus |
| PI3K | Phosphoinositide 3-kinase |
| PM | power of movement |
| Polr2b | polymerase (RNA) II (DNA directed) polypeptide B |
| qPCR | quantitative real-time RT-PCR |
| qPCR | real-time RT-PCR |
| RCT | randomized control trial |
| RNA | ribonucleic acid |
| RNA-seq | RNA sequencing |
| RPMI-1640 | Roswell Park Memorial Institute medium |
| RT-PCR | reverse transcription polymerase chain reaction |
| rTMS | Repetitive Transcranial Magnetic Stimulation |
| S-4-CPG | S-4-carboxy-phenylglycine |
| Sdha | succinate dehydrogenase complex, subunit A |
| SEM | standard error of the mean |
| SNP | single-nucleotide polymorphism |
| SNRI | serotonin-norepinephrine reuptake inhibitor |
| SP | substance P (Chapter 1) |
| SP | sulfapyridine (Chapter 3) |
| SPT | sucrose preference test |
| SSRI | selective serotonin reuptake inhibitor |
| SSZ | sulfasalazine |

| | |
|---------------|---|
| Taf1b | TATA box binding protein (Tbp)-associated factor, RNA polymerase I, B |
| TAM | tumour-associated macrophage |
| TCA | tricyclic antidepressant |
| TeCA | tetracyclic antidepressant |
| TNF- α | necrosis factor alpha |
| TrkB | tropomyosin-related kinase B |
| TST | tail suspension test |
| Val66Met | methionine for valine substitution at amino acid 66 |
| VEGF | vascular endothelial growth factor |
| VTA | ventral tegmental area |

Declaration of Academic Achievement

This dissertation is presented as a combination of four manuscripts – two published papers and two submitted manuscript, as follows:

Nashed, M. G., Frey, B. N., Rosebush, P., Singh, G. (2016).

Oncodynamic Effect of Cancer on Depression. In G. Singh (Ed.), *Oncodynamics: Effects of Cancer Cells on the Body* (pp. 105-127). Cham: Springer International Publishing, Switzerland.

Nashed, M. G., Seidlitz, E. P., Frey, B. N., Singh, G. (2015). Depressive-

like behaviours and decreased dendritic branching in the medial prefrontal cortex of mice with tumors: A novel validated model of cancer-induced depression. *Behav Brain Res*, 294, 25-35.

Nashed, M. G., Ungard, R. G., Young, K., Zacal, N. J., Seidlitz, E. P.,

Frey, B. N., Singh, G. Inhibiting glutamate release with sulfasalazine in a mouse model of cancer-induced depression. Submitted to *Neuropsychopharmacology* on January 26th, 2016 (submission number NPP-16-0097; under revision for re-submission to NPP at the time of dissertation completion)

Nashed, M. G., Linher-Melville, K., Frey, B. N., Singh, G. RNA-

sequencing profiles hippocampal gene expression in a validated mouse model of cancer-induced depression. Submitted to *Neuro-Oncology* on February 27th, 2016 (submission number N-O-D-16-00153).

In addition, I co-authored the following publications during my Ph.D. candidacy:

Nashed, M. G., Balenko, M. D., Singh, G. (2014). Cancer-induced oxidative stress and pain. *Curr Pain Headache Rep*, 18(1), 384.

Miladinovic, T., **Nashed, M. G.**, Singh, G. (2015). Overview of Glutamatergic Dysregulation in Central Pathologies. *Biomolecules*, 5(4), 3112-3141.

CHAPTER 1

Oncodynamic Effect of Cancer on Depression

Mina G. Nashed, Benicio N. Frey, Patricia Rosebush, Gurmit Singh

In G. Singh (Ed.), *Oncodynamics: Effects of Cancer Cells on the Body*

(pp. 105-127). Cham: Springer International Publishing, Switzerland.

Preface

In this chapter, an author-generated version of the manuscript entitled “Oncodynamic Effect of Cancer on Depression”, published as a book chapter in G. Singh (Ed.), *Oncodynamics: Effects of Cancer Cells on the Body* (pp. 105-127). Cham: Springer International Publishing, Switzerland, is presented. This chapter is reprinted with permission from Springer Publishing (see Appendix 3 for Licence Agreement).

For this manuscript, I performed a thorough literature review on all topics discussed. I wrote the manuscript, generated the table and figure therein, and modified the manuscript based on editor suggestions. Dr. Benicio Frey and Dr. Patricia Rosebush provided clinical input on the content of the manuscript. They also reviewed and provided feedback on the structure of the chapter. Dr. Gurmit Singh provided intellectual direction and edited the manuscript.

Context and Background Information

The book for which this chapter was written introduces the term *oncodynamics* to the field of oncology and defines the term as “the impact of abnormal cues generated by tumors on the physiological functioning of the body”. This chapter specifically focuses on the oncodynamic effect that cancer has on the development of depression. A detailed discussion is provided for topics that are relevant for the rationale of this dissertation.

The chapter begins with an introduction highlighting the prevalence of depression in cancer patients, and the lack of specific treatment strategies developed for cancer-induced depression (CID). A discussion of the history of depression is provided and highlights the 19th century shift in our understanding of depression as a biologically mediated illness. The modern clinical criteria of major depressive disorder (MDD) are provided, followed by a detailed discussion of the major neurobiological theories of depression. This discussion covers the monoamine hypothesis of affective disorders, the involvement of neurotrophins (such as brain derived neurotrophic factor; BDNF), stress, inflammation, and glutamatergic signalling. Antidepressants are considered in the context of the neurobiology of depression. In particular, the benefits and limitations of modern antidepressants based on the monoamine hypothesis of the 1950s' are emphasised. Antidepressant treatment for cancer patients is then considered, and it is concluded that more high quality clinical trials are needed to assess the efficacy of antidepressants for CID. The last section of the chapter reviews the common physiological abnormalities associated with both cancer and depression. The common pro-inflammatory state, physiological stress, and glutamatergic dysregulation associated with cancer and depression are considered as plausible oncodynamic mechanisms of CID. This dissertation predominantly focuses on glutamatergic dysregulation in CID.

Since this manuscript was prepared as a book chapter, it does not include the hypothesis and objectives of this dissertation. Therefore, the hypothesis is stated here:

Cancer can induce depression through defined biological mechanisms, which represent a distinct subtype of depression. Glutamatergic signalling is involved in the induction and maintenance of cancer-induced depression, and is modifiable by pharmacological intervention at the tumour site.

This hypothesis was investigated through 3 objectives, which are explored in Chapters 2, 3, and 4:

Objective 1: To develop a validated behavioural mouse model of CID.

Objective 2: To investigate the antidepressant efficacy of pharmacologically inhibiting system x_c^- glutamate release at the tumour site.

Objective 3: To investigate the CID model at the level of gene expression in comparison to a stress model of depressive-like behaviours.

Oncodynamic Effect of Cancer on Depression

Mina Nashed, BSc, MSc

Benicio Frey, MSc, MD, PhD

Patricia Rosebush, MScN, MD, FRCP(C)

Gurmit Singh, PhD

Contents

Introduction

Depression

Antidepressants

Cancer-Induced Depression

Conclusion

References

Abstract

Depressive disorders are among the most prevalent psychiatric illnesses in the general population. In cancer patients, the prevalence of depression is dramatically increased. In addition to the psychosocial impact of a negative diagnosis, recent evidence suggests that cancer-induced depression is mediated by biological processes. This oncodynamic effect of cancer on the development of depression is poorly understood, leading to ineffective treatment of cancer-induced depression with drugs that are developed for depressive disorders in the general population. This chapter begins by outlining the clinical profile of major depressive disorder. We then provide a discussion of the most prominent neurobiological hypotheses of depression, including the monoamine hypothesis, the role of neurotrophins, physiological stress, inflammation, and glutamatergic signalling. The efficacy of current antidepressants is then discussed for depression in the general population and in cancer patients. This leads to a discussion of the biological basis of cancer-induced depression, including the effects of physiological stress, inflammation, and glutamatergic signalling. We conclude that more research is needed to determine oncodynamic events in the development of cancer-induced depression. Development of validated animal models is the first step in delineating contributing biological mechanisms, which will ultimately lead to more targeted drug development and improved efficacy.

Introduction

The psychosocial impact of a cancer diagnosis undoubtedly contributes to co-morbid depression in cancer patients. While depression in the general population occurs with a lifetime prevalence of ~8 – 12% [4], it can reach as high as 57% in breast cancer patients and can be as staggering 95% in high grade glioma [77]. In addition to the psychosocial contribution, recent preclinical and clinical evidence suggests the involvement of biological mechanisms in cancer-induced depression (CID). This biological underpinning, and the development of the capacity to investigate it at the basic level, has a potentially profound impact on the quality of life of cancer patients. Currently, treatment for CID is limited to therapies developed for non-cancer-related major depressive disorder (MDD) despite lack of convincing evidence for the efficacy of these treatments in cancer patients [73]. A more effective strategy for treating CID begins with the investigation of the oncodynamic effect of cancer on depression at the most basic level. A better understanding of this interaction would provide the framework for developing new pharmacotherapy aimed at novel targets. This chapter will discuss what is currently known about the oncodynamic effect of cancer on depression by first reviewing depression at the clinical and etiological level, then examining cancer signalling events that are likely to contribute to CID.

Depression

The term melancholia (ancient Greek for “black bile”) was first used by Hippocrates around 400 B.C. to describe a disease state of persistent fear and despair [101]. According to the humoral theory, this disease state arose from excess black bile—one of the four bodily liquids, or humors. In the early 19th century, a “clinico-anatomical” view of disease asserted that symptoms of illnesses could be correlated with anatomical lesions [10]. During the second half of the 19th century, this conceptual shift led to greater focus on the brain in an effort to better understand melancholia. Today, insight from preclinical, biochemical, genetic, post-mortem, and neuroimaging studies have led to a greater understanding and classification of mood disorders. In addition to developing cognitive behavioural therapy, the last several decades have seen a proliferation of psychotropic drugs, which target specific biological pathways, enter the market. In the case of antidepressants, while the efficacy and tolerance have generally improved, low clinical response rates underscore the importance of continued progress in understanding the neurobiology of depression.

Diagnosis & Classification of Depression

Mood disorders are characterized by persistent periods of intensely reduced or elevated mood that interfere with normal functioning. The subcategory of mood disorders that is defined by reduced mood is termed *depressive disorders*. According to the current fifth edition of the *Diagnostic and Statistical Manual of*

Mental Disorders (DSM-5) of the American Psychiatric Association (APA), the common feature of this subcategory is the presence of sad, empty, or irritable mood [5]. This can be accompanied by various somatic and cognitive changes that impede day-to-day functioning. Differences between depressive disorders depend on duration and timing of symptoms, as well as presumed aetiology.

In the case of *Major Depressive Disorder* (MDD; commonly called major depression, clinical depression, or simply depression), changes in affect, cognition, and neurovegetative function occur in discrete episodes with inter-episodic remission [5]. Episodes must persist for at least 2 weeks, although typically last considerably longer, and at least one episode is required to make a diagnosis of MDD. If the mood disturbances persist for 2 or more years without periods of remission, a diagnosis of *persistent depressive disorder* (or dysthymia) is given. The depressive episodes required to make a diagnosis of MDD or dysthymia are characterized by the presence of 5 (or more) of 9 symptoms, summarized in Table 1 below. In addition, at least one of the symptoms must be either (1) depressed mood or (2) anhedonia (loss of interest or pleasure).

Table 1. Symptoms for major depressive episode

-
1. Depressed mood most of the day, nearly every day
 2. Markedly diminished interest or pleasure in all, or almost all, activities most of the day, nearly every day
 3. Significant weight loss when not dieting or weight gain, or decrease or increase in appetite nearly every day.
 4. Insomnia or hypersomnia nearly every day.
 5. Psychomotor agitation or retardation nearly every day
 6. Fatigue or loss of energy nearly every day.
 7. Feelings of worthlessness or excessive or inappropriate guilt nearly every day
 8. Diminished ability to think or concentrate, or indecisiveness, nearly every day
 9. Recurrent thoughts of death, recurrent suicidal ideation without a specific plan, or a suicide attempt or a specific plan for committing suicide.
-

Neurobiology of Depression

There are several neurochemical and neuroanatomical correlates of depression, which have led to multiple etiological hypotheses. In reviewing these hypotheses, it is worth noting that no single model can sufficiently account for all aspects and variations of depression. Rather than a unified hypothesis of depression, it is likely that the true aetiology of a complex and heterogeneous mental disorder such as depression incorporates components from all current theories.

The Monoamine Hypothesis of Affective Disorders

Monoamine neurotransmitters are a class of neurotransmitters derived from aromatic amino acids, and most notably include serotonin, norepinephrine, and dopamine. In the 1950's, the role of monoamines in mood disorders became apparent through a series of inadvertent discoveries, which eventually culminated in the *monoamine hypothesis of affective disorders* [101]. In 1955, some patients

being treated with the antihypertensive agent reserpine were found to become depressed after treatment [48, 95]. It was later shown that reserpine depletes vesicular storage of brain serotonin, which in turn reduces the available serotonin for synaptic transmission [48, 101, 135]. Conversely, the antimycobacterial agent iproniazid was shown to improve mood in tubercular patients with depression [22, 48]. Iproniazid inhibits monoamine oxidase (MAO), the enzyme that degrades free monoamines in the presynaptic nerve terminal. By inhibiting MAO, iproniazid enhances central serotonin and norepinephrine transmission. This discovery prompted the development of other monoamine oxidase inhibitors (MAOIs). Further support for the monoamine hypothesis came when imipramine, a drug initially developed as an anxiolytic for agitated patients with psychosis, was shown to have antidepressant effects [48, 69]. Imipramine, now classified as a tricyclic antidepressant (TCA), acts by blocking monoamine reuptake transporters, thereby increasing the level of serotonin and norepinephrine in the synapse. Together, MAOIs and TCAs constitute first generation antidepressants. In the late 1980's, momentum for the monoamine hypothesis prompted a second generation of antidepressants to enter development. These drugs aimed to increase receptor specificity and, therefore, decrease adverse side effects and increase tolerability. This second generation of antidepressants includes selective serotonin reuptake inhibitors (SSRIs), which are currently the most prescribed class of antidepressants, as well as serotonin-norepinephrine reuptake inhibitors (SNRIs). Although current antidepressants that target monoamine transmission are

clinically efficacious for some patients, their delayed antidepressant effect has proven to be problematic for the monoamine hypothesis. SSRIs increase monoamine transmission within hours of administration and begin to cause side effects within hours or days [48, 68]. However, enhanced mood requires weeks of chronic treatment. Additionally, monoamine depletion studies have found that acute reduction of monoamines can decrease mood in patients with a personal or family history of depression but not in healthy controls [68, 104, 123]. Rather than a direct effect of monoamine neurotransmission on mood state, it is now thought that antidepressants induce secondary transcriptional and translational changes that ultimately lead to synaptogenesis and neurogenesis [68, 101, 113]. For example, the transcription factor CREB (cAMP response element binding protein) is downstream of serotonin receptors and regulates expression of brain-derived neurotrophic factor (BDNF). Clinical studies report decreased levels of CREB in the cortex of depressed patients, and experimentally increased CREB activity in the hippocampus of rodents has been reported to induce antidepressant-like effects on behavioural tests [12, 101]. Additionally, CREB levels in the hippocampus are increased following chronic administration of antidepressants, such as the SSRI fluoxetine [12, 106]. These neuroplastic changes require several weeks and are necessary to achieve behavioural changes, which is consistent with the delayed response to antidepressants. Although the monoamine hypothesis has been the most clinically relevant theory of depression, leading to the development of first and second generation antidepressants, the delayed clinical response to

increased monoamines suggests that monoamine deficiency is not a primary abnormality in the aetiology of depression.

Neurotrophins, BDNF, and the Anatomy of Depression

In the brain, the monoamines serotonin and norepinephrine are largely released by the raphe nuclei and the locus coeruleus, respectively. These brainstem structures project to regions in the cerebral cortex and limbic system that regulate emotion, reward, attention, and executive function. Specifically, neuroimaging and volumetric post-mortem studies have identified reduced neural activity and dendritic atrophy in the hippocampus and the prefrontal cortex (PFC) [25, 60, 102, 134]. Although functional imaging studies have produced limited overlap in the brain regions identified in depression, meta-analytic results suggest that the regions with the most consistently reduced neural activity include the PFC, insula, cerebellum, and the parahippocampal gyrus (PHG; the major inflow tract to the hippocampus) [32, 45]. More consistent results have been provided through structural neuroimaging studies. These results were summarized in a meta-analysis, which revealed consistent volume reductions in frontal regions (anterior cingulate, orbitofrontal, and prefrontal cortex), as well as in the hippocampus and dorsal striatum [45, 63]. Moreover, volume reductions have been shown to be attenuated with antidepressant treatment [134].

The precise mechanism of region-specific volume reductions in depression has not been established. However, the role of BDNF has attracted interest in recent years. Stress-induced downregulation in hippocampal BDNF expression

has been well documented in preclinical studies [26]. Conversely, chronic treatment with antidepressants has been shown to upregulate hippocampal and PFC BDNF expression [87]. Post-mortem studies on humans support preclinical results, showing decreased levels of hippocampal BDNF in untreated subjects compared to subjects treated with antidepressant at the time of death [16, 26, 58, 87]. These correlation studies have prompted investigation into a more causal role of BDNF regulation in depression. To explore the possibility of a causal association, a single-nucleotide polymorphism (SNP) in BDNF was investigated, which substitutes methionine for valine at amino acid 66 (Val66Met), leading to improper storage of BDNF in neurons [30, 68]. Consequently, less BDNF is secreted from the nerve terminals. When implemented into a biological system, knock-in mice with this polymorphism exhibited increased anxiety-related behaviours when exposed to stressors [17, 68]. Antidepressants have also been shown to increase other growth factors in the hippocampus, such as vascular endothelial growth factor (VEGF), likely through the activation of transcriptional regulators such as CREB [68, 143]. However, a direct neuroprotective role of growth factors such as BDNF has not been straightforward to establish due to region-specificity. For example, in the ventral tegmental area (VTA; most notably involved in reward response and drug addiction) and the nucleus accumbens (NAc; also involved in reward processing), infusion of BDNF causes increased depressive-like behaviours in mice [67].

Stress and Cytokines

There is strong evidence in the literature that dysregulation of the hypothalamic-pituitary-adrenal axis (HPA) is an important factor in the biological aetiology of depression. In response to perceived stress by the cortical regions, the hypothalamus releases corticotropin-releasing hormone (CRH). CRH then stimulates the anterior pituitary gland to release adrenocorticotrophic hormone (ACTH), which in turn stimulates the adrenal cortex to release cortisol, a glucocorticoid. In a negative feedback mechanism, excess cortisol inhibits the hypothalamus and anterior pituitary, halting further production of cortisol. Although the first depressive episode usually involves a stressful psychosocial “trigger”, later episodes of depression become increasingly “endogenous” as the illness progresses [45]. Even in the absence of exogenous triggers, increased plasma, urine, and cerebrospinal fluid (CSF) cortisol levels have been well documented in a subset of patients with depression [57, 85, 110, 111]. Chronic exposure to elevated levels of glucocorticoids can have a deleterious impact on brain structures involved in cognition and emotional functions [82]. In fact, hypercortisolaemia has been shown to cause structural remodelling in the hippocampus, amygdala, and PFC [90]. In the hippocampus, certain types of acute stress have been demonstrated to suppress neurogenesis in the dentate gyrus, leading to atrophy—an effect that has also been observed in patients with Cushing’s syndrome, which is primarily characterized by increased ACTH release from the pituitary gland and hypercortisolaemia [139]. This stress-induced

atrophy has been postulated to be the underlying mechanism of the volumetric reductions observed in the hippocampus and PFC of patients with depression. Further support for the role of chronic stress in depression has come from preclinical studies. The most successful and widely used murine models of depression have, in fact, relied on the clinical observations of stress as a risk factor in depression [103]. Chronic mild stress, chronic unpredictable stress, social defeat paradigms, as well as direct chronic administration of corticosterone have all provided some measure of construct validity in modelling depression by causing anhedonia in the sucrose preference test [39, 103, 114, 146, 147]. These paradigms have also demonstrated face validity by modelling demonstrable symptoms of depression (e.g. decreased investigative and locomotor activity), and predictive validity through the reversal of depressive-like behaviours following chronic antidepressant treatment [103, 146]. It is important to note, however, that true construct validity cannot be achieved in models of depression, as this would require re-creating the disease aetiology, which remains largely unknown. At the molecular level, there is evidence that hypercortisolaemia is associated with modulation of the serotonergic system. The serotonin receptor subtype 5-HT_{1A} has been strongly implicated in depression and anxiety, with reduced receptor numbers and affinity reported in some patients [126]. Recently, preclinical and clinical evidence has suggested a causal role of stress-induced hypercortisolaemia on 5-HT_{1A} receptor downregulation [72, 80].

“Sickness behaviour” constitutes a set of clinically recognized behaviours that human and animal subjects exhibit at the onset of infectious disease [44]. These behaviours, which are due to activation of the inflammatory response, share many characteristics with depression, such as anhedonia and cognitive impairment [45]. Cytokines are the molecular mediators of inflammatory responses. Pro-inflammatory cytokines such as interleukin 1 (IL-1), IL-6, and tumour necrosis factor alpha (TNF- α) have been found to be elevated in the plasma and CSF of patients with depression [151]. In rodents, direct injection of low doses of IL-1 has also been shown to induce “sickness behaviour” [28, 68]. In humans, depressive symptoms have been reported as a common side effect of treatment with interferon alpha (IFN- α), a pro-inflammatory agent, occurring in approximately 30-50% of patients [52]. Conversely, evidence suggests that anti-inflammatory treatment such as non-steroidal anti-inflammatory drugs (NSAIDs) can be effective adjuvant drugs, particularly for treatment-resistant depression [65]. Despite strong evidence for a possible role of inflammation in the aetiology of depression, the neurobiological mechanism involved remains unknown. Further investigations should focus on the effect of neuroimmunological mediators (i.e. microglia) on surrounding glia and neurons [68].

Glutamate

Glutamate is the anionic form of the amino acid glutamic acid. In the nervous system, glutamate is the most abundant neurotransmitter [92] and plays a key role in cognitive processes that are dependent on synaptic plasticity, such as

learning and memory [89]. Peripherally, glutamate is released as a response to induced inflammation and activation of peripheral nociceptive fibres [19, 109]. Additionally, direct injection of glutamate has been shown to increase sensitivity to thermal and mechanical stimuli in murine models [11, 54].

Ketamine is a widely used general anaesthetic, and is pharmacologically classified as an antagonist to N-Methyl-D-aspartate receptors (NMDAR), a type of ionotropic glutamate receptors. In recent years, ketamine has become the focus of accumulating reports assessing its antidepressant effects in both humans and animal models [97, 153]. In 2000, Berman and colleagues carried out the first clinical study that reported on ketamine's rapid antidepressant properties. The antidepressant effects of ketamine were robust for the 9 patients involved in the randomized trial [9] and were then replicated in a larger study involving 18 treatment-resistant patients [153]. Since then, glutamate signalling has become well established as a factor in the neurostructural changes in depression [29, 125], with extensive preclinical [8, 38, 39, 75] and clinical evidence [53, 152] to support the validity of glutamate modulation for treating depression.

In 2010, interested in the potential for new depression therapeutics, Li and colleagues carried out a study on rats that began to elucidate a possible antidepressant mechanism for ketamine. They found that administration of ketamine rapidly activated the mammalian target of rapamycin (mTOR) pathway, leading to increased synaptogenesis in the prefrontal cortex [74]. Additionally, blocking mTOR signalling effectively blocked ketamine's ability to induce

synaptogenesis. It is now suggested that antagonism of NMDARs by ketamine causes an increased concentration of extracellular glutamate, resulting in fast excitation of neurons through increased activity of α -amino-3-hydroxy-5-methyl-4-isoxazolepropionic acid receptors (AMPA), another type of ionotropic glutamate receptors [27]. This fast excitation causes an influx of calcium ions through voltage-gated calcium channels, which in turn stimulates the release of BDNF. BDNF subsequently stimulates tropomyosin-related kinase B (TrkB) and downstream signalling pathways including PI3K-Akt and MAPK. These pathways stimulate mTOR, a serine-threonine protein kinase, which in turn regulates genes that increase the density of synaptic proteins, ultimately leading to synaptogenesis and antidepressant behavioural responses [27]. Although ketamine is also known to interact with other signalling systems, including the dopamine D2 receptors, opioid receptors, and sigma (σ) receptors [66, 119], there is considerable evidence to suggest that the primary antidepressant response of ketamine is mediated by the NMDAR. For example, other NMDA antagonists, including MK-801 and CPPene, have also shown effectiveness in inducing antidepressive effects in animal models [7, 84]. Moreover, the behavioural antidepressant effects of ketamine in animal models of depression have been shown to act independently of σ receptors [119]. In addition to ketamine, the antidepressant action of tianeptine, a clinically used TCA, has recently been attributed to glutamatergic regulation, possibly through the modulation of both AMPAR and NMDAR [91].

Clinically, concentrations of glutamate are elevated in the serum or plasma of patients with MDD [3, 61, 88, 94]. At the brain level, studies using magnetic resonance spectroscopy (MRS) reveal a decreased unresolved glutamate/glutamine signal (Glx) and glutamate alone signal (Glu) in brain regions that are relevant to depression, such as the PFC and anterior cingulate cortex [6, 46].

Antidepressants

Treatment for MDD has improved significantly since the serendipitous discovery of MAOIs and the formation of the monoamine hypothesis of depression in the 1950's. However, with the underlying aetiology of the illness still unclear, efforts to create increasingly targeted therapy has been relatively stagnant. Monotherapy with first and second-generation antidepressants often fails to alleviate symptoms, and it may take multiple attempts with different antidepressants and adjunct therapy to achieve clinical efficacy. Treating depression becomes even more difficult when it presents as comorbidity, in part due to a lack of understanding of the relationship between the primary disease and depression. Few studies have examined depression in cancer patients at the basic level, and thus treatment options for CID are limited to those therapies developed for use in non-cancer-related MDD. In this section, we will consider the clinical efficacy of antidepressants in MDD as well as CID.

Antidepressants in Major Depressive Disorder

The Sequenced Treatment Alternatives to Relieve Depression (STAR*D) trial was the largest effort to date on the efficacy of antidepressants. It was commissioned by the National Institute of Mental Health (NIMH) and completed in 2006 [124]. In 2008, data from the trial became available. The study recruited 4,041 adult patients (1,127 dropped out; 2,876 were analyzable) with MDD from primary care and psychiatric settings [50, 124]. As the primary outcome measure for remission, STAR*D used the Hamilton Depression Rating Scale (HAM-D) to measure the severity of depression. The HAM-D is a commonly used 52-item questionnaire that rates severity of depression on a 17-point scale, with scores of 0-7 considered normal [42]. In level 1 treatment, patients received citalopram monotherapy, one of the most prescribed SSRIs, and remission rates were approximately 28% based on HAM-D scores [51]. In levels 2, 3, and 4 of the trial, patients who did not achieve remission in the previous level were either switched to a different antidepressant or received an augmentation to citalopram treatment. Switches to new antidepressants consisted of other SSRIs, SNRIs, TCAs, or other agents that act on monoamine transmission. In the case of treatment augmentation, a wide range of agents were used, including anxiolytics, lithium, and thyroid hormone T3 [51]. In each level of the trial, the treatment-resistant patients from the previous level were randomized to the new treatment regimens. Remission rates in levels 2, 3, and 4 of the trial were all below 30%. With only a third of MDD patients responding to initial monotherapy, systematic reviews of

randomized control trials (RCTs) have sought to better define the role of antidepressants in the clinical setting. In 2009, Cipriani et al. showed that of the commonly prescribed second generation antidepressants, escitalopram and sertraline were the most efficacious and best tolerated, leading to fewer discontinuations [18]. In another meta-analysis, Fournier et al. investigated antidepressant efficacy relative to initial symptom severity [33]. They concluded that patients with severe MDD benefit substantially from antidepressant treatment, whereas benefit is minimal in mild or moderate MDD. In addition to pharmacological modulation, cognitive behavioural therapy (CBT) has been shown to be beneficial for patients with depression, even in the case of severe MDD [24, 49]. In some cases of severe MDD that is not responsive to antidepressants, electroconvulsive therapy (ECT) may be used. ECT has been extensively shown to be effective in achieving remission in treatment-resistant patients [93]. However, due to the requirement of anaesthetic, ECT is rarely used as a first line of treatment. More recently, Repetitive Transcranial Magnetic Stimulation (rTMS) has also been shown to provide some benefit as adjunct therapy in treatment resistant patients [93].

Antidepressants in Cancer-Induced Depression

In stark contrast to the large-scale and high-quality RCTs available for primary MDD, few studies have investigated antidepressant efficacy and alternative or adjunct therapies in cancer patients. This is surprising considering the high prevalence of depression comorbidity in cancer, a clinical observation

that spans decades [13, 31, 35, 62, 78, 144]. Difficulties in studying and treating CID are found at the preclinical and clinical levels. At the preclinical level, the lack of validated animal models for CID has restricted inquiry into the possible biological mechanisms involved. Cancer patients with comorbid depression are, therefore, limited to antidepressant treatment developed for non-cancer patients. Clinically, depression is underdiagnosed and undertreated in cancer patients, largely owing to the psychosocial complication of what might be considered “appropriate sadness” in terminally ill patients compared to treatable psychiatric disease [13, 78, 137]. In addition, factors such as cancer type, cancer stage, and demographic convolute an already complex mental disorder. Thus, in the absence of more precisely tailored treatment, antidepressants (particularly SSRIs) remain the first line of treatment in the oncologic setting.

Although few studies have examined the efficacy of antidepressants in CID, a handful of systematic reviews have compiled such studies in an attempt to draw clinical conclusions. In 2006, 2007, and 2011, three groups examined the literature for antidepressant efficacy in cancer. The first review focused on SSRIs and found that four of the five studies reported positive results, and one study using fluoxetine showed no difference in incidence of depression compared to placebo [145]. The second review, which had overlapping studies with the first, also examined the efficacy of mianserin (a tetracyclic antidepressant; TeCA) in two included studies [120]. In this review, three placebo-controlled trials (including the two mianserin studies) showed positive results. Of the remaining

four studies, the two placebo-controlled trials did not detect a difference between treatment and placebo, while the two trials comparing active treatments found temporal improvement of depressive scores but no group differences. The third review in 2011 updated the previous results with one additional study, which did not detect a difference between placebo and paroxetine or desipramine [105]. Underscoring the lack of high-quality studies on the topic, a 2013 Cochrane review found no eligible RCTs, controlled trials, cohort studies or case-control studies investigating antidepressant efficacy in patients with primary brain tumours [122]. Studies under consideration were excluded for a wide range of issues, such as reporting on usual clinical care rather than systematically evaluating specific treatments. Most recently, another systematic review has investigated antidepressant efficacy in breast cancer specifically [15]. This review identified two eligible studies with mixed results, both of which have been included in other systematic reviews [105, 120, 145]. Concerns raised in this review included small sample sizes, and therefore, a significant risk of bias. Overall, these systematic reviews highlight the inadequacy of currently available literature on the question of antidepressant efficacy in cancer patients. From these studies, broad clinical conclusions cannot be drawn, which points to a need for larger and better designed clinical trials as well as a capacity to study CID at the basic level.

In addition to pharmacotherapy, psychological interventions such as CBT, supportive psychotherapy, and group psychotherapy may be efficacious for cancer

patients either as primary treatment or in combination with antidepressants [2, 73, 79]. However, in clinical trials of antidepressants, physiological interventions, including regular hospice care, may be a confounding variable that can mask antidepressant effect [79]. Therefore, intervention models under investigation need to be well designed and appropriately analyzed to control for such confounds.

Cancer-Induced Depression

Strong clinical and preclinical evidence exists in the literature to support a causal role of cancer on depression. In the introduction to this chapter, the prevalence of depression in the oncologic setting was discussed in comparison to depression in the general population. While the staggeringly high prevalence of depression in cancer patients suggests a strong correlation, the impact of psychosocial factors make it difficult to establish causation or biological mechanisms. However, early clinical studies reveal that psychological changes relating to depression may in fact *precede* the diagnosis of cancer [40, 55, 112]. More recently, a breast cancer study, which included 428 women, reported that over 25% of women with breast cancer exhibited symptoms of depression prior to being informed of their cancer diagnosis [142]. Using data from the World Mental Health Survey Initiative, another study performed a retrospective analysis on the mental health of cancer patients, which included nineteen countries and more than 52,000 patients [107]. The study found that depression symptoms appear predictive of a later cancer diagnosis. By demonstrating an increased prevalence

of depression in patients who have cancer but are unaware of their diagnosis, these clinical findings effectively eliminate the confounding psychosocial effect of a cancer diagnosis, and suggest a possible causal role of cancer on mental health at the biological level. In addition to clinical support, this oncodynamic impact of cancer on depression is supported through common biological systems between cancer and depression; namely, inflammation, physiological stress, and glutamatergic dysregulation. In order to investigate the possible causal role of these systems in the induction of depression by cancer cells, validated CID animal models need to be established. In 2009, Pyter et al. reported that peripheral mammary tumours induce behavioural changes such as anhedonia in rats and increase plasma biomarkers such as cytokines and corticosterone [115]. Similarly, in 2011 Lamkin et al. were able to replicate these findings using ovarian cancer in mice [71]. To investigate possible neurological correlates in CID, Yang et al. recently showed that tumour-bearing mice had reduced proliferating and progenitor neurons in the dentate gyrus of the hippocampus when compared to control animals [149]. Although these studies have provided compelling insight into the association between cancer and depression, more rigorous validation of CID models is needed. Behavioural and relevant neuroanatomical comparisons to existing validated models of depression would yield more convincing animal models. In addition, reversal trials using antidepressants on the positive control depressive models would further establish the validity of the behavioural tests used prior to evaluating the CID models. Properly validated CID models would be

an essential tool in manipulating inflammatory, stress, and glutamatergic systems in the investigation of the causal oncodynamic effect of cancer on depressive symptoms. To date, only correlative associations have been established between cancer and depression, although a causal relationship has been postulated based on the clinical studies discussed in earlier in this chapter. Expanding on what is currently known about the common biological systems that are involved in cancer and depression, we can discuss the most plausible oncodynamic mechanisms of CID. These proposed mechanisms of CID are summarized in **Figure 1**.

Oncodynamic Effect Through Inflammation

A well-established characteristic of most cancer cells is their ability to exploit the host's immune system at multiple stages of tumour development and metastasis [1, 20, 21, 34, 41, 43]. Specifically, cancer cells recruit an array of cytokine-producing leukocytes, such as tumour-associated macrophages (TAMs) [20, 100]. Cancer cells themselves are also capable of expressing various cytokines, such as TNF- α and IL-6, that attract more leukocytes [20]. In doing so, cancer cells employ the same mechanisms that are normally activated to repair tissue in response to tissue damage [70]. For example, in order to repair normal tissue damage, the extracellular matrix (ECM) that binds cells together must be broken down in order to allow for the recruitment of new cells to the site of injury. Platelets aggregating at the site of injury release platelet derived growth factor (PDGF), which in turn stimulate fibroblasts to secrete matrix metalloproteinases (MMPs). These enzymes break down the ECM of damaged cells and allow the

arrival of new cells [70]. Cancer cells that secrete PDGF can exploit this mechanism by recruiting MMP-secreting fibroblasts to break down the ECM of healthy epithelial cells and by replacing them with multiplying cancer cells [70, 76].

As previously discussed in this chapter, depression is strongly associated with pro-inflammatory mediators in clinical and preclinical studies. The ability of cancer cells to directly secrete pro-inflammatory mediators highlights one possible oncodynamic pathway of CID. We can further postulate on the specific downstream effect of this oncodynamic event through closer investigation of inflammatory consequences in depression. Clinical studies investigating the cytokine profile of cancer patients have shown that IL-6, which is directly secreted by cancer cells [127], is elevated in the plasma of cancer patients who also exhibit depressive symptoms, compared to cancer patients who do not exhibit depressive symptoms [56, 99, 138]. In another study, the increased plasma concentration of IL-6 in ovarian cancer patients was associated with the vegetative symptoms of depression (such as fatigue and weight loss), but not with affective symptoms or overall depression [83]. Similar effects on vegetative, but not affective, depression symptoms have been observed with IFN- α therapy-induced inflammation [14, 70, 98]. Taken together, these results suggest that cancer cell-secreted IL-6 (and possibly other inflammatory mediators) induces an oncodynamic effect on depression, which specifically exacerbates vegetative symptoms.

Oncodynamic Effect Through Physiological Stress

Physiological stress through activation of the sympathetic nervous system is an adaptive response to environmental stressors. As previously discussed, dysregulation of this response is strongly implicated in the aetiology of depression. Undoubtedly, the psychosocial impact of a cancer diagnosis is one source of this dysregulation. The induction of chronic physiological stress in cancer patients is supported by the clinical observation of increased plasma cortisol in advanced cancer patients [81, 128]. Additionally, plasma levels of cortisol are higher with increased tumour burden, metastasis, and pervasiveness of the cancer [116, 129, 141]. This suggests a direct impact of cancer cells on physiological stress, in addition to the psychosocial contribution. However, the mechanism of cancer-induced activation of the stress response has not been investigated, with the notable exception of adrenal tumours that autonomously produce and secrete cortisol [36]. Other studies have investigated general HPA activation in cancer patients, but not the mechanism of activation, and often in the context of investigating depressive symptoms [83, 138]. Although clinical studies suggest a direct oncodynamic effect of cancer on the dysregulation of the physiological stress response (and ultimately depression), a discussion on the biological mechanisms is lacking in the literature.

Oncodynamic Effect Through Glutamatergic Signalling

As early as the 1980's, results from clinical investigations have demonstrated elevated plasma levels of glutamate in cancer patients [108, 118]. More recently, the mechanism of glutamate release by cancer cells as well downstream consequences of this release have garnered attention in the literature. Initial studies focused on glioma cell lines and found that glutamate secretion into the extracellular environment involved the glutamate/cystine antiporter system x_c^- [59]. This excess glutamate secretion causes excitotoxicity and death of surrounding neurons through over-activation of NMDARs [131, 150]. The same mechanism of glutamate secretion through system x_c^- was later characterized in multiple cancer cell lines, including metastatic breast and prostate cancers, through *in vitro* and *in vivo* studies [130, 131, 132, 133, 140].

Earlier in this chapter, the emerging role of glutamatergic signalling in the aetiology of depression was discussed. Excess glutamate secretion by cancer cells provides a biologically plausible cause of glutamate dysregulation in depression. This connection is particularly convincing in the case of gliomas, which secrete very high amounts of glutamate and which are also associated with a very high incidence of depression, as previously discussed. Neuronal hyperactivation due to glioma-secreted glutamate would interfere with neuroplastic and synaptoplastic events in the mPFC and the hippocampus, ultimately leading to depression. In peripheral cancers, the effect of glutamate on depression may not be as direct. Because of glutamate's key role in many neuronal signalling events, glutamate

distribution and extracellular fluid (ECF) concentrations in the brain are tightly controlled. The vast majority of glutamate in the brain is stored in astrocytes, while glutamate in the ECF is maintained at very low concentrations relative to plasma levels in the periphery [47, 86, 136]. The blood-brain-barrier (BBB) is a crucial structure in the maintenance of this concentration difference between plasma and brain ECF glutamate. Excitatory amino acid transporters (EAATs) on the abluminal (brain-facing) membrane of the BBB transport glutamate from the ECF to the peripherally circulating blood. The luminal (blood-facing) membrane lacks EAATs, thus preventing the entrance of glutamate from the blood into the brain under normal physiological conditions. However, recent evidence has suggested that pathological conditions disrupt the BBB, leading to increased permeability. Substance P (SP) is a pro-inflammatory neuropeptide that has been implicated in nociception [23], depression [64, 96, 148], and is expressed in breast cancer cells [117]. It was recently shown that breast cancer cell-secreted SP is involved in the transmigration of cancer cells across the BBB [121]. To do this, SP activates an inflammatory response in the endothelial cells that comprise the BBB, which ultimately increases their permeability. Therefore, under pathological conditions such as metastatic disease, tight regulation of brain glutamate may be impaired by breaches in the BBB. This represents one possible mechanism through which glutamate secreted by peripheral tumours can affect brain physiology and induce depression.

An alternative oncodynamic mechanism would be analogous to pain transmission. Glutamate released by peripheral cancer cells causes pain in a model of bone metastasis, which is attenuated using an antagonist of system x_c^- [140]. In this paradigm, glutamate does not need to cross the BBB in order to transmit a pain signal. Nociceptive fibres are activated peripherally and the signal is transmitted through the ascending pathway to cortical regions that perceive pain [37]. Similarly, it is plausible that peripheral glutamate activates CNS pathways indirectly through signal transmission, culminating in brain alterations consistent with depression. Therefore, although a mechanism has not been investigated in the literature, preclinical and clinical evidence suggests that cancer-secreted glutamate imparts an oncodynamic effect on the development of CID. In this section, two biologically plausible mechanisms for this oncodynamic effect have been suggested.

cancer cells also release large amounts of glutamate. Substance P (SP) released by cancer cells impairs the blood-brain barrier (BBB), causing increased permeability, which may allow peripherally secreted glutamate to enter the brain. Alternatively, peripherally secreted glutamate may act on the spinal cord through signal transduction pathways that project to brain regions involved in depression. Peripheral cancer cells also secrete cytokines, which may be a causal factor in vegetative depressive symptoms. Tumour burden has also been shown to influence the hypothalamic-pituitary-adrenal (HPA) axis, which leads to chronic physiological stress and depressive symptoms.

Conclusion

Depression in cancer patients is a highly prevalent comorbidity, which affects quality of life and survivorship. Although psychosocial factors contribute to depression in the cancer setting, the clinical evidence reviewed in this chapter suggests a more causal role of cancer on the induction of depression. Through careful consideration of the overlapping biological mechanisms involved in depression aetiology and cancer physiology, we can postulate on the initial oncodynamic signalling event(s) that lead to the induction of depression. However, a robustly validated preclinical model of CID is lacking in the literature. Therefore, the capacity to investigate the oncodynamic mechanism of CID

through manipulation of a valid model has yet to be established. Future direction in this field of research should focus on developing the capacity to investigate the mechanism(s) of CID, while being attentive to advancements in the understanding of depression aetiology.

References

1. Aggarwal BB, Shishodia S, Sandur SK et al. (2006) Inflammation and cancer: how hot is the link? *Biochemical pharmacology* 72:1605-1621
2. Akechi T (2012) Psychotherapy for depression among patients with advanced cancer. *Japanese journal of clinical oncology* 42:1113-1119
3. Altamura CA, Mauri MC, Ferrara A et al. (1993) Plasma and platelet excitatory amino acids in psychiatric disorders. *The American journal of psychiatry* 150:1731-1733
4. Andrade L, Caraveo-Anduaga JJ, Berglund P et al. (2003) The epidemiology of major depressive episodes: results from the International Consortium of Psychiatric Epidemiology (ICPE) Surveys. *International journal of methods in psychiatric research* 12:3-21
5. Association AP (2013) *Diagnostic and Statistical Manual of Mental Disorders, Fifth Edition.*
6. Auer DP, Putz B, Kraft E et al. (2000) Reduced glutamate in the anterior cingulate cortex in depression: an in vivo proton magnetic resonance spectroscopy study. *Biological psychiatry* 47:305-313
7. Autry AE, Adachi M, Nosyreva E et al. (2011) NMDA receptor blockade at rest triggers rapid behavioural antidepressant responses. *Nature* 475:91-95
8. Banasr M, Chowdhury GM, Terwilliger R et al. (2010) Glial pathology in an animal model of depression: reversal of stress-induced cellular,

- metabolic and behavioral deficits by the glutamate-modulating drug riluzole. *Molecular psychiatry* 15:501-511
9. Berman RM, Cappiello A, Anand A et al. (2000) Antidepressant effects of ketamine in depressed patients. *Biological psychiatry* 47:351-354
 10. Berrios GE (1988) Melancholia and depression during the 19th century: a conceptual history. *The British journal of psychiatry : the journal of mental science* 153:298-304
 11. Bhawe G, Karim F, Carlton SM et al. (2001) Peripheral group I metabotropic glutamate receptors modulate nociception in mice. *Nature neuroscience* 4:417-423
 12. Blendy JA (2006) The role of CREB in depression and antidepressant treatment. *Biological psychiatry* 59:1144-1150
 13. Caplette-Gingras A, Savard J (2008) Depression in women with metastatic breast cancer: a review of the literature. *Palliative & supportive care* 6:377-387
 14. Capuron L, Gummnick JF, Musselman DL et al. (2002) Neurobehavioral effects of interferon-alpha in cancer patients: phenomenology and paroxetine responsiveness of symptom dimensions. *Neuropsychopharmacology : official publication of the American College of Neuropsychopharmacology* 26:643-652

15. Carvalho AF, Hyphantis T, Sales PM et al. (2014) Major depressive disorder in breast cancer: a critical systematic review of pharmacological and psychotherapeutic clinical trials. *Cancer treatment reviews* 40:349-355
16. Chen B, Dowlatshahi D, Macqueen GM et al. (2001) Increased hippocampal BDNF immunoreactivity in subjects treated with antidepressant medication. *Biological psychiatry* 50:260-265
17. Chen ZY, Jing D, Bath KG et al. (2006) Genetic variant BDNF (Val66Met) polymorphism alters anxiety-related behavior. *Science* 314:140-143
18. Cipriani A, Furukawa TA, Salanti G et al. (2009) Comparative efficacy and acceptability of 12 new-generation antidepressants: a multiple-treatments meta-analysis. *Lancet* 373:746-758
19. Conn PJ, Pin JP (1997) Pharmacology and functions of metabotropic glutamate receptors. *Annual review of pharmacology and toxicology* 37:205-237
20. Coussens LM, Werb Z (2002) Inflammation and cancer. *Nature* 420:860-867
21. Coussens LM, Zitvogel L, Palucka AK (2013) Neutralizing tumor-promoting chronic inflammation: a magic bullet? *Science* 339:286-291
22. Crane GE (1956) The psychiatric side-effects of iproniazid. *The American journal of psychiatry* 112:494-501

23. De Felipe C, Herrero JF, O'brien JA et al. (1998) Altered nociception, analgesia and aggression in mice lacking the receptor for substance P. *Nature* 392:394-397
24. Driessen E, Hollon SD (2010) Cognitive behavioral therapy for mood disorders: efficacy, moderators and mediators. *The Psychiatric clinics of North America* 33:537-555
25. Duman RS, Aghajanian GK (2012) Synaptic dysfunction in depression: potential therapeutic targets. *Science* 338:68-72
26. Duman RS, Monteggia LM (2006) A neurotrophic model for stress-related mood disorders. *Biological psychiatry* 59:1116-1127
27. Duman RS, Voleti B (2012) Signaling pathways underlying the pathophysiology and treatment of depression: novel mechanisms for rapid-acting agents. *Trends in neurosciences* 35:47-56
28. Dunn AJ, Swiergiel AH, De Beaurepaire R (2005) Cytokines as mediators of depression: what can we learn from animal studies? *Neuroscience and biobehavioral reviews* 29:891-909
29. Duric V, Banasr M, Stockmeier CA et al. (2013) Altered expression of synapse and glutamate related genes in post-mortem hippocampus of depressed subjects. *The international journal of neuropsychopharmacology / official scientific journal of the Collegium Internationale Neuropsychopharmacologicum (CINP)* 16:69-82

30. Egan MF, Kojima M, Callicott JH et al. (2003) The BDNF val66met polymorphism affects activity-dependent secretion of BDNF and human memory and hippocampal function. *Cell* 112:257-269
31. Endicott J (1984) Measurement of depression in patients with cancer. *Cancer* 53:2243-2249
32. Fitzgerald PB, Laird AR, Maller J et al. (2008) A meta-analytic study of changes in brain activation in depression. *Human brain mapping* 29:683-695
33. Fournier JC, Derubeis RJ, Hollon SD et al. (2010) Antidepressant drug effects and depression severity: a patient-level meta-analysis. *JAMA : the journal of the American Medical Association* 303:47-53
34. Franklin RA, Liao W, Sarkar A et al. (2014) The cellular and molecular origin of tumor-associated macrophages. *Science* 344:921-925
35. Fris I, Litin EM, Pearson JS (1967) Comparison of psychiatric symptoms in carcinoma of the pancreas with those in some other intra-abdominal neoplasms. *The American journal of psychiatry* 123:1553-1562
36. Goh G, Scholl UI, Healy JM et al. (2014) Recurrent activating mutation in PRKACA in cortisol-producing adrenal tumors. *Nature genetics* 46:613-617
37. Gordon-Williams RM, Dickenson AH (2007) Central neuronal mechanisms in cancer-induced bone pain. *Current opinion in supportive and palliative care* 1:6-10

38. Gourley SL, Espitia JW, Sanacora G et al. (2012) Antidepressant-like properties of oral riluzole and utility of incentive disengagement models of depression in mice. *Psychopharmacology* 219:805-814
39. Gourley SL, Taylor JR (2009) Recapitulation and reversal of a persistent depression-like syndrome in rodents. *Current protocols in neuroscience / editorial board, Jacqueline N. Crawley ... [et al.] Chapter 9:Unit 9* 32
40. Green AI, Austin CP (1993) Psychopathology of pancreatic cancer. A psychobiologic probe. *Psychosomatics* 34:208-221
41. Grivennikov SI, Greten FR, Karin M (2010) Immunity, inflammation, and cancer. *Cell* 140:883-899
42. Hamilton M (1960) A rating scale for depression. *Journal of neurology, neurosurgery, and psychiatry* 23:56-62
43. Hanahan D, Weinberg RA (2011) Hallmarks of cancer: the next generation. *Cell* 144:646-674
44. Hart BL (1988) Biological basis of the behavior of sick animals. *Neuroscience and biobehavioral reviews* 12:123-137
45. Hasler G (2010) Pathophysiology of depression: do we have any solid evidence of interest to clinicians? *World psychiatry : official journal of the World Psychiatric Association (WPA)* 9:155-161
46. Hasler G, Van Der Veen JW, Tumonis T et al. (2007) Reduced prefrontal glutamate/glutamine and gamma-aminobutyric acid levels in major

- depression determined using proton magnetic resonance spectroscopy.
Archives of general psychiatry 64:193-200
47. Hawkins RA (2009) The blood-brain barrier and glutamate. The American journal of clinical nutrition 90:867S-874S
 48. Hirschfeld RM (2000) History and evolution of the monoamine hypothesis of depression. The Journal of clinical psychiatry 61 Suppl 6:4-6
 49. Hoifodt RS, Strom C, Kolstrup N et al. (2011) Effectiveness of cognitive behavioural therapy in primary health care: a review. Family practice 28:489-504
 50. Howland RH (2008) Sequenced Treatment Alternatives to Relieve Depression (STAR*D). Part 1: study design. Journal of psychosocial nursing and mental health services 46:21-24
 51. Howland RH (2008) Sequenced Treatment Alternatives to Relieve Depression (STAR*D). Part 2: Study outcomes. Journal of psychosocial nursing and mental health services 46:21-24
 52. Hoyo-Becerra C, Schlaak JF, Hermann DM (2014) Insights from interferon-alpha-related depression for the pathogenesis of depression associated with inflammation. Brain, behavior, and immunity
 53. Ibrahim L, Diazgranados N, Franco-Chaves J et al. (2012) Course of improvement in depressive symptoms to a single intravenous infusion of ketamine vs add-on riluzole: results from a 4-week, double-blind, placebo-

- controlled study. *Neuropsychopharmacology* : official publication of the American College of Neuropsychopharmacology 37:1526-1533
54. Jackson DL, Graff CB, Richardson JD et al. (1995) Glutamate participates in the peripheral modulation of thermal hyperalgesia in rats. *European journal of pharmacology* 284:321-325
55. Jacobsson L, Ottosson JO (1971) Initial mental disorders in carcinoma of pancreas and stomach. *Acta psychiatrica Scandinavica. Supplementum* 221:120-127
56. Jehn CF, Kuehnhardt D, Bartholomae A et al. (2006) Biomarkers of depression in cancer patients. *Cancer* 107:2723-2729
57. Juruena MF, Cleare AJ, Pariante CM (2004) The hypothalamic pituitary adrenal axis, glucocorticoid receptor function and relevance to depression. *Revista brasileira de psiquiatria (Sao Paulo, Brazil : 1999)* 26:189-201
58. Karege F, Vaudan G, Schwald M et al. (2005) Neurotrophin levels in postmortem brains of suicide victims and the effects of antemortem diagnosis and psychotropic drugs. *Brain research. Molecular brain research* 136:29-37
59. Kato S, Negishi K, Mawatari K et al. (1992) A mechanism for glutamate toxicity in the C6 glioma cells involving inhibition of cystine uptake leading to glutathione depletion. *Neuroscience* 48:903-914
60. Kempton MJ, Salvador Z, Munafo MR et al. (2011) Structural neuroimaging studies in major depressive disorder. *Meta-analysis and*

- comparison with bipolar disorder. Archives of general psychiatry 68:675-690
61. Kim JS, Schmid-Burgk W, Claus D et al. (1982) Increased serum glutamate in depressed patients. Archiv fur Psychiatrie und Nervenkrankheiten 232:299-304
 62. Koenig R, Levin SM, Brennan MJ (1967) The emotional status of cancer patients as measured by a psychological test. Journal of chronic diseases 20:923-930
 63. Koolschijn PC, Van Haren NE, Lensvelt-Mulders GJ et al. (2009) Brain volume abnormalities in major depressive disorder: a meta-analysis of magnetic resonance imaging studies. Human brain mapping 30:3719-3735
 64. Kormos V, Gaszner B (2013) Role of neuropeptides in anxiety, stress, and depression: from animals to humans. Neuropeptides 47:401-419
 65. Kornstein SG, Schneider RK (2001) Clinical features of treatment-resistant depression. The Journal of clinical psychiatry 62 Suppl 16:18-25
 66. KorteKaas R, Maguire RP, Van Waarde A et al. (2008) Despite irreversible binding, PET tracer [11C]-SA5845 is suitable for imaging of drug competition at sigma receptors-the cases of ketamine and haloperidol. Neurochemistry international 53:45-50
 67. Krishnan V, Han MH, Graham DL et al. (2007) Molecular adaptations underlying susceptibility and resistance to social defeat in brain reward regions. Cell 131:391-404

68. Krishnan V, Nestler EJ (2008) The molecular neurobiology of depression. *Nature* 455:894-902
69. Kuhn R (1958) The treatment of depressive states with G 22355 (imipramine hydrochloride). *The American journal of psychiatry* 115:459-464
70. Lamkin DM (2010) Inflammatory processes and depressive-like behavior in a syngeneic model of ovarian cancer. University of Iowa
71. Lamkin DM, Lutgendorf SK, Lubaroff D et al. (2011) Cancer induces inflammation and depressive-like behavior in the mouse: modulation by social housing. *Brain, behavior, and immunity* 25:555-564
72. Lanzenberger R, Wadsak W, Spindelegger C et al. (2010) Cortisol plasma levels in social anxiety disorder patients correlate with serotonin-1A receptor binding in limbic brain regions. *The international journal of neuropsychopharmacology / official scientific journal of the Collegium Internationale Neuropsychopharmacologicum (CINP)* 13:1129-1143
73. Li M, Fitzgerald P, Rodin G (2012) Evidence-based treatment of depression in patients with cancer. *Journal of clinical oncology : official journal of the American Society of Clinical Oncology* 30:1187-1196
74. Li N, Lee B, Liu RJ et al. (2010) mTOR-dependent synapse formation underlies the rapid antidepressant effects of NMDA antagonists. *Science* 329:959-964

75. Li N, Liu RJ, Dwyer JM et al. (2011) Glutamate N-methyl-D-aspartate receptor antagonists rapidly reverse behavioral and synaptic deficits caused by chronic stress exposure. *Biological psychiatry* 69:754-761
76. Link CJ, Jr., Kohn E, Reed E (1996) The relationship between borderline ovarian tumors and epithelial ovarian carcinoma: epidemiologic, pathologic, and molecular aspects. *Gynecologic oncology* 60:347-354
77. Litofsky NS, Farace E, Anderson F, Jr. et al. (2004) Depression in patients with high-grade glioma: results of the Glioma Outcomes Project. *Neurosurgery* 54:358-366; discussion 366-357
78. Lloyd-Williams M (2000) Difficulties in diagnosing and treating depression in the terminally ill cancer patient. *Postgraduate medical journal* 76:555-558
79. Lloyd-Williams M, Payne S, Reeve J et al. (2013) Antidepressant medication in patients with advanced cancer--an observational study. *QJM : monthly journal of the Association of Physicians* 106:995-1001
80. Lopez JF, Chalmers DT, Little KY et al. (1998) A.E. Bennett Research Award. Regulation of serotonin1A, glucocorticoid, and mineralocorticoid receptor in rat and human hippocampus: implications for the neurobiology of depression. *Biological psychiatry* 43:547-573
81. Lundstrom S, Furst CJ (2003) Symptoms in advanced cancer: relationship to endogenous cortisol levels. *Palliative medicine* 17:503-508

82. Lupien SJ, McEwen BS, Gunnar MR et al. (2009) Effects of stress throughout the lifespan on the brain, behaviour and cognition. *Nature reviews. Neuroscience* 10:434-445
83. Lutgendorf SK, Weinrib AZ, Penedo F et al. (2008) Interleukin-6, cortisol, and depressive symptoms in ovarian cancer patients. *Journal of clinical oncology : official journal of the American Society of Clinical Oncology* 26:4820-4827
84. Maeng S, Zarate CA, Jr., Du J et al. (2008) Cellular mechanisms underlying the antidepressant effects of ketamine: role of alpha-amino-3-hydroxy-5-methylisoxazole-4-propionic acid receptors. *Biological psychiatry* 63:349-352
85. Mahar I, Bambico FR, Mechawar N et al. (2014) Stress, serotonin, and hippocampal neurogenesis in relation to depression and antidepressant effects. *Neuroscience and biobehavioral reviews* 38:173-192
86. Mann GE, Yudilevich DL, Sobrevia L (2003) Regulation of amino acid and glucose transporters in endothelial and smooth muscle cells. *Physiological reviews* 83:183-252
87. Martinowich K, Manji H, Lu B (2007) New insights into BDNF function in depression and anxiety. *Nature neuroscience* 10:1089-1093
88. Mauri MC, Ferrara A, Boscati L et al. (1998) Plasma and platelet amino acid concentrations in patients affected by major depression and under fluvoxamine treatment. *Neuropsychobiology* 37:124-129

89. Mcentee WJ, Crook TH (1993) Glutamate: its role in learning, memory, and the aging brain. *Psychopharmacology* 111:391-401
90. Mcewen BS (2007) Physiology and neurobiology of stress and adaptation: central role of the brain. *Physiological reviews* 87:873-904
91. Mcewen BS, Chattarji S, Diamond DM et al. (2010) The neurobiological properties of tianeptine (Stablon): from monoamine hypothesis to glutamatergic modulation. *Molecular psychiatry* 15:237-249
92. Meldrum BS (2000) Glutamate as a neurotransmitter in the brain: review of physiology and pathology. *The Journal of nutrition* 130:1007s-1015s
93. Micallef-Trigona B (2014) Comparing the effects of repetitive transcranial magnetic stimulation and electroconvulsive therapy in the treatment of depression: a systematic review and meta-analysis. *Depression research and treatment* 2014:135049
94. Mitani H, Shirayama Y, Yamada T et al. (2006) Correlation between plasma levels of glutamate, alanine and serine with severity of depression. *Progress in neuro-psychopharmacology & biological psychiatry* 30:1155-1158
95. Muller JC, Pryor WW, Gibbons JE et al. (1955) Depression and anxiety occurring during Rauwolfia therapy. *Journal of the American Medical Association* 159:836-839
96. Munoz M, Covenas R (2014) Involvement of substance P and the NK-1 receptor in human pathology. *Amino acids* 46:1727-1750

97. Murrough JW (2012) Ketamine as a novel antidepressant: from synapse to behavior. *Clinical pharmacology and therapeutics* 91:303-309
98. Musselman DL, Lawson DH, Gumnick JF et al. (2001) Paroxetine for the prevention of depression induced by high-dose interferon alfa. *The New England journal of medicine* 344:961-966
99. Musselman DL, Miller AH, Porter MR et al. (2001) Higher than normal plasma interleukin-6 concentrations in cancer patients with depression: preliminary findings. *The American journal of psychiatry* 158:1252-1257
100. Nashed MG, Balenko MD, Singh G (2014) Cancer-induced oxidative stress and pain. *Current pain and headache reports* 18:384
101. Nestler EJ, Barrot M, Dileone RJ et al. (2002) Neurobiology of depression. *Neuron* 34:13-25
102. Nestler EJ, Gould E, Manji H et al. (2002) Preclinical models: status of basic research in depression. *Biological psychiatry* 52:503-528
103. Nestler EJ, Hyman SE (2010) Animal models of neuropsychiatric disorders. *Nature neuroscience* 13:1161-1169
104. Neumeister A, Nugent AC, Waldeck T et al. (2004) Neural and behavioral responses to tryptophan depletion in unmedicated patients with remitted major depressive disorder and controls. *Archives of general psychiatry* 61:765-773

105. Ng CG, Boks MP, Zainal NZ et al. (2011) The prevalence and pharmacotherapy of depression in cancer patients. *Journal of affective disorders* 131:1-7
106. Nibuya M, Nestler EJ, Duman RS (1996) Chronic antidepressant administration increases the expression of cAMP response element binding protein (CREB) in rat hippocampus. *The Journal of neuroscience : the official journal of the Society for Neuroscience* 16:2365-2372
107. O'Neill S, Posada-Villa J, Medina-Mora ME et al. (2014) Associations between DSM-IV mental disorders and subsequent self-reported diagnosis of cancer. *Journal of psychosomatic research* 76:207-212
108. Ollenschlager G, Karner J, Karner-Hanusch J et al. (1989) Plasma glutamate--a prognostic marker of cancer and of other immunodeficiency syndromes? *Scandinavian journal of clinical and laboratory investigation* 49:773-777
109. Omote K, Kawamata T, Kawamata M et al. (1998) Formalin-induced release of excitatory amino acids in the skin of the rat hindpaw. *Brain research* 787:161-164
110. Pariante CM, Lightman SL (2008) The HPA axis in major depression: classical theories and new developments. *Trends in neurosciences* 31:464-468
111. Parker KJ, Schatzberg AF, Lyons DM (2003) Neuroendocrine aspects of hypercortisolism in major depression. *Hormones and behavior* 43:60-66

112. Passik SD, Roth AJ (1999) Anxiety symptoms and panic attacks preceding pancreatic cancer diagnosis. *Psycho-oncology* 8:268-272
113. Pittenger C, Duman RS (2008) Stress, depression, and neuroplasticity: a convergence of mechanisms. *Neuropsychopharmacology : official publication of the American College of Neuropsychopharmacology* 33:88-109
114. Pollak DD, Rey CE, Monje FJ (2010) Rodent models in depression research: classical strategies and new directions. *Annals of medicine* 42:252-264
115. Pyter LM, Pineros V, Galang JA et al. (2009) Peripheral tumors induce depressive-like behaviors and cytokine production and alter hypothalamic-pituitary-adrenal axis regulation. *Proceedings of the National Academy of Sciences of the United States of America* 106:9069-9074
116. Rasmuson T, Ljungberg B, Grankvist K et al. (2001) Increased serum cortisol levels are associated with high tumour grade in patients with renal cell carcinoma. *Acta oncologica (Stockholm, Sweden)* 40:83-87
117. Reddy BY, Greco SJ, Patel PS et al. (2009) RE-1-silencing transcription factor shows tumor-suppressor functions and negatively regulates the oncogenic TAC1 in breast cancer cells. *Proceedings of the National Academy of Sciences of the United States of America* 106:4408-4413

118. Rivera S, Lopez-Soriano FJ, Azcon-Bieto J et al. (1987) Blood amino acid compartmentation in mice bearing Lewis lung carcinoma. *Cancer research* 47:5644-5646
119. Robson MJ, Elliott M, Seminerio MJ et al. (2012) Evaluation of sigma (sigma) receptors in the antidepressant-like effects of ketamine in vitro and in vivo. *European neuropsychopharmacology : the journal of the European College of Neuropsychopharmacology* 22:308-317
120. Rodin G, Lloyd N, Katz M et al. (2007) The treatment of depression in cancer patients: a systematic review. *Supportive care in cancer : official journal of the Multinational Association of Supportive Care in Cancer* 15:123-136
121. Rodriguez PL, Jiang S, Fu Y et al. (2014) The proinflammatory peptide substance P promotes blood-brain barrier breaching by breast cancer cells through changes in microvascular endothelial cell tight junctions. *International journal of cancer. Journal international du cancer* 134:1034-1044
122. Rooney A, Grant R (2013) Pharmacological treatment of depression in patients with a primary brain tumour. *The Cochrane database of systematic reviews* 5:Cd006932
123. Ruhe HG, Mason NS, Schene AH (2007) Mood is indirectly related to serotonin, norepinephrine and dopamine levels in humans: a meta-analysis of monoamine depletion studies. *Molecular psychiatry* 12:331-359

124. Rush AJ, Fava M, Wisniewski SR et al. (2004) Sequenced treatment alternatives to relieve depression (STAR*D): rationale and design. *Controlled clinical trials* 25:119-142
125. Sanacora G, Treccani G, Popoli M (2012) Towards a glutamate hypothesis of depression: an emerging frontier of neuropsychopharmacology for mood disorders. *Neuropharmacology* 62:63-77
126. Savitz J, Lucki I, Drevets WC (2009) 5-HT(1A) receptor function in major depressive disorder. *Progress in neurobiology* 88:17-31
127. Schafer ZT, Brugge JS (2007) IL-6 involvement in epithelial cancers. *The Journal of clinical investigation* 117:3660-3663
128. Schaur RJ, Fellier H, Gleispach H et al. (1979) Tumor host relations. I. Increased plasma cortisol in tumor-bearing humans compared with patients with benign surgical diseases. *Journal of cancer research and clinical oncology* 93:281-285
129. Schaur RJ, Semmelrock HJ, Schauenstein E et al. (1979) Tumor host relations. II. Influence of tumor extent and tumor site on plasma cortisol of patients with malignant diseases. *Journal of cancer research and clinical oncology* 93:287-292
130. Seidlitz EP, Sharma MK, Saikali Z et al. (2009) Cancer cell lines release glutamate into the extracellular environment. *Clinical & experimental metastasis* 26:781-787

131. Seidlitz EP, Sharma MK, Singh G (2010) A by-product of glutathione production in cancer cells may cause disruption in bone metabolic processes. *Canadian journal of physiology and pharmacology* 88:197-203
132. Seidlitz EP, Sharma MK, Singh G (2010) Extracellular glutamate alters mature osteoclast and osteoblast functions. *Canadian journal of physiology and pharmacology* 88:929-936
133. Sharma MK, Seidlitz EP, Singh G (2010) Cancer cells release glutamate via the cystine/glutamate antiporter. *Biochemical and biophysical research communications* 391:91-95
134. Sheline YI, Gado MH, Kraemer HC (2003) Untreated depression and hippocampal volume loss. *The American journal of psychiatry* 160:1516-1518
135. Shore PA, Silver SL, Brodie BB (1955) Interaction of reserpine, serotonin, and lysergic acid diethylamide in brain. *Science* 122:284-285
136. Smith QR (2000) Transport of glutamate and other amino acids at the blood-brain barrier. *The Journal of nutrition* 130:1016s-1022s
137. Somerset W, Stout SC, Miller AH et al. (2004) Breast cancer and depression. *Oncology (Williston Park, N.Y.)* 18:1021-1034; discussion 1035-1026, 1047-1028
138. Soygur H, Palaoglu O, Akarsu ES et al. (2007) Interleukin-6 levels and HPA axis activation in breast cancer patients with major depressive

- disorder. *Progress in neuro-psychopharmacology & biological psychiatry* 31:1242-1247
139. Starkman MN, Gebarski SS, Berent S et al. (1992) Hippocampal formation volume, memory dysfunction, and cortisol levels in patients with Cushing's syndrome. *Biological psychiatry* 32:756-765
140. Ungard RG, Seidlitz EP, Singh G (2014) Inhibition of breast cancer-cell glutamate release with sulfasalazine limits cancer-induced bone pain. *Pain* 155:28-36
141. Van Der Pompe G, Antoni MH, Heijnen CJ (1996) Elevated basal cortisol levels and attenuated ACTH and cortisol responses to a behavioral challenge in women with metastatic breast cancer. *Psychoneuroendocrinology* 21:361-374
142. Van Esch L, Roukema JA, Ernst MF et al. (2012) Combined anxiety and depressive symptoms before diagnosis of breast cancer. *Journal of affective disorders* 136:895-901
143. Warner-Schmidt JL, Duman RS (2007) VEGF is an essential mediator of the neurogenic and behavioral actions of antidepressants. *Proceedings of the National Academy of Sciences of the United States of America* 104:4647-4652
144. Watts S, Leydon G, Birch B et al. (2014) Depression and anxiety in prostate cancer: a systematic review and meta-analysis of prevalence rates. *BMJ open* 4:e003901

145. Williams S, Dale J (2006) The effectiveness of treatment for depression/depressive symptoms in adults with cancer: a systematic review. *British journal of cancer* 94:372-390
146. Willner P (1997) Validity, reliability and utility of the chronic mild stress model of depression: a 10-year review and evaluation. *Psychopharmacology* 134:319-329
147. Yan HC, Cao X, Das M et al. (2010) Behavioral animal models of depression. *Neuroscience bulletin* 26:327-337
148. Yang LM, Yu L, Jin HJ et al. (2014) Substance P receptor antagonist in lateral habenula improves rat depression-like behavior. *Brain research bulletin* 100:22-28
149. Yang M, Kim J, Kim JS et al. (2014) Hippocampal dysfunctions in tumor-bearing mice. *Brain, behavior, and immunity* 36:147-155
150. Ye ZC, Sontheimer H (1999) Glioma cells release excitotoxic concentrations of glutamate. *Cancer research* 59:4383-4391
151. Young JJ, Bruno D, Pomara N (2014) A review of the relationship between proinflammatory cytokines and major depressive disorder. *Journal of affective disorders* 169c:15-20
152. Zarate CA, Jr., Brutsche NE, Ibrahim L et al. (2012) Replication of ketamine's antidepressant efficacy in bipolar depression: a randomized controlled add-on trial. *Biological psychiatry* 71:939-946

153. Zarate CA, Jr., Singh JB, Carlson PJ et al. (2006) A randomized trial of an N-methyl-D-aspartate antagonist in treatment-resistant major depression. Archives of general psychiatry 63:856-864

CHAPTER 2

Depressive-like behaviours and decreased dendritic branching in the medial prefrontal cortex of mice with tumors: A novel validated model of cancer-induced depression

Mina G. Nashed, Eric P. Seidlitz, Benicio N. Frey, Gurmit Singh

Behav Brain Res 294: 25-35

Preface

In this chapter, an author-generated version of the manuscript entitled “Depressive-like behaviours and decreased dendritic branching in the medial prefrontal cortex of mice with tumors: A novel validated model of cancer-induced depression”, published in *Behavioural Brain Research* November 2015, is presented. The paper is reproduced with permission from **Elsevier**, as stated on the copyright agreement:

Authors can use their articles, in full or in part, for a wide range of scholarly, non-commercial purposes as outlined below:

- *Use by an author in the author’s classroom teaching (including distribution of copies, paper or electronic)*
- *Distribution of copies (including through e-mail) to known research colleagues for their personal use (but not for Commercial Use)*
- *Inclusion in a thesis or dissertation (provided that this is not to be published commercially)*
- *Use in a subsequent compilation of the author’s works*
- *Extending the Article to book-length form*
- *Preparation of other derivative works (but not for Commercial Use)*
- *Otherwise using or re-using portions or excerpts in other works*

These rights apply for all Elsevier authors who publish their article as either a subscription article or an open access article. In all cases we require that all Elsevier authors always include a full acknowledgement and, if appropriate, a link to the final published version hosted on Science Direct.

(<http://www.sciencedirect.com/science/article/pii/S016643281530111X>)

For this paper, I performed the behavioural assays, animal drug treatments, cancer cell culturing and inoculations, tissue harvest and processing, dendritic analysis, blood collection and processing, CORT ELISA, and data analysis. Furthermore, I created all of the figures, tables, and both wrote and revised the manuscript. Dr. Eric Seidlitz revised the manuscript and provided critical training for techniques, input regarding experimental groups, design, and interpretation. Dr. Benicio Frey and Dr. Gurmit Singh provided intellectual direction and revised the manuscript. Please note that American spellings are used throughout the article, as required by the journal.

Context and Background Information

In the introductory chapter of this manuscript, I argued that it is necessary to develop an animal model in order to begin exploring the pathophysiology of cancer-induced depression (CID) at the basic level. The manuscript presented in this chapter establishes the first validated preclinical model of CID.

Immunodeficient models with human tumour cell xenografts were initially explored and rejected based on observed confounding behaviours, which diminished test reliability (Appendix 1). For example, immunodeficient BALB/c nu/nu mice exhibited a leg-grabbing behaviour on the tail suspension test (TST), which rendered it ineffective at determining escape vs. despair behaviours.

Other studies have recently established an associated between tumour burden and depressive-like behaviours, with a particular focus on the role of

inflammation (Lamkin et al., 2011; Norden et al., 2015; Pyter, Pineros, Galang, McClintock, & Prendergast, 2009; Yang et al., 2014). However, these studies do not validate their models using positive control models of depressive-like behaviours. To validate that the behavioural alterations observed in a new model are due to the induction of a depressive state, the same alterations must first be observed using the same assays in an established model of a depressive-like state. Furthermore, the alterations observed in the positive control model must be reversible by antidepressant treatment to establish that the assays are sensitive to antidepressant effects. This is particularly important to control for the significant variability in animal behaviours of different strains and in different laboratory conditions (Krackow et al., 2010).

In this manuscript, a positive control model was established using chronic administration of corticosterone (CORT). A group of CORT mice were also treated chronically with fluoxetine (FLX), a popular clinical antidepressant. The CID model was induced with subcutaneous inoculation of murine 4T1 mammary carcinoma cells. Both the CORT and CID models displayed anhedonic and despair behaviours. The depressive-like behaviours observed in the CORT model were reversible by FLX treatment. In addition to the behavioural assays, a neuroanatomical assessment was conducted on the medial prefrontal cortex (mPFC) in both models. Dendritic atrophy and reduced neuronal activity have been demonstrated in the mPFC of depressed patients (Fitzgerald, Laird, Maller, & Daskalakis, 2008; Kempton et al., 2011; Koolschijn, van Haren, Lensvelt-

Mulders, Hulshoff Pol, & Kahn, 2009). Our results demonstrated reduced mPFC apical and basilar dendritic arbour branching in CORT and CID mice. FLX treatment partially reversed these deficits in CORT mice.

This manuscript represents the first validated preclinical model of CID. Similar to the positive control CORT model, this model exhibited robust depressive-like behaviours and neuroanatomical deficits in the mPFC.

**Depressive-like behaviours and decreased dendritic branching in
the medial prefrontal cortex of mice with tumors: A novel
validated model of cancer-induced depression**

^{1,2}Mina G. Nashed[#], ^{1,2}Eric P. Seidlitz, ^{3,4}Benicio N. Frey, ^{1,2}Gurmit Singh*

¹*Department of Pathology & Molecular Medicine, McMaster University, Hamilton, ON, L8N 3Z5, Canada.*

²*Michael G. DeGrootte Institute for Pain Research and Care, McMaster University, Hamilton, ON, L8N 3Z5, Canada.*

³*Department of Psychiatry and Behavioural Neurosciences, McMaster University, Hamilton, ON, L8N 3Z5, Canada.*

⁴*Mood Disorders Program and Women's Health Concerns Clinic, St. Joseph's Healthcare Hamilton, ON, L8P 3P6,
Canada.*

Abbreviated Title: A Model of Cancer-Induced Depression

Submitting Author

*** Corresponding author**

Address: Department of Pathology & Molecular Medicine, McMaster University, 1280 Main
Street West, Hamilton, ON L8N 3Z5, Canada.

Tel.: +1 905 525 9140x28144.

E-mail address: singhg@mcmaster.ca

Key Words:

cancer, depression, animal model, anhedonia, behavioural despair, medial prefrontal cortex

Abstract Word Count: 252

Article Word Count: 5,038

Number of Figures: 7

Number of Tables: 3

Abstract

Depression is commonly comorbid in cancer patients and has detrimental effects on disease progression. Evidence suggests that biological mechanisms may induce the onset of cancer-induced depression (CID). The present investigation aims to establish a validated preclinical animal model of CID. Female BALB/c mice were allocated to four groups: control (n = 12), chronic oral exposure to corticosterone (CORT) (n = 12), CORT exposure followed by chronic low dose fluoxetine (FLX) treatment (n = 12), and subcutaneous inoculation of 4T1 mammary carcinoma cells (n = 13). Anhedonia was evaluated using the sucrose preference test (SPT), and behavioural despair was evaluated using the forced swim test (FST) and tail suspension test (TST). Sholl analyses were used to examine the dendritic morphology of Golgi-Cox impregnated neurons from the medial prefrontal cortex (mPFC). CORT exposure and tumor burden were both associated with decreased sucrose preference, increased FST immobility, and decreased basilar and apical dendritic branching of neurons in the mPFC. CORT-induced behavioural and dendritic morphological changes were reversible by FLX. No differences in TST immobility were observed between groups. On the secondary TST outcome measure, CORT exposure and tumor burden were associated with a trend towards decreased power of movement. CORT exposure induced a positive control model of a depressive-like state, with FLX treatment confirming the predictive validity of the model. This verified the sensitivity of behavioural and histological tests, which were used to assess the CID model. The

induction of a depressive-like state in this model represents the first successfully validated animal model of CID.

Introduction

Major depressive disorder (MDD) is one of the most commonly diagnosed psychiatric disorders in primary care settings. Its lifetime prevalence is ~8 – 12 % [1], increasing to as high as 57 % in breast cancer patients and a staggering 95 % in high-grade glioma [2]. Depression in cancer patients has often been conceptualized as “reactive depression” due to the expected psychosocial influence of a cancer diagnosis [3]. However, treating the onset of depression as purely reactive in cancer patients does not account for any possible biological influence of the cancer itself. There is considerable clinical evidence that psychological changes relating to depression actually precede the diagnosis of cancer [4-6]. Over 25 % of women with breast cancer exhibit symptoms of depression prior to being informed of their cancer diagnosis [7], and depression symptoms appear to be predictive of a later cancer diagnosis [8]. These clinical findings suggest a biologically causative effect of cancer on the initiation of depressive symptoms, independent of confounding factors such as a patient’s knowledge of a psychologically stressful cancer diagnosis.

A major impediment to the mechanistic study, drug development, and effective treatment of CID has been the lack of valid animal models that would facilitate preclinical research. The current investigation aims to address this need by developing a robust, validated mouse model of CID. To accomplish this, we first aimed to demonstrate that our chosen tests were sensitive to depressive-like behaviours induced by an existing, well-established animal model of non-cancer

related depression-like state. Predictive validity of the model was also assessed by intervention with a clinical antidepressant, fluoxetine (FLX). Anhedonia, the diminished ability to experience pleasure, is considered a core symptom of MDD [9, 10]. In the present investigation, anhedonia was assessed with the sucrose preference test (SPT), which is based on the neurobiological assumption that intake of sucrose-sweetened water is a valid measure of sensitivity to reward [11]. Another common measure of depressive-like behaviour in animals is “behavioural despair”, which we assessed using the forced swim test (FST) [12] and tail suspension test (TST) [13]. In these paradigms, despair is characterized by the duration of immobility (i.e. lack of escape behaviour) when exposed to forced swimming or tail suspension. To induce a positive control model of a depressive-like state, we exposed mice chronically to corticosterone (CORT), which provides a well-established preclinical model of depressive-like behaviours [14-21]. FLX, a selective serotonin reuptake inhibitor (SSRI), was used at a low chronic dose to reverse CORT-induced behavioural changes [22, 23]. CORT-induced depressive-like behaviours and their reversal by FLX established the sensitivity of the behavioural tests. In parallel with this, a group of animals were inoculated with 4T1 mammary carcinoma cells subcutaneously to determine if a depressive-like state could be induced by cancer alone, and if this model could conform to the requirements of a robust preclinical animal model.

Depression has been associated with dendritic atrophy and reduced neuronal activity in specific brain regions, particularly the hippocampus and

medial prefrontal cortex (mPFC) [24-28]. Therefore, a histological analysis of dendritic branching of pyramidal neurons in the mPFC was performed to investigate structural evidence of an induced depressive-like state and corroborate results from the behavioural analyses.

We hypothesized that the behavioural tests and the dendritic analyses would reliably identify depressive-like behaviours and structural changes in the mPFC in the CORT model of a depressive-like state, and that these changes would be reversible by chronic administration of FLX. We further hypothesized that our subcutaneous tumor model would exhibit depressive-like behaviours and dendritic atrophy using the same analyses, thereby validating an animal model of CID for further use in mechanistic studies and pharmaceutical development.

In the current investigation, reversal of CORT-induced behavioural and dendritic changes by FLX confirmed the predictive validity of this model and verified the sensitivity of the behavioural and histological tests. Using these tests, tumor burden was shown to be associated with depressive-like behaviours and decreased dendritic branching in the mPFC, demonstrating a physiological association between cancer and a depressive-like state, and validating this animal model of CID.

Materials and Methods

Mice

Forty-nine female BALB/c mice aged 4-6 weeks were obtained from Charles River Laboratories (St. Constant, QC, Canada). Female mice were selected as male mice appear to more frequently gnaw and bite at tumor sites [29]. Mice were single-housed in sterile cages maintained at 24 °C with a 12-h light/dark cycle, and were provided *ad libitum* access to autoclaved food and water. All procedures were performed according to guidelines established by the Canadian Council on Animal Care under a protocol reviewed and approved by the *Animal Research Ethics Board* of McMaster University.

Drug treatments

To induce a positive control model of a depressive-like state, mice were administered chronic oral CORT as outlined previously [15]. Briefly, the pH of sterile water was increased to 12-13 using 10 N NaOH and CORT hemisuccinate (Steraloids, Newport, RI, USA) was added and allowed to dissolve overnight at 4 °C to slow its decay. Once dissolved, the pH was neutralized to 7.0-7.5 using 10 N HCl. The resulting CORT solution (35 µg/mL) was administered *ad libitum* to mice in place of their normal drinking water over a 21-day period. Mean dose was calculated to be 6.53 ± 0.16 mg/kg/day in these animals.

For the reversal of CORT-induced depressive-like behaviours, CORT treatment in drinking water was stopped, and the SSRI FLX was administered *ad*

libitum in drinking water for a 21-day period. FLX hydrochloride (Sigma-Aldrich, St. Louis, MO, USA) was dissolved in sterile drinking water at a concentration of 150 µg/mL to obtain dosages between 10 and 18 mg/kg/day [23]. The mean dose of FLX consumed was 16.46 ± 0.16 mg/kg/day. FLX was administered in opaque bottles to protect it from light.

Tumor cell inoculation

Murine 4T1 mammary carcinoma cells are derived from a spontaneously arising mammary tumor in BALB/c mice [30, 31]. 4T1 cells (American Type Culture Collection, Manassas, VA, USA) were maintained in culture according to supplier specifications. Mice were anesthetized by isoflurane inhalation and inoculated with 15,000 4T1 cells in serum-free RPMI 1640 media (Life Technologies, Burlington, ON, Canada) subcutaneously on the right side of their lower backs. This tumor site was selected instead of the orthotopic site to avoid movement constraints and potential confounding behaviours in the FST and TST. All other mice that did not receive 4T1 injections were sham-inoculated with serum-free RPMI 1640 media. Tumor size was monitored using a digital caliper every 3-4 days once tumors became palpable at day 8. Mice were weighed weekly and overall health status was monitored every 3-4 days initially, and then daily during the final week prior to endpoint. All mice were euthanized 28 days after the mice in the tumor group were inoculated with cancer cells.

Behavioural analyses

Sucrose preference was evaluated as a measure of anhedonia. Mice were first habituated to 3 % sucrose over a 72-h period. During this period, regular drinking water was replaced with 3 % sucrose solution. This concentration of sucrose has been shown in our preliminary experiments to provide a robust sucrose preference of approximately 70 % in BALB/c mice, which allows for reliable detection of both elevations and reductions in preference (data not shown). The SPT was performed prior to any intervention at baseline and again after experimental treatments. During each testing period, mice were presented with a two-bottle option of water and 3 % sucrose solution for 48 h in their home cages. At 24 h, the positions of the two bottles were switched to eliminate any effect of location bias. Bottles were weighed before and after testing and preference was calculated as the percentage of sucrose solution intake relative to total fluid intake [32].

Two tests were used to assess behavioural despair: the automated dual-sensor FST (BioSeb, Vitrolles, France) and the automated TST (BioSeb, Vitrolles, France). For the FST, mice were individually placed into 20 cm diameter beakers with 10 cm depth of sterile water warmed to 28 °C to counter hypothermia [33]. This system combines overhead video with input from vibration sensors attached to the beakers to distinguish between active state of swimming/climbing and inactive state of immobility/floating. The total testing duration was 6 min, with the first minute discounted from analysis to allow for behavioural stabilization.

The primary outcome measure of the FST was the duration of time spent immobile. For the TST, a piece of masking tape was placed around the tail of each animal. To suspend the mice, the tape was pierced with a hook attached to a strain gauge on the TST apparatus. Again, the total testing duration was 6 min, with the first minute discounted from analysis. Input from the strain gauge was used to compute immobility time, as well as secondary measures including power of movement (P.M.; arbitrary units).

Experimental groups

The FST and TST were performed once prior to endpoint to avoid confounding learned behaviours that could arise from repeated testing (e.g. leg-grabbing on the TST). However, multiple exposures to the SPT did not confound later testing, and was found to be necessary to habituate mice to the sucrose solution. The SPT was initially performed at baseline and scores were used to divide animals into four experimental groups such that the means and standard deviations of sucrose preference were uniform between groups at baseline. The four groups were then randomly assigned to treatments: no treatment control (n = 12), CORT-only (+CORT/-FLX; n = 12), CORT followed by FLX (+CORT/+FLX; n = 12), and subcutaneous tumor (n = 13). The detailed timeline of the experiment is presented in **Figure 1**.

Euthanasia and tissue processing

Euthanasia was performed by isoflurane anesthesia and cardiac puncture exsanguination for endpoint blood collection, followed by decapitation.

Euthanasia and endpoint monitoring were performed in accordance with protocols approved by the *Animal Research Ethics Board* of McMaster University. Brains were immediately removed, rinsed with sterile phosphate-buffered saline, and placed in Golgi-Cox impregnation solution (Hitobiotec Inc., Wilmington, DE, USA) for 2 weeks at room temperature. Following impregnation, brains were rapidly frozen in cooled isopentane. 200 μm sections were obtained using a cryostat and air dried on gelatin-coated slides at room temperature in the dark. Golgi-Cox impregnation was visualized by immersion of slides in an ammonium hydroxide-based solution provided with the Hito Golgi-Cox OptimStain Kit. Slides were dehydrated in increasing concentrations of ethanol, then cleared in xylene and coverslips applied using a xylene-based resinous mounting medium. Mounted sections were viewed by light microscopy.

Dendritic analysis

Eight mice from each experimental group were randomly selected for dendritic analysis (N = 32). Golgi-Cox stained brain sections between +2.45 and +1.45 relative to bregma were examined under light microscopy to identify pyramidal neurons in layer II–III of the mPFC [34]. Pyramidal neurons were identified by their characteristic triangular soma, basilar dendritic tree, and apical

dendrites extending towards the pial surface [35, 36]. Only neurons that appeared fully intact and were unobscured by other neurons were selected for imaging, yielding between 6 and 10 viable neurons for each animal. Z-stacked images were captured for each neuron in 2 μm increments using OpenLab 5 (PerkinElmer, Waltham, MA, USA). Neurons were digitally reconstructed using the Simple Neurite Tracer plugin for the open source software Fiji (ImageJ platform) [37], with the investigator blind to condition. Cumulative basilar and apical branch lengths were recorded following neuronal reconstruction. Assessing the variability between the 6 and 10 neurons selected from each brain provided a mean within-animal standard error of the mean (SEM) of $9.4 \pm 0.7 \%$ for total basilar branch length, and $13.2 \pm 0.8 \%$ for total apical branch length. Cumulative basilar and apical branch lengths were also used to assess group differences in overall dendritic morphology.

To more closely examine the extent of basilar and apical dendritic branching, Sholl analyses were performed, in which a grid of concentric rings spaced 10 μm apart was overlaid onto the neuronal image centered at the soma and the number of ring intersections with dendrites was computed for each neuron as a branching index [38, 39]. Sholl analyses were performed using a Fiji plugin [40].

Blood collection and CORT ELISA

At baseline, mice were anesthetized by isoflurane inhalation and approximately 100 μL of blood was collected from the orbital sinus. At endpoint,

mice were euthanized and blood samples were collected intracardially using sterile 18 G needles and 1 mL syringes. Blood samples were allowed to coagulate followed by centrifugation to extract serum. A mouse/rat CORT enzyme-linked immunosorbent assay (ELISA) (Alpco, Salem, NH, USA) was used to determine serum levels of CORT, with all samples analyzed in triplicate.

Data analysis

Comparisons between control versus +CORT/-FLX versus +CORT/+FLX aimed to establish test sensitivity by detecting a depressive-like state in the positive control CORT model and reversal of this state through FLX treatment. In parallel to establishing test sensitivity, comparisons between control versus tumor aimed to establish the CID model by detecting a depressive-like state in tumor-bearing animals relative to control animals. Lastly, comparisons between the +CORT/-FLX versus tumor assessed any differences in the depressive-like states of the positive control CORT model and the tumor model.

Behavioural results for the SPT, FST, and TST were expressed as mean scores for mice in each experimental group. For the dendritic analysis, branch length was expressed as mean total branch length for 8 mice from each experimental group. For these data, one-way analysis of variance (ANOVA) was used to analyze between-group effects. Grubb's test was used to identify any outliers for each behavioural test.

Sholl analysis results were expressed as mean ring intersections summed into 20 μm bins for each experimental group. Weight was expressed as mean

body weight for each experimental group, corrected for tumor mass in the tumor group. For these data, a two-way repeated-measures ANOVA (Sholl: group \times distance from soma; weight: group \times experimental days) was used to analyze between-group effects.

For all one-way ANOVAs, planned comparisons were performed between all groups, with the exception of tumor animals versus +CORT/+FLX animals as this comparison would not yield meaningful results. Since these comparisons were planned *a priori* and involve a particular set of pairwise comparisons, Bonferroni's correction for multiple comparisons was used for all one-way ANOVAs. For all two-way repeated-measures ANOVAs, selection of particular pairwise comparisons is not possible. These tests involved comparisons of each group to every other group. However, the comparisons between tumor animals versus +CORT/+FLX animals are not reported. For two-way repeated-measures ANOVAs, *post hoc* analyses were performed using Tukey's multiple comparison test. All statistical tests were performed using GraphPad Prism software version 6.0 for Macintosh (GraphPad Software, Inc., La Jolla, CA, USA).

Tumor growth was measured every 3-4 days when tumors became palpable. Growth was expressed as mean tumor mass (in grams) over time. Calipers were used to measure tumor length, width, and depth, and hemi-ellipsoid tumor volume was calculated as $V = L \times W \times H \times 0.5236$ [41, 42]. To correct for tumor mass when measuring body weight, tumor volume was converted to mass, assuming soft-tissue density of 1 g/cm³ [43, 44].

Serum samples were pooled to produce a single sample for each group, and CORT levels were analyzed at baseline and endpoint. Samples were pooled for economical reasons and to allow for technical replicates. CORT levels were then reported as the percent of baseline levels, such that 100% represents the same concentration of serum CORT at endpoint as measured at baseline prior to model induction.

Results

Weight and tumor size monitoring

The main effect of treatment group approached significance ($F_{(3,47)} = 2.77$, $P = 0.052$), and there was a significant interaction between group and time ($F_{(12,188)} = 4.28$, $P < 0.0001$) (**Figure 2**). Post hoc analysis revealed significantly reduced weight of +CORT/-FLX animals compared to +CORT/+FLX animals at day 4 ($P = 0.005$), day 12 ($P = 0.032$), and day 18 ($P = 0.002$). Other non-significant trends were also noted. On average, CORT-treated mice weighed slightly less than control, and there was a trend toward increased weight in the FLX-treated mice compared to control. After day 12 of tumor growth, tumor-bearing mice weighed slightly less than control mice. All mice in the tumor group exhibited exponential tumor growth over 25 days, with a final mean tumor mass of 0.27 ± 0.03 g (**Figure 3**).

Behavioural analyses

In the SPT, 1 animal from the control group and 1 animal from the tumor group were excluded from analysis as they were determined to be outliers. There was a significant main effect of treatment group observed in the SPT ($F_{(3,43)} = 4.45$, $P = 0.008$). Planned analysis revealed that CORT-treated mice showed a reduction in preference for 3 % sucrose solution compared to control ($P = 0.008$) (**Figure 4A**). Mice that received FLX treatment had a sucrose preference that was intermediate between control and CORT-only mice. This partial recovery of

preference did not significantly differ from either group (+CORT/+FLX vs. Control: $P = 0.55$; +CORT/+FLX vs. +CORT/-FLX: $P = 0.41$). Tumor-bearing mice showed a significantly reduced sucrose preference compared to control mice ($P = 0.035$), and did not differ from CORT-treated mice ($P > 0.99$).

There was a significant main effect of treatment observed in the FST ($F_{(3,45)} = 6.12, P = 0.001$). Planned analysis revealed that CORT-treated mice showed a significantly increased immobility time compared to control ($P = 0.013$) (**Figure 4B**), which was reversed by FLX ($P = 0.011$). Tumor-bearing mice showed a significantly increased immobility time compared to control mice ($P = 0.039$), and did not differ from CORT-treated mice ($P > 0.99$).

Two measures for the TST were reported: immobility time (**Figure 4C**) and P.M. (**Figure 4D**). There was no main effect of treatment group in the TST immobility or P.M. ($F_{(3,45)} = 1.68, P = 0.18$) or P.M. ($F_{(3,45)} = 0.86, P = 0.47$). However, the 3 experimental groups exhibited a non-significant trend towards decreased P.M.

Dendritic analyses

Layer II-III pyramidal neurons in the mPFC were identified in Golgi-Cox impregnated coronal sections of mouse brains. **Figure 5** illustrates the identification of the mPFC in coronal sections, complete neuronal impregnation, and digital reconstructions of neurons from all experimental groups.

Differences in overall dendritic morphology were assessed by examining cumulative basilar and apical branch lengths (**Figure 6**). There was a significant

main effect of treatment group on the basilar branch length ($F_{(3,28)} = 3.18$, $P = 0.039$) and apical branch length ($F_{(3,28)} = 7.34$, $P < 0.001$). Planned analyses revealed a non-significant trend for shorter basilar branch length in CORT-treated mice compared to control mice ($P = 0.13$), while apical branch length was significantly reduced ($P < 0.001$). FLX-treated mice had higher basilar branch compared to CORT-only mice, which approached significance ($P = 0.072$), although apical branch length was intermediate between control and CORT-only mice and not significantly different from either group (+CORT/+FLX vs. Control: $P = 0.10$; +CORT/+FLX vs. +CORT/-FLX: $P = 0.17$). Basilar branch length was reduced in tumor-bearing mice compared to control mice, but did not reach statistical significance ($P = 0.58$), and was also not different compared to CORT-treated mice ($P > 0.99$). Apical branch length was reduced in tumor-bearing mice compared to control mice, which approached significance ($P = 0.073$), and was not different compared to CORT-treated mice ($P = 0.23$).

The extent of dendritic branching was assessed by Sholl analyses. **Table 1** illustrates the details of the Sholl analyses, showing group differences in basilar and apical intersections at each 20 μm bin. **Figure 7** visually highlights the results of the Sholl analysis, showing the pattern of group difference for basilar (**Figure 7A**) and apical (**Figure 7B**) branching. For both basilar and apical arbors there were significant main group effects (basilar: $F_{(3,28)} = 3.22$, $P = 0.038$; apical: $F_{(3,28)} = 7.38$, $P < 0.001$) and significant interactions of group and distance from soma (basilar: $F_{(30,280)} = 2.62$, $P < 0.0001$; apical: $F_{(51,476)} = 1.74$, $P = 0.002$). *Post hoc*

analysis at each 20 μm interval from the soma revealed that CORT-treated mice had significantly reduced basilar branching compared to control mice between 30 and 40 μm ($P = 0.048$), and significantly reduced apical branching between 90 and 240 μm (90-100 μm : $P = 0.031$; 110-200 μm : $P < 0.001$; 210-220 μm : $P = 0.018$; 230-240 μm : $P = 0.025$). FLX-treated mice had significantly increased basilar branching compared to CORT-only mice between 90 and 120 μm (90-100 μm : $P = 0.029$; 110-120 μm : $P = 0.012$), and significantly increased apical branching between 150 and 160 μm ($P = 0.048$). Apical branching was only partially recovered by FLX treatment since FLX-treated mice had significantly reduced apical branching compared to control mice between 170 and 180 μm ($P = 0.037$). Tumor-bearing mice had significantly reduced basilar branching compared to control mice between 30 and 60 μm (all intervals: $P < 0.001$), and significantly reduced apical branching between 110 and 180 μm (110-120 μm : $P = 0.012$; 130-140 μm : $P = 0.002$; 150-160 μm : $P = 0.002$; 170-180 μm : $P = 0.016$). Basilar and apical branching was not different between tumor-bearing mice and CORT-treated mice at any interval.

Serum CORT ELISA

Endpoint serum CORT, normalized to baseline levels, was elevated in CORT-treated mice (28 days after CORT cessation) compared to control mice (**Table 2**). In the FLX-treated group, serum CORT was elevated compared to control mice, but slightly less than CORT-only mice. Statistical considerations

were not applicable as individual animal samples were pooled, yielding one sample for each group.

Discussion

Clinical evidence indicates that there is an alarmingly high prevalence of depression comorbidity in cancer patients [45, 46]. Depression has also been shown to be predictive of cancer progression and increased mortality [47-51]. Currently, treatment options for CID are limited to therapies developed for use in non-cancer MDD. Although cancer patients in their last year of life are four times more likely than the general population to be prescribed an antidepressant [52], at present, the few existing studies that have examined the efficacy of antidepressants in cancer patients have provided inconsistent results [53-55]. While some studies have demonstrated moderate efficacy, others have shown no changes in the incidence or level of depression between patients prescribed a placebo or antidepressant, even for two of the most widely prescribed antidepressants, fluoxetine and paroxetine [53]. These clinical findings highlight the need for mechanistic investigations and the development of novel targeted therapies for CID, which requires the establishment of validated animal CID models. Several recent studies focusing on the role of cancer-mediated inflammation as an underlying cause of depression have provided preclinical evidence supporting CID as a symptom needing specialized treatment [29, 56-58]. These studies demonstrate depressive-like behaviours in tumor-bearing rodents using tests designed to measure behavioural despair and/or anhedonia. Results from the CID model in the current investigation were consistent with these studies. The positive control CORT model and reversal with FLX provided further

confirmation of the sensitivity of our tests in detecting a depressive-like state and antidepressant effect, respectively. Results for all behavioural and dendritic analyses are summarized in **Table 3**. Prior studies investigating CID lack supporting evidence from histological analyses of brain regions known to be relevant to depression. In this investigation, a histological examination of the mPFC was performed, which further validated our CID model.

We used a simple and non-invasive chronic CORT exposure model as a positive control to induce a classical, stress-mediated depressive-like state [15, 16, 59]. Exposure to oral CORT causes a persistent depressive-like state in rodents, which can last several weeks after cessation of the treatment period [15, 60]. The antidepressant FLX was used to confirm the predictive validity of the CORT model. FLX was utilized given that it has previously been reported to be efficacious when chronically administered at similar doses (10 – 18 mg/kg/day) [22, 23]. Antidepressants such as FLX that have limited effects acutely but are effective when administered chronically in animal models are thought to better represent clinical antidepressant mechanisms [61]. To verify the biological correlates of this positive control model, serum CORT was assessed using an ELISA and found to be elevated at endpoint, three weeks following cessation of CORT treatment (**Table 2**). By comparison, the FLX-treated group had a lower serum CORT level compared to the positive control model, although results should be cautiously interpreted in the absence of a statistical analysis due to pooling of samples. These results are consistent with reports that FLX inhibits P-

glycoprotein at the blood-brain barrier, causing increased activation of glucocorticoid receptors in the brain and negative feedback on the HPA-axis [62, 63].

In animal models of a depressive-like state, anhedonia is typically assessed using the SPT. In the present study, animals in the positive control CORT group exhibited a significantly reduced sucrose preference 3 weeks after cessation of CORT administration (**Figure 4A**). The observed decrease in sucrose preference was partially reversed by FLX. A complete reversal of depressive-like behaviours by FLX should not be expected. Clinically, only about 1/3 of depressed subjects treated with a single SSRI achieve full remission [64] and treatment response depends in part on the severity of depressive-like symptoms [65]. Preclinical studies support these observations, with FLX treatment reversing approximately 40 – 50 % of swim-induced immobility on the FST [66]. Our proposed animal model of CID also exhibited an anhedonic response in the SPT, which was similar in magnitude to, and did not differ statistically from, CORT-induced anhedonia.

The FST and TST were initially developed as behavioural assays to screen for novel antidepressants [33, 67, 68] and inherently induce acute stress, which is reversed by administration of antidepressants. Recently, the FST and TST have also demonstrated sensitivity in detecting depressive-like states in animal models of chronic mild stress, including oral CORT administration [59, 69]. In the present study, these behavioural assays were used to assess the depressive-like state of CORT-treated as well as tumor-bearing mice. The tests served to confirm the

predictive validity of the CORT model to induce a depressive-like state and to reverse this state through chronic low-dose FLX treatment. In the FST, our CID model exhibited nearly the same level of behavioural despair as that induced by CORT treatment, which was reversible by FLX treatment. In contrast, there were no differences observed between groups in immobility as measured by the TST. However, trends for the power of movement measure suggest behavioural despair in CORT-treated mice, which was not reversed by FLX, as well as behavioural despair in the CID model. Although both the FST and TST were developed as measures of despair, the divergent results from these tests suggest that these particular tests may detect different pathophysiological mechanisms. Levels of immobility as measured by the FST, but not the TST, are significantly altered after repeated ketamine treatment, suggesting that FST may be more sensitive to glutamatergic dysregulation [70]. It is also possible that the FST with video and sensor inputs, as well as a more precise calibration method, was more sensitive in differentiating between mobile and immobile states. Taken together, the behavioural results reported here demonstrate sensitivity in detecting depressive-like behaviours in the positive control model, which are at least partly reversed by FLX. Although any statistically significant differences in depressive-like behaviours between tumor and control animals would have been sufficient to validate the CID model, the robustness of response on these assays is important for the model's future utility. The CID model developed in this study demonstrated similar magnitudes of anhedonia and behavioural despair as the

positive control CORT model, which we have shown to be sensitive to reversal by FLX. We can, therefore, expect our CID model to reliably detect treatments that would be efficacious for CID.

Clinical and post-mortem studies using neuroimaging and volumetric analyses have consistently identified dendritic atrophy and reduced brain activation in the mPFC of depressed patients [24, 26, 27, 71-73]. To examine changes in dendritic branching in the mPFC, Golgi-Cox stained neurons were imaged, digitally reconstructed, and traced and dendritic arbors were analyzed by Sholl analysis. Golgi-Cox staining has the unique quality of fully penetrating only a small fraction of neurons, thereby facilitating the visualization of dendritic branching within individual neurons [74]. Results from analyzing dendritic branch length and the Sholl analyses indicate CORT-induced atrophy of apical and, to a lesser extent, basilar dendrites, which was partially reversed by FLX (**Figs. 6 & 7**). These results support previous observations using murine stress models of a depressive-like state, which report atrophy primarily in apical but not basilar dendrites of the mPFC [35]. Studies using hippocampal samples generally report similar findings [75-79], although one recent study found significantly decreased basilar, but not apical, branching in the hippocampal CA1 region of mice exposed to chronic oral CORT [80]. In a study that examined the mPFC, a clear but ultimately non-significant trend towards decreased cumulative basilar branch length and extent of branching using the Sholl analysis were observed [35]. Similar to the behavioural findings, our CID model exhibited basilar and apical

dendritic atrophy that was comparable in magnitude to the positive control CORT model. In addition to behavioural tests, these findings provide a histological assay to further investigate the central effects of novel treatments for CID. Hippocampi from mice used in the present investigation were also preserved for future differential gene expression studies using next-generation sequencing.

As mentioned previously, few clinical studies have been undertaken to assess the efficacy of current antidepressants on CID, with several existing studies reporting inconsistent findings. The pathophysiology of CID should not be assumed to parallel non-cancer related MDD without further careful investigation into the etiology, physiology, and treatment of cancer patients with depression. Care should be taken in using antidepressants such as FLX to assess the predictive validity of a preclinical CID model. Our future investigations into the mechanisms that underlie CID will assess the efficacy of FLX, as well as several other pharmacological agents, in attenuating CID using the animal model developed in this study. Several of these agents will target the glutamatergic pathway, given that glutamatergic dysregulation is important in both cancer and depression.

Conclusion

The lack of validated animal models has been one of the main obstacles in studying the underlying biology of CID. By evaluating the sensitivity of multiple behavioural assays, as well as dendritic analyses in the mPFC, we have established and validated the first mouse model of CID. Our findings will facilitate further research into the mechanisms underlying CID, and ultimately help to support the development of much needed novel, targeted therapies.

Acknowledgements

The authors thank Natalie Zacal and Robert Ungard for their help with animal work and tissue processing. We also thank Robert Ungard and Dr. Katja Linher-Melville for their critical feedback on the manuscript.

Conflict of interest

Dr. Frey has received grant/research support from Alternative Funding Plan Innovations Award, Brain & Behaviour Research Foundation, CIHR, Eli Lilly, Hamilton Health Sciences Foundation, J.P. Bickell Foundation, Ontario Brain Institute, Ontario Mental Health Foundation, Pfizer and Society for Women's Health Research, and has received consultant and/or speaker fees from AstraZeneca, Bristol-Myers Squibb, Lundbeck, Pfizer, Servier and Sunovion. The other authors declare no competing financial interest.

Funding

This study was funded by operating grants from the Canadian Institute of Health Research (CIHR) and the Canadian Breast Cancer Foundation (CBCF).

References

- [1] Andrade L, Caraveo-Anduaga JJ, Berglund P, Bijl RV, De Graaf R, Vollebergh W, et al. The epidemiology of major depressive episodes: results from the International Consortium of Psychiatric Epidemiology (ICPE) Surveys. *International journal of methods in psychiatric research*. 2003;12:3-21.
- [2] Litofsky NS, Farace E, Anderson F, Jr., Meyers CA, Huang W, Laws ER, Jr. Depression in patients with high-grade glioma: results of the Glioma Outcomes Project. *Neurosurgery*. 2004;54:358-66; discussion 66-7.
- [3] Paykel ES. Basic concepts of depression. *Dialogues in clinical neuroscience*. 2008;10:279-89.
- [4] Green AI, Austin CP. Psychopathology of pancreatic cancer. A psychobiologic probe. *Psychosomatics*. 1993;34:208-21.
- [5] Jacobsson L, Ottosson JO. Initial mental disorders in carcinoma of pancreas and stomach. *Acta psychiatrica Scandinavica Supplementum*. 1971;221:120-7.
- [6] Passik SD, Roth AJ. Anxiety symptoms and panic attacks preceding pancreatic cancer diagnosis. *Psycho-oncology*. 1999;8:268-72.
- [7] Van Esch L, Roukema JA, Ernst MF, Nieuwenhuijzen GA, De Vries J. Combined anxiety and depressive symptoms before diagnosis of breast cancer. *Journal of affective disorders*. 2012;136:895-901.
- [8] O'Neill S, Posada-Villa J, Medina-Mora ME, Al-Hamzawi AO, Piazza M, Tachimori H, et al. Associations between DSM-IV mental disorders and

subsequent self-reported diagnosis of cancer. *Journal of psychosomatic research*.

2014;76:207-12.

[9] American Psychiatric Association. *Diagnostic and Statistical Manual of Mental Disorders (5th ed.)*. Washington, DC2013.

[10] Krishnan V, Nestler EJ. The molecular neurobiology of depression. *Nature*. 2008;455:894-902.

[11] Willner P. Validity, reliability and utility of the chronic mild stress model of depression: a 10-year review and evaluation. *Psychopharmacology*. 1997;134:319-29.

[12] Porsolt RD, Bertin A, Jalfre M. Behavioral despair in mice: a primary screening test for antidepressants. *Archives internationales de pharmacodynamie et de therapie*. 1977;229:327-36.

[13] Steru L, Chermat R, Thierry B, Simon P. The tail suspension test: a new method for screening antidepressants in mice. *Psychopharmacology*. 1985;85:367-70.

[14] David DJ, Samuels BA, Rainer Q, Wang JW, Marsteller D, Mendez I, et al. Neurogenesis-dependent and -independent effects of fluoxetine in an animal model of anxiety/depression. *Neuron*. 2009;62:479-93.

[15] Gourley SL, Taylor JR. Recapitulation and reversal of a persistent depression-like syndrome in rodents. *Current protocols in neuroscience / editorial board, Jacqueline N Crawley [et al]*. 2009;Chapter 9:Unit 9 32.

- [16] Gourley SL, Wu FJ, Kiraly DD, Ploski JE, Kedves AT, Duman RS, et al. Regionally specific regulation of ERK MAP kinase in a model of antidepressant-sensitive chronic depression. *Biological psychiatry*. 2008;63:353-9.
- [17] Gregus A, Wintink AJ, Davis AC, Kalynchuk LE. Effect of repeated corticosterone injections and restraint stress on anxiety and depression-like behavior in male rats. *Behavioural brain research*. 2005;156:105-14.
- [18] Johnson SA, Fournier NM, Kalynchuk LE. Effect of different doses of corticosterone on depression-like behavior and HPA axis responses to a novel stressor. *Behavioural brain research*. 2006;168:280-8.
- [19] Kalynchuk LE, Gregus A, Boudreau D, Perrot-Sinal TS. Corticosterone increases depression-like behavior, with some effects on predator odor-induced defensive behavior, in male and female rats. *Behavioral neuroscience*. 2004;118:1365-77.
- [20] Murray F, Smith DW, Hutson PH. Chronic low dose corticosterone exposure decreased hippocampal cell proliferation, volume and induced anxiety and depression like behaviours in mice. *European journal of pharmacology*. 2008;583:115-27.
- [21] Zhao Y, Ma R, Shen J, Su H, Xing D, Du L. A mouse model of depression induced by repeated corticosterone injections. *European journal of pharmacology*. 2008;581:113-20.

- [22] Detke MJ, Johnson J, Lucki I. Acute and chronic antidepressant drug treatment in the rat forced swimming test model of depression. *Experimental and clinical psychopharmacology*. 1997;5:107-12.
- [23] Dulawa SC, Holick KA, Gundersen B, Hen R. Effects of chronic fluoxetine in animal models of anxiety and depression. *Neuropsychopharmacology : official publication of the American College of Neuropsychopharmacology*. 2004;29:1321-30.
- [24] Duman RS, Aghajanian GK. Synaptic dysfunction in depression: potential therapeutic targets. *Science*. 2012;338:68-72.
- [25] Eisch AJ, Petrik D. Depression and hippocampal neurogenesis: a road to remission? *Science*. 2012;338:72-5.
- [26] Fitzgerald PB, Laird AR, Maller J, Daskalakis ZJ. A meta-analytic study of changes in brain activation in depression. *Human brain mapping*. 2008;29:683-95.
- [27] Kempton MJ, Salvador Z, Munafo MR, Geddes JR, Simmons A, Frangou S, et al. Structural neuroimaging studies in major depressive disorder. Meta-analysis and comparison with bipolar disorder. *Archives of general psychiatry*. 2011;68:675-90.
- [28] Koolschijn PC, van Haren NE, Lensvelt-Mulders GJ, Hulshoff Pol HE, Kahn RS. Brain volume abnormalities in major depressive disorder: a meta-analysis of magnetic resonance imaging studies. *Human brain mapping*. 2009;30:3719-35.

- [29] Yang M, Kim J, Kim JS, Kim SH, Kim JC, Kang MJ, et al. Hippocampal dysfunctions in tumor-bearing mice. *Brain, behavior, and immunity*. 2014;36:147-55.
- [30] Dexter DL, Kowalski HM, Blazar BA, Fligiel Z, Vogel R, Heppner GH. Heterogeneity of tumor cells from a single mouse mammary tumor. *Cancer research*. 1978;38:3174-81.
- [31] Pulaski BA, Ostrand-Rosenberg S. Mouse 4T1 breast tumor model. *Current protocols in immunology / edited by John E Coligan [et al]*. 2001;Chapter 20:Unit 20.2.
- [32] Towell A, Muscat R, Willner P. Effects of pimozide on sucrose consumption and preference. *Psychopharmacology*. 1987;92:262-4.
- [33] Petit-Demouliere B, Chenu F, Bourin M. Forced swimming test in mice: a review of antidepressant activity. *Psychopharmacology*. 2005;177:245-55.
- [34] Franklin KBJ, Paxinos G. *The mouse brain in stereotaxic coordinates*. San Diego: Academic Press; 1997.
- [35] Cook SC, Wellman CL. Chronic stress alters dendritic morphology in rat medial prefrontal cortex. *Journal of neurobiology*. 2004;60:236-48.
- [36] Silva-Gómez A. Decreased dendritic spine density on prefrontal cortical and hippocampal pyramidal neurons in postweaning social isolation rats. *Brain research*. 2003;983:128-36.

[37] Longair MH, Baker DA, Armstrong JD. Simple Neurite Tracer: open source software for reconstruction, visualization and analysis of neuronal processes.

Bioinformatics (Oxford, England). 2011;27:2453-4.

[38] Gensel JC, Schonberg DL, Alexander JK, McTigue DM, Popovich PG.

Semi-automated Sholl analysis for quantifying changes in growth and differentiation of neurons and glia. Journal of neuroscience methods.

2010;190:71-9.

[39] Sholl DA. Dendritic organization in the neurons of the visual and motor cortices of the cat. Journal of anatomy. 1953;87:387-406.

[40] Ferreira TA, Blackman AV, Oyrer J, Jayabal S, Chung AJ, Watt AJ, et al.

Neuronal morphometry directly from bitmap images. Nature methods.

2014;11:982-4.

[41] Lein M, Jung K, Le DK, Hasan T, Ortel B, Borchert D, et al. Synthetic inhibitor of matrix metalloproteinases (batimastat) reduces prostate cancer growth in an orthotopic rat model. The Prostate. 2000;43:77-82.

[42] Tomayko MM, Reynolds CP. Determination of subcutaneous tumor size in athymic (nude) mice. Cancer chemotherapy and pharmacology. 1989;24:148-54.

[43] Jensen MM, Jorgensen JT, Binderup T, Kjaer A. Tumor volume in subcutaneous mouse xenografts measured by microCT is more accurate and reproducible than determined by ¹⁸F-FDG-microPET or external caliper. BMC medical imaging. 2008;8:16.

- [44] Montelius M, Ljungberg M, Horn M, Forssell-Aronsson E. Tumour size measurement in a mouse model using high resolution MRI. *BMC medical imaging*. 2012;12:12.
- [45] Massie MJ. Prevalence of depression in patients with cancer. *Journal of the National Cancer Institute Monographs*. 2004:57-71.
- [46] Mitchell AJ, Chan M, Bhatti H, Halton M, Grassi L, Johansen C, et al. Prevalence of depression, anxiety, and adjustment disorder in oncological, haematological, and palliative-care settings: a meta-analysis of 94 interview-based studies. *The Lancet Oncology*. 2011;12:160-74.
- [47] Brown KW, Levy AR, Rosberger Z, Edgar L. Psychological distress and cancer survival: a follow-up 10 years after diagnosis. *Psychosomatic medicine*. 2003;65:636-43.
- [48] Pinquart M, Duberstein PR. Depression and cancer mortality: a meta-analysis. *Psychological medicine*. 2010;40:1797-810.
- [49] Pirl WF, Greer JA, Traeger L, Jackson V, Lennes IT, Gallagher ER, et al. Depression and survival in metastatic non-small-cell lung cancer: effects of early palliative care. *Journal of clinical oncology : official journal of the American Society of Clinical Oncology*. 2012;30:1310-5.
- [50] Satin JR, Linden W, Phillips MJ. Depression as a predictor of disease progression and mortality in cancer patients: a meta-analysis. *Cancer*. 2009;115:5349-61.

- [51] Stommel M, Given BA, Given CW. Depression and functional status as predictors of death among cancer patients. *Cancer*. 2002;94:2719-27.
- [52] Brelin S, Loge JH, Skurtveit S, Johannesen TB, Aass N, Ottesen S, et al. Antidepressants to cancer patients during the last year of life--a population-based study. *Psycho-oncology*. 2013;22:506-14.
- [53] Ng CG, Boks MP, Zainal NZ, de Wit NJ. The prevalence and pharmacotherapy of depression in cancer patients. *Journal of affective disorders*. 2011;131:1-7.
- [54] Rodin G, Lloyd N, Katz M, Green E, Mackay JA, Wong RK, et al. The treatment of depression in cancer patients: a systematic review. *Supportive care in cancer : official journal of the Multinational Association of Supportive Care in Cancer*. 2007;15:123-36.
- [55] Williams S, Dale J. The effectiveness of treatment for depression/depressive symptoms in adults with cancer: a systematic review. *British journal of cancer*. 2006;94:372-90.
- [56] Lamkin DM, Lutgendorf SK, Lubaroff D, Sood AK, Beltz TG, Johnson AK. Cancer induces inflammation and depressive-like behavior in the mouse: modulation by social housing. *Brain, behavior, and immunity*. 2011;25:555-64.
- [57] Norden DM, Bicer S, Clark Y, Jing R, Henry CJ, Wold LE, et al. Tumor growth increases neuroinflammation, fatigue and depressive-like behavior prior to alterations in muscle function. *Brain, behavior, and immunity*. 2015;43:76-85.

- [58] Pyter LM, Pineros V, Galang JA, McClintock MK, Prendergast BJ. Peripheral tumors induce depressive-like behaviors and cytokine production and alter hypothalamic-pituitary-adrenal axis regulation. *Proceedings of the National Academy of Sciences of the United States of America*. 2009;106:9069-74.
- [59] Gourley SL, Kiraly DD, Howell JL, Olausson P, Taylor JR. Acute hippocampal brain-derived neurotrophic factor restores motivational and forced swim performance after corticosterone. *Biological psychiatry*. 2008;64:884-90.
- [60] Ardayfio P, Kim KS. Anxiogenic-like effect of chronic corticosterone in the light-dark emergence task in mice. *Behavioral neuroscience*. 2006;120:249-56.
- [61] Lam RW. Onset, time course and trajectories of improvement with antidepressants. *European neuropsychopharmacology : the journal of the European College of Neuropsychopharmacology*. 2012;22 Suppl 3:S492-8.
- [62] Pariante CM, Kim RB, Makoff A, Kerwin RW. Antidepressant fluoxetine enhances glucocorticoid receptor function in vitro by modulating membrane steroid transporters. *British journal of pharmacology*. 2003;139:1111-8.
- [63] Weber CC, Eckert GP, Muller WE. Effects of antidepressants on the brain/plasma distribution of corticosterone. *Neuropsychopharmacology : official publication of the American College of Neuropsychopharmacology*. 2006;31:2443-8.
- [64] Howland RH. Sequenced Treatment Alternatives to Relieve Depression (STAR*D). Part 2: Study outcomes. *Journal of psychosocial nursing and mental health services*. 2008;46:21-4.

- [65] Fournier JC, DeRubeis RJ, Hollon SD, Dimidjian S, Amsterdam JD, Shelton RC, et al. Antidepressant drug effects and depression severity: a patient-level meta-analysis. *JAMA : the journal of the American Medical Association*. 2010;303:47-53.
- [66] Sanchez C, Meier E. Behavioral profiles of SSRIs in animal models of depression, anxiety and aggression. Are they all alike? *Psychopharmacology*. 1997;129:197-205.
- [67] Cryan JF, Mombereau C, Vassout A. The tail suspension test as a model for assessing antidepressant activity: review of pharmacological and genetic studies in mice. *Neuroscience and biobehavioral reviews*. 2005;29:571-625.
- [68] Yan HC, Cao X, Das M, Zhu XH, Gao TM. Behavioral animal models of depression. *Neuroscience bulletin*. 2010;26:327-37.
- [69] Xu Z, Zhang Y, Hou B, Gao Y, Wu Y, Zhang C. Chronic corticosterone administration from adolescence through early adulthood attenuates depression-like behaviors in mice. *Journal of affective disorders*. 2011;131:128-35.
- [70] Chatterjee M, Jaiswal M, Palit G. Comparative evaluation of forced swim test and tail suspension test as models of negative symptom of schizophrenia in rodents. *ISRN psychiatry*. 2012;2012:595141.
- [71] Hasler G. Pathophysiology of depression: do we have any solid evidence of interest to clinicians? *World psychiatry : official journal of the World Psychiatric Association (WPA)*. 2010;9:155-61.

- [72] Nestler EJ, Gould E, Manji H, Buncan M, Duman RS, Greshenfeld HK, et al. Preclinical models: status of basic research in depression. *Biological psychiatry*. 2002;52:503-28.
- [73] Sheline YI, Gado MH, Kraemer HC. Untreated depression and hippocampal volume loss. *The American journal of psychiatry*. 2003;160:1516-8.
- [74] Gibb R, Kolb B. A method for vibratome sectioning of Golgi-Cox stained whole rat brain. *Journal of neuroscience methods*. 1998;79:1-4.
- [75] Alfarez DN, Karst H, Velzing EH, Joels M, Krugers HJ. Opposite effects of glucocorticoid receptor activation on hippocampal CA1 dendritic complexity in chronically stressed and handled animals. *Hippocampus*. 2008;18:20-8.
- [76] Magarinos AM, McEwen BS. Stress-induced atrophy of apical dendrites of hippocampal CA3c neurons: involvement of glucocorticoid secretion and excitatory amino acid receptors. *Neuroscience*. 1995;69:89-98.
- [77] Magarinos AM, McEwen BS, Flugge G, Fuchs E. Chronic psychosocial stress causes apical dendritic atrophy of hippocampal CA3 pyramidal neurons in subordinate tree shrews. *The Journal of neuroscience : the official journal of the Society for Neuroscience*. 1996;16:3534-40.
- [78] Watanabe Y, Gould E, McEwen BS. Stress induces atrophy of apical dendrites of hippocampal CA3 pyramidal neurons. *Brain research*. 1992;588:341-5.

[79] Woolley CS, Gould E, McEwen BS. Exposure to excess glucocorticoids alters dendritic morphology of adult hippocampal pyramidal neurons. *Brain research*. 1990;531:225-31.

[80] Gourley SL, Swanson AM, Koleske AJ. Corticosteroid-induced neural remodeling predicts behavioral vulnerability and resilience. *The Journal of neuroscience : the official journal of the Society for Neuroscience*. 2013;33:3107-12.

Tables & Figures

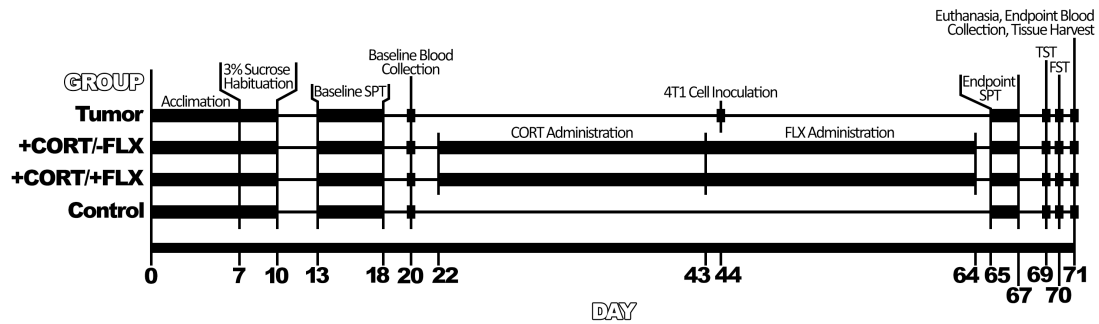


Figure 1. Timeline of the experiment. Day 0 represents the day of animal arrival.

Procedures for each of the 4 groups are listed along the timeline at the days that they were performed. (SPT, sucrose preference test; TST, tail suspension test; FST, forced swim test; CORT, corticosterone; FLX, fluoxetine).

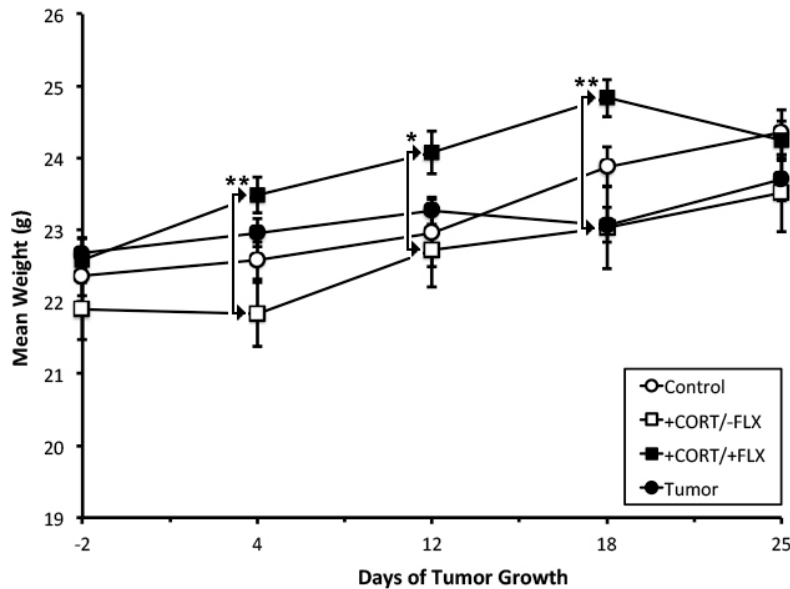


Figure 2. Mean body weight of mice in the 4 experimental groups. Data are presented for the duration of tumor growth. Mice that were administered corticosterone alone (+CORT/-FLX; $n = 12$) weight less than mice that were administered fluoxetine following CORT treatment (+CORT/+FLX; $n = 12$) at day 4 ($P = 0.005$), day 12 ($P = 0.032$), and day 18 ($P = 0.002$). There was a trend toward decreased weight for +CORT/-FLX mice and increased weight for +CORT/+FLX mice compared to control mice ($n = 12$). There was also a trend toward decreased weight for mice that were inoculated with 4T1 mammary carcinoma cells (tumor; $n = 13$) compared to control mice after 12 days of tumor growth (corrected for tumor mass). Data are expressed as mean \pm SEM. Two-way repeated-measures ANOVA with Tukey's post hoc test for multiple comparisons were used to analyze group differences over time (* $P < 0.05$, ** $P < 0.01$).

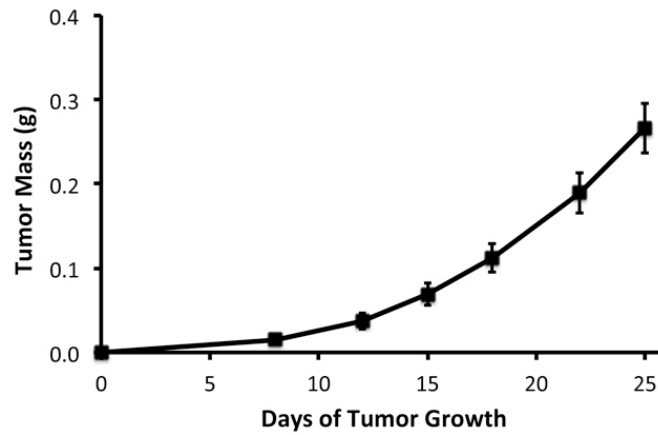


Figure 3. Tumor growth in mice subcutaneously inoculated with 15,000 4T1 mammary carcinoma cells (n = 13). Tumor growth pattern was exponential and tumor mass reached an average of 0.27 ± 0.03 g by day 25 of tumor growth. Data are expressed as mean \pm SEM.

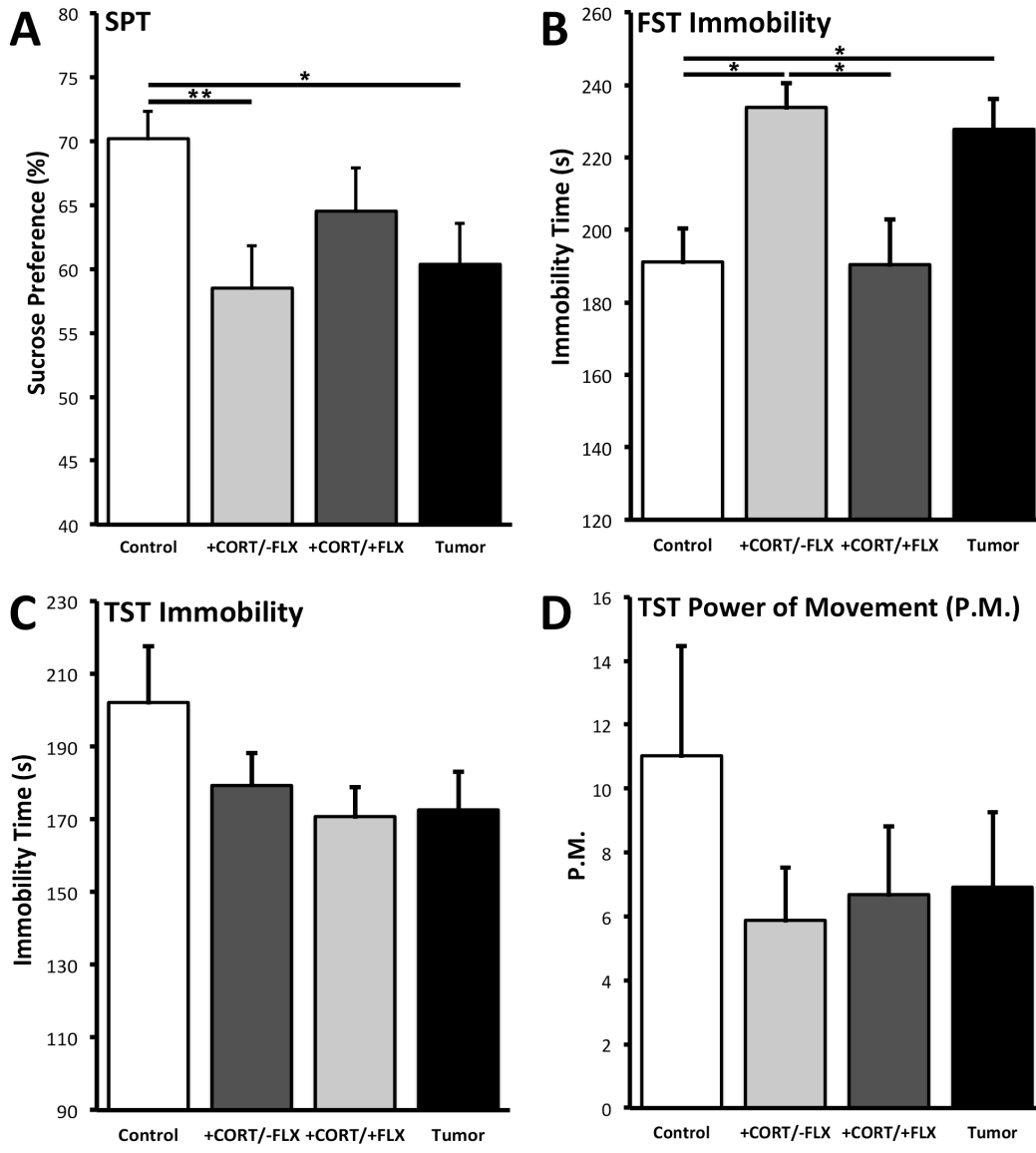


Figure 4. Behavioural results for the 4 experimental groups: control (n = 12), corticosterone treatment (+CORT/-FLX; n = 12), CORT treatment followed by fluoxetine treatment (+CORT/+FLX; n = 12), and 4T1 mammary carcinoma cell inoculation (tumor; n = 13). (A) In the sucrose preference test (SPT) preference is calculated as $(\text{sucrose water consumption}/\text{total fluid intake}) \times 100$, where 50% represents equal consumption of sucrose water and regular water. CORT

treatment was associated with reduced preference for sucrose solution compared to control ($P = 0.008$). FLX-treatment partially recovered sucrose preference, but not to statistical significance (compared to control, $P = 0.55$; compared to +CORT/-FLX, $P = 0.41$). Tumor burden was associated with decreased sucrose preference ($P = 0.035$) and did not differ from CORT-treated mice ($P > 0.99$). (B) In the forced swim test (FST) CORT treatment was associated with increased immobility time ($P = 0.013$), which was reversed by FLX treatment ($P = 0.011$). Tumor burden was associated with increased immobility compared to control ($P = 0.039$), and did not differ from CORT-treated mice ($P > 0.99$). In the tail suspension test (TST), no significant differences were observed in immobility (C) or power of movement (P.M.) (D). However, CORT-treated mice displayed a trend towards decreased P.M., which did not appear to be affected by FLX treatment. Tumor-bearing mice also displayed a trend towards decreased P.M. compared to control mice. Data are presented as mean \pm SEM. One-way ANOVA with Bonferroni's correction for multiple comparisons were used to analyze group differences (* $P < 0.05$, ** $P < 0.01$).

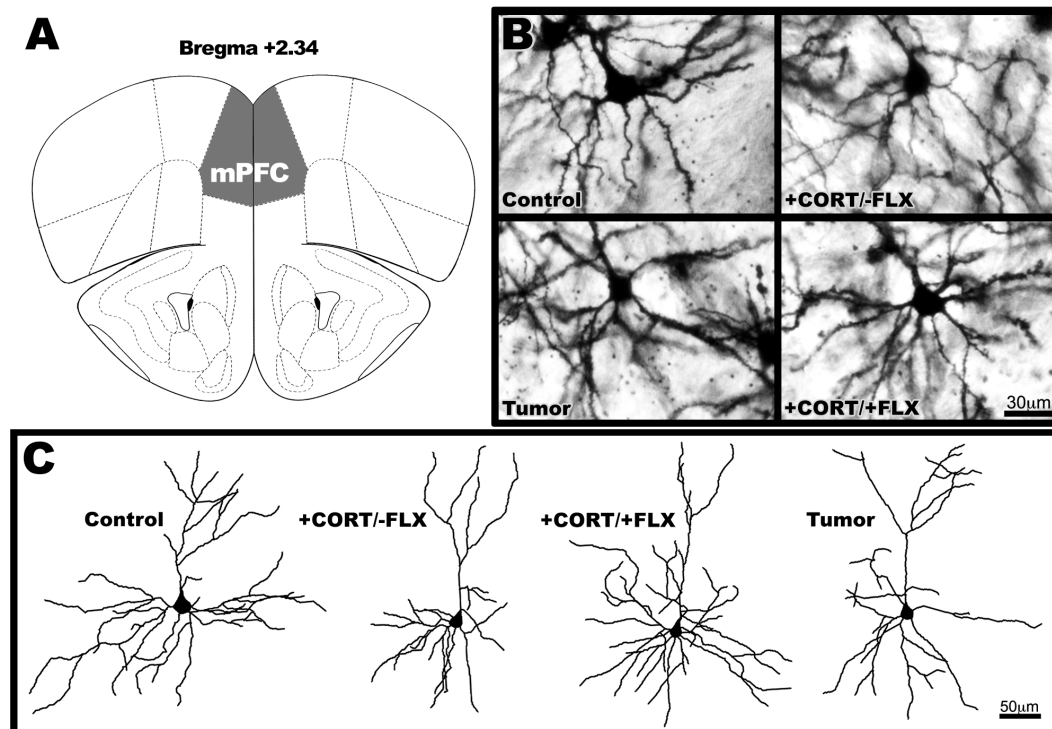


Figure 5. (A) A coronal section schematic highlighting the medial prefrontal cortex (mPFC) in a mouse brain (adapted from Franklin [34]). (B) Golgi-Cox impregnated layer II-III pyramidal neurons from the mPFC under light microscopy on a single z-plane axis. A representative neuron is shown for each of the 4 experimental groups: control, corticosterone treatment (+CORT/-FLX), CORT treatment followed by fluoxetine treatment (+CORT/+FLX), and 4T1 mammary carcinoma cell inoculation (tumor). (C) Digital reconstructions of the representative neurons in panel B.

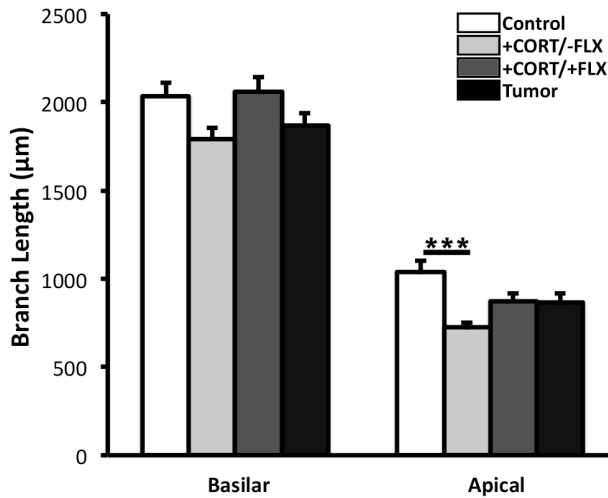


Figure 6. Basilar and apical branch length for the 4 experimental groups: control (n = 8), corticosterone treatment (+CORT/-FLX; n = 8), CORT treatment followed by fluoxetine treatment

(+CORT/+FLX; n = 8), and 4T1 mammary carcinoma cell inoculation (tumor; n = 8). There was a non-significant trend toward lower mean basilar branch length in CORT-treated mice compared to control mice ($P = 0.13$). FLX treatment was associated with increased basilar branch length compared to CORT-only mice, which approached significance ($P = 0.072$). There was a non-significant trend toward lower mean basilar branch length in tumor-bearing mice compared to control mice ($P = 0.58$), and was also not different compared to CORT-treated mice ($P > 0.99$). CORT treatment reduced apical branch length ($P < 0.001$). This reduction was partially reversed with FLX treatment, though not to statistical significance (compared to control, $P = 0.10$; compared to +CORT/-FLX, $P = 0.17$). Tumor burden was associated with decreased apical branch length, which approached significance ($P = 0.073$), and was not different compared to CORT-treated mice ($P = 0.23$). Data are presented as mean \pm SEM. One-way ANOVA with Bonferroni's correction for multiple comparisons were used to analyze group differences (***) $P < 0.001$).

Table 1

Details of Sholl analyses comparing number of intersections between groups. Data have been summed into 20 μm bins and presented as means \pm SEM.

| Distance from soma (μm) | Control | | +CORT/-FLX | | +CORT/+FLX | | Tumor | | Sig. |
|--------------------------------------|---------------|------|---------------|------|---------------|------|---------------|------|----------------|
| | Intersections | SEM | Intersections | SEM | Intersections | SEM | Intersections | SEM | |
| Basilar Dendrite | | | | | | | | | |
| 10 – 20 | 17.90 | 0.55 | 17.73 | 1.07 | 17.81 | 0.40 | 15.64 | 1.08 | n.s. |
| 30 – 40 | 28.74 | 0.68 | 25.40 | 1.12 | 27.61 | 0.78 | 23.30 | 1.20 | <i>a, d</i> |
| 50 – 60 | 30.24 | 0.94 | 27.28 | 1.02 | 28.15 | 1.06 | 24.24 | 1.28 | <i>d</i> |
| 70 – 80 | 26.06 | 1.15 | 22.95 | 1.06 | 25.64 | 1.14 | 22.97 | 1.19 | n.s. |
| 90 – 100 | 20.33 | 1.08 | 17.30 | 1.28 | 20.88 | 1.01 | 18.63 | 1.49 | <i>c</i> |
| 110 – 120 | 13.93 | 0.94 | 11.48 | 1.17 | 15.43 | 0.99 | 13.78 | 1.17 | <i>c</i> |
| 130 – 140 | 8.21 | 0.75 | 6.93 | 1.01 | 10.13 | 0.86 | 9.85 | 1.39 | n.s. |
| 150 – 160 | 4.67 | 0.52 | 3.79 | 0.77 | 5.68 | 0.68 | 5.90 | 1.04 | n.s. |
| 170 – 180 | 2.21 | 0.32 | 1.73 | 0.36 | 2.68 | 0.62 | 3.44 | 0.97 | n.s. |
| 190 – 200 | 0.91 | 0.13 | 0.60 | 0.18 | 1.01 | 0.35 | 1.78 | 0.61 | n.s. |
| > 200 | 0.83 | 0.26 | 0.12 | 0.06 | 0.96 | 0.48 | 1.18 | 0.48 | n.s. |
| Apical Dendrite | | | | | | | | | |
| 10 – 20 | 2.40 | 0.15 | 2.41 | 0.08 | 2.38 | 0.09 | 2.72 | 0.19 | n.s. |
| 30 – 40 | 4.63 | 0.26 | 5.06 | 0.45 | 4.85 | 0.29 | 5.30 | 0.64 | n.s. |
| 50 – 60 | 6.42 | 0.34 | 6.32 | 0.35 | 6.04 | 0.47 | 6.35 | 0.69 | n.s. |
| 70 – 80 | 7.32 | 0.58 | 6.60 | 0.40 | 6.60 | 0.36 | 6.50 | 0.80 | n.s. |
| 90 – 100 | 8.14 | 0.57 | 6.28 | 0.45 | 7.07 | 0.56 | 6.45 | 0.67 | <i>a</i> |
| 110 – 120 | 8.11 | 0.70 | 5.31 | 0.35 | 6.63 | 0.41 | 6.02 | 0.53 | <i>a, d</i> |
| 130 – 140 | 8.04 | 0.79 | 4.67 | 0.31 | 6.36 | 0.37 | 5.59 | 0.27 | <i>a, d</i> |
| 150 – 160 | 7.56 | 0.99 | 4.11 | 0.31 | 5.85 | 0.26 | 5.08 | 0.36 | <i>a, c, d</i> |
| 170 – 180 | 6.51 | 0.91 | 3.58 | 0.26 | 4.68 | 0.38 | 4.51 | 0.59 | <i>a, b, d</i> |
| 190 – 200 | 5.48 | 0.96 | 2.90 | 0.13 | 3.90 | 0.46 | 3.85 | 0.62 | <i>a</i> |
| 210 – 220 | 4.43 | 0.72 | 2.43 | 0.18 | 3.23 | 0.51 | 3.39 | 0.62 | <i>a</i> |
| 230 – 240 | 3.66 | 0.64 | 1.75 | 0.11 | 2.29 | 0.53 | 2.80 | 0.76 | <i>a</i> |
| 250 – 260 | 2.49 | 0.51 | 1.29 | 0.18 | 1.69 | 0.53 | 2.24 | 0.66 | n.s. |
| 270 – 280 | 1.50 | 0.22 | 0.90 | 0.22 | 1.34 | 0.46 | 1.48 | 0.43 | n.s. |
| 290 – 300 | 0.99 | 0.14 | 0.64 | 0.20 | 1.05 | 0.45 | 1.14 | 0.36 | n.s. |
| 310 – 320 | 0.52 | 0.16 | 0.36 | 0.16 | 0.80 | 0.40 | 0.82 | 0.33 | n.s. |
| 330 – 340 | 0.32 | 0.13 | 0.09 | 0.06 | 0.51 | 0.38 | 0.63 | 0.31 | n.s. |
| > 350 | 0.39 | 0.28 | 0.08 | 0.08 | 1.04 | 0.82 | 0.56 | 0.36 | n.s. |

Two-way repeated-measures ANOVAs (group \times distance from soma) with

Tukey's post hoc test for multiple comparisons were used to analyze group

differences.

a Denotes significant difference between +CORT/–FLX and control.

b Denotes significant difference between +CORT/+FLX and control.

c Denotes significant difference between +CORT/–FLX and +CORT/+FLX.

d Denotes significant difference between tumor and control.

n.s. Denotes no significant differences between any group.

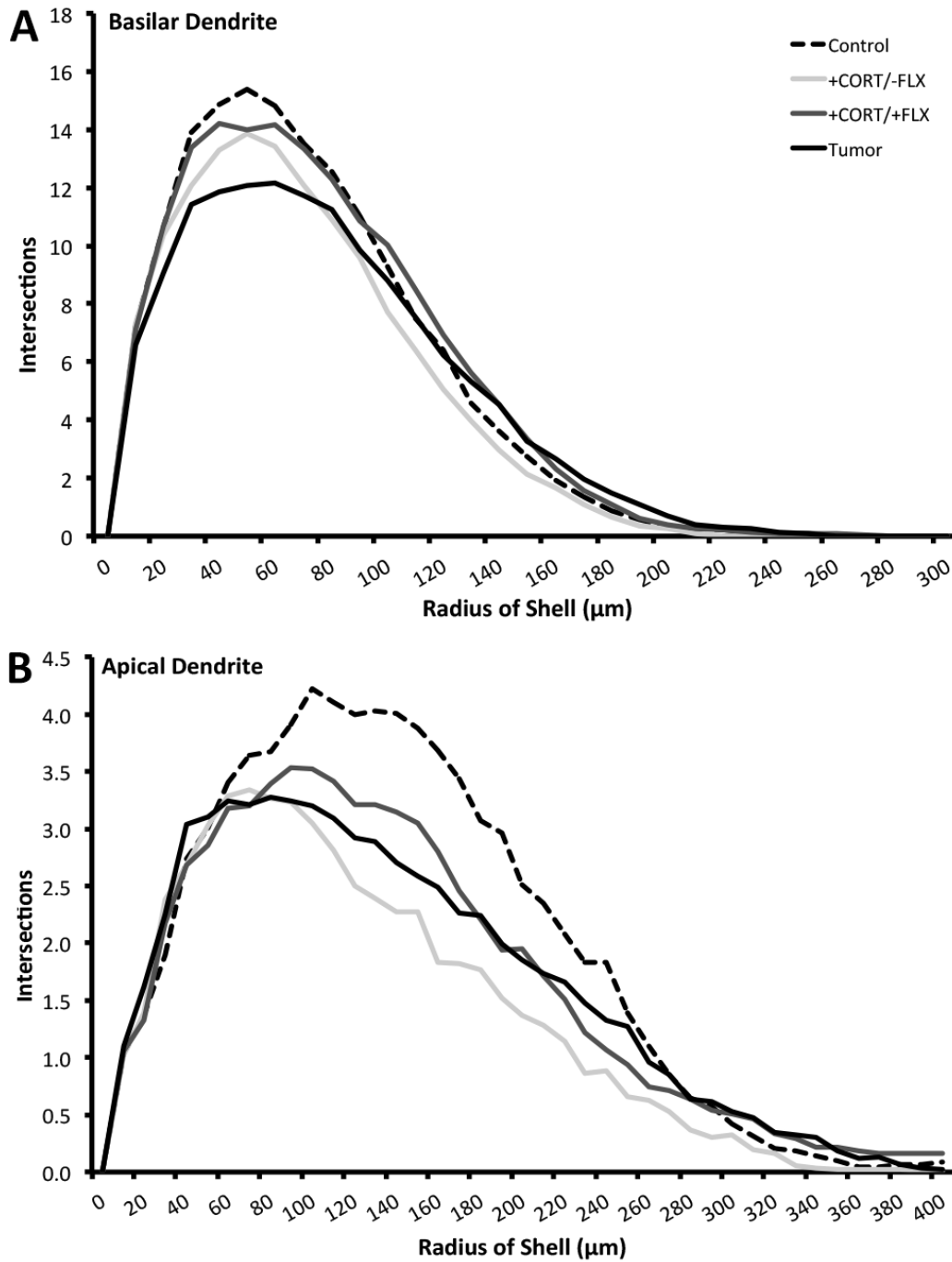


Figure 7. Sholl analyses of (A) basilar and (B) apical dendrites with 10 μm spaced concentric rings for the 4 experimental groups: control (n = 8), corticosterone treatment (+CORT/-FLX; n = 8), CORT treatment followed by

fluoxetine treatment (+CORT/+FLX; n = 8), and 4T1 mammary carcinoma cell inoculation (tumor; n = 8). Intersections of dendrites with rings denote the extent of dendritic branching. Basilar and apical branching was reduced by CORT-treatment, and partially recovered by FLX. Tumor burden was associated with reduced basilar and apical branching compared to control. Data are presented as mean number of intersections for each group at every 10 μm interval.

Table 2

Endpoint serum levels of corticosterone (CORT) for: control, corticosterone treatment (+CORT/-FLX), and CORT treatment followed by fluoxetine treatment (+CORT/+FLX).

| Group | % of baseline serum [CORT] |
|------------|----------------------------|
| Control | 104.8 |
| +CORT/-FLX | 180.1 |
| +CORT/+FLX | 159.5 |

Baseline and endpoint serum CORT was pooled by group and time point, then measured using an enzyme-linked immunosorbent assay (ELISA), which was run in triplicate. Data are expressed as a percentage of baseline levels $[(\text{endpoint [CORT]}/\text{baseline [CORT]}) \times 100]$. Treatment with CORT was associated with elevated serum CORT. FLX-treated mice had elevated serum CORT, although it was slightly less elevated than in CORT-only mice.

Table 3

Summary of results for behavioural and dendritic analyses.

| Test | Comparison | | | |
|----------------------------|-------------------|-------------------|-------------------|--------------|
| | Control | Control | +CORT/-FLX | Control |
| | vs. +CORT/-FLX | vs. +CORT/+FLX | vs. +CORT/+FLX | vs. Tumor |
| SPT | + | ~ | ~ | + |
| FST | + | - | + | + |
| TST (immobility) | - | - | - | - |
| TST (P.M.) | ~ | ~ | - | ~ |
| Branch Length (basilar) | ~ | - | ~ | ~ |
| Branch Length (apical) | + | ~ | ~ | ~ |
| Sholl (basilar) | + | - | + | + |
| Sholl (apical) | + | + | + | + |

+ denotes statistically significant differences between groups. - denotes no statistical differences between groups. ~ denotes trends towards group differences that were not statistically significant (SPT, sucrose preference test; TST, tail suspension test; FST, forced swim test; CORT, corticosterone; FLX, fluoxetine).

CHAPTER 3

Inhibiting glutamate release with sulfasalazine in a mouse model of cancer-induced depression

Mina G. Nashed, Robert G. Ungard, Kimberly Young, Natalie J. Zacal, Eric P.

Seidlitz, Jennifer Fazzari, Benicio N. Frey, Gurmit Singh

Submitted to: *Neuropsychopharmacology*

Preface

In this chapter, an author-generated version of the manuscript entitled “Inhibiting glutamate release with sulfasalazine in a mouse model of cancer-induced depression”, prepared for submission January 2016 to *Neuropsychopharmacology*, is presented. This manuscript was under revision for re-submission to NPP at the time of dissertation completion. The submission number is NPP-16-0097. As this is a manuscript in submission, no copyright license documentation is required.

For this paper, I performed the cell culturing and treatment, ^{14}C -cystine uptake assay, behavioural assays, animal drug treatments, cancer cell inoculations, brain tissue processing, clonogenic assay, and data analysis. Furthermore, I created all of the figures, tables, and both wrote and revised the manuscript. Robert Ungard, Natalie Zacal, and Dr. Eric Seidlitz performed tissue harvest and blood collection, and revised the manuscript. Kimberly Young performed blood sample processing, aided in the behavioural assays, and revised the manuscript. Jennifer Fazzari performed the serum glutamate assay, and I performed the relevant analysis of this data. Serum samples were sent to Eve Technologies (Calgary, AB, Canada) for cytokine quantification. Dr. Benicio Frey and Dr. Gurmit Singh provided intellectual direction and revised the manuscript. Please note that American spellings are used throughout the article, as required by the journal.

Context and Background Information

In Chapter 1, I discussed the oncodynamic effect of cancer on the development on depression and presented several plausible mechanisms, including glutamatergic dysregulation by cancer cells. In Chapter 2, a manuscript was presented that established a validated mouse model of cancer-induced depression (CID). In the present chapter, a study was conducted to investigate whether pharmacologically inhibiting glutamate secretion at the tumour site is a viable antidepressant strategy for CID.

As previously discussed, glutamate is becoming increasingly recognized for its role in the pathophysiology of depression. We have also previously shown that multiple breast and prostate cancer cell lines secrete large amounts of glutamate through the glutamate/cystine antiporter system x_c^- (Seidlitz, Sharma, Saikali, Ghert, & Singh, 2009; Sharma, Seidlitz, & Singh, 2010). In the present chapter, I extend these findings to show that murine 4T1 mammary carcinoma cells, which are used in the CID model, also release large amounts of glutamate. Furthermore, 4T1 glutamate release is significantly attenuated by sulfasalazine (SSZ), a system x_c^- inhibitor.

Using the CID model and the same behavioural assays presented in Chapter 2, drug treatments were tested. Treatments with the antidepressant fluoxetine (FLX) and the system x_c^- inhibitor SSZ prevented anhedonic and despair behaviours in tumour-bearing mice. SSZ is predominantly cleaved into 5-aminosalicylic acid (5-ASA) and sulfapyridine (SP) in the gut. Since 5-ASA is a

known anti-inflammatory drug and depression may involve an inflammatory component, the SSZ metabolites were also investigated. Treatment with 5-ASA/SP prevented the development of anhedonic, but not despair, behaviours. Cytokine analysis revealed that neither SSZ nor 5-ASA/SP were effective at preventing interleukin 1 β (IL-1 β) and IL-6 elevation in CID mice. Therefore, it is likely that the observed antidepressant effect of SSZ is predominantly due to the intact form of the drug inhibiting system x_c^- . Further investigations will better characterize the antidepressant mechanism of SSZ and system x_c^- inhibition.

There is evidence to suggest that pro-inflammatory cytokines, which are commonly elevated in both cancer and depression, contribute to the weakening of the blood-brain barrier (BBB) (Rochfort & Cummins, 2015; Wang et al., 2014). The analysis in this chapter focuses on cytokines that are known to be involved in depression, and reveals elevated levels of IL-6 and possibly IL-1 β in tumour-bearing mice. These data provide a plausible mechanism of BBB weakening in cancer, which may contribute to bidirectional glutamate transport across the BBB. Further studies are warranted to investigate this possibility as discussed in the “Future Directions” section of Chapter 5.

**Behavioral Effects of Inhibiting Glutamate Released by Cancer
Cells using Sulfasalazine in a Mouse Model of Cancer-Induced
Depression**

^{1,2}Mina G. Nashed, M.Sc.; ^{1,2}Robert G. Ungard, M.Sc.; ^{1,2}Kimberly Young,
B.H.Sc.; ^{1,2}Natalie J. Zacal, M.Sc.; ^{1,2}Eric P. Seidlitz, M.Sc., Ph.D.; ^{1,2}Jennifer
Fazzari, B.Sc.; ^{3,4}Benicio N. Frey, M.D., M.Sc., Ph.D.; ^{1,2}Gurmit Singh, Ph.D.*

¹*Department of Pathology & Molecular Medicine, McMaster University, Hamilton, ON, Canada*

²*Michael G. DeGroot Institute for Pain Research and Care, McMaster University, Hamilton, ON, Canada.*

³*Department of Psychiatry and Behavioural Neurosciences, McMaster University, Hamilton, ON, L8N 3K7, Canada.*

⁴*Mood Disorders Program and Women's Health Concerns Clinic, St. Joseph's Healthcare Hamilton, ON, L8P 3K7,
Canada.*

Running Title: Glutamate Modulation in Cancer-Induced Depression

*** Corresponding author.**

Address: Department of Pathology & Molecular Medicine, McMaster University, 1280 Main
Street West, Hamilton, ON L8N 3Z5, Canada.

Tel.: +1 905 525 9140x28144.

E-mail address: singhg@mcmaster.ca

URL: <http://www.singhlab.ca>

Abstract

Despite the lack of robust evidence of effectiveness, current treatment options for cancer-induced depression (CID) are limited to those developed for non-cancer related depression. We have recently developed a mouse model to investigate the pathophysiology of CID and explore novel targets for therapy. Similar to other cancer cell lines, we demonstrated that murine 4T1 mammary carcinoma cells release large amounts of glutamate through the glutamate-cystine antiporter system x_c^- . Using female BALB/c mice subcutaneously inoculated with 4T1 mammary carcinoma cells, we investigated the antidepressant-like efficacy of sulfasalazine (SSZ), a system x_c^- inhibitor. Overall, SSZ was at least as effective as fluoxetine at preventing the development of cancer-induced anhedonia and behavioral despair. The same robust effect was not observed with the metabolites of SSZ, 5-aminosalicylic acid (5-ASA) and sulfapyridine (SP). Although 5-ASA is a known anti-inflammatory agent, neither treatment with SSZ nor 5-ASA/SP prevented tumor-induced increases in serum levels of interleukin-1 β (IL-1 β) and IL-6, which are known to be increased in depressive disorders. This demonstrates that the observed antidepressant-like effect of SSZ was primarily attributable to the intact form of the drug, which inhibits system x_c^- , rather than an anti-inflammatory mediated decrease in depressive behaviors. This study represents the first attempt at targeting cancer cells to alleviate CID, rather than targeting the downstream impact of tumor burden on the central nervous system. In doing so,

we have also begun to characterize the mechanism of CID, which appears to involve excess release of glutamate by cancer cells.

Introduction

Depression is commonly reported by cancer patients (Mitchell *et al*, 2011), and increases mortality in this population (Pinquart and Duberstein, 2010).

Accordingly, the effective management of depression is essential to improving both quality of life and survivorship in cancer patients. Although late-stage cancer patients are far more likely than the general population to be prescribed an antidepressant (Brelvi *et al*, 2013), a recent meta-analysis did not find a significant difference in efficacy between antidepressants and placebo in treating cancer patients with depression symptoms (Ostuzzi *et al*, 2015). This study, in addition to previous systematic reviews, emphasizes the scarcity of high quality evidence for the effect of antidepressants in cancer-induced depression (CID) (Ng *et al*, 2011; Ostuzzi *et al*, 2015; Rodin *et al*, 2007; Williams and Dale, 2006).

To investigate the underlying pathophysiology of CID and to explore novel targeted therapies, we have recently developed a validated mouse model of CID (Nashed *et al*, 2015). In this model, BALB/c mice that were subcutaneously inoculated with 4T1 mammary carcinoma cells exhibited similar behavioral and neurostructural deficits to those associated with a chronic stress-induced depressive-like state.

Glutamate dysregulation has been strongly linked to depressive disorders. For instance, glutamate is elevated in the plasma of patients with MDD (Mitani *et al*, 2006), and magnetic resonance spectroscopy (MRS) studies have revealed a

decreased glutamate/glutamine (Glx) and glutamate (Glu) signals in brain regions that are relevant to depression, such as the prefrontal cortex and anterior cingulate cortex (Auer *et al*, 2000; Hasler *et al*, 2007). Moreover, ketamine, a glutamate receptor antagonist, has a rapid antidepressant effect in treatment-resistant patients and preclinical models of depression (Li *et al*, 2010; Murrugh, 2012; Zarate *et al*, 2006).

Although the underlying biological basis of CID is not yet established, evidence suggests that glutamate signaling may be involved. Glutamate released by the glutamate/cystine antiporter system x_c^- from glioma cells is sufficient to directly induce excitotoxic cell death through chronic glutamate receptor activation of nearby neurons (de Groot and Sontheimer, 2011). We have previously reported that multiple breast and prostate cancer cell lines secrete significant amounts of glutamate into the extracellular environment through system x_c^- (Seidlitz *et al*, 2009; Sharma *et al*, 2010). Although peripheral glutamate does not cross the blood-brain barrier (BBB) under normal conditions (Smith, 2000), pathological conditions may increase BBB permeability and allow for bidirectional glutamate transport. For example, breast cancer cells have been shown to release high levels of substance P (Reddy *et al*, 2009) and cytokines, including IL-1 β , IL-6, IL-17A, and TNF- α (Esquivel-Velazquez *et al*, 2015). Both substance P (Rodriguez *et al*, 2014) and cytokines that are associated with depression and cancer have been shown to disrupt BBB integrity (Huppert *et al*, 2010; Patel and Frey, 2015; Rochfort and Cummins, 2015; Wang *et al*, 2014). Intravenous administration of

glutamate decelerates the elimination of glutamate in the brain parenchyma (Teichberg *et al*, 2009). Therefore, irrespective of BBB integrity, excess peripheral glutamate may also cause an accumulation of glutamate in the brain through decreased brain-to-blood glutamate efflux. Therefore, it is plausible that inhibiting glutamate release by peripheral cancer cells would impact CNS glutamate regulation and produce an antidepressant effect.

Recently, it was shown that adult mice deficient in system x_c^- exhibited reduced anxiety- and depressive-like behaviors (Bentea *et al*, 2015), which further supports the role of glutamatergic dysregulation in depression, and identify system x_c^- as a potential therapeutic target. In the present study, we hypothesize that chronic pharmacological inhibition of peripheral cancer cell system x_c^- through oral sulfasalazine (SSZ) treatment will prevent depressive-like behaviors in our CID model. To test our hypothesis, we used fluoxetine (FLX) treatment to establish a positive control group of treated CID. Although only intact SSZ inhibits system x_c^- , orally ingested SSZ is predominantly cleaved into 5-aminosalicylic acid (5-ASA) and sulfapyridine (SP) in the gut (National Center for Biotechnology Information, 2005; Sontheimer and Bridges, 2012). 5-ASA is a known anti-inflammatory drug (Kruis *et al*, 2001), and may therefore independently impact depressive behaviors. To clarify the mechanism of any observed antidepressant-like effects of SSZ, a comparison with the effects of its metabolites, 5-ASA and SP, was included. Additionally, we quantified serum

levels of IL-1 β , IL-6, IL-17A, and TNF- α to provide further insight into the anti-inflammatory impact of chronic treatment with SSZ and its metabolites.

Materials and Methods

Cell culture

4T1 murine mammary carcinoma cells (American Type Culture Collection, Manassas, VA, USA) and TM40A murine non-tumorigenic mammary epithelial cells (kindly supplied by Dr. Joseph Jerry, University of Massachusetts, Amherst, MA, USA) were maintained according to supplier specifications. Culturing methods are detailed in “Supplementary Materials and Methods”.

Cell treatment

The system x_c^- inhibitor SSZ (Sigma-Aldrich) was prepared in accordance with manufacturer’s recommendations in 1 M NH_4OH to produce a stock solution of 0.1 M SSZ. Control cells were treated with vehicle 1 M NH_4OH .

Glutamate release through system x_c^-

Glutamate release through system x_c^- was quantified using the cellular uptake of radiolabeled ^{14}C -cystine. In cancer cells, cystine uptake is coupled with glutamate release mediated by a 1:1 exchange via system x_c^- (Seidlitz *et al*, 2010). Therefore, measuring the uptake of radiolabeled ^{14}C -cystine provides a proportional measure of glutamate release. Furthermore, the specificity of this assay in assessing system x_c^- activity is supported by xCT knockdown results. An approximate 2-fold knockdown of xCT mRNA expression in human breast cancer cells (MDA-MB-

231) causes an approximate 2-fold decrease in ^{14}C -cystine uptake (unpublished data).

The cystine uptake protocol was adapted from previous reports (Lutgen *et al*, 2013; Shih *et al*, 2006). Briefly, 250,000 cells were seeded in 6-well plates. All wells were incubated with ^{14}C -cystine, either in the presence or absence of 200 μM of SSZ, for 30 minutes. Cells were then lysed, and the lysate was analyzed using a scintillation counter to quantify radioactivity. The lysate was also used to quantify the amount of protein for each well, and cystine uptake was normalized to total protein. Assay procedures are further detailed in “Supplementary Materials and Methods”.

Mice

Fifty-nine female BALB/c mice aged 4-6 weeks were obtained from Charles River Laboratories (St. Constant, QC, Canada). Mice were single-housed in cages maintained at 24 °C with a 12-h light/dark cycle, and were provided *ad libitum* access to food and water. Single housing eliminates the protective effect of group housing on depressive-like behaviors observed in tumor-bearing mice (Lamkin *et al*, 2011). All animal procedures were performed according to guidelines established by the Canadian Council on Animal Care under a protocol reviewed and approved by the *Animal Research Ethics Board* of McMaster University.

Tumor cell inoculation

Tumor cell inoculations were performed as previously described (Nashed *et al*, 2015). Briefly, mice were inoculated with 15,000 4T1 cells in sterile phosphate buffered saline (PBS) subcutaneously above their right flank. Control mice were sham-inoculated with sterile PBS. Mice were weighed weekly (Supplementary Materials and Methods, **Figure S1**) and tumor size was monitored using a digital caliper every 3-4 days once tumors became palpable at day 8 (Supplementary Materials and Methods, **Figure S2**). All mice were euthanized 28-29 days after cancer cell inoculation.

Drug treatments

All drugs were administered *ad libitum* to the mice in place of their normal drinking water. This method of drug treatment was chosen to minimize repeated stressful injections and excessive handling, which might confound the behavioral results. Drug treatments were initiated on the day of tumor cell inoculation and continued until endpoint.

FLX hydrochloride (Sigma-Aldrich) was dissolved in drinking water at a concentration of 100 µg/mL to obtain a target mean drug dose of approximate 20 mg/kg/day, which is the highest chronic dose reported to be effective in mice (Abuhamdah *et al*, 2015; Dulawa *et al*, 2004). SSZ was dissolved in a small volume of 1 M NH₄OH, which was then adjusted to pH 8.5 using 1 M HCl. The concentrated SSZ solution was then diluted 1:30 in drinking water to a final

concentration of 0.3 mg/mL. In humans, only approximately 12% of orally ingested SSZ escapes colonic cleavage and is absorbed into systemic circulation (Sontheimer *et al*, 2012). Based on these bioavailability data, mean water consumption, and mean weight of mice, it was estimated that 0.3 mg/mL of SSZ would translate into a dose of approximately 8 mg/kg/day. This target dose was chosen to be comparable to a dose that we have previously demonstrated to effectively reduce cancer-induced bone pain (Ungard *et al*, 2014). The SSZ metabolites, 5-ASA and SP (Sigma-Aldrich), were prepared the same way as SSZ to a final concentration of 0.09 mg/mL for 5-ASA and 0.15 mg/mL for SP. These target concentrations were chosen to match the expected concentrations of metabolites produced from oral treatment with 0.3 mg/mL of SSZ. As such, a liberal estimation of 80% colonic cleavage of SSZ into equal parts 5-ASA and SP was assumed (National Center for Biotechnology Information, 2005) and concentrations were adjusted based on the molecular weights of each metabolite.

FLX and SSZ are known to have an aversive taste. Therefore, all vehicles included 2% orange extract (McCormick Canada Inc., London, ON, Canada) to increase the palatability of drug solutions. Sweetening the water was avoided in order to maintain sucrose preference test (SPT) sensitivity at post-treatment measurement. All drugs were administered in opaque bottles for light protection.

Behavioral analyses

Behavioral tests were performed as previously described (Nashed *et al*, 2015). Anhedonia was evaluated using the sucrose preference test (SPT) and behavioral despair was evaluated using the forced swim test (FST) and the tail suspension test (TST). For the SPT, mice were first habituated to sucrose solution and a 2-bottle setup in their home cages for 72 h. For baseline and post-treatment testing, mice were presented with a two-bottle option of water and 3% sucrose solution for 48 h. At 24 h, the positions of the two bottles were switched to reduce location bias. Bottles were weighed before and after testing, and preference was calculated as the percentage of sucrose solution intake relative to total fluid intake (Towell *et al*, 1987).

The FST and TST were performed using automated systems (BioSeb, Vitrolles, France). For the FST, mice were individually placed into beakers of water. For the TST, mice were suspended by their tails, and strain gauge input was used to assess mobility. For both tests, the total duration was 6 minutes, with the first minute of the test discounted from analysis to allow for behavioral stabilization (Miller *et al*, 2010; Park *et al*, 2012). Immobility time was the primary outcome measure, and power of movement (PM) was reported as a secondary measure for the TST. Although this study utilizes female mice, it has been demonstrated that estrous cycle does not impact sucrose preference or behavioral despair in healthy and tumor-bearing female mice (Lamkin *et al*, 2011).

Experimental groups

Five groups of mice were randomly assigned to treatments: healthy + vehicle control (n = 11), tumor + vehicle control (n = 12), tumor + FLX (n = 12), tumor + SSZ (n = 12), and tumor + combination 5-ASA/SP (n = 12).

Euthanasia and tissue harvesting

Euthanasia was performed by isoflurane anesthesia and cardiac puncture exsanguination for endpoint blood collection, followed by decapitation. Blood samples were collected intracardially using sterile 25 G needles and 1 mL syringes. Blood samples were allowed to coagulate for 30-60 minutes at room temperature, and then centrifuged to extract serum (Tuck *et al*, 2009). Brains were immediately removed, rinsed and placed in sterile Hanks' Balanced Salt Solution (HBSS) for further processing (see *Brain Metastases* below).

Brain Metastases

Brain metastases were investigated using a clonogenic assay as outlined by Pulaski and Ostrand-Rosenberg (2001). This assay exploits the fact that, unlike mouse host cells, 4T1 tumor cells are resistant to 6-thioguanine (6-TG). Briefly, brains were minced and dissociated in a cocktail of collagenase type IV and elastase in HBSS. Samples were cultured in complete media containing 60 μ M 6-TG for 10-14 days. Cells were then fixed with methanol and stained with methylene blue, and the number of colonies were quantified. Clonogenic assay procedures are further detailed in “Supplementary Materials and Methods”.

Serum Glutamate

Serum proteins were precipitated from samples using 1 volume of chilled 100% (w/v) trichloroacetic acid (TCA) to 3 volumes of serum. Samples were centrifuged and the supernatant removed and neutralized with potassium hydroxide (KOH). Protein pellets were quantified for each sample using the BioRad assay as described in “Supplementary Materials and Methods”. Serum glutamate in the supernatant was analyzed using the AMPLEX Red glutamic acid assay kit (Invitrogen/Molecular Probes, Eugene, OR, USA) and analyzed on a CytoFluor Series 4000 Fluorescence Multi-Well Plate Reader (PerSeptive Biosystems, Framingham, MA, USA). Serum glutamate was normalized to total serum protein for each sample.

Serum Cytokines

Serum samples from each mouse sent to Eve Technologies (Calgary, AB, Canada) for cytokine quantification of IL-1 β , IL-6, IL-17A, and TNF- α . Cytokine quantification is further detailed in “Supplementary Materials and Methods”.

Data Analyses

Three independent planned pairwise comparisons were used to analyze results from the ¹⁴C-cystine uptake assay: 4T1 vs. TM40A, TM40A vs. TM40A + 200 μ M SSZ, and 4T1 vs. 4T1 + 200 μ M SSZ. For each comparison, results from 3 independent experiments (each performed in triplicates) are represented as mean

fold-changes in counts per minute (CMP)/mg protein relative to controls. All pairwise comparisons were evaluated using one-tailed Student *t*-tests.

One-way analysis of variance (ANOVA) was used to analyze the behavioral data (SPT, FST, and TST), serum glutamate, and serum cytokines. For these data, 4 planned comparisons were analyzed. Control mice were compared with tumor mice to establish benchmark tumor-induced changes for each assay. Tumor mice were compared with each intervention group (FLX, SSZ, and 5-ASA) to explore drug effects on each assay. The Holm-Šidák correction was used to correct for multiple comparisons.

In this investigation we used a peripheral tumor model for CID. Therefore, we are primarily interested in attenuating depressive behaviors by targeting peripheral tumor cells. However, 4T1 cells are capable of metastasizing to the brain (Pulaski and Ostrand-Rosenberg, 2001). Therefore, as a secondary measure for all behavioral data, linear regression analyses were performed to investigate whether brain metastases were predictive of tumor-induced or drug-induced behavioral changes.

For all analyses, the significance level was set at $\alpha = 0.05$. Grubb's test was used to identify and exclude any outliers. The Shapiro-Wilk test of was used to determine normality. Data that was not normally distributed was subsequently transformed to achieve approximate normality prior to further statistical considerations. Data are presented as mean \pm the SEM. Statistical analyses were

performed using GraphPad Prism software version 6.0 for Macintosh (GraphPad Software, Inc., La Jolla, CA, USA). All graphs were prepared on Microsoft Excel 2011 version 14.1.0 (Microsoft, Redmond, WA, USA).

Results

Glutamate release through system x_c^-

Cystine uptake, and consequently glutamate release, by tumorigenic 4T1 cells was more than 3-fold higher than that observed by non-tumorigenic TM40A control cells ($P = 0.032$; **Figure 1 A**). Treatment with 200 μ M of SSZ decreased cystine uptake to 0.39-fold for TM40A cells ($P < 0.001$) and decreased cystine uptake to 0.25-fold for 4T1 cells (0.25-fold) ($P < 0.001$; **Figure 1 B**).

Behavioral analyses

Mice in the tum+FLX group consumed a mean FLX dose of 21.59 ± 0.56 mg/kg/day. Mice in the tum+SSZ group consumed a mean SSZ dose of 71.41 ± 2.98 mg/kg/day, or 8.57 ± 0.36 mg/kg/day when corrected for systemic absorption of intact SSZ (Sontheimer *et al*, 2012). Mice in the tum+5-ASA/SP group consumed a mean 5-ASA dose of 20.32 ± 0.54 mg/kg/day, and a mean SP dose of 33.86 ± 0.89 mg/kg/day.

In the SPT, lower preference for sucrose solution indicates anhedonia, which is a core symptom of depression characterized by the loss of ability to experience pleasure. Our results revealed a significant main effect of treatment group ($F_{(4,53)} = 3.84$, $P = 0.008$). As expected, untreated tumor mice showed lower sucrose preference compared to control mice ($P = 0.026$) (**Figure 2 A**). Treatment with FLX, SSZ, and 5-ASA/SP were all associated with higher sucrose preference compared to untreated tumor mice ($P = 0.040$, $P = 0.002$, $P = 0.035$, respectively).

In the FST and TST, longer immobility times indicate behavioral despair, a depressive behavior that is sensitive to antidepressant treatment. Our results revealed a significant main effect of treatment group on FST immobility ($F_{(4,52)} = 4.36, P = 0.004$). As expected, untreated tumor mice had higher immobility time compared to control mice ($P = 0.033$) (**Figure 2 B**). FLX and SSZ were associated with lower immobility times compared to untreated tumor mice ($P = 0.033, P = 0.019$, respectively). 5-ASA/SP treatment did not prevent the tumor-induced increase in immobility time.

Two measures for the TST are reported: immobility time (**Figure 2 C**) and PM (**Figure 2 D**). PM did not follow a normal distribution. \log_{10} transformation of these data achieved approximate normality. There was no main effect of treatment group on TST immobility ($F_{(4,54)} = 1.70, P = 0.163$) or \log_{10} PM ($F_{(4,54)} = 1.32, P = 0.276$). Here we independently replicated our previous finding that the TST is not sensitive in detecting behavioral despair in the CID model (Nashed *et al*, 2015).

Approximately 35% of tumor-bearing mice developed brain metastases 4 weeks after inoculation, which is consistent with previous observations (Pulaski *et al*, 2001). Among mice that developed brain metastases, the number of metastatic colonies was not normally distributed. \log_{10} transformation of this data achieved approximate normality. Subsequently, regression analyses revealed that brain metastases did not predict sucrose preference in any direction for any of the tumor groups (**Figure 3 A**). Brain metastases were moderately predictive of increased immobility time on the FST for the tumor group treated with SSZ ($P = 0.019$)

(**Figure 3 B**). A possible explanation for this is that mice with brain metastases were less responsive to SSZ treatment on this measure. In the TST, metastases were moderately predictive of lower immobility time and higher PM for untreated tumor mice ($P = 0.005$ and $P = 0.004$, respectively) (**Figure 3 C**). This result was counterintuitive, but may help explain the consistent lack of sensitivity of this test in detecting tumor-induced behavioral despair and drug effects. In addition, brain metastases were moderately predictive of higher PM for the mice treated with 5-ASA/SP ($P = 0.013$), but did not predict PM for mice treated with SSZ or FLX.

Serum Glutamate

There was no main effect of treatment group on serum glutamate ($F_{(4,47)} = 1.87$, $P = 0.132$). However, trends observed in serum glutamate levels are consistent with the expected glutamate release by 4T1 cells in tumor-bearing mice, and with the hypothesized inhibition of this glutamate release by SSZ (**Figure 4**).

Serum Cytokines

There was a significant main effect of treatment group on IL-1 β serum level ($F_{(4,51)} = 2.62$, $P = 0.046$). FLX-treated mice had a significantly lower level of serum IL-1 β compared to untreated tumor mice ($P = 0.022$) (**Figure 5 A**). Serum levels of IL-1 β did not differ for mice treated with SSZ or 5-ASA/SP compared to untreated tumor mice. There was a significant main effect of treatment group on IL-6 serum level ($F_{(4,44)} = 7.79$, $P < 0.0001$). Untreated tumor mice had higher levels of serum IL-6 compared to control mice ($P = 0.015$) (**Figure 5 B**). Serum

levels of IL-6 did not differ for mice treated with FLX, SSZ or 5-ASA/SP compared to untreated tumor mice. IL-17A and TNF- α levels were not different between groups (**Figure 5 C and D**).

Discussion

In the present study, murine 4T1 mammary carcinoma cells had greater cystine uptake, and consequently greater glutamate release, compared to non-tumorigenic TM40A mammary epithelial cells derived from the same mouse strain (**Figure 1 A**). Furthermore, we demonstrated that SSZ inhibits cystine uptake in both TM40A cells and 4T1 cells (**Figure 1 B**), suggesting that system x_c^- is primarily responsible for glutamate release. These results are consistent with previous studies from our group showing that human breast and prostate cancer cell lines release large amounts of glutamate into their microenvironment through the glutamate/cystine antiporter system x_c^- (Seidlitz *et al*, 2009; Sharma *et al*, 2010). We also found that the use of SSZ (a system x_c^- inhibitor) and FLX (used as a positive control) in tumor-bearing mice exerted antidepressant-like effects, namely increased sucrose preference and decreased FST immobility. Results from all behavioral tests, serum glutamate, and serum cytokine analyses are summarized in **Table 1**.

To establish a benchmark for antidepressant-like efficacy in the present study, we used the selective serotonin reuptake inhibitor (SSRI) FLX. FLX effectively attenuates depressive-like behaviors in animal models when administered chronically (Abuhamdah *et al*, 2015; Dulawa *et al*, 2004). SSRIs are useful for treating acute depressive episodes and preventing subsequent episodes in MDD subjects (Gilaberte *et al*, 2001). The rapid progression of tumor growth in our CID model was more suitable for testing the prophylactic efficacy of FLX, SSZ, and 5-

ASA/SP, rather than reversal of depressive-like behaviors. In our CID model, chronic treatment with SSZ was at least as effective as FLX in preventing depressive-like behaviors. Both drug treatments also showed non-significant trends toward lower immobility time and higher mean PM on the TST when compared with untreated tumor mice. Treatment with the SSZ metabolites, 5-ASA/SP, was associated with higher sucrose preference compared to untreated tumor mice. However, these compounds had no effect on the behavioral despair tests. This suggests that the observed antidepressant-like effect of SSZ in the FST immobility was primarily due to intact SSZ.

Serum cytokine analysis suggested that neither 70 mg/kg/day of SSZ nor 20 mg/kg/day of 5-ASA were effective at preventing the increase in IL-6 that was induced by tumor burden (**Figure 5 A and B**). A previous study found that 5-ASA, which is used to treat inflammatory bowel disease, decreased intestinal inflammation at doses as low as 8.3 mg/kg/day in rats (Horvath *et al*, 2008). The lack of effect we observed on serum cytokines may be due to the fact that only about 10% of 5-ASA is absorbed systemically, where it is rendered largely inactive by extensive acetylation (Tokui *et al*, 2002). Although anti-inflammatory agents, such as celecoxib, can exert antidepressant effects in a subset of individuals with MDD (Kohler *et al*, 2014), 5-ASA did not produce antidepressant-like effects in our CID model perhaps due to its limited absorption. By contrast, FLX administration was associated with lower serum IL-1 β compared to untreated tumor mice (**Figure 5 A**). This result is consistent with

meta-analysis results in MDD showing that FLX reduces serum levels of IL-1 β but not TNF- α , with mixed results for IL-6 (Hannestad *et al*, 2011).

Results from the serum cytokine analysis also provide plausibility for a direct depressive mechanism of peripherally released glutamate on the CNS. In our CID model, tumor burden was associated with increased IL-6, and possibly IL-1 β . These cytokines have been demonstrated to reduce BBB integrity, thereby increasing permeability (Rochfort *et al*, 2015; Wang *et al*, 2014). Future analyses of BBB integrity and systemic administration of radiolabeled glutamate would be useful in better characterizing the impact of peripherally released glutamate on the CNS.

Intraperitoneal administration of SSZ inhibits tumor growth in a glioma model (Chung *et al*, 2005), and affects CNS extracellular glutamate levels in healthy rats (Lutgen *et al*, 2014). These data suggest that SSZ is able to cross the BBB. Interestingly, in healthy rats, 8 and 16 mg/kg of SSZ reduced extracellular glutamate in the brain without affecting behavioral despair on the FST (Lutgen *et al*, 2014). This may be due to the relatively limited impact of system x_c⁻ inhibition on cystine uptake in cortical astrocytes and neurons, which utilize additional mechanisms of glutamate regulation and glutathione biosynthesis (Chung *et al*, 2005). In contrast, cancer cells are heavily dependent on system x_c⁻ for glutathione production, and are therefore much more sensitive to inhibitory drugs, such as SSZ (Chung *et al*, 2005; Sharma *et al*, 2010; Ungard *et al*, 2014). It is, therefore, unlikely that a central influence of SSZ is primarily responsible for the

antidepressant-like effect observed in the present study. Rather, it is more plausible that this effect is largely attributable to inhibition of excess glutamate release by peripheral cancer cells. This is consistent with our observation that intact SSZ, but not 5-ASA/SP, prevented the development of behavioral despair. Furthermore, it has been demonstrated that the anti-tumor effects of SSZ are entirely attributable to system x_c^- inhibition, rather than its reported anti-inflammatory and apoptotic influence through nuclear factor- κ B (NF- κ B) inhibition (Chung and Sontheimer, 2009). Serum glutamate analysis did not yield any significant results, which may in part be attributable to regulatory mechanisms. Glutamate scavenging by glutamate-oxaloacetate transaminase (GOT) and glutamate-pyruvate transaminase (GPT) would make it difficult to detect dynamic glutamate dysregulation at a single time point (Leibowitz *et al*, 2012). Nevertheless, trends in serum glutamate were consistent with SSZ inhibition of glutamate release by cancer cells (**Figure 4**). Caution should still be taken when interpreting the results of this study due to the lack of specificity of SSZ to system x_c^- . Oral SSZ was chosen for the current investigation due to the clinical relevance of this model. SSZ is a clinically useful and well-tolerated system x_c^- inhibitor (Gout *et al*, 2001). Valuable insight may be derived from further investigation of more specific system x_c^- inhibitors, such as S-4-carboxy-phenylglycine (S-4-CPG) (Garzon-Muvdi *et al*, 2013). However, the pharmacokinetics of orally administered S-4-CPG has not been described, and this model would likely require daily intraperitoneal injections or surgically implanted

osmotic pumps. Stress induced by either of these modes of drug delivery would need to be carefully considered. Genetically modulating system x_c^- activity represents a more specific method of investigating the impact of cancer cell-derived glutamate on CID. To this end, we are currently developing an xCT knockdown 4T1 cancer cell line to be used in future *in vivo* studies.

In summary, we have demonstrated that chronic oral administration of SSZ is at least as effective as FLX at preventing the development of depressive-like behaviors in a preclinical model of CID. This finding carries clinical significance, particularly considering recent evidence that SSZ inhibits tumor progression (Chung *et al*, 2005; Chung *et al*, 2009) and cancer-induced bone pain (Ungard *et al*, 2014). Our results suggest that one of the mechanisms of antidepressant-like action of SSZ may be through inhibition of glutamate release via system x_c^- at the peripheral tumor site, rather than anti-inflammatory action of SSZ metabolites. FLX was also efficacious in preventing the development of depressive-like behaviors in tumor-bearing mice. It may, therefore, be interesting to investigate the effects of standard antidepressants augmented with SSZ in the treatment of CID. While this investigation focuses on peripheral modulation of glutamate signaling in CID, further assessment of central glutamate signaling, using ketamine and other recently described glutamatergic modulators, would further enhance our understanding of CID. Overall, our results represent a potential new pathway for drug development in the treatment of CID. This approach can target the effects of cancer cells directly to prevent depressive symptoms, rather than

targeting downstream effects on the CNS. These results have significant implications for the pathophysiology of CID and present a novel preclinical model for the development of more targeted therapy.

Acknowledgements

The authors would like to thank Dr. Lehana Thabane (Professor and Associate Chair, Department of Clinical Epidemiology & Biostatistics, McMaster University) for his advice and guidance regarding the statistical considerations for this study. We also thank Dr. Katja Linher-Melville for contributing her unpublished data to the discussion on the cystine uptake assay. Experiments in this study were completed as part of the doctoral thesis of M.G.N. This project was funded by operating grants from the Canadian Institutes of Health Research (CIHR) and the Canadian Breast Cancer Foundation (CBCF).

Financial Disclosure

Dr. Frey has received grant/research support from Alternative Funding Plan Innovations Award, Brain & Behaviour Research Foundation, CIHR, Eli Lilly, Hamilton Health Sciences Foundation, J.P. Bickell Foundation, Ontario Brain Institute, Ontario Mental Health Foundation, Pfizer and Society for Women's Health Research, and has received consultant and/or speaker fees from AstraZeneca, Bristol-Myers Squibb, Lundbeck, Pfizer, Servier and Sunovion. Other authors declare no competing financial interest.

References

- Abuhamdah RM, Hussain MD, Chazot PL, Ennaceur A (2015). Effects of chronic fluoxetine treatment on anxious behaviour of balb/c mice in a 3-dimensional maze. *Stress* **18**(6): 677-685.
- Auer DP, Putz B, Kraft E, Lipinski B, Schill J, Holsboer F (2000). Reduced glutamate in the anterior cingulate cortex in depression: An in vivo proton magnetic resonance spectroscopy study. *Biol Psychiatry* **47**(4): 305-313.
- Bentea E, Demuyser T, Van Liefferinge J, Albertini G, Deneyer L, Nys J, *et al* (2015). Absence of system xc- in mice decreases anxiety and depressive-like behavior without affecting sensorimotor function or spatial vision. *Prog Neuropsychopharmacol Biol Psychiatry* **59C**: 49-58.
- Brelvi S, Loge JH, Skurtveit S, Johannesen TB, Aass N, Ottesen S, *et al* (2013). Antidepressants to cancer patients during the last year of life--a population-based study. *Psychooncology* **22**(3): 506-514.
- Chung WJ, Lyons SA, Nelson GM, Hamza H, Gladson CL, Gillespie GY, *et al* (2005). Inhibition of cystine uptake disrupts the growth of primary brain tumors. *J Neurosci* **25**(31): 7101-7110.
- Chung WJ, Sontheimer H (2009). Sulfasalazine inhibits the growth of primary brain tumors independent of nuclear factor-kappaB. *J Neurochem* **110**(1): 182-193.

de Groot J, Sontheimer H (2011). Glutamate and the biology of gliomas. *Glia*

59(8): 1181-1189.

Dulawa SC, Holick KA, Gundersen B, Hen R (2004). Effects of chronic

fluoxetine in animal models of anxiety and depression.

Neuropsychopharmacology **29**(7): 1321-1330.

Esquivel-Velazquez M, Ostoa-Saloma P, Palacios-Arreola MI, Nava-Castro KE,

Castro JI, Morales-Montor J (2015). The role of cytokines in breast cancer

development and progression. *J Interferon Cytokine Res* **35**(1): 1-16.

Garzon-Muvdi T, Pradilla G, Ruzevick JJ, Bender M, Edwards L, Grossman R, *et*

al (2013). A glutamate receptor antagonist, s-4-carboxyphenylglycine (s-4-cpg),

inhibits vasospasm after subarachnoid hemorrhage in haptoglobin 2-2 mice

[corrected]. *Neurosurgery* **73**(4): 719-728; discussion 729.

Gilaberte I, Montejo AL, de la Gandara J, Perez-Sola V, Bernardo M, Massana J,

et al (2001). Fluoxetine in the prevention of depressive recurrences: A double-

blind study. *J Clin Psychopharmacol* **21**(4): 417-424.

Gout PW, Buckley AR, Simms CR, Bruchovsky N (2001). Sulfasalazine, a potent

suppressor of lymphoma growth by inhibition of the x(c)- cystine transporter:

A new action for an old drug. *Leukemia* **15**(10): 1633-1640.

- Hannestad J, DellaGioia N, Bloch M (2011). The effect of antidepressant medication treatment on serum levels of inflammatory cytokines: A meta-analysis. *Neuropsychopharmacology* **36**(12): 2452-2459.
- Hasler G, van der Veen JW, Tumonis T, Meyers N, Shen J, Drevets WC (2007). Reduced prefrontal glutamate/glutamine and gamma-aminobutyric acid levels in major depression determined using proton magnetic resonance spectroscopy. *Arch Gen Psychiatry* **64**(2): 193-200.
- Horvath K, Varga C, Berko A, Posa A, Laszlo F, Whittle BJ (2008). The involvement of heme oxygenase-1 activity in the therapeutic actions of 5-aminosalicylic acid in rat colitis. *Eur J Pharmacol* **581**(3): 315-323.
- Huppert J, Closhen D, Croxford A, White R, Kulig P, Pietrowski E, *et al* (2010). Cellular mechanisms of il-17-induced blood-brain barrier disruption. *FASEB J* **24**(4): 1023-1034.
- Kohler O, Benros ME, Nordentoft M, Farkouh ME, Iyengar RL, Mors O, *et al* (2014). Effect of anti-inflammatory treatment on depression, depressive symptoms, and adverse effects: A systematic review and meta-analysis of randomized clinical trials. *JAMA Psychiatry* **71**(12): 1381-1391.
- Kruis W, Schreiber S, Theuer D, Brandes JW, Schutz E, Howaldt S, *et al* (2001). Low dose balsalazide (1.5 g twice daily) and mesalazine (0.5 g three times

daily) maintained remission of ulcerative colitis but high dose balsalazide (3.0 g twice daily) was superior in preventing relapses. *Gut* **49**(6): 783-789.

Lamkin DM, Lutgendorf SK, Lubaroff D, Sood AK, Beltz TG, Johnson AK (2011). Cancer induces inflammation and depressive-like behavior in the mouse: Modulation by social housing. *Brain Behav Immun* **25**(3): 555-564.

Leibowitz A, Boyko M, Shapira Y, Zlotnik A (2012). Blood glutamate scavenging: Insight into neuroprotection. *Int J Mol Sci* **13**(8): 10041-10066.

Li N, Lee B, Liu RJ, Banasr M, Dwyer JM, Iwata M, *et al* (2010). Mtor-dependent synapse formation underlies the rapid antidepressant effects of nmda antagonists. *Science* **329**(5994): 959-964.

Lutgen V, Qualmann K, Resch J, Kong L, Choi S, Baker DA (2013). Reduction in phencyclidine induced sensorimotor gating deficits in the rat following increased system xc(-) activity in the medial prefrontal cortex. *Psychopharmacology (Berl)* **226**(3): 531-540.

Lutgen V, Resch J, Qualmann K, Raddatz NJ, Panhans C, Olander EM, *et al* (2014). Behavioral assessment of acute inhibition of system xc (-) in rats. *Psychopharmacology (Berl)* **231**(24): 4637-4647.

- Miller BH, Schultz LE, Gulati A, Su AI, Pletcher MT (2010). Phenotypic characterization of a genetically diverse panel of mice for behavioral despair and anxiety. *PLoS One* **5**(12): e14458.
- Mitani H, Shirayama Y, Yamada T, Maeda K, Ashby CR, Jr., Kawahara R (2006). Correlation between plasma levels of glutamate, alanine and serine with severity of depression. *Prog Neuropsychopharmacol Biol Psychiatry* **30**(6): 1155-1158.
- Mitchell AJ, Chan M, Bhatti H, Halton M, Grassi L, Johansen C, *et al* (2011). Prevalence of depression, anxiety, and adjustment disorder in oncological, haematological, and palliative-care settings: A meta-analysis of 94 interview-based studies. *Lancet Oncol* **12**(2): 160-174.
- Murrough JW (2012). Ketamine as a novel antidepressant: From synapse to behavior. *Clin Pharmacol Ther* **91**(2): 303-309.
- Nashed MG, Seidlitz EP, Frey BN, Singh G (2015). Depressive-like behaviours and decreased dendritic branching in the medial prefrontal cortex of mice with tumors: A novel validated model of cancer-induced depression. *Behav Brain Res* **294**: 25-35.
- National Center for Biotechnology Information (2005). Pubchem compound database; cid=5384001. <https://pubchem.ncbi.nlm.nih.gov/compound/5384001>.

- Ng CG, Boks MP, Zainal NZ, de Wit NJ (2011). The prevalence and pharmacotherapy of depression in cancer patients. *J Affect Disord* **131**(1-3): 1-7.
- Ostuzzi G, Matcham F, Dauchy S, Barbui C, Hotopf M (2015). Antidepressants for the treatment of depression in people with cancer. *Cochrane Database Syst Rev* **6**: Cd011006.
- Park MJ, Yoo SW, Choe BS, Dantzer R, Freund GG (2012). Acute hypoglycemia causes depressive-like behaviors in mice. *Metabolism* **61**(2): 229-236.
- Patel JP, Frey BN (2015). Disruption in the blood-brain barrier: The missing link between brain and body inflammation in bipolar disorder? *Neural Plast* **2015**: 708306.
- Pinquart M, Duberstein PR (2010). Depression and cancer mortality: A meta-analysis. *Psychol Med* **40**(11): 1797-1810.
- Pulaski BA, Ostrand-Rosenberg S (2001). Mouse 4t1 breast tumor model. *Curr Protoc Immunol* **Chapter 20**: Unit 20.22.
- Reddy BY, Greco SJ, Patel PS, Trzaska KA, Rameshwar P (2009). Re-1-silencing transcription factor shows tumor-suppressor functions and negatively regulates the oncogenic *tac1* in breast cancer cells. *Proc Natl Acad Sci U S A* **106**(11): 4408-4413.

- Rochfort KD, Cummins PM (2015). The blood-brain barrier endothelium: A target for pro-inflammatory cytokines. *Biochem Soc Trans* **43**(4): 702-706.
- Rodin G, Lloyd N, Katz M, Green E, Mackay JA, Wong RK, *et al* (2007). The treatment of depression in cancer patients: A systematic review. *Support Care Cancer* **15**(2): 123-136.
- Rodriguez PL, Jiang S, Fu Y, Avraham S, Avraham HK (2014). The proinflammatory peptide substance p promotes blood-brain barrier breaching by breast cancer cells through changes in microvascular endothelial cell tight junctions. *Int J Cancer* **134**(5): 1034-1044.
- Seidlitz EP, Sharma MK, Saikali Z, Ghert M, Singh G (2009). Cancer cell lines release glutamate into the extracellular environment. *Clin Exp Metastasis* **26**(7): 781-787.
- Seidlitz EP, Sharma MK, Singh G (2010). A by-product of glutathione production in cancer cells may cause disruption in bone metabolic processes. *Can J Physiol Pharmacol* **88**(3): 197-203.
- Sharma MK, Seidlitz EP, Singh G (2010). Cancer cells release glutamate via the cystine/glutamate antiporter. *Biochem Biophys Res Commun* **391**(1): 91-95.
- Shih AY, Erb H, Sun X, Toda S, Kalivas PW, Murphy TH (2006). Cystine/glutamate exchange modulates glutathione supply for neuroprotection from oxidative stress and cell proliferation. *J Neurosci* **26**(41): 10514-10523.

Smith QR (2000). Transport of glutamate and other amino acids at the blood-brain barrier. *J Nutr* **130**(4S Suppl): 1016s-1022s.

Sontheimer H, Bridges RJ (2012). Sulfasalazine for brain cancer fits. *Expert Opin Investig Drugs* **21**(5): 575-578.

Teichberg VI, Cohen-Kashi-Malina K, Cooper I, Zlotnik A (2009). Homeostasis of glutamate in brain fluids: An accelerated brain-to-blood efflux of excess glutamate is produced by blood glutamate scavenging and offers protection from neuropathologies. *Neuroscience* **158**(1): 301-308.

Tokui K, Asai Y, Arakawa T, Matsumoto T, Nabeshima T (2002). Comparative absorption of 5-aminosalicylic acid (5-asa) after administration of a 5-asa enema and salazosulfapyridine (sasp) after an sasp suppository in japanese volunteers. *Biol Pharm Bull* **25**(2): 264-267.

Towell A, Muscat R, Willner P (1987). Effects of pimozide on sucrose consumption and preference. *Psychopharmacology (Berl)* **92**(2): 262-264.

Tuck MK, Chan DW, Chia D, Godwin AK, Grizzle WE, Krueger KE, *et al* (2009). Standard operating procedures for serum and plasma collection: Early detection research network consensus statement standard operating procedure integration working group. *J Proteome Res* **8**(1): 113-117.

- Ungard RG, Seidlitz EP, Singh G (2014). Inhibition of breast cancer-cell glutamate release with sulfasalazine limits cancer-induced bone pain. *Pain* **155**(1): 28-36.
- Wang Y, Jin S, Sonobe Y, Cheng Y, Horiuchi H, Parajuli B, *et al* (2014). Interleukin-1beta induces blood-brain barrier disruption by downregulating sonic hedgehog in astrocytes. *PLoS One* **9**(10): e110024.
- Williams S, Dale J (2006). The effectiveness of treatment for depression/depressive symptoms in adults with cancer: A systematic review. *Br J Cancer* **94**(3): 372-390.
- Zarate CA, Jr., Singh JB, Carlson PJ, Brutsche NE, Ameli R, Luckenbaugh DA, *et al* (2006). A randomized trial of an n-methyl-d-aspartate antagonist in treatment-resistant major depression. *Arch Gen Psychiatry* **63**(8): 856-864.

Figures & Tables

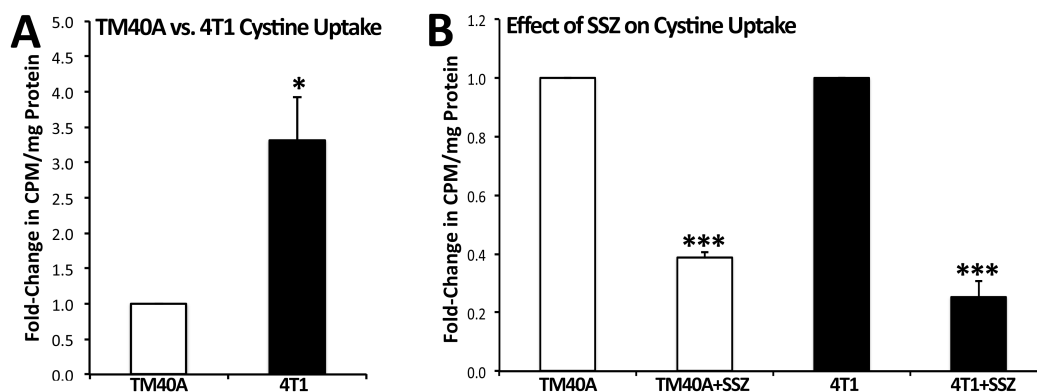


Figure 1. ¹⁴C-cystine uptake assay on 4T1 cancer cells and TM40A mammary epithelial cells, both derived from BALB/c mice. (A) Cystine uptake by 4T1 cells was more than 3-fold higher than TM40A cells ($P = 0.032$). (B) 200 μ M SSZ caused a decrease in TM40A cystine uptake to 0.39-fold ($P < 0.001$) and a decrease in 4T1 cystine uptake to 0.25-fold ($P < 0.001$). Results are represented as means from 3 experiments (performed in duplicates) \pm SEM. Statistical significance was assessed through one-tailed Student t -tests. * $P < 0.05$. *** $P < 0.001$.

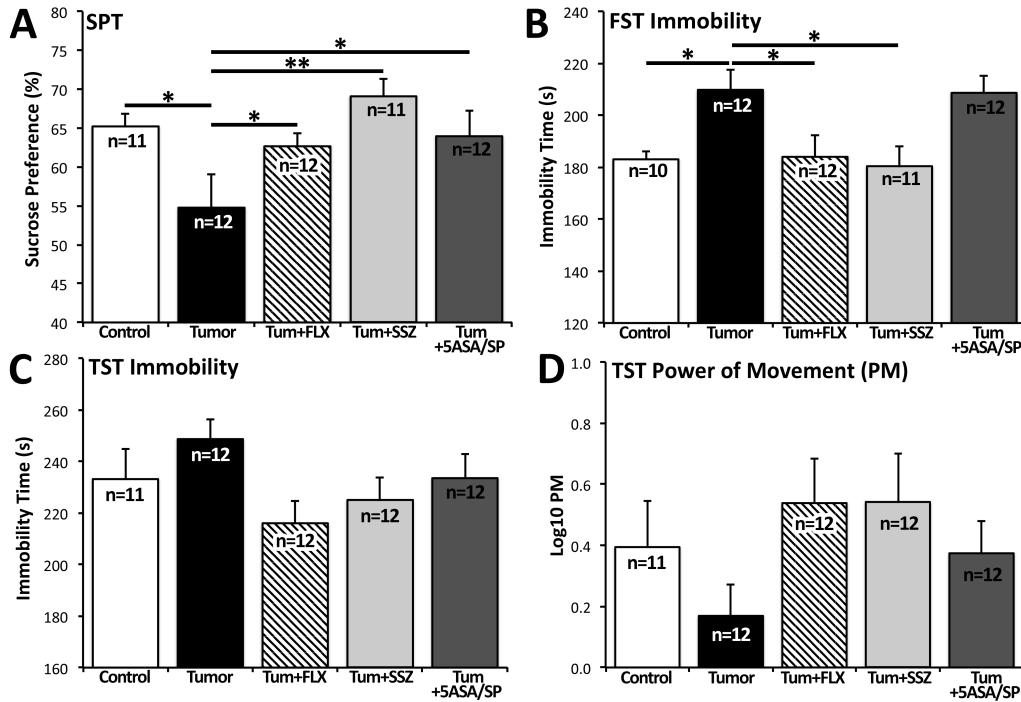


Figure 2. Behavioral results for the 5 experimental groups: control, tumor, tum+FLX, tum+SSZ, tum+5-ASA/SP. (A) In the sucrose preference test (SPT) preference is calculated as (sucrose water consumption/total fluid intake) \times 100, where 50% represents equal consumption of sucrose water and regular water. Tumor mice showed a lower sucrose preference compared to control ($P = 0.026$). Treatments with FLX, SSZ, and 5-ASA/SP were associated with higher sucrose preference compared to untreated tumor mice ($P = 0.040$, $P = 0.002$, $P = 0.035$, respectively). (B) In the forced swim test (FST), tumor mice had higher immobility time compared to control mice ($P = 0.033$). FLX and SSZ were associated with lower immobility times compared to untreated tumor mice ($P = 0.033$, $P = 0.019$, respectively). (C) In the tail suspension test (TST), no

significant changes were observed. Trends indicated a lower immobility time and higher \log_{10} PM associated with FLX and SSZ treatments compared to untreated mice. Data are presented as mean \pm SEM. Results were analyzed using one-way ANOVA. The Holm-Šidák correction was used to correct for multiple comparisons. * $P < 0.05$, ** $P < 0.01$.

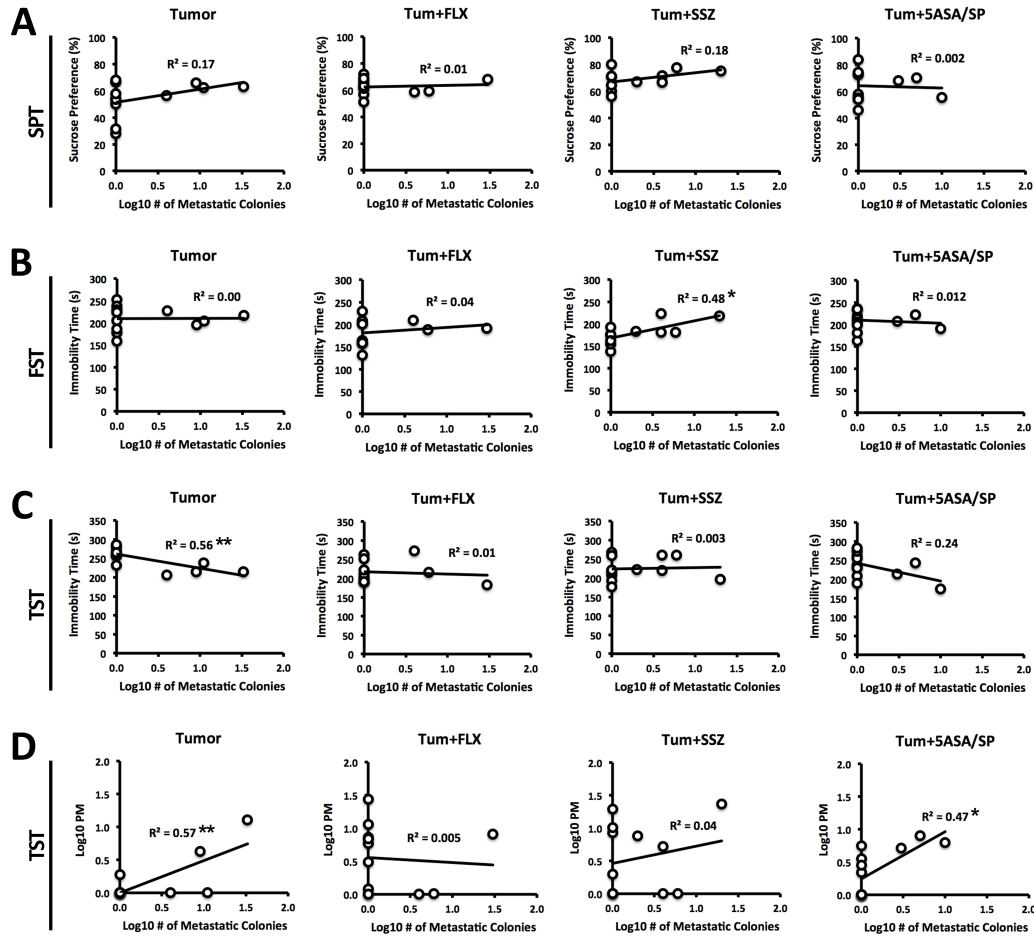


Figure 3. Brain metastasis regression analyses for the 4 tumor groups: tumor, tum+FLX, tum+SSZ, tum+5-ASA/SP. (A) Brain metastases were not predictive of sucrose preference for any of the tumor groups. (B) Brain metastases were predictive of lower FST immobility time for mice treated with SSZ ($P = 0.019$). (C) Brain metastases were predictive of lower immobility time for untreated tumor-bearing mice ($P = 0.005$). (D) Brain metastases were predictive of higher PM for untreated tumor mice ($P = 0.004$) and 5-ASA/SP treated mice ($P = 0.013$). Results were analyzed using linear regression analyses. * $P < 0.05$, ** $P < 0.001$.

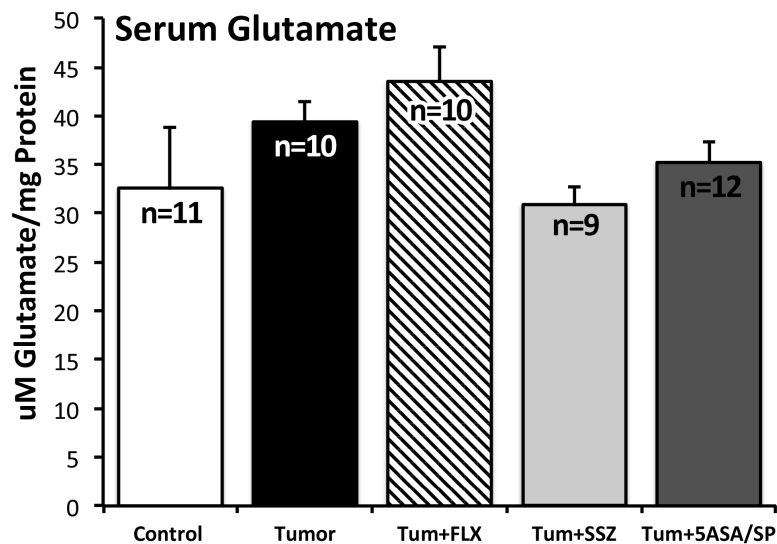


Figure 4. Serum level of glutamate for the 5 experimental groups: control, tumor, tum+FLX, tum+SSZ, tum+5-ASA/SP. Data are presented as mean \pm SEM. No significant differences were observed between treatment groups. Trends were consistent with the expected increase of serum glutamate in tumor-bearing mice, and the expected inhibition of cancer cell glutamate release by SSZ. Results were analyzed using one-way ANOVA. The Holm-Šidák correction was used to correct for multiple comparisons.

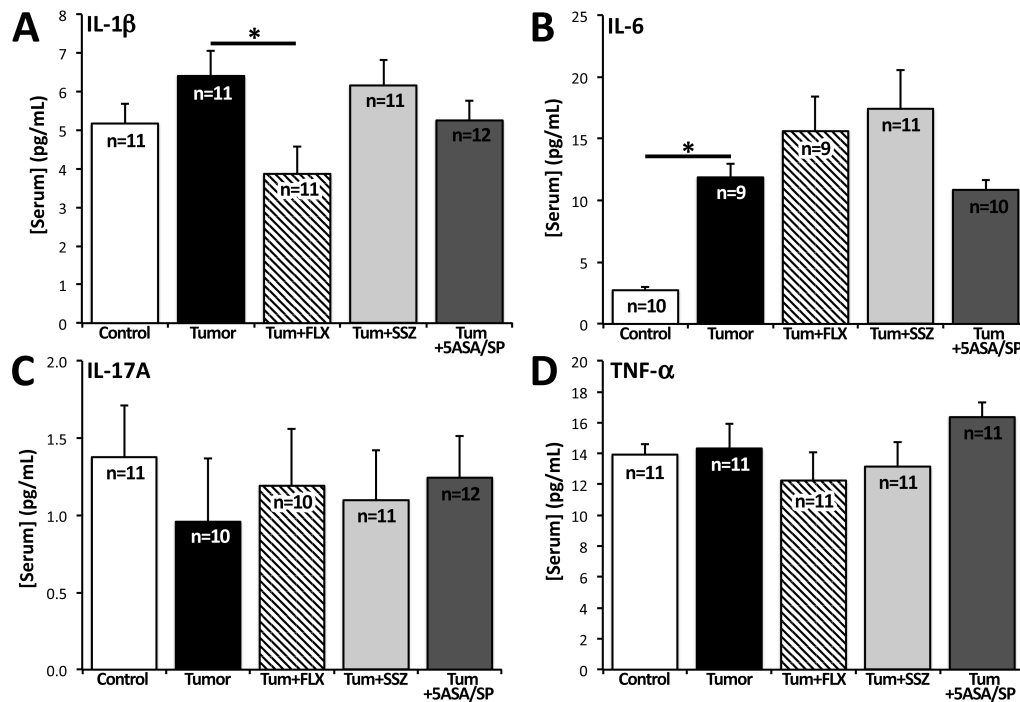


Figure 5. Serum level of pro-inflammatory cytokines for the 5 experimental groups: control, tumor, tum+FLX, tum+SSZ, tum+5-ASA/SP. (A) FLX-treated mice had a significantly lower level of serum IL-1 β compared to untreated tumor mice ($P = 0.022$). (B) Untreated tumor-bearing mice had higher levels of serum IL-6 compared to control mice ($P = 0.015$). (C) Serum IL-17A did not differ between any experimental groups. (D) Serum TNF- α did not differ between any experimental groups. Data are presented as mean \pm SEM. Results were analyzed using one-way ANOVA. The Holm-Šidák correction was used to correct for multiple comparisons. * $P < 0.05$.

Table 1

Summary of results for behavioral and cytokine analyses.

| Comparison | SPT | FST | TST (Immob.) | TST (PM) | Serum Glu | IL-1 β | IL-6 | IL- 17A | TNF- α |
|---------------------------|-----|-----|-----------------|-------------|--------------|--------------|------|------------|---------------|
| Control vs. Tumor | ↓ | ↑ | – | – | – | – | ↑ | – | – |
| Tumor vs. Tum+FLX | ↑ | ↓ | – | – | – | ↓ | – | – | – |
| Tumor vs. Tum+SSZ | ↑↑ | ↓ | – | – | – | – | – | – | – |
| Tumor vs. Tum+5-ASA/SP | ↑ | – | – | – | – | – | – | – | – |

“–” denotes no differences between groups. One arrow denote a mean difference between groups with $0.05 > P > 0.01$. Two arrows denote a mean difference between groups with $P < 0.01$. The direction of the arrows represents the direction of change of mean for that particular measure. SPT, sucrose preference test; TST, tail suspension test; FST, forced swim test; FLX, fluoxetine; SSZ, sulfasalazine; 5-ASA, 5-aminosalicylic acid; SP, sulfapyridine; Glu, glutamate; IL, interleukin; TNF- α , tumor necrosis factor- α .

Supplemental Materials and Methods

Cell Culture

4T1 cells were maintained in Roswell Park Memorial Institute medium (RPMI-1640; Life Technologies, Carlsbad, CA) supplemented with 10% fetal bovine serum (FBS) and 1% antibiotic/antimycotic (Life Technologies). TM40A cells were maintained in Dulbecco's Modified Eagle Medium: Nutrient Mixture F-12 (DMEM:F12; Life Technologies) supplemented with 10% FBS, 10 $\mu\text{g}/\text{mL}$ insulin, 1% antibiotic/antimycotic (Life Technologies), and 20 ng/mL mouse Epidermal Growth Factor (mEGF; Sigma-Aldrich, St. Louis, MO, USA). All cells were incubated at 37 °C and 5% CO_2 .

Glutamate release through system x_c^-

For both 4T1 and TM40A cells, 250,000 cells per well were seeded in a 6-well plate and allowed to adhere overnight. Media was then replaced with 300 μL 1 \times Hank's Balanced Salt Solution (HBSS; Invitrogen, Burlington, ON, Canada) containing either vehicle 1 M NH_4OH or 200 μM of SSZ and 0.45 μL of 20 $\mu\text{Ci}/\text{mL}$ ^{14}C -cystine (PerkinElmer, Waltham, MA, USA) added to each well. Following incubation at 37 °C for 30 minutes, HBSS was aspirated and cells were lysed using lysis buffer (0.1 N NaOH containing 0.1% Triton X-100; Sigma). 100 μL of the lysate was added to 1 mL of Ecoscint-H solution (National Diagnostics, Atlanta, GA, USA) in a scintillation vial. A Beckman LS6500 scintillation

counter (Beckman Coulter, Inc, Brea, CA USA) was used to quantify the radioactivity of each vial.

Cystine uptake was normalized to total protein using the BioRad protein assay (BioRad Laboratories, Inc, Hercules, CA, USA). This assay was performed in triplicate in a 96-well plate. A 1:4 dilution of BioRad solution was added to 10 μ L samples of lysate and incubated for 5 minutes. The plate was then analyzed using a BioTek PowerWave XL plate reader (BioTek Instruments, Inc, Winooski, VT, USA) at 570 nm. Quantification of protein in each sample allowed for the standardization of the counts per minute (CPM) reading by the scintillator to total protein.

Mice Weights and Tumor Volume

All mice were weighed once per week. Weight was expressed as mean body weight for each experimental group, corrected for tumor mass in the tumor group (**Figure S1**). Tumor growth was measured every 3-4 days when tumors became palpable. Growth was expressed as mean tumor mass (in grams) over time (**Figure S2**). Calipers were used to measure tumor length, width, and depth, and hemi-ellipsoid tumor volume was calculated as $V = L \times W \times H \times 0.5236$ (Lein *et al*, 2000; Tomayko and Reynolds, 1989). To correct for tumor mass when measuring body weight, tumor volume was converted to mass, assuming soft-tissue density of 1 g/cm^3 (Jensen *et al*, 2008; Montelius *et al*, 2012). For these data, two-way repeated-measures ANOVA (group \times experimental days) were used to

analyze between-group effects, followed by Tukey's *post hoc* test for multiple comparisons.

Brain Metastases

Brain samples were first rinsed in HBSS to remove surface blood, and then minced using surgical scissors. The minced brains were dissociated in a filter-sterilized cocktail of 2 mg/mL collagenase type IV (Worthington Biochemical, Lakewood, NJ, USA) and 30 units of elastase (MP Biomedical, Santa Ana, CA, USA) in HBSS. Samples were incubated while mixing for 120 minutes at 37 °C, and then filtered through 70- μ m nylon cell strainers (Life Technologies) to remove any undigested tissue. Filtered samples were centrifuged and the supernatant discarded, and the resultant pellets were washed and centrifuged in HBSS 2 times. Following the final wash, pellets were resuspended in Iscove's Modified Dulbecco's Media (IMDM) supplemented with 10% FBS, 1% antibiotic/antimycotic (Life Technologies), and 60 μ M 6-TG (Sigma-Aldrich) and plated onto 10-cm tissue culture dishes. Dishes were incubated at 37 °C and 5% CO₂ for 10-14 days. Cells were then fixed in methanol and stained with 0.03% (w/v) methylene blue solution. Colonies were quantified for each dish, with each colony representing one clonogenic metastatic cell.

Serum Cytokines

Serum samples were diluted 2-fold in sterile PBS and 75 μ L of serum samples were sent to Eve Technologies (Calgary, AB, Canada) for cytokine quantification of IL-1 β , IL-6, IL-17A, and TNF- α . Eve Technologies uses Multiplexing LASER Bead Technology with each metabolite corresponding to a unique fluorophore signature. Capture antibodies are coupled with the metabolite's particular beads and a bead analyzer (Bio-Plex 200) is used to quantify the metabolite.

Supplemental Figures

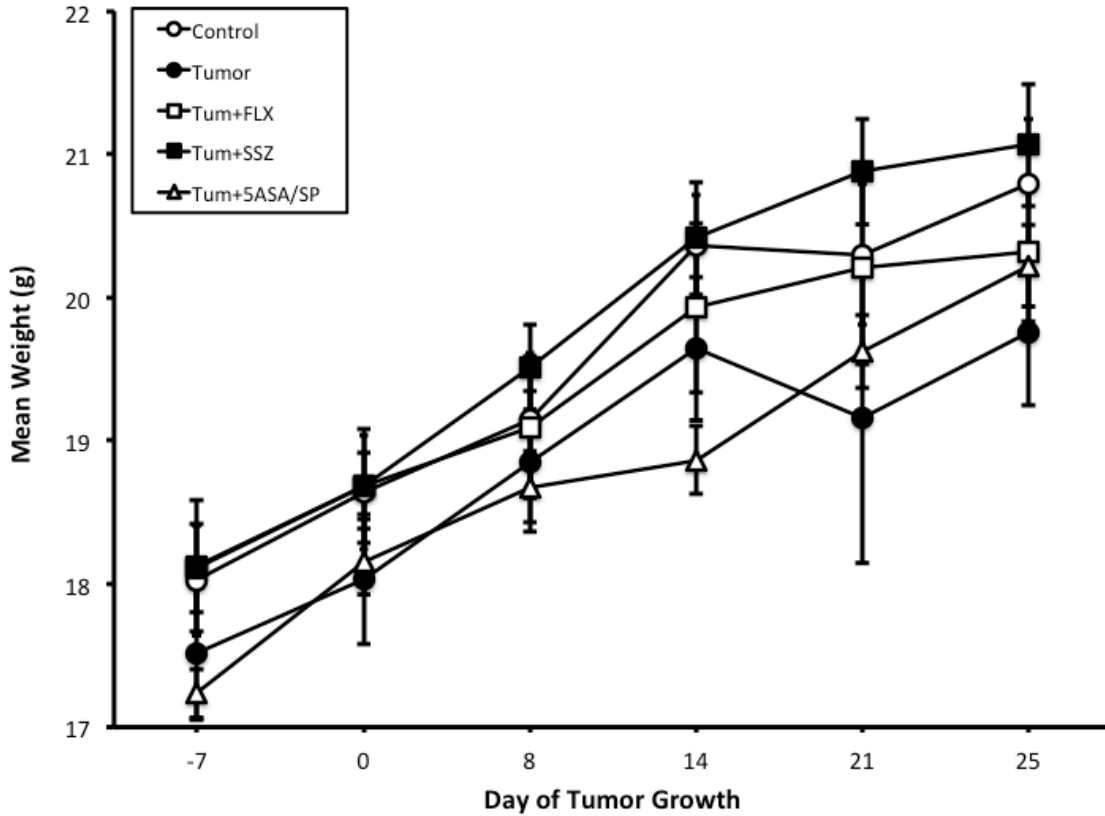


Figure S1. Mean body weight of mice in the 5 experimental groups (Control, n = 11; Tumor, n = 12; Tum+FLX, n = 12; Tum+SSZ; n = 12, Tum+5-ASA/SP, n = 12). Data are presented for the duration of tumor growth and weights were corrected for tumor mass. Data are expressed as mean \pm SEM. Two-way repeated-measures ANOVA with Tukey's *post hoc* test for multiple comparisons were used to analyze group differences over time. None of the groups at any time point revealed significant differences in (corrected) weight.

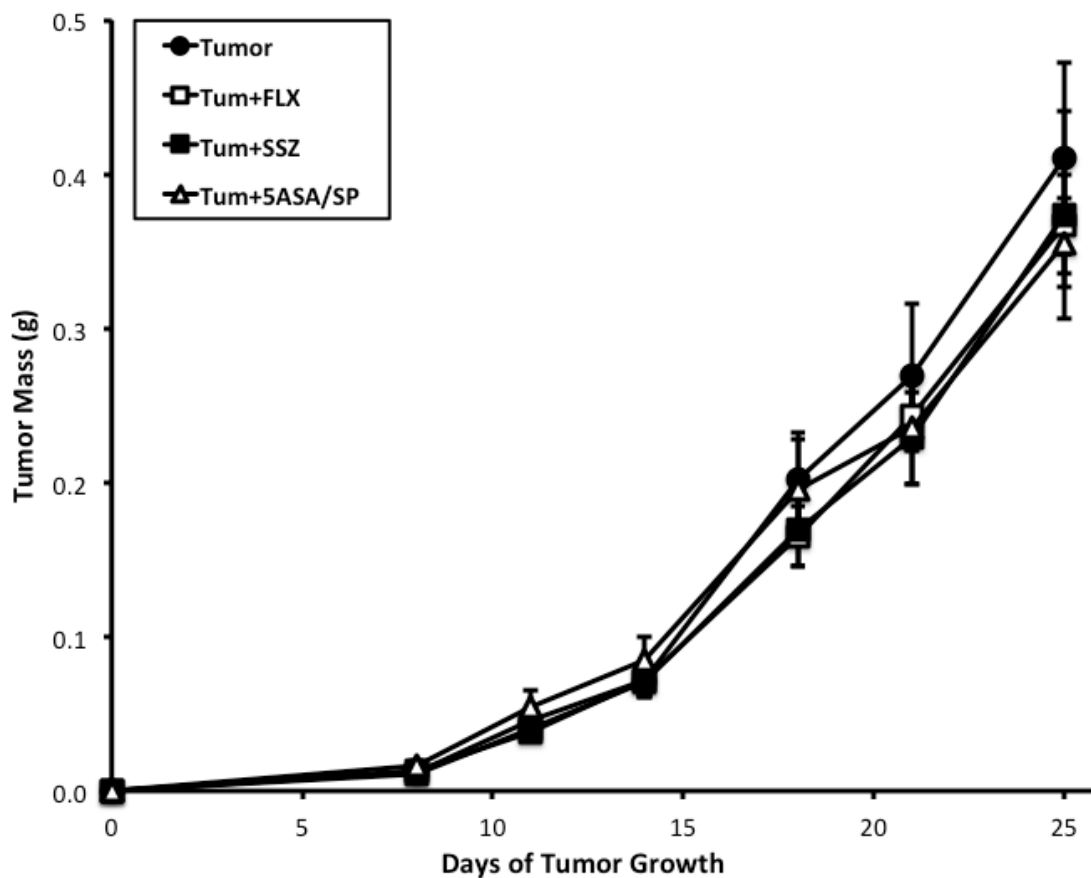


Figure S2. Tumor growth in mice subcutaneously inoculated with 15,000 4T1 mammary carcinoma cells (Tumor, $n = 12$; Tum+FLX, $n = 12$; Tum+SSZ, $n = 12$, Tum+5-ASA/SP, $n = 12$). Tumor growth pattern was exponential and tumor mass reached a cumulative mean of 0.38 ± 0.02 g by day 26 of tumor growth. Data are expressed as mean \pm SEM. Two-way repeated-measures ANOVA with Tukey's post hoc test for multiple comparisons were used to analyze group differences over time. None of the groups at any time point revealed significant differences in tumor size.

References

- Jensen MM, Jorgensen JT, Binderup T, Kjaer A (2008). Tumor volume in subcutaneous mouse xenografts measured by microCT is more accurate and reproducible than determined by 18F-FDG-microPET or external caliper. *BMC medical imaging* **8**: 16.
- Lein M, Jung K, Le DK, Hasan T, Ortel B, Borchert D, *et al* (2000). Synthetic inhibitor of matrix metalloproteinases (batimastat) reduces prostate cancer growth in an orthotopic rat model. *The Prostate* **43**(2): 77-82.
- Montelius M, Ljungberg M, Horn M, Forssell-Aronsson E (2012). Tumour size measurement in a mouse model using high resolution MRI. *BMC medical imaging* **12**: 12.
- Tomayko MM, Reynolds CP (1989). Determination of subcutaneous tumor size in athymic (nude) mice. *Cancer chemotherapy and pharmacology* **24**(3): 148-154.

CHAPTER 4

RNA-sequencing profiles hippocampal gene expression in a validated mouse model of cancer-induced depression

Mina G. Nashed, Katja Linher-Melville, Benicio N. Frey, Gurmit Singh

Submitted to: *Translational Psychiatry*

Preface

In this chapter, an author-generated version of the manuscript entitled “RNA-sequencing profiles hippocampal gene expression in a validated mouse model of cancer-induced depression”, prepared for submission February 2016 to *Neuro-Oncology*, is presented. The submission number for this manuscript is N-O-D-16-00153. As this is a manuscript in submission, no copyright license documentation is required.

For this paper, I performed the hippocampal excisions, aided in RNA extraction, and performed the analyses for qRT-PCR, RNA-seq, and gene enrichment. Furthermore, I created all of the figures, tables, and both wrote and revised the manuscript. Katja Linher-Melville performed RNA extraction, qRT-PCR, aided in qRT-PCR analysis, and revised the manuscript. RNA samples were sent to Farncombe Metagenomics Facility (McMaster University) for sequencing. Dr. Benicio Frey and Dr. Gurmit Singh provided intellectual direction and revised the manuscript. Please note that American spellings are used throughout the article, as required by the journal.

Context and Background Information

In Chapter 2, a validated pre-clinical model of cancer-induced depression (CID) is presented. This model was validated by comparison to an established model of a stress-induced depressive state, which was induced by chronic oral administration of corticosterone (CORT). In the present chapter, hippocampi were

excised from naïve, CORT, and CID mice. RNA was then extracted and sequenced for analysis of differential gene expression. This represents the first efforts into investigating CID as a distinct form of depression at the basic level. The primary purpose of this study was to assess hippocampal similarities and differences between the CORT and CID models at the level of gene expression, and incite further mechanistic studies and development of novel treatment targets for CID.

RNA sequencing (RNA-seq) results were validated by quantitative real-time reverse transcription polymerase chain reaction (qRT-PCR). Differential expression analysis identified a large overlap of differentially expressed genes (DEGs) between the CORT and CID models. This was the first instance in which genetic alterations that are associated with depression in a relevant brain region have been demonstrated in a cancer model. Enrichment analyses for biological pathways and terms further revealed that these alterations were related to ion homeostasis and neuronal communication. The CID model was associated with additional DEGs that were not identified for the CORT model. These DEGs were enriched in pathways and terms relating to neuronal development, intercellular signalling cascade, learning, and memory. It is, therefore, plausible that CID represents a distinct form of depression, which has some degree of overlapping pathophysiology with non-cancer-related depression. Further validation of the hippocampal alterations at the protein activity level is warranted. Knockdown models and pharmacological interventions would be valuable tools in establishing

causal relationships between the alterations in hippocampal gene expression and a depressive phenotype.

RNA-Sequencing Profiles Hippocampal Gene Expression in a Validated Mouse Model of Cancer-Induced Depression

^{1,2}Mina G. Nashed, M.Sc.; ^{1,2}Katja Linher-Melville, Ph.D.; ^{3,4}Benicio N. Frey, M.D., Ph.D.; ^{1,2}Gurmit Singh, Ph.D.*

¹Department of Pathology & Molecular Medicine, McMaster University, Hamilton, ON, L8N 3Z5, Canada

²Michael G. DeGroot Institute for Pain Research and Care, McMaster University, Hamilton, ON, L8N 3Z5, Canada.

³Department of Psychiatry and Behavioural Neurosciences, McMaster University, Hamilton, ON, L8N 3Z5, Canada.

⁴Mood Disorders Program and Women's Health Concerns Clinic, St. Joseph's Healthcare Hamilton, ON, L8P 3P6, Canada.

Running Title: RNA-Seq in a Model of Cancer-Induced Depression

*** Corresponding author.**

Address: Department of Pathology & Molecular Medicine, McMaster University, 1280 Main Street West, Hamilton, ON L8N 3Z5, Canada.

Tel.: +1 905 525 9140x28144.

E-mail address: singhg@mcmaster.ca

URL: <http://www.singhlab.ca>

Funding

This project was funded by operating grants from the Canadian Institutes of Health Research (CIHR) and the Canadian Breast Cancer Foundation (CBCF).

Conflict of Interest

Dr. Frey has received grant/research support from Alternative Funding Plan Innovations Award, Eli Lilly, and Pfizer, and has received consultant and/or speaker fees from AstraZeneca, Bristol-Myers Squibb, Lundbeck, Pfizer, Servier and Sunovion. Other authors declare no competing financial interest.

Abstract

Background: To investigate the pathophysiology of cancer-induced depression (CID), we have recently developed a validated CID mouse model. Given that the efficacy of antidepressants in cancer patients is controversial, it remains unclear whether CID is a biologically distinct form of depression.

Methods: We used RNA-sequencing (RNA-seq) to investigate differentially expressed genes (DEGs) in hippocampi of animals from our CID model relative a positive control model of depressive-like behaviour induced with chronic corticosterone (CORT). To validate RNA-seq results, we performed quantitative real-time RT-PCR (qRT-PCR) on a subset of DEGs. Enrichment analysis using DAVID was performed on DEGs to identify enriched KEGG pathways and biological process gene ontologies (GO:BP).

Results: qRT-PCR results significantly predicted RNA-seq results. RNA-seq revealed that most DEGs identified in the CORT model overlapped with the CID model. Enrichment analyses identified KEGG pathways and GO:BP terms associated with ion homeostasis and neuronal communication for both the CORT and CID model. In addition, CID DEGs were enriched in pathways and terms relating to neuronal development, intracellular signalling, learning, and memory.

Conclusion: This study is the first to investigate CID at the mRNA level. We have shown that most hippocampal mRNA changes that are associated with a depressive-like state are also associated with cancer. Several other changes occur

at the mRNA level in cancer, suggesting that the CID model may represent a biologically distinct form of a depressive-like state.

Introduction

Gene expression profiling has long been an integral aspect of cancer research. Techniques such as DNA-microarray analysis continue to provide significant insights into aspects related to cancer diagnosis, prognosis, and treatment¹⁻⁴. However, these techniques have not been applied to investigate the impact of cancer on neurological processes. Expression profiling is also becoming increasingly prevalent in the study of psychiatric disorders. In major depressive disorder (MDD), gene expression changes may be specific to brain regions that are known to be impacted by depression, such as the prefrontal cortex, hippocampus, amygdala, anterior cingulate cortex, and striatum. In the hippocampus, microarray studies have identified downregulation of NF- κ B signalling, upregulation of the γ -aminobutyric acid (GABA)-ergic gene *MARLIN1* (Multiple coiled-coil GABABR1-binding protein), glutamate AMPA receptor subunits, and genes involved in calcium signalling (e.g. *SYT4*), as well as expression changes in second messenger systems⁵⁻⁷. Furthermore, other genetic analyses on MDD patients and suicide victims have demonstrated impaired hippocampal brain-derived neurotrophic factor (BDNF) signalling⁸, downregulation of glucocorticoid receptors⁹ and synapsin¹⁰, as well as expression changes in serotonergic signalling¹¹.

While microarrays remain relevant and are widely used, they have several inherent limitations¹². One limitation is the requirement of *a priori* knowledge of the genome under investigation, with incomplete, incorrect, or out-dated genome

annotations affecting result quality. Cross-hybridization between similar sequences can also affect the results, and the reliance on reverse transcription polymerase chain reaction (RT-PCR) to produce a sufficient quantity of cDNA (micrograms) introduces additional bias. In addition, microarrays are semi-quantitative and report only relative expression levels, making it difficult to detect differential expression in low-abundance sequences relative to background noise. High-abundance sequences can also be difficult to quantify due to signal saturation. Next-generation sequencing (NGS), which is becoming more widely available to researchers due to recent decreases in cost, addresses many of these limitations inherent to microarrays¹². NGS directly sequences starting material (nanograms), making it much more sensitive for detecting low and high-abundance sequences, as well as allowing for the detection of novel sequences without *a priori* knowledge of the genome. Due to these advantages, NGS techniques, such as RNA sequencing (RNA-seq), are being more frequently utilized in profiling studies for numerous pathologies, including cancer¹³ and psychiatric disorders¹⁴⁻¹⁶. However, we found only one study that used RNA-seq to investigate hippocampal gene expression in depression. This study identified microRNA 182 (miR-182) signalling to be disrupted in postmortem hippocampal dentate gyrus granule cells of patients with MDD¹⁴.

Depression is disproportionately prevalent in cancer patients, and can negatively impact both quality of life and survivorship^{17,18}. Despite inconsistent clinical evidence, modern antidepressants such as selective serotonin reuptake

inhibitors (SSRIs) remain the primary therapy for cancer-induced depression (CID)¹⁹⁻²². To investigate the pathophysiology of CID, we have recently developed and validated a mouse model of CID using subcutaneous inoculation of 4T1 mammary carcinoma cells in BALB/c mice²³. This model was validated against a positive control model for depressive-like behaviour induced by chronic administration of corticosterone (CORT). In order to further explore the cerebral molecular mechanisms involved in CID, here we investigated hippocampal gene expression profiles of the CID and CORT models relative to naïve animals using next-generation RNA-seq, and validated the results using quantitative real-time RT-PCR (qRT-PCR). To contextualize the data obtained from RNA-seq, we performed enrichment analyses on DEGs to identify enriched biological process gene ontologies (GO:BP)^{24,25}, as well as enriched Kyoto Encyclopedia of Genes and Genomes (KEGG) pathways^{26,27}.

To our knowledge, this is the first investigation to assess central transcriptional alterations induced by peripheral cancer. This study is also among only a few that have applied NGS technology to investigate transcriptional alterations associated with a depressive-like state. Here, we report that there was a significant overlap of DEGs identified for both depressive models. Interestingly, additional DEGs, as well as KEGG pathways and GO:BP terms, were specifically associated with the CID model, and we therefore posit that clinical CID may represent a biologically distinct form of depression. Further delineation of the

mechanisms underlying this specific depressive-like state could facilitate the development of more specific CID pharmacotherapies.

Materials and Methods

Mice

Female BALB/c mice, which were previously randomized into three experimental groups to develop a validated mouse model of CID²³, were included in the present study. The groups were naïve control, chronic oral CORT (positive control for depressive-like state), and CID. Mice in the CORT group were exposed to a 35 µg/mL solution of CORT *ad libitum* for 21 days. Mice in the CID group were inoculated subcutaneously with 15,000 4T1 mammary carcinoma cells in serum-free RPMI 1640 media just above their right flank. Mice were euthanized after 28 days of tumour growth. Naïve mice received sham inoculations of serum-free RPMI 1640 media. For the current investigation, hippocampi from six mice in each group were excised, and RNA was extracted. All animal procedures were performed according to guidelines established by the Canadian Council on Animal Care under a protocol reviewed and approved by the *Animal Research Ethics Board* of McMaster University.

Tissue Collection

Mice subcutaneously inoculated with 4T1 mammary carcinoma cells were sacrificed at day 71 of the previously described experiment²³, brains from all groups of animals were harvested, immediately placed into RNAlater RNA Stabilization Reagent (Ambion, Waltham, MA, USA), and stored at -80°C.

Hippocampi were extracted via brain microdissection under a stereoscopic microscope.

RNA Isolation

Total RNA was isolated from each sample using the RNeasy Kit (Qiagen, Hilden, Germany) using 18-gauge needles fitted to a 1cc syringe to completely dissociate the hippocampi. Eluates were DNase-treated using the DNA-free Kit (DNase Treatment and Removal Reagents; Ambion, Waltham, MA, USA). Following spectrophotometric analysis, 40 ng of total RNA were subjected to RNA-seq, with remaining RNA samples stored at -80°C.

RNA-Sequencing

RNA samples were sent to the Farncombe Metagenomics Facility (McMaster University, Ontario, Canada) for RNA sequencing. The quality of RNA was assessed using the RNA 6000 Nano kit on a 2100 Bioanalyzer instrument (Agilent Technologies, Santa Clara, CA, USA). A RNA library was prepared using the NEBNext Ultra Directional RNA Library Prep Kit for Illumina and poly-A mRNA was enriched using the NEBNext Poly(A) mRNA Magnetic Isolation Module (New England Biolabs, Ipswich, MA, USA). Libraries were sequenced on two lanes of the Illumina HiSeq 1500 platform using the HiSeq Rapid V2 chemistry with onboard cluster generation and 70 bp single-end reads (Illumina, San Diego, CA, USA). To mitigate lane effects, each biological

replicate was split between two lanes and the reads were later combined for analysis.

Quantitative Real-Time RT-PCR

Total RNA was reverse transcribed into cDNA using the SuperScript III kit (Life Technologies, Waltham, MA, USA).

Nine target DEGs were selected for relative qRT-PCR analysis using SYBR Green premix (Takara Bio, Kyoto, Japan) to validate the results derived from RNA-seq. All target and housekeeping gene primers based on sequences specific for *Mus musculus* were derived from PrimerBank (<http://pga.mgh.harvard.edu/primerbank/index.html>), with annealing temperatures of 60°C. Official gene symbols, primer sequences, product sizes, and specific melting peaks for each target gene product are listed in supplementary **Table S1**. The specifications of the three housekeeping genes used in this study are summarized in supplementary **Table S2** [Polr2b: polymerase (RNA) II (DNA directed) polypeptide B; Sdha: succinate dehydrogenase complex, subunit A; Taf1b: TATA box binding protein (Tbp)-associated factor, RNA polymerase I, B]. A MiniOpticon 48-well Real-Time PCR System linked to CFX Manager software (BioRad Hercules, CA, USA) was utilized to carry out duplicate target gene amplifications for each cDNA sample in parallel to duplicate housekeeping gene reactions. Housekeepers were selected based on stringent efficiency testing by evaluating the slopes derived from plotting the log of a 2-fold serial dilution of

murine brain cDNA (template) versus the C_T of each target gene compared to each housekeeper. A further test was carried out by plotting ΔC_T values (target C_T at each template dilution minus housekeeper C_T at the equivalent dilution) across the dilution series. Amplification efficiencies were tested for each primer pair, with efficiency (E) = $[10 \text{ raised to } (-1/S)] - 1$. The integrity of each product was verified by gel electrophoresis.

Data Analyses

RNA-sequencing

RNA-seq data was analyzed using the Tuxedo protocol, as described previously²⁸. The Galaxy Project, a web-based platform for biomedical data analysis, was used to perform several of the steps outlined in the Tuxedo protocol²⁹⁻³¹. Briefly, the sequencing quality of the FASTQ files was evaluated using the FastQC tool (<http://www.bioinformatics.babraham.ac.uk/projects/fastqc/>). This identified overrepresented sequences corresponding with remnant index sequences, which were removed by inputting index sequences into the FASTX Clip tool (http://hannonlab.cshl.edu/fastx_toolkit/). Tophat was then used to align reads from individual biological replicates to the GRCm38/mm10 assembly. Cufflinks was used to create assembled transcripts, which were combined with the corresponding GRCm38/mm10 reference transcriptome annotation using Cuffmerge to create a transcriptome assembly. Cuffdiff was used to assess transcript abundance (in Fragments Per Kilobase of transcript per Million mapped

reads: FPKM) and differential gene expression by merging the transcriptome assembly with the individual aligned reads created by Tophat. The false discovery rate (FDR) adjusted p -value (i.e. q -value) was set to less than 0.05.

The Bioconductor package CummeRbund was used to visualize Cuffdiff output files in RStudio version 0.99.467³²⁻³⁴. This platform was used to create scatter and volcano plots for each pairwise comparison, as well as an expression level plot and heatmap comparing all 3 experimental groups. EulerAPE version 3 was used to produce a Venn diagram to visualize the overlap of DEGs between pairwise comparisons³⁵.

Quantitative Real-Time RT-PCR

qRT-PCR data was analyzed using the $2^{-\Delta\Delta C_T}$ method³⁶. For each of the 9 selected target genes, the mean ΔC_T for the 6 biological replicates in each group being compared was calculated as the mean C_T of the target gene minus the mean C_T of the appropriate housekeeping gene. For each pairwise comparison, $\Delta\Delta C_T$ was then calculated as the mean ΔC_T of the non-control group minus the ΔC_T of the control group, and the resulting $\Delta\Delta C_T$ value was converted to $2^{-\Delta\Delta C_T}$, representing fold-change. In all pairwise comparisons, fold-changes were calculated relative to the control group. In the comparison between CORT and CID, the CORT group was used as the control. To determine the overall experimental standard error of mean (SEM), SEMs derived from the ΔC_T values were used to calculate upper and lower values of $2^{-\Delta\Delta C_T}$. This resulted in a final

SEM asymmetrically distributed around the mean $2^{-\Delta\Delta C_T}$ as a consequence of converting data derived from an exponential process into a linear representation³⁶.

The 9 selected target DEGs were represented across 12 pairwise comparisons, due to some genes being differentially expressed in more than one comparison. For each pairwise comparison, results from qRT-PCR were graphically represented alongside the corresponding fold-changes derived from RNA-seq, which were calculated based on reported FPKM values. FPKM values were not log-transformed because both $2^{-\Delta\Delta C_T}$ fold-changes and FPKM are approximately log-normally distributed²⁸, whereas ΔC_T and $\log_{10}(\text{FPKM})$ are approximately normally distributed. Therefore, the appropriate comparison of $2^{-\Delta\Delta C_T}$ fold-changes is untransformed FPKM. In addition, linear regression was used to test the concordance between qRT-PCR and RNA-seq results, with α set to 0.05³⁷. The regression analysis was performed using SPSS Statistics Version 22 (IBM, Armonk, NY, USA). All graphs were prepared on Microsoft Excel 2011 version 14.1.0 (Microsoft, Redmond, WA, USA).

Enrichment

Ontological and KEGG pathway enrichment analyses were performed using DAVID, an online bioinformatics tool for functional interpretation of gene sets^{38,39}. For each pairwise comparison, the list of DEGs was imported into DAVID's "functional annotation" tool, with *Mus musculus* selected as the reference species. Enriched KEGG pathways and GO:BP terms were identified

with the Expression Analysis Systematic Explorer (EASE) threshold (maximum EASE score/p-value) set to a default of 0.1. The EASE score is a modified Fisher Exact test score utilized by DAVID to identify significant gene enrichment. Fold-enrichment was also reported, representing the ratio of the proportion of input genes in a list of DEGs relative to the number of genes that term or pathway represents within the reference mouse genome⁴⁰. KEGG pathways or GO:BP terms with fold-enrichment below 2 were excluded.

Network visualizations for each pairwise list of DEGs were performed using Cytoscape, a bioinformatics software package⁴¹. Biological function of genes is strongly related to their co-expression⁴², and the GeneMANIA app in Cytoscape was used to construct gene co-expression networks using the following parameters: networks = co-expression, network weighting = gene ontology biological process based, number of related genes displayed = 0⁴³. Node fill color was set to reflect gene expression fold-changes from RNA-seq results and node border color was used to identify genes of KEGG pathways. GO:BP results were visualized separately from the networks and displayed as bar graphs of fold-enrichment for each term.

Results

RNA-sequencing

Three pairwise comparisons of differential gene expression were performed using RNA-seq, namely control vs. CORT, control vs. CID, and CORT vs. CID, with each group consisting of 6 biological replicates. On average, samples yielded 1073 ± 427 Mbases (range: 642 – 2590 Mbases), and 15.3 ± 6.1 million reads (range: 9.1 – 37.0 million reads). Mean coverage was computed using the Lander/Waterman equation ($C = LN/G$), where C denotes coverage, G denotes genome length (or transcriptome length for RNA-seq), L denotes average read length, and N denotes the average number of reads⁴⁴. Galaxy was used to derive the total length of annotated transcripts. The Base Coverage tool in Galaxy (<https://toolshed.g2.bx.psu.edu/view/devteam/basecoverage/b8a9e718caa3>) was executed on the most recent mouse genome assembly (GRCm38/mm10: December 2011 *Mus musculus* assembly). The resultant transcriptome length was used to compute coverage as follows: $C = (70 \text{ bp} \times 15.3 \text{ million reads}) / (80.6 \text{ Mbp}) = 13.3\times$. This indicates that, on average, each transcript base was sequenced approximately 13 to 14 times.

Figure 1 provides a visual representation of individual gene data in each pairwise comparison. Scatter plots (**Figure 1 A**) highlight the overall gene expression similarities and differences between the two conditions within each comparison. Volcano plots (**Figure 1 B**) highlight genes that were differentially

expressed in each comparison by plotting $-\log_{10}(p\text{-value})$ against $\log_2(\text{fold-change})$ of individual genes. **Figure 2** visually summarizes differential gene expression patterns between all 3 groups. The density plot (**Figure 2 A**) illustrates expression level distribution. Sections on the plot where groups do not overlap represent differential expression. The Venn diagram (**Figure 2 B**) further characterizes differential gene expression for each pairwise comparison, showing the number of shared DEGs between comparisons. A total of 68 DEGs were identified in the control vs. CORT comparison, 170 in the control vs. CID comparison, and 82 in the CORT vs. CID comparison. Forty-six of the 68 DEGs identified in the control vs. CORT comparisons were also identified in the control vs. CID comparison. Fifty out of the 170 DEGs identified in the control vs. CID comparison were also identified in the CORT vs. CID comparison. The heatmap (**Figure 2 C**) provides a visual representation of the expression level [in $\log_{10}(\text{FPKM}+1)$] for all DEGs across the 3 groups. A full list of DEGs identified for each pairwise comparison is included in supplementary **Table S3**.

Quantitative Real-Time RT-PCR

Nine genes, covering 12 pairwise comparisons, were selected for qRT-PCR analysis to validate the RNA-seq results. It is noteworthy that most DEGs identified by RNA-seq were characterized by moderate downregulation; thus 7 of the 12 qRT-PCR validations were performed on moderately downregulated genes with fold-changes near 0.7. In addition, 2 validations were performed on highly downregulated genes, 1 on a moderately upregulated gene, and 2 on highly

upregulated genes. Therefore, validation with qRT-PCR covered a large range of differential expression levels across all 3 pairwise comparisons. **Figure 3** illustrates each of the pairwise qRT-PCR validations compared to RNA-seq-derived fold-changes. In all cases, data represent the mean of 6 biological replicates, with error bars indicating SEM. qRT-PCR mean fold-changes in gene expression were consistent with those derived from RNA-seq. Linear regression analysis revealed that qRT-PCR results significantly predicted RNA-seq results ($F = 147.7$, $R^2 = 0.937$, $p < 0.001$) (**Figure 4**).

Enrichment Analyses

Co-expression networks of DEGs from each pairwise comparison were constructed using the GeneMania application in Cytoscape (**Figure 5 A**). Node fill colors indicate that most genes across comparisons were downregulated relative to the control. Results from KEGG pathway enrichment analysis, performed using DAVID, are indicated on the networks using node border colors. This analysis revealed 3 enriched pathways in the control vs. CORT comparison, namely calcium signalling, neuroactive ligand-receptor interaction, and nitrogen metabolism. Nine pathways were enriched in the control vs. CID comparison, namely MAPK signalling, calcium signalling, neuroactive ligand-receptor interaction, vascular smooth muscle contraction, Alzheimer's disease, GnRH signalling, phosphatidylinositol signalling, long-term potentiation, and long-term depression. Neuroactive ligand-receptor interaction was also enriched in all 3

comparisons, with common genes downregulated in CORT and CID relative to control, and to a greater degree in CID relative to CORT.

Analysis of GO:BP revealed 22 enriched terms for the control vs. CORT DEGs (**Figure 5 B**). These terms were mostly related to ion transport, chemical homeostasis, cellular communication and neurotransmission, and regulation of heart rate. Sixty-six terms were enriched for the control vs. CID DEGs. These terms were related to ion transport, chemical homeostasis, cellular communication and neurotransmission, neuronal development and ensheathment, erythrocyte development, intracellular signalling cascade, oxygen transport, and locomotion. Thirty-six terms were enriched for the CORT vs. CID DEGs. These terms were related to chemical homeostasis, cellular communication and neurotransmission, neuronal development and ensheathment, lipid metabolism, inflammation, kinase activity, and cell adhesion.

Discussion

Structural neuroimaging studies on patients with MDD have consistently demonstrated volume reductions in cortical and subcortical brain regions^{45,46}. In particular, data on more than 1700 MDD patients from the ENIGMA consortium revealed significantly reduced hippocampal volumes relative to more than 7000 healthy controls⁴⁷. Moreover, regional brain volume reductions may be attenuated with antidepressant therapy⁴⁸. Functional neuroimaging has similarly demonstrated abnormal hippocampal and prefrontal cortical (PFC) activation in individuals with MDD⁴⁹. In a recent study on a mouse model of CID, we found reduced basilar and apical dendritic branching in the medial PFC (mPFC) of CORT and CID mice compared with naïve controls²³. In the present study, we utilized the previously excised hippocampi from those same mice and extracted RNA to investigate differential gene expression across models. RNA-seq was then performed on hippocampal RNA using carefully selected parameters to ensure sufficient sensitivity for the detection of DEGs. It has recently been shown that increasing the number of biological replicates has a greater impact on the power of detecting DEGs than increasing the number of reads beyond 10 million⁵⁰. Therefore, including 6 biological replicates in each group with a mean of 15.3 million reads per replicate provided sufficiently powerful detection of DEGs in the present study.

We have employed 3 pairwise comparisons to explore the pathophysiology of CID. To establish transcriptional changes related to a non-cancer depressive-like

state, naïve control mice were compared with a positive control model induced by chronic administration of CORT. To explore transcriptional changes related to CID, the same naïve control mice were compared with our CID model. Finally, to directly investigate differences between the two depressive models, the CORT model was compared with the CID model. We found that most DEGs identified in the control vs. CORT comparison were also identified in the control vs. CID comparison. However, considerably more DEGs were identified in the control vs. CID comparison, which were not identified in the control vs. CORT comparison (Figure 2). Importantly, these findings alone suggest a substantial overlap in hippocampal changes associated with both depressive models, in addition to other changes that appear to be specific to the CID model. This may be an indication that clinical CID is biologically distinct from primary depression at the level of central transcriptional modifications. To validate the results obtained from RNA-seq, DEGs from 12 comparisons covering a wide range of expression fold-changes were analyzed by qRT-PCR. Results from this analysis revealed consistent gene fold-changes between the two methodologies, and qRT-PCR significantly predicted RNA-seq results (Figures 3 & 4).

Previous gene expression studies have identified DEGs relating to neurodevelopmental processes and neurotransmission in *postmortem* hippocampi of individuals with depression and suicide⁵⁻⁷. In the present study, GO:BP terms relating to these processes were enriched in both depressive models. As previously mentioned, the GABAergic gene *MARLIN1* and *GRIA2* (AMPA

receptor subunit 2) have been found to be upregulated in the hippocampi of patients with MDD and suicide victims^{6,7}. Our results show downregulation of hippocampal *Grm4* (metabotropic glutamate receptor 4) and *Grin2c* [N-methyl-D-aspartate (NMDA) receptor NR2C subunit] in both depressive models. We also observed hippocampal downregulation of *Gabrd* (GABA_A receptor δ subunit) in the CORT model, and downregulation of *Gabra3* (GABA_A receptor α -3 subunit) and *Gria4* (AMPA receptor subunit 4) in the CID model. In both depressive models, further investigation into glutamatergic dysregulation may be particularly relevant given the proposed role of glutamate signalling in the pathophysiology of depression^{51,52} and the fast-acting antidepressant effect of NMDA receptor antagonists such as ketamine^{53,54}. To our knowledge, specific hippocampal knockdowns of the genes identified in this study have not been investigated. However, consistent with the observed downregulation of *Gabrd* in the CORT model, there is evidence to suggest that pregnancy-related deficiency in hippocampal GABA_A receptor δ subunit is associated with postpartum depression⁵⁵. Furthermore, AMPA receptor subunit 1 knockout mice exhibit depressive-like behaviours⁵⁶. This might be particularly relevant for the CID model, which exhibited hippocampal downregulation of *Gria4*, whereas the CORT model did not show altered AMPA signalling in this study.

In addition to coding RNA, both depressive models were associated with downregulation of microRNA (miRNA) 568, and CORT was associated with upregulation of miRNA 8109. Although these miRNAs have yet to be

functionally annotated, a whole-miRNome investigation may help to better characterize transcriptional changes associated with CID, particularly in light of recent results implicating microRNA dysregulation in the hippocampi of patients with MDD¹⁴. In addition, a recent whole-miRNome study identified 30 differentially expressed miRNAs in the blood of MDD patients after antidepressant administration⁵⁷. Interestingly, KEGG pathways identified for those miRNAs included neuroactive ligand-receptor interaction, long-term potentiation, and long-term depression, which we have also identified as enriched KEGG pathways in the present CID model.

CID was associated with alterations in biological processes of interest beyond what was observed with the CORT model. For example, we observed an enriched set of DEGs involved in MAPK signalling, similar to a previous RNA-seq study reporting MAPK dysregulation in the ventral tegmental area of mouse models of emotional and physical stress¹⁶. We also observed DEGs in phosphatidylinositol signalling, which, along with MAPK signalling, act downstream of brain-derived neurotrophic factor (BDNF) activation, a key pathway for neuroplasticity widely implicated in the pathophysiology of MDD⁵⁸. DEGs relating to Alzheimer's disease, long-term potentiation, and long-term depression were also associated with our CID model. This may suggest a role for memory and learning impairment in the neurobiology of CID.

This study identified novel pathways that are potentially involved in the neurobiology of CID. It remains possible that not all transcriptional modifications

are causally related to the induced depressive-like state. Validation with hippocampus-specific knockdown studies and pharmacological manipulations of pathways identified here would be required to firmly establish causality. However, since cancer cell inoculation is the sole initiating event in the CID model, we strongly suspect that the DEGs and pathways identified in this study are causally linked to the observed depressive-like behaviours. This is supported by the large overlap of DEGs between the CID model and the positive control CORT model. Furthermore, pathways relating to learning and memory that were specific to CID are supported by clinical results, which implicate cognitive impairment in a subset of patients with depression⁵⁹ and cancer⁶⁰.

Transcriptional changes leading to altered mRNA levels do not necessarily reflect alterations in protein activity⁶¹. Therefore, DEGs and pathways identified in this study should be validated through proteomics.

This study represents the first efforts to identify central transcriptional alterations associated with a model of CID as distinct from a stress-induced depressive-like state. We have shown that cancer induces downregulation of hippocampal genes involved in neuronal communication and ion homeostasis that are similarly downregulated by CORT. In addition, CID was associated with additional transcriptional alterations related to memory, intracellular signalling cascade, locomotion, and neuronal development. Intervention studies through pharmacology, as well as proteomics, are needed to further characterize the molecular pathways of CID.

Acknowledgements

The authors would like to thank Dr. Meghan Verschoor for her input regarding the enrichment analyses of differentially expressed genes. Experiments in this study were completed as part of the doctoral thesis of M.G.N.

Funding

This project was funded by operating grants from the Canadian Institutes of Health Research (CIHR) and the Canadian Breast Cancer Foundation (CBCF).

Conflict of Interest

Dr. Frey has received grant/research support from Alternative Funding Plan Innovations Award, Eli Lilly, and Pfizer, and has received consultant and/or speaker fees from AstraZeneca, Bristol-Myers Squibb, Lundbeck, Pfizer, Servier and Sunovion. Other authors declare no competing financial interest.

References

1. Bos PD, Zhang XH, Nadal C, et al. Genes that mediate breast cancer metastasis to the brain. *Nature*. 2009; 459(7249):1005-1009.
2. Markert JM, Fuller CM, Gillespie GY, et al. Differential gene expression profiling in human brain tumors. *Physiological genomics*. 2001; 5(1):21-33.
3. Mischel PS, Cloughesy TF, Nelson SF. DNA-microarray analysis of brain cancer: molecular classification for therapy. *Nature reviews. Neuroscience*. 2004; 5(10):782-792.
4. Subramanian A, Tamayo P, Mootha VK, et al. Gene set enrichment analysis: a knowledge-based approach for interpreting genome-wide expression profiles. *Proceedings of the National Academy of Sciences of the United States of America*. 2005; 102(43):15545-15550.
5. Gao L, Gao Y, Xu E, Xie J. Microarray Analysis of the Major Depressive Disorder mRNA Profile Data. *Psychiatry Investig*. 2015; 12(3):388-396.
6. Sequeira A, Klempan T, Canetti L, et al. Patterns of gene expression in the limbic system of suicides with and without major depression. *Molecular psychiatry*. 2007; 12(7):640-655.
7. Sequeira A, Mamdani F, Ernst C, et al. Global brain gene expression analysis links glutamatergic and GABAergic alterations to suicide and major depression. *PloS one*. 2009; 4(8):e6585.

8. Egan MF, Kojima M, Callicott JH, et al. The BDNF val66met polymorphism affects activity-dependent secretion of BDNF and human memory and hippocampal function. *Cell*. 2003; 112(2):257-269.
9. DeRijk RH, Schaaf M, Stam FJ, et al. Very low levels of the glucocorticoid receptor beta isoform in the human hippocampus as shown by Taqman RT-PCR and immunocytochemistry. *Brain research. Molecular brain research*. 2003; 116(1-2):17-26.
10. Vawter MP, Thatcher L, Usen N, Hyde TM, Kleinman JE, Freed WJ. Reduction of synapsin in the hippocampus of patients with bipolar disorder and schizophrenia. *Molecular psychiatry*. 2002; 7(6):571-578.
11. Pang TY, Du X, Zajac MS, Howard ML, Hannan AJ. Altered serotonin receptor expression is associated with depression-related behavior in the R6/1 transgenic mouse model of Huntington's disease. *Human molecular genetics*. 2009; 18(4):753-766.
12. Hurd PJ, Nelson CJ. Advantages of next-generation sequencing versus the microarray in epigenetic research. *Brief Funct Genomic Proteomic*. 2009; 8(3):174-183.
13. LeBlanc VG, Marra MA. Next-Generation Sequencing Approaches in Cancer: Where Have They Brought Us and Where Will They Take Us? *Cancers (Basel)*. 2015; 7(3):1925-1958.

14. Kohen R, Dobra A, Tracy JH, Haugen E. Transcriptome profiling of human hippocampus dentate gyrus granule cells in mental illness. *Translational psychiatry*. 2014; 4:e366.
15. Lyddon R, Dwork AJ, Keddache M, Siever LJ, Dracheva S. Serotonin 2c receptor RNA editing in major depression and suicide. *The world journal of biological psychiatry : the official journal of the World Federation of Societies of Biological Psychiatry*. 2013; 14(8):590-601.
16. Warren BL, Vialou VF, Iniguez SD, et al. Neurobiological sequelae of witnessing stressful events in adult mice. *Biological psychiatry*. 2013; 73(1):7-14.
17. Litofsky NS, Farace E, Anderson F, Jr., Meyers CA, Huang W, Laws ER, Jr. Depression in patients with high-grade glioma: results of the Glioma Outcomes Project. *Neurosurgery*. 2004; 54(2):358-366; discussion 366-357.
18. Giese-Davis J, Collie K, Rancourt KM, Neri E, Kraemer HC, Spiegel D. Decrease in depression symptoms is associated with longer survival in patients with metastatic breast cancer: a secondary analysis. *Journal of clinical oncology : official journal of the American Society of Clinical Oncology*. 2011; 29(4):413-420.
19. Li M, Fitzgerald P, Rodin G. Evidence-based treatment of depression in patients with cancer. *Journal of clinical oncology : official journal of the American Society of Clinical Oncology*. 2012; 30(11):1187-1196.

20. Ng CG, Boks MP, Zainal NZ, de Wit NJ. The prevalence and pharmacotherapy of depression in cancer patients. *Journal of affective disorders*. 2011; 131(1-3):1-7.
21. Rodin G, Lloyd N, Katz M, et al. The treatment of depression in cancer patients: a systematic review. *Supportive care in cancer : official journal of the Multinational Association of Supportive Care in Cancer*. 2007; 15(2):123-136.
22. Williams S, Dale J. The effectiveness of treatment for depression/depressive symptoms in adults with cancer: a systematic review. *British journal of cancer*. 2006; 94(3):372-390.
23. Nashed MG, Seidlitz EP, Frey BN, Singh G. Depressive-like behaviours and decreased dendritic branching in the medial prefrontal cortex of mice with tumors: A novel validated model of cancer-induced depression. *Behavioural brain research*. 2015; 294:25-35.
24. Ashburner M, Ball CA, Blake JA, et al. Gene ontology: tool for the unification of biology. The Gene Ontology Consortium. *Nature genetics*. 2000; 25(1):25-29.
25. Gene Ontology Consortium. Gene Ontology Consortium: going forward. *Nucleic acids research*. 2015; 43(Database issue):D1049-1056.
26. Kanehisa M, Goto S. KEGG: kyoto encyclopedia of genes and genomes. *Nucleic acids research*. 2000; 28(1):27-30.

27. Kanehisa M, Goto S, Sato Y, Kawashima M, Furumichi M, Tanabe M. Data, information, knowledge and principle: back to metabolism in KEGG. *Nucleic acids research*. 2014; 42(Database issue):D199-205.
28. Trapnell C, Roberts A, Goff L, et al. Differential gene and transcript expression analysis of RNA-seq experiments with TopHat and Cufflinks. *Nature protocols*. 2012; 7(3):562-578.
29. Blankenberg D, Von Kuster G, Coraor N, et al. Galaxy: a web-based genome analysis tool for experimentalists. *Current protocols in molecular biology / edited by Frederick M. Ausubel ... [et al.]*. 2010; Chapter 19:Unit 19.10.11-21.
30. Giardine B, Riemer C, Hardison RC, et al. Galaxy: a platform for interactive large-scale genome analysis. *Genome research*. 2005; 15(10):1451-1455.
31. Goecks J, Nekrutenko A, Taylor J, Galaxy T. Galaxy: a comprehensive approach for supporting accessible, reproducible, and transparent computational research in the life sciences. *Genome biology*. 2010; 11(8):R86.
32. Gentleman RC, Carey VJ, Bates DM, et al. Bioconductor: open software development for computational biology and bioinformatics. *Genome biology*. 2004; 5(10):R80.
33. *cummeRbund: Analysis, exploration, manipulation, and visualization of Cufflinks high-throughput sequencing data*. [computer program]: R package version 2.10.0.; 2013.

34. *RStudio: Integrated Development for R* [computer program]. Boston, MA2015.
35. Micallef L, Rodgers P. eulerAPE: drawing area-proportional 3-Venn diagrams using ellipses. *PloS one*. 2014; 9(7):e101717.
36. Livak KJ, Schmittgen TD. Analysis of relative gene expression data using real-time quantitative PCR and the 2(-Delta Delta C(T)) Method. *Methods*. 2001; 25(4):402-408.
37. Zhen AW, Nguyen NH, Gibert Y, et al. The small molecule, genistein, increases hepcidin expression in human hepatocytes. *Hepatology (Baltimore, Md.)*. 2013; 58(4):1315-1325.
38. Huang da W, Sherman BT, Lempicki RA. Systematic and integrative analysis of large gene lists using DAVID bioinformatics resources. *Nature protocols*. 2009; 4(1):44-57.
39. Huang da W, Sherman BT, Lempicki RA. Bioinformatics enrichment tools: paths toward the comprehensive functional analysis of large gene lists. *Nucleic acids research*. 2009; 37(1):1-13.
40. Verschoor ML, Verschoor CP, Singh G. Ets-1 global gene expression profile reveals associations with metabolism and oxidative stress in ovarian and breast cancers. *Cancer & metabolism*. 2013; 1(1):17.
41. Shannon P, Markiel A, Ozier O, et al. Cytoscape: a software environment for integrated models of biomolecular interaction networks. *Genome research*. 2003; 13(11):2498-2504.

42. Stuart JM, Segal E, Koller D, Kim SK. A gene-coexpression network for global discovery of conserved genetic modules. *Science*. 2003; 302(5643):249-255.
43. Warde-Farley D, Donaldson SL, Comes O, et al. The GeneMANIA prediction server: biological network integration for gene prioritization and predicting gene function. *Nucleic acids research*. 2010; 38(Web Server issue):W214-220.
44. Lander ES, Waterman MS. Genomic mapping by fingerprinting random clones: a mathematical analysis. *Genomics*. 1988; 2(3):231-239.
45. Hasler G. Pathophysiology of depression: do we have any solid evidence of interest to clinicians? *World psychiatry : official journal of the World Psychiatric Association (WPA)*. 2010; 9(3):155-161.
46. Koolschijn PC, van Haren NE, Lensvelt-Mulders GJ, Hulshoff Pol HE, Kahn RS. Brain volume abnormalities in major depressive disorder: a meta-analysis of magnetic resonance imaging studies. *Human brain mapping*. 2009; 30(11):3719-3735.
47. Schmaal L, Veltman DJ, van Erp TG, et al. Subcortical brain alterations in major depressive disorder: findings from the ENIGMA Major Depressive Disorder working group. *Molecular psychiatry*. 2015.
48. Sheline YI, Gado MH, Kraemer HC. Untreated depression and hippocampal volume loss. *The American journal of psychiatry*. 2003; 160(8):1516-1518.

49. Fitzgerald PB, Laird AR, Maller J, Daskalakis ZJ. A meta-analytic study of changes in brain activation in depression. *Human brain mapping*. 2008; 29(6):683-695.
50. Liu Y, Zhou J, White KP. RNA-seq differential expression studies: more sequence or more replication? *Bioinformatics (Oxford, England)*. 2014; 30(3):301-304.
51. Mitani H, Shirayama Y, Yamada T, Maeda K, Ashby CR, Jr., Kawahara R. Correlation between plasma levels of glutamate, alanine and serine with severity of depression. *Progress in neuro-psychopharmacology & biological psychiatry*. 2006; 30(6):1155-1158.
52. Hasler G, van der Veen JW, Tumonis T, Meyers N, Shen J, Drevets WC. Reduced prefrontal glutamate/glutamine and gamma-aminobutyric acid levels in major depression determined using proton magnetic resonance spectroscopy. *Archives of general psychiatry*. 2007; 64(2):193-200.
53. Berman RM, Cappiello A, Anand A, et al. Antidepressant effects of ketamine in depressed patients. *Biological psychiatry*. 2000; 47(4):351-354.
54. Murrough JW. Ketamine as a novel antidepressant: from synapse to behavior. *Clinical pharmacology and therapeutics*. 2012; 91(2):303-309.
55. Maguire J, Mody I. GABA(A)R plasticity during pregnancy: relevance to postpartum depression. *Neuron*. 2008; 59(2):207-213.
56. Chourbaji S, Vogt MA, Fumagalli F, et al. AMPA receptor subunit 1 (GluR-A) knockout mice model the glutamate hypothesis of depression. *FASEB*

- journal : official publication of the Federation of American Societies for Experimental Biology*. 2008; 22(9):3129-3134.
57. Bocchio-Chiavetto L, Maffioletti E, Bettinsoli P, et al. Blood microRNA changes in depressed patients during antidepressant treatment. *European neuropsychopharmacology : the journal of the European College of Neuropsychopharmacology*. 2013; 23(7):602-611.
58. Duman RS, Voleti B. Signaling pathways underlying the pathophysiology and treatment of depression: novel mechanisms for rapid-acting agents. *Trends in neurosciences*. 2012; 35(1):47-56.
59. Kim HK, Nunes PV, Oliveira KC, Young LT, Lafer B. Neuropathological relationship between major depression and dementia: A hypothetical model and review. *Progress in neuro-psychopharmacology & biological psychiatry*. 2016; 67:51-57.
60. Spoletini I, Caltagirone C, Ceci M, Gianni W, Spalletta G. Management of pain in cancer patients with depression and cognitive deterioration. *Surgical oncology*. 2010; 19(3):160-166.
61. Feder ME, Walser JC. The biological limitations of transcriptomics in elucidating stress and stress responses. *Journal of evolutionary biology*. 2005; 18(4):901-910.

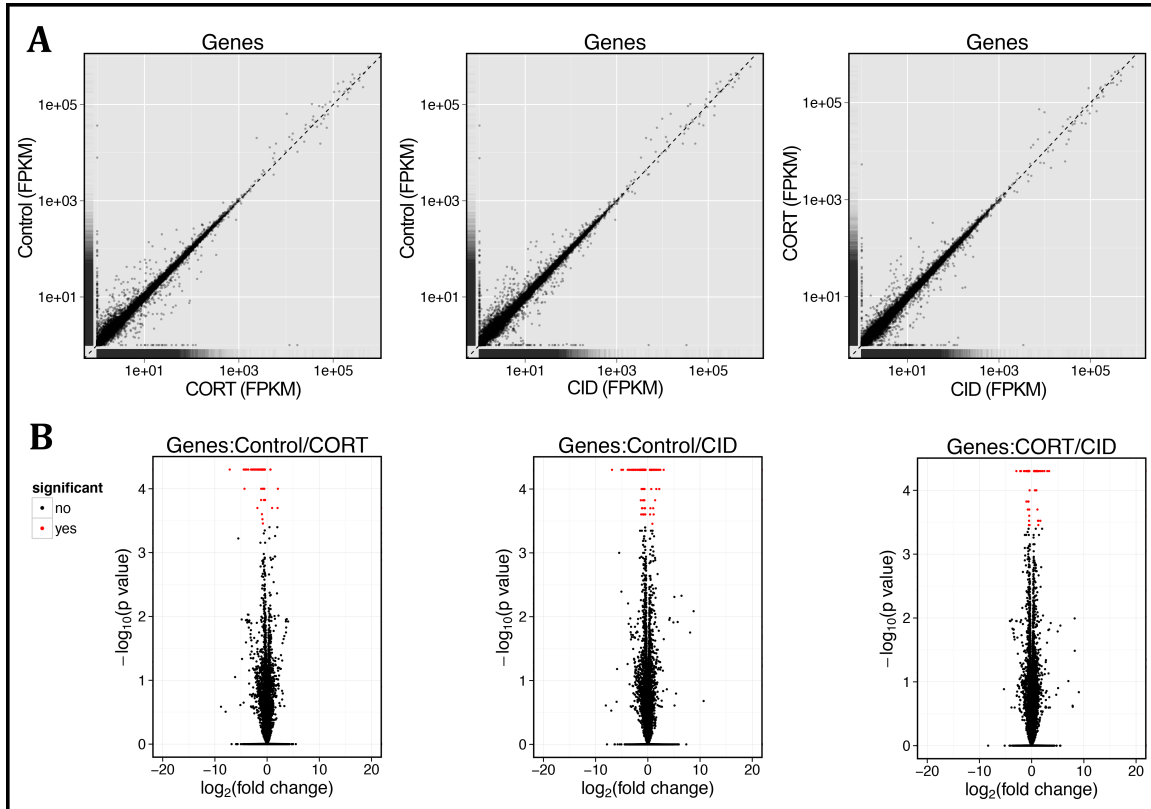
Figures & Tables

Figure 1. Visual representation of individual gene data in each pairwise comparison. **(A)** Scatter plots for each comparison showing overall gene expression similarities and differences. FPKM: Fragments Per Kilobase of transcript per Million mapped reads. **(B)** Volcano plots highlighting genes that were differentially expressed in each comparison.

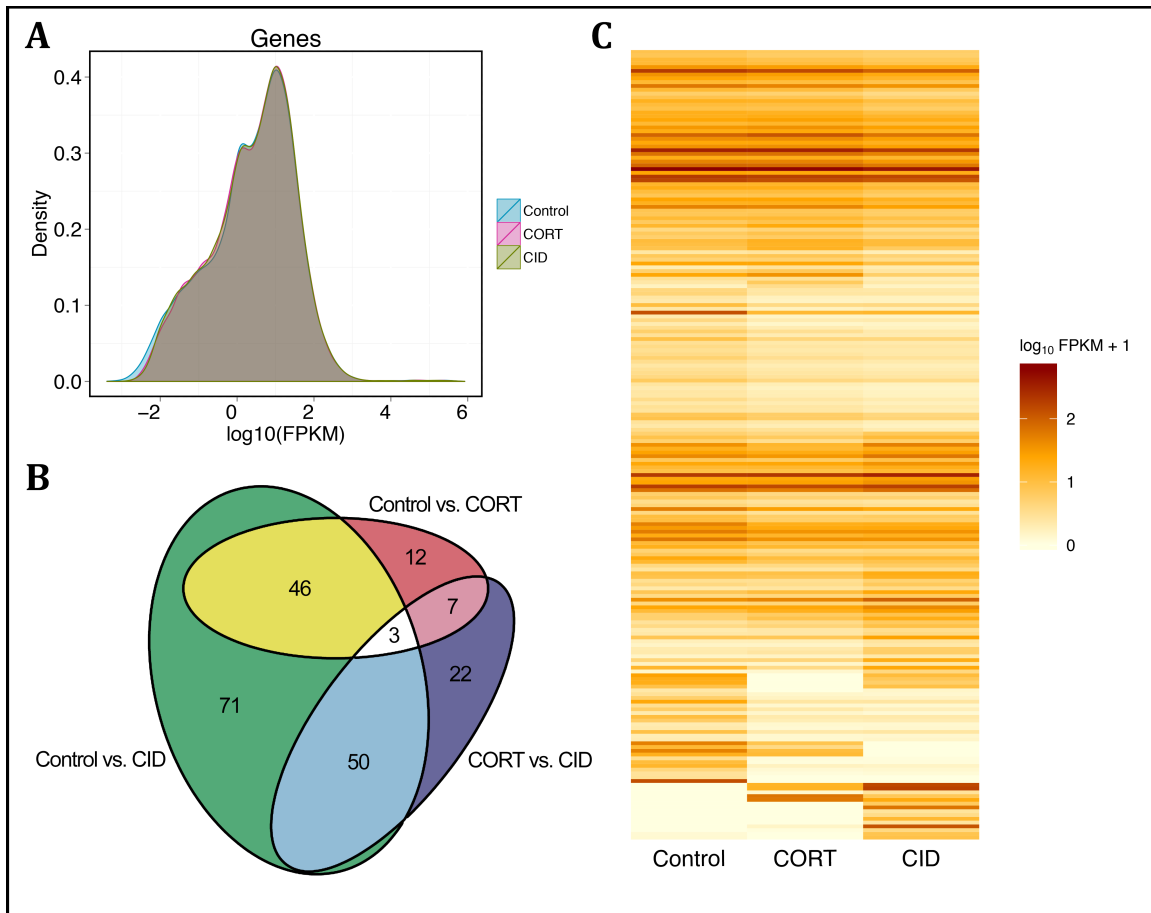


Figure 2. Visual summary of differential gene expression patterns between all 3 groups. (A) Density plot illustrating expression level distribution, with non-overlapping segments of the plot representing differential expression. (B) Venn diagram showing the number of shared DEGs between each comparisons. (C) Heatmap showing the level of expression [in $\log_{10}(\text{FPKM} + 1)$] for all DEGs across the 3 groups. FPKM: Fragments Per Kilobase of transcript per Million mapped reads.

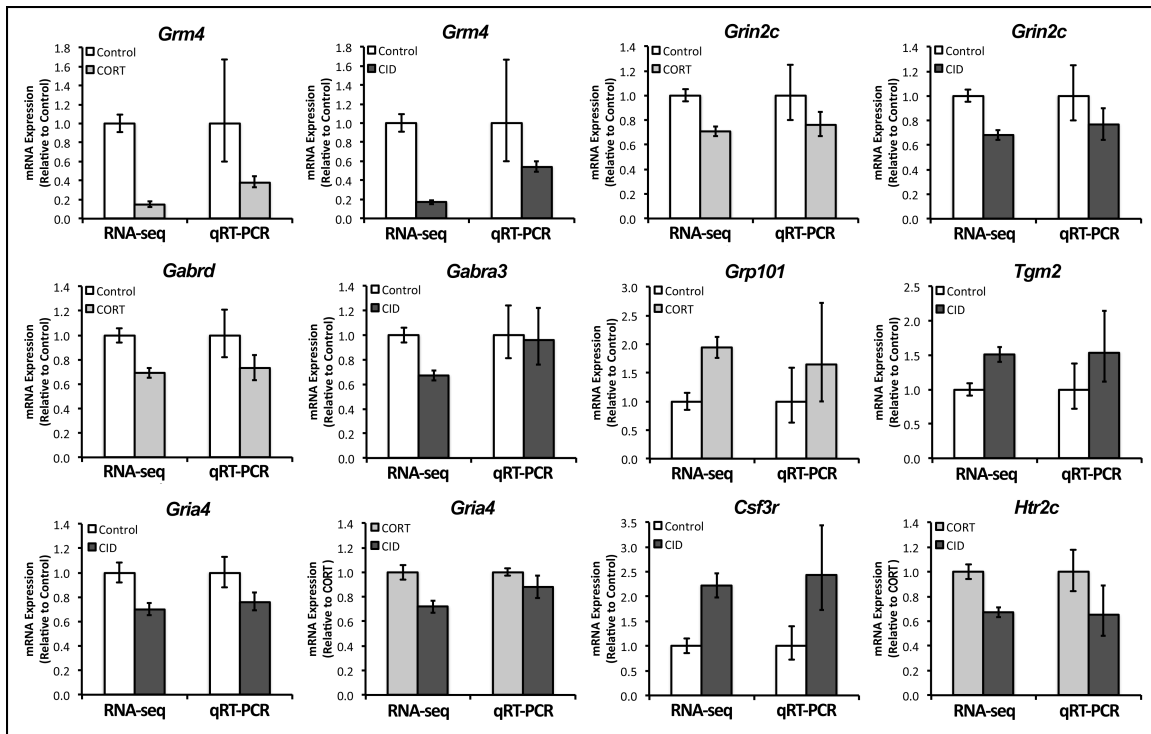


Figure 3. qRT-PCR fold-changes compared with RNA-seq fold-changes. 9 genes across 12 comparisons indicate similar results between both methods. For each group, data represents the mean of 6 biological replicates, with error bars indicating the SEM.

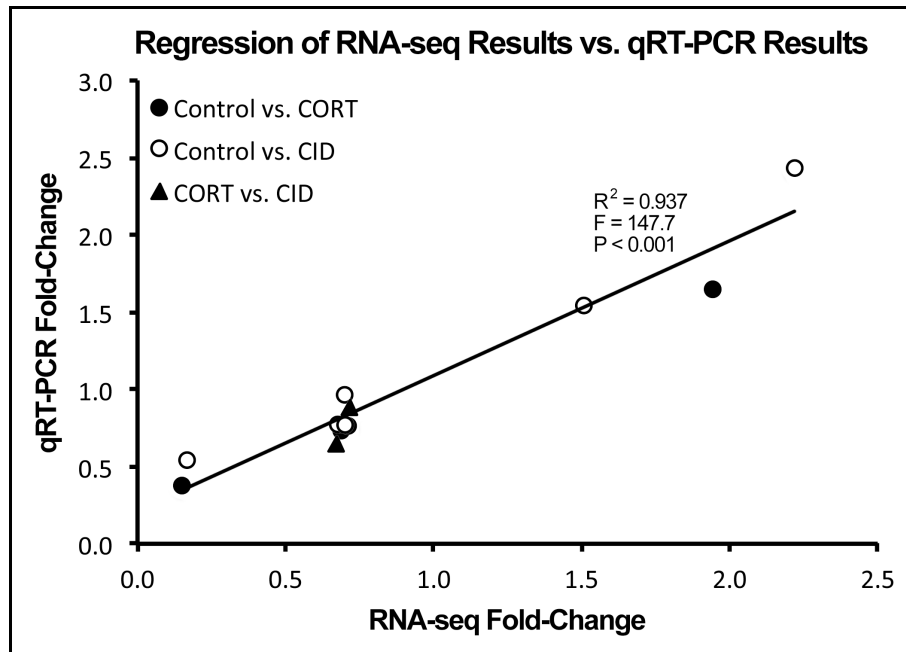


Figure 4. Linear regression analysis of qRT-PCR results compared with RNA-seq results. All pairwise comparisons and a wide range of fold-changes are represented in the analysis. Regression revealed high concordance between the two methods, which was statistically significant ($F = 147.7$, $R^2 = 0.937$, $p < 0.001$). Statistical analysis was performed using SPSS, with α set to 0.05.

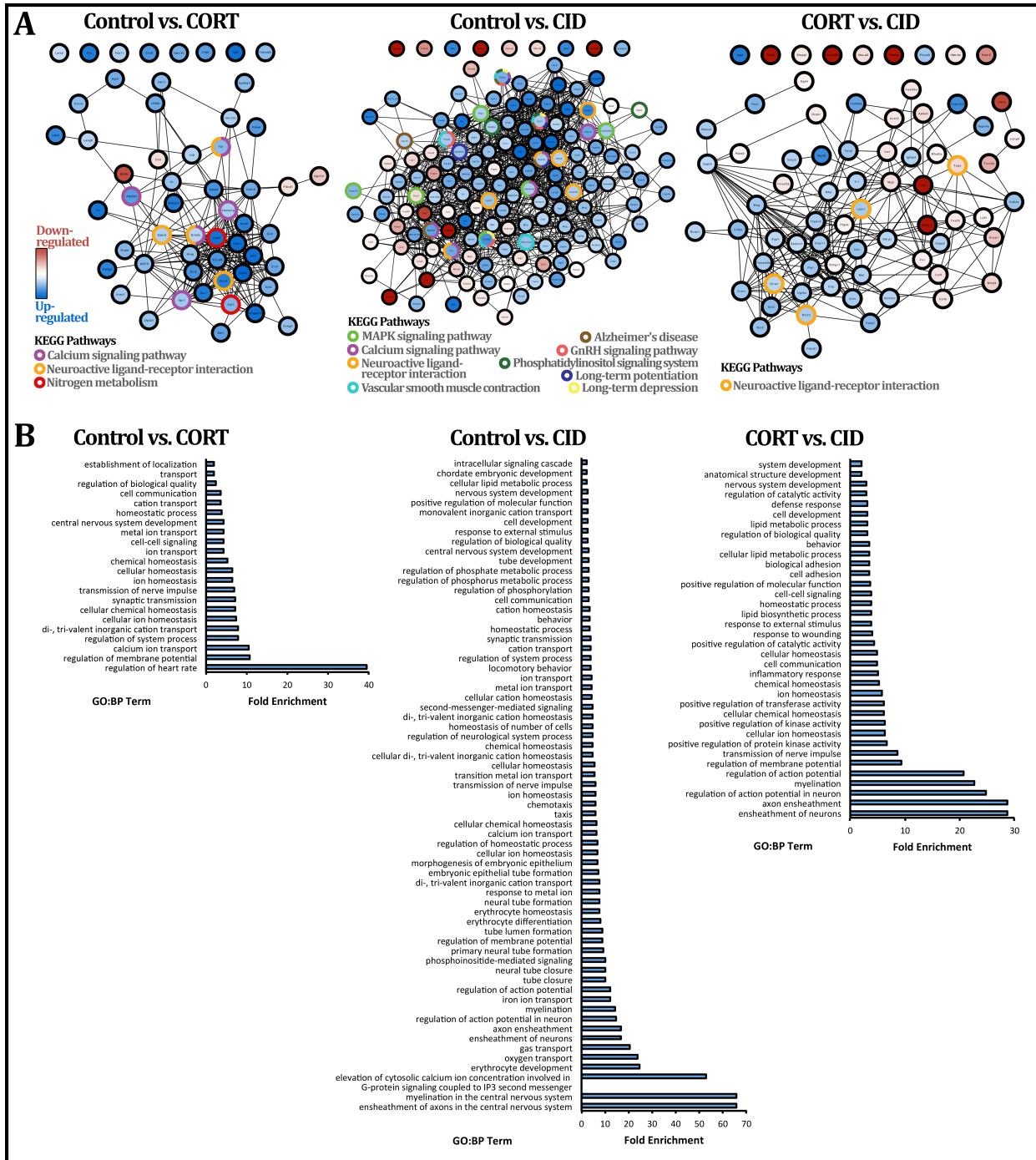


Figure 5. Enrichment analyses of DEGs identified using RNA-seq. **(A)** Co-expression networks of DEGs from each pairwise comparison were created using the GeneMANIA application in Cytoscape. Node fill colors represent expression fold-changes compared to the control, and node border colors represent KEGG pathways identified using DAVID. **(B)** Bar graphs illustrating fold-enrichments of GO:BP terms identified for DEGs from each pairwise comparison using DAVID. EASE threshold was set to 0.1 and fold-enrichments below 2 were excluded.

Supplemental Information

Table S1. Primers utilized for relative qRT-PCR analysis.

| Gene Symbol | Primer Sequence (5' to 3') | House-keeper | Product Size (bp) | Melt Peak |
|---------------|--|---------------|-------------------|-----------|
| <i>Grm4</i> | FOR: GACCGCATCAACAACGACC REV: GTGCCGTCCTTCTCGATGAG | <i>Sdha</i> | 137 | 87.5-88.0 |
| <i>Grin2c</i> | FOR: GGGATCTGCCATAACGAGAAG REV: GCACTGAGTGTCGAAGTTTCCA | <i>Polr2b</i> | 157 | 86.0-86.5 |
| <i>Gabrd</i> | FOR: CCAGCATTGACCATATCTCAGAG REV: TCATGGAACCAGGCAGATTTG | <i>Taf1b</i> | 190 | 85.5 |
| <i>Gpr101</i> | FOR: AGATGACCAACCGACGTAGTT REV: TGGCTCCCCAGATCATGGAA | <i>Taf1b</i> | 141 | 84.0-84.5 |
| <i>Gabra3</i> | FOR: AGACAGACATGGCATGATGAAAG REV: GGTGTGGTCATATTGTGAGCC | <i>Sdha</i> | 146 | 80.0 |
| <i>Tgm2G</i> | FOR: GACAATGTGGAGGAGGGATCT REV: CTCTAGGCTGAGACGGTACAG | <i>Taf1b</i> | 120 | 85.0 |
| <i>Csf3r</i> | FOR: CTGATCTTCTTGCTACTCCCCA REV: GGTGTAGTTCAAGTGAGGCAG | <i>Taf1b</i> | 249 | 86.5 |
| <i>Htr2c</i> | FOR: TGCTGGTGGGACTACTTGTC REV: GACGCAGTTGAAAATAGCACATC | <i>Sdha</i> | 124 | 81.0-81.5 |
| <i>Gria4</i> | FOR: TTTGCAGGCAGATTGTCTTG REV: GGGGCTGGTGTTATGAAGAA | <i>Sdha</i> | 180 | 82.5-83.0 |

Table S2. Housekeeping gene primers utilized for relative qRT-PCR analysis.

| Gene Symbol | Primer Sequence (5' to 3') | Product Size (bp) | Melt Peak |
|--------------------|---|--------------------------|------------------|
| <i>Polr2b</i> | FOR: ATGGCTTAACAGATCGTGACCT REV: GCGACATTCTCCTGTATAGGCA | 176 | 81.0-81.5 |
| <i>Grin2c</i> | FOR: TCCTACCCGATCACATACTGTT REV: GCTCTGTCATGTAATGGATGGCA | 152 | 84.0-84.5 |
| <i>Sdha</i> | FOR: GATTTGCCTCGTTTCCCAGAC REV: GCCATAGCCTGCACATCATATT | 215 | 81.0-81.5 |

Table S3. List of differentially expressed genes (DEGs) and fold changes for each pairwise comparison.

| Control vs. CORT | | | | |
|------------------|-----------------|---|-------------|---------|
| XLOC Name | Gene Symbol | Gene Name | Fold-Change | q-value |
| XLOC_009476 | <i>Cbln3</i> | cerebellin 3 precursor protein | 0.01 | 0.009 |
| XLOC_030509 | <i>Cbln1</i> | cerebellin 1 precursor protein | 0.04 | 0.009 |
| XLOC_016233 | <i>Sp5</i> | trans-acting transcription factor 5 | 0.05 | 0.017 |
| XLOC_022558 | <i>En2</i> | engrailed 2 | 0.05 | 0.009 |
| XLOC_012954 | <i>Arhgef33</i> | Rho guanine nucleotide exchange factor (GEF) 33 | 0.06 | 0.009 |
| XLOC_021168 | <i>Car8</i> | carbonic anhydrase 8 | 0.07 | 0.009 |
| XLOC_014015 | <i>Ttr</i> | transthyretin | 0.08 | 0.009 |
| XLOC_032531 | <i>Zic1</i> | zinc finger protein of the cerebellum 1 | 0.12 | 0.009 |
| XLOC_003357 | <i>Nts</i> | neurotensin | 0.12 | 0.009 |
| XLOC_003296 | <i>Mybpc1</i> | myosin binding protein C, slow-type | 0.14 | 0.009 |
| XLOC_013378 | <i>Grm4</i> | glutamate receptor, metabotropic 4 | 0.15 | 0.009 |
| XLOC_020670 | <i>Inadl</i> | InaD-like (Drosophila) | 0.17 | 0.009 |
| XLOC_022039 | <i>Pla2g5</i> | phospholipase A2, group V | 0.18 | 0.009 |
| XLOC_010841 | <i>Shisa8</i> | shisa family member 8 | 0.19 | 0.009 |
| XLOC_024662 | <i>Ubn2</i> | ubnuclein 2 | 0.21 | 0.009 |
| XLOC_029786 | <i>Gm2694</i> | predicted gene 2694 | 0.25 | 0.009 |
| XLOC_031477 | <i>Zic4</i> | zinc finger protein of the cerebellum 4 | 0.28 | 0.03 |
| XLOC_022021 | <i>Epha8</i> | Eph receptor A8 | 0.28 | 0.009 |
| XLOC_002196 | <i>Slc1a6</i> | solute carrier family 1 (high affinity aspartate/glutamate transporter), member 6 | 0.29 | 0.009 |
| XLOC_011547 | <i>Clic6</i> | chloride intracellular channel 6 | 0.31 | 0.009 |
| XLOC_025639 | <i>Pdia4</i> | protein disulfide isomerase associated 4 | 0.33 | 0.009 |
| XLOC_004080 | <i>Atp2a3</i> | ATPase, Ca ⁺⁺ transporting, ubiquitous | 0.34 | 0.009 |
| XLOC_001562 | <i>Pld5</i> | phospholipase D family, member 5 | 0.34 | 0.009 |
| XLOC_008713 | <i>Gm1821</i> | predicted gene 1821 | 0.35 | 0.009 |
| XLOC_003781 | <i>Ebfl</i> | early B cell factor 1 | 0.37 | 0.009 |
| XLOC_009106 | <i>Zic2</i> | zinc finger protein of the cerebellum 2 | 0.41 | 0.009 |
| XLOC_009695 | <i>Zic5</i> | zinc finger protein of the cerebellum 5 | 0.42 | 0.009 |
| XLOC_001263 | <i>Inhbb</i> | inhibin beta-B | 0.43 | 0.009 |
| XLOC_030069 | <i>Cdh15</i> | cadherin 15 | 0.44 | 0.009 |
| XLOC_031818 | <i>Rgl3</i> | ral guanine nucleotide dissociation stimulator-like 3 | 0.45 | 0.024 |
| XLOC_004543 | <i>Gprc5c</i> | G protein-coupled receptor, family C, group 5, member C | 0.45 | 0.017 |

| | | | | |
|--------------------|-----------------|---|------|-------|
| XLOC_011401 | <i>Mir568</i> | microRNA 568 | 0.47 | 0.009 |
| XLOC_000525 | <i>Syt2</i> | synaptotagmin II | 0.47 | 0.009 |
| XLOC_029888 | <i>Car7</i> | carbonic anhydrase 7 | 0.51 | 0.009 |
| XLOC_010729 | <i>Pvalb</i> | parvalbumin | 0.52 | 0.009 |
| XLOC_008640 | <i>Gdf10</i> | growth differentiation factor 10 | 0.52 | 0.009 |
| XLOC_008180 | <i>F2r</i> | coagulation factor II (thrombin) receptor | 0.53 | 0.009 |
| XLOC_030017 | <i>Vat1l</i> | vesicle amine transport protein 1 homolog-like (T. californica) | 0.54 | 0.009 |
| XLOC_026564 | <i>Ercc2</i> | excision repair cross-complementing rodent repair deficiency, complementation group 2 | 0.54 | 0.009 |
| XLOC_021100 | <i>Tnfrsf25</i> | tumor necrosis factor receptor superfamily, member 25 | 0.54 | 0.009 |
| XLOC_006619 | <i>Syndig1l</i> | synapse differentiation inducing 1 like | 0.55 | 0.009 |
| XLOC_030690 | <i>Kcng4</i> | potassium voltage-gated channel, subfamily G, member 4 | 0.58 | 0.017 |
| XLOC_014386 | <i>Nrep</i> | neuronal regeneration related protein | 0.59 | 0.009 |
| XLOC_008982 | <i>Hr</i> | hairless | 0.59 | 0.009 |
| XLOC_014343 | <i>Zfp521</i> | zinc finger protein 521 | 0.61 | 0.017 |
| XLOC_025040 | <i>Itp1l</i> | inositol 1,4,5-trisphosphate receptor 1 | 0.63 | 0.009 |
| XLOC_016017 | <i>Kcnt1</i> | potassium channel, subfamily T, member 1 | 0.64 | 0.009 |
| XLOC_013763 | <i>Mtcl1</i> | microtubule crosslinking factor 1 | 0.66 | 0.024 |
| XLOC_032469 | <i>Unc13c</i> | unc-13 homolog C (C. elegans) | 0.67 | 0.009 |
| XLOC_005264 | <i>Cacna1g</i> | calcium channel, voltage-dependent, T type, alpha 1G subunit | 0.67 | 0.009 |
| XLOC_031796 | <i>Fdx1l</i> | ferredoxin 1-like | 0.69 | 0.024 |
| XLOC_005397 | <i>Jup</i> | junction plakoglobin | 0.69 | 0.017 |
| XLOC_022183 | <i>Gabrd</i> | gamma-aminobutyric acid (GABA) A receptor, subunit delta | 0.69 | 0.009 |
| XLOC_026419 | <i>Leng8</i> | leukocyte receptor cluster (LRC) member 8 | 0.71 | 0.009 |
| XLOC_005535 | <i>Grin2c</i> | glutamate receptor, ionotropic, NMDA2C (epsilon 3) | 0.71 | 0.009 |
| XLOC_023798 | <i>Miat</i> | myocardial infarction associated transcript (non-protein coding) | 0.73 | 0.009 |
| XLOC_015363 | <i>Malat1</i> | metastasis associated lung adenocarcinoma transcript 1 (non-coding RNA) | 0.75 | 0.009 |
| XLOC_031709 | <i>Lars2</i> | leucyl-tRNA synthetase, mitochondrial | 0.77 | 0.024 |
| XLOC_017579 | <i>Fibcd1</i> | fibrinogen C domain containing 1 | 1.54 | 0.009 |
| XLOC_002515 | <i>Dcn</i> | decorin | 1.58 | 0.009 |
| XLOC_033696 | <i>Gpr101</i> | G protein-coupled receptor 101 | 1.94 | 0.03 |
| XLOC_009455 | <i>Myh6</i> | myosin, heavy polypeptide 6, cardiac muscle, alpha | 4.01 | 0.03 |
| XLOC_029781 | <i>Mir8109</i> | microRNA 8109 | 4.18 | 0.017 |
| XLOC_005745 | <i>NA</i> | not annotated | 0.00 | 0.009 |
| XLOC_021216 | <i>NA</i> | not annotated | 0.00 | 0.009 |
| XLOC_030849 | <i>NA</i> | not annotated | 0.00 | 0.009 |

| XLOC_026396 | NA | not annotated | ∞ | 0.03 |
|-----------------|----------------------|---|-------------|---------|
| XLOC_009725 | NA | not annotated | ∞ | 0.03 |
| Control vs. CID | | | | |
| XLOC Name | Gene Symbol | Gene Name | Fold-Change | q-value |
| XLOC_009476 | <i>Cbln3</i> | cerebellin 3 precursor protein | 0.01 | 0.009 |
| XLOC_022558 | <i>En2</i> | engrailed 2 | 0.03 | 0.009 |
| XLOC_030509 | <i>Cbln1</i> | cerebellin 1 precursor protein | 0.04 | 0.009 |
| XLOC_021168 | <i>Car8</i> | carbonic anhydrase 8 | 0.07 | 0.009 |
| XLOC_012954 | <i>Arhgef33</i> | Rho guanine nucleotide exchange factor (GEF) 33 | 0.08 | 0.009 |
| XLOC_016233 | <i>Sp5</i> | trans-acting transcription factor 5 | 0.09 | 0.009 |
| XLOC_014015 | <i>Ttr</i> | transthyretin | 0.09 | 0.009 |
| XLOC_003357 | <i>Nts</i> | neurotensin | 0.11 | 0.009 |
| XLOC_003296 | <i>Mybpc1</i> | myosin binding protein C, slow-type | 0.13 | 0.009 |
| XLOC_032531 | <i>Zic1</i> | zinc finger protein of the cerebellum 1 | 0.13 | 0.009 |
| XLOC_029786 | <i>Gm2694</i> | predicted gene 2694 | 0.15 | 0.009 |
| XLOC_010841 | <i>Shisa8</i> | shisa family member 8 | 0.15 | 0.009 |
| XLOC_013378 | <i>Grm4</i> | glutamate receptor, metabotropic 4 | 0.17 | 0.009 |
| XLOC_020670 | <i>Inadl</i> | InaD-like (Drosophila) | 0.19 | 0.009 |
| XLOC_001562 | <i>Pld5</i> | phospholipase D family, member 5 | 0.19 | 0.009 |
| XLOC_005886 | <i>Ispd</i> | isoprenoid synthase domain containing | 0.20 | 0.009 |
| XLOC_031477 | <i>Zic4</i> | zinc finger protein of the cerebellum 4 | 0.25 | 0.009 |
| XLOC_000525 | <i>Syt2</i> | synaptotagmin II | 0.26 | 0.009 |
| XLOC_019560 | <i>Trpc3</i> | transient receptor potential cation channel, subfamily C, member 3 | 0.27 | 0.009 |
| XLOC_022039 | <i>Pla2g5</i> | phospholipase A2, group V | 0.27 | 0.009 |
| XLOC_002196 | <i>Slc1a6</i> | solute carrier family 1 (high affinity aspartate/glutamate transporter), member 6 | 0.32 | 0.009 |
| XLOC_011547 | <i>Clic6</i> | chloride intracellular channel 6 | 0.34 | 0.009 |
| XLOC_031129 | <i>Ccdc153</i> | coiled-coil domain containing 153 | 0.35 | 0.009 |
| XLOC_025639 | <i>Pdia4</i> | protein disulfide isomerase associated 4 | 0.35 | 0.009 |
| XLOC_015683 | <i>5830416P10Rik</i> | RIKEN cDNA 5830416P10 gene | 0.36 | 0.049 |
| XLOC_026919 | <i>Slc17a6</i> | solute carrier family 17 (sodium-dependent inorganic phosphate cotransporter), member 6 | 0.38 | 0.009 |
| XLOC_004080 | <i>Atp2a3</i> | ATPase, Ca ⁺⁺ transporting, ubiquitous | 0.38 | 0.009 |
| XLOC_010729 | <i>Pvalb</i> | parvalbumin | 0.39 | 0.009 |
| XLOC_026090 | <i>Lrrc23</i> | leucine rich repeat containing 23 | 0.39 | 0.024 |
| XLOC_009106 | <i>Zic2</i> | zinc finger protein of the cerebellum 2 | 0.40 | 0.009 |
| XLOC_022021 | <i>Epha8</i> | Eph receptor A8 | 0.41 | 0.009 |

| | | | | |
|--------------------|----------------------|---|------|-------|
| XLOC_001263 | <i>Inhbb</i> | inhibin beta-B | 0.41 | 0.009 |
| XLOC_000127 | <i>1500015O10Rik</i> | RIKEN cDNA 1500015O10 gene | 0.41 | 0.037 |
| XLOC_025720 | <i>Pde1c</i> | phosphodiesterase 1C | 0.42 | 0.009 |
| XLOC_005282 | <i>Nxph3</i> | neurexophilin 3 | 0.42 | 0.009 |
| XLOC_003781 | <i>Ebfl</i> | early B cell factor 1 | 0.43 | 0.009 |
| XLOC_009695 | <i>Zic5</i> | zinc finger protein of the cerebellum 5 | 0.44 | 0.009 |
| XLOC_004543 | <i>Gprc5c</i> | G protein-coupled receptor, family C, group 5, member C | 0.44 | 0.017 |
| XLOC_000224 | <i>Vwc2l</i> | von Willebrand factor C domain-containing protein 2-like | 0.44 | 0.017 |
| XLOC_008180 | <i>F2r</i> | coagulation factor II (thrombin) receptor | 0.44 | 0.009 |
| XLOC_023031 | <i>Fam222a</i> | family with sequence similarity 222, member A | 0.45 | 0.009 |
| XLOC_031558 | <i>6430571L13Rik</i> | RIKEN cDNA 6430571L13 gene | 0.45 | 0.049 |
| XLOC_000021 | <i>Sulfl</i> | sulfatase 1 | 0.46 | 0.030 |
| XLOC_023589 | <i>Kctd8</i> | potassium channel tetramerisation domain containing 8 | 0.46 | 0.009 |
| XLOC_030017 | <i>Vat1l</i> | vesicle amine transport protein 1 homolog-like (T. californica) | 0.47 | 0.009 |
| XLOC_016927 | <i>Plcb4</i> | phospholipase C, beta 4 | 0.48 | 0.009 |
| XLOC_030690 | <i>Kcng4</i> | potassium voltage-gated channel, subfamily G, member 4 | 0.49 | 0.009 |
| XLOC_031818 | <i>Rgl3</i> | ral guanine nucleotide dissociation stimulator-like 3 | 0.50 | 0.030 |
| XLOC_019332 | <i>Olfm3</i> | olfactomedin 3 | 0.51 | 0.009 |
| XLOC_015602 | <i>Opalin</i> | oligodendrocytic myelin paranodal and inner loop protein | 0.51 | 0.009 |
| XLOC_023332 | <i>Medag</i> | mesenteric estrogen dependent adipogenesis | 0.51 | 0.009 |
| XLOC_029888 | <i>Car7</i> | carbonic anhydrase 7 | 0.51 | 0.009 |
| XLOC_009841 | <i>Cdh18</i> | cadherin 18 | 0.52 | 0.017 |
| XLOC_000776 | <i>Dusp10</i> | dual specificity phosphatase 10 | 0.52 | 0.037 |
| XLOC_006619 | <i>Syndig1l</i> | synapse differentiation inducing 1 like | 0.52 | 0.009 |
| XLOC_022576 | <i>Kcnk3</i> | potassium channel, subfamily K, member 3 | 0.53 | 0.024 |
| XLOC_023356 | <i>Steap2</i> | six transmembrane epithelial antigen of prostate 2 | 0.53 | 0.009 |
| XLOC_021166 | <i>Tox</i> | thymocyte selection-associated high mobility group box | 0.54 | 0.024 |
| XLOC_018007 | <i>Hipk3</i> | homeodomain interacting protein kinase 3 | 0.54 | 0.009 |
| XLOC_009911 | <i>Nov</i> | nephroblastoma overexpressed gene | 0.55 | 0.009 |
| XLOC_033238 | <i>Gjb1</i> | gap junction protein, beta 1 | 0.55 | 0.037 |
| XLOC_027488 | <i>Syt9</i> | synaptotagmin IX | 0.55 | 0.009 |
| XLOC_023202 | <i>Rasa4</i> | RAS p21 protein activator 4 | 0.55 | 0.037 |
| XLOC_026187 | <i>Tspan9</i> | tetraspanin 9 | 0.56 | 0.009 |
| XLOC_004246 | <i>Sept4</i> | septin 4 | 0.57 | 0.009 |
| XLOC_011401 | <i>Mir568</i> | microRNA 568 | 0.57 | 0.009 |
| XLOC_010490 | <i>Enpp2</i> | ectonucleotide pyrophosphatase/phosphodiesterase 2 | 0.57 | 0.009 |

| | | | | |
|--------------------|----------------------|---|------|-------|
| XLOC_014343 | <i>Zfp521</i> | zinc finger protein 521 | 0.57 | 0.009 |
| XLOC_014386 | <i>Nrep</i> | neuronal regeneration related protein | 0.58 | 0.009 |
| XLOC_008640 | <i>Gdf10</i> | growth differentiation factor 10 | 0.58 | 0.009 |
| XLOC_013534 | <i>Mog</i> | myelin oligodendrocyte glycoprotein | 0.58 | 0.009 |
| XLOC_006319 | <i>Adssl1</i> | adenylosuccinate synthetase like 1 | 0.59 | 0.017 |
| XLOC_008982 | <i>Hr</i> | hairless | 0.59 | 0.009 |
| XLOC_026719 | <i>Ppp1r14a</i> | protein phosphatase 1, regulatory (inhibitor) subunit 14A | 0.60 | 0.017 |
| XLOC_021981 | <i>Rps6kal</i> | ribosomal protein S6 kinase polypeptide 1 | 0.60 | 0.024 |
| XLOC_018553 | <i>Bcas1</i> | breast carcinoma amplified sequence 1 | 0.60 | 0.009 |
| XLOC_002839 | <i>Abracl</i> | ABRA C-terminal like | 0.60 | 0.049 |
| XLOC_021435 | <i>Lpar1</i> | lysophosphatidic acid receptor 1 | 0.61 | 0.009 |
| XLOC_033359 | <i>Plp1</i> | proteolipid protein (myelin) 1 | 0.62 | 0.009 |
| XLOC_013763 | <i>Mtcl1</i> | microtubule crosslinking factor 1 | 0.62 | 0.009 |
| XLOC_017682 | <i>Ermn</i> | ermin, ERM-like protein | 0.62 | 0.009 |
| XLOC_031128 | <i>Mcam</i> | melanoma cell adhesion molecule | 0.63 | 0.049 |
| XLOC_026564 | <i>Erc2</i> | excision repair cross-complementing rodent repair deficiency, complementation group 2 | 0.63 | 0.009 |
| XLOC_016017 | <i>Kcnt1</i> | potassium channel, subfamily T, member 1 | 0.63 | 0.024 |
| XLOC_028168 | <i>Mag</i> | myelin-associated glycoprotein | 0.64 | 0.009 |
| XLOC_000343 | <i>Efhd1</i> | EF hand domain containing 1 | 0.64 | 0.009 |
| XLOC_014296 | <i>Mbp</i> | myelin basic protein | 0.64 | 0.009 |
| XLOC_032536 | <i>1190002N15Rik</i> | RIKEN cDNA 1190002N15 gene | 0.64 | 0.009 |
| XLOC_031559 | <i>Cacna2d2</i> | calcium channel, voltage-dependent, alpha 2/delta subunit 2 | 0.65 | 0.017 |
| XLOC_025040 | <i>Itp1</i> | inositol 1,4,5-trisphosphate receptor 1 | 0.65 | 0.009 |
| XLOC_009257 | <i>Prkcd</i> | Prkcd | 0.65 | 0.009 |
| XLOC_018878 | <i>Cldn11</i> | claudin 11 | 0.66 | 0.009 |
| XLOC_005264 | <i>Cacna1g</i> | calcium channel, voltage-dependent, T type, alpha 1G subunit | 0.66 | 0.009 |
| XLOC_022190 | <i>Tmem88b</i> | transmembrane protein 88B | 0.66 | 0.009 |
| XLOC_029494 | <i>Ank1</i> | ankyrin 1, erythroid | 0.67 | 0.030 |
| XLOC_033746 | <i>Gabra3</i> | gamma-aminobutyric acid (GABA) A receptor, subunit alpha 3 | 0.67 | 0.009 |
| XLOC_005535 | <i>Grin2c</i> | glutamate receptor, ionotropic, NMDA2C (epsilon 3) | 0.68 | 0.009 |
| XLOC_031829 | <i>Anln</i> | anillin, actin binding protein | 0.68 | 0.037 |
| XLOC_027700 | <i>Inpp5a</i> | inositol polyphosphate-5-phosphatase A | 0.68 | 0.030 |
| XLOC_020028 | <i>Ugt8a</i> | UDP galactosyltransferase 8A | 0.69 | 0.030 |
| XLOC_002577 | <i>Ptprr</i> | protein tyrosine phosphatase, receptor type, R | 0.69 | 0.044 |
| XLOC_031725 | <i>Gria4</i> | glutamate receptor, ionotropic, AMPA4 (alpha 4) | 0.70 | 0.049 |

| | | | | |
|--------------------|----------------------|---|------|-------|
| XLOC_032578 | <i>Trf</i> | transferrin | 0.70 | 0.009 |
| XLOC_008068 | <i>Uqcrb</i> | ubiquinol-cytochrome c reductase binding protein | 0.70 | 0.009 |
| XLOC_015841 | <i>Fam107b</i> | family with sequence similarity 107, member B | 0.71 | 0.044 |
| XLOC_004539 | <i>Ttyh2</i> | tweety homolog 2 (Drosophila) | 0.71 | 0.037 |
| XLOC_004386 | <i>Cnp</i> | 2',3'-cyclic nucleotide 3' phosphodiesterase | 0.71 | 0.009 |
| XLOC_019030 | <i>Serpini1</i> | serine (or cysteine) peptidase inhibitor, clade I, member 1 | 0.72 | 0.009 |
| XLOC_018170 | <i>Mal</i> | myelin and lymphocyte protein, T cell differentiation protein | 0.72 | 0.009 |
| XLOC_012740 | <i>Rcan2</i> | regulator of calcineurin 2 | 0.73 | 0.009 |
| XLOC_005891 | <i>Etv1</i> | ets variant 1 | 0.73 | 0.049 |
| XLOC_017226 | <i>Slc32a1</i> | solute carrier family 32 (GABA vesicular transporter), member 1 | 0.73 | 0.009 |
| XLOC_025580 | <i>AK161964</i> | pleiotrophin | 0.75 | 0.009 |
| XLOC_015536 | <i>Rfx3</i> | regulatory factor X, 3 (influences HLA class II expression) | 1.30 | 0.009 |
| XLOC_007242 | <i>Rreb1</i> | ras responsive element binding protein 1 | 1.34 | 0.037 |
| XLOC_010400 | <i>Pdzd2</i> | PDZ domain containing 2 | 1.34 | 0.009 |
| XLOC_021853 | <i>Mfsd2a</i> | major facilitator superfamily domain containing 2A | 1.40 | 0.030 |
| XLOC_008713 | <i>Gm1821</i> | predicted gene 1821 | 1.43 | 0.009 |
| XLOC_015363 | <i>Malat1</i> | metastasis associated lung adenocarcinoma transcript 1 (non-coding RNA) | 1.45 | 0.009 |
| XLOC_033875 | <i>Xist</i> | inactive X specific transcripts | 1.45 | 0.009 |
| XLOC_018470 | <i>Tgm2</i> | transglutaminase 2, C polypeptide | 1.51 | 0.049 |
| XLOC_009619 | <i>Dgkh</i> | diacylglycerol kinase, eta | 1.57 | 0.009 |
| XLOC_019452 | <i>Adgrl4</i> | adhesion G protein-coupled receptor L4 | 1.58 | 0.017 |
| XLOC_017497 | <i>Ptgds</i> | prostaglandin D2 synthase (brain) | 1.60 | 0.009 |
| XLOC_001048 | <i fn1<="" i=""></i> | fibronectin 1 | 1.60 | 0.009 |
| XLOC_010672 | <i>Ly6i</i> | lymphocyte antigen 6 complex, locus I | 1.61 | 0.009 |
| XLOC_028173 | <i>Fxyd5</i> | FXYD domain-containing ion transport regulator 5 | 1.79 | 0.044 |
| XLOC_003003 | <i>Srgn</i> | serglycin | 1.82 | 0.049 |
| XLOC_020628 | <i>Acer2</i> | alkaline ceramidase 2 | 1.87 | 0.049 |
| XLOC_029918 | <i>Fam65a</i> | family with sequence similarity 65, member A | 1.87 | 0.009 |
| XLOC_008030 | <i>Ctla2a</i> | cytotoxic T lymphocyte-associated protein 2 alpha | 1.98 | 0.009 |
| XLOC_031393 | <i>Aldh1a2</i> | aldehyde dehydrogenase family 1, subfamily A2 | 2.04 | 0.030 |
| XLOC_026272 | <i>Mgp</i> | matrix Gla protein | 2.10 | 0.009 |
| XLOC_002269 | <i>Apba3</i> | amyloid beta (A4) precursor protein-binding, family A, member 3 | 2.11 | 0.009 |
| XLOC_000513 | <i>Fmod</i> | fibromodulin | 2.12 | 0.009 |
| XLOC_025169 | <i>Vwf</i> | Von Willebrand factor homolog | 2.16 | 0.037 |
| XLOC_020851 | <i>Csf3r</i> | colony stimulating factor 3 receptor (granulocyte) | 2.22 | 0.009 |

| | | | | |
|---------------------|--------------------|---|--------------------|----------------|
| XLOC_010738 | <i>Rac2</i> | RAS-related C3 botulinum substrate 2 | 2.28 | 0.049 |
| XLOC_028803 | <i>Hbb-bs</i> | hemoglobin, beta adult s chain | 2.53 | 0.009 |
| XLOC_027760 | <i>Lsp1</i> | lymphocyte specific 1 | 2.63 | 0.024 |
| XLOC_003748 | <i>Hba-a2</i> | hemoglobin alpha, adult chain 2 | 2.66 | 0.009 |
| XLOC_017282 | <i>Mmp9</i> | matrix metalloproteinase 9 | 2.88 | 0.009 |
| XLOC_028802 | <i>Hbb-b2</i> | hemoglobin, beta adult minor chain | 3.07 | 0.017 |
| XLOC_003397 | <i>Lyz2</i> | lysozyme 2 | 3.20 | 0.009 |
| XLOC_003750 | <i>Hba-a2</i> | hemoglobin alpha, adult chain 2 | 3.32 | 0.009 |
| XLOC_010172 | <i>Tnrc6b</i> | trinucleotide repeat containing 6b | 3.87 | 0.009 |
| XLOC_004039 | <i>Dvl2</i> | dishevelled 2, dsh homolog (Drosophila) | 4.34 | 0.009 |
| XLOC_015509 | <i>Anxa1</i> | annexin A1 | 4.35 | 0.009 |
| XLOC_013024 | <i>Fndc1</i> | fibronectin type III domain containing 1 | 4.55 | 0.017 |
| XLOC_009248 | <i>Pde12</i> | phosphodiesterase 12 | 5.25 | 0.009 |
| XLOC_013661 | <i>Lrg1</i> | leucine-rich alpha-2-glycoprotein 1 | 8.21 | 0.009 |
| XLOC_031633 | <i>Ltf</i> | lactotransferrin | ∞ | 0.009 |
| XLOC_011372 | <i>Gm5483</i> | predicted gene 5483 | ∞ | 0.009 |
| XLOC_004219 | <i>Wfdc21</i> | WAP four-disulfide core domain 21 | ∞ | 0.009 |
| XLOC_011787 | <i>Stfa2</i> | stefin A2 | ∞ | 0.009 |
| XLOC_011371 | <i>Stfa2l1</i> | stefin A2 like 1 | ∞ | 0.009 |
| XLOC_011430 | <i>Retnlg</i> | resistin like gamma | ∞ | 0.009 |
| XLOC_019135 | <i>S100a8</i> | S100 calcium binding protein A8 (calgranulin A) | ∞ | 0.009 |
| XLOC_022746 | NA | not annotated | 0.42 | 0.009 |
| XLOC_026331 | NA | not annotated | 0.00 | 0.030 |
| XLOC_001735 | NA | not annotated | 0.00 | 0.049 |
| XLOC_013895 | NA | not annotated | 0.00 | 0.009 |
| XLOC_020205 | NA | not annotated | 0.00 | 0.009 |
| XLOC_032849 | NA | not annotated | 0.00 | 0.049 |
| XLOC_021216 | NA | not annotated | 0.00 | 0.009 |
| XLOC_001774 | NA | not annotated | 0.00 | 0.049 |
| XLOC_020220 | NA | not annotated | ∞ | 0.024 |
| XLOC_020241 | NA | not annotated | ∞ | 0.009 |
| XLOC_020206 | NA | not annotated | ∞ | 0.024 |
| XLOC_009720 | NA | not annotated | ∞ | 0.030 |
| CORT vs. CID | | | | |
| XLOC Name | Gene Symbol | Gene Name | Fold-Change | q-value |
| XLOC_005886 | <i>Ispd</i> | isoprenoid synthase domain containing | 0.13 | 0.009 |
| XLOC_029781 | <i>Mir8109</i> | microRNA 8109 | 0.22 | 0.009 |

| | | | | |
|-------------|----------------|--|------|-------|
| XLOC_009455 | <i>Myh6</i> | myosin, heavy polypeptide 6, cardiac muscle, alpha | 0.22 | 0.009 |
| XLOC_031129 | <i>Ccdc153</i> | coiled-coil domain containing 153 | 0.24 | 0.009 |
| XLOC_018892 | <i>Sox2ot</i> | SOX2 overlapping transcript | 0.36 | 0.009 |
| XLOC_019193 | <i>Fam63a</i> | family with sequence similarity 63, member A | 0.39 | 0.009 |
| XLOC_003334 | <i>Vezt</i> | Vezatin, adherens junction component | 0.48 | 0.009 |
| XLOC_001902 | <i>Rsph4a</i> | Radial spoke head protein 4 homolog A | 0.50 | 0.024 |
| XLOC_001973 | <i>Fabp7</i> | fatty acid binding protein 7 | 0.54 | 0.009 |
| XLOC_000525 | <i>Syt2</i> | synaptotagmin II | 0.55 | 0.009 |
| XLOC_008177 | <i>Crhbp</i> | corticotropin releasing hormone binding protein | 0.56 | 0.009 |
| XLOC_004923 | <i>Gjc2</i> | gap junction gamma-2 | 0.60 | 0.030 |
| XLOC_001940 | <i>Cd24a</i> | CD24a antigen | 0.60 | 0.009 |
| XLOC_009911 | <i>Nov</i> | nephroblastoma overexpressed gene | 0.61 | 0.009 |
| XLOC_009793 | <i>Plxcd3</i> | phosphatidylinositol-specific phospholipase C, X domain containing 3 | 0.62 | 0.024 |
| XLOC_022170 | <i>Tprgl</i> | transformation related protein 63 regulated like | 0.62 | 0.009 |
| XLOC_033359 | <i>Plp1</i> | proteolipid protein (myelin) 1 | 0.63 | 0.009 |
| XLOC_028168 | <i>Mag</i> | myelin-associated glycoprotein | 0.63 | 0.009 |
| XLOC_017682 | <i>Ermn</i> | ermin, ERM-like protein | 0.63 | 0.009 |
| XLOC_021435 | <i>Lpar1</i> | lysophosphatidic acid receptor 1 | 0.65 | 0.024 |
| XLOC_031829 | <i>Anln</i> | anillin, actin binding protein | 0.65 | 0.009 |
| XLOC_022190 | <i>Tmem88b</i> | transmembrane protein 88B | 0.66 | 0.009 |
| XLOC_020028 | <i>Ugt8a</i> | UDP galactosyltransferase 8A | 0.66 | 0.009 |
| XLOC_032691 | <i>Rbms3</i> | RNA binding motif, single stranded interacting protein 3 | 0.66 | 0.024 |
| XLOC_017579 | <i>Fibcd1</i> | fibrinogen C domain containing 1 | 0.66 | 0.009 |
| XLOC_033395 | <i>Htr2c</i> | 5-Hydroxytryptamine (serotonin) receptor 2C, G protein-coupled | 0.67 | 0.009 |
| XLOC_019272 | <i>Tspan2</i> | tetraspanin 2 | 0.67 | 0.009 |
| XLOC_018878 | <i>Cldn11</i> | claudin 11 | 0.67 | 0.009 |
| XLOC_032578 | <i>Trf</i> | transferrin | 0.68 | 0.009 |
| XLOC_018170 | <i>Mal</i> | myelin and lymphocyte protein, T cell differentiation protein | 0.68 | 0.009 |
| XLOC_004367 | <i>Igfbp4</i> | insulin-like growth factor binding protein 4 | 0.69 | 0.009 |
| XLOC_010490 | <i>Enpp2</i> | ectonucleotide pyrophosphatase/phosphodiesterase 2 | 0.70 | 0.009 |
| XLOC_024618 | <i>Strip2</i> | striatin interacting protein 2 | 0.70 | 0.009 |
| XLOC_018553 | <i>Bcas1</i> | breast carcinoma amplified sequence 1 | 0.70 | 0.009 |
| XLOC_004386 | <i>Cnp</i> | 2',3'-cyclic nucleotide 3' phosphodiesterase | 0.71 | 0.009 |
| XLOC_017226 | <i>Slc32a1</i> | solute carrier family 32 (GABA vesicular transporter), member 1 | 0.72 | 0.009 |
| XLOC_014296 | <i>Mbp</i> | myelin basic protein | 0.72 | 0.009 |
| XLOC_031725 | <i>Gria4</i> | glutamate receptor, ionotropic, AMPA4 (alpha 4) | 0.72 | 0.037 |

| | | | | |
|--------------------|----------------------|---|------|-------|
| XLOC_010639 | <i>Ndrgl</i> | N-myc downstream regulated gene 1 | 0.73 | 0.030 |
| XLOC_014347 | <i>Aqp4</i> | aquaporin 4 | 0.73 | 0.009 |
| XLOC_004246 | <i>Sept4</i> | septin 4 | 0.74 | 0.009 |
| XLOC_019030 | <i>Serpini1</i> | serine (or cysteine) peptidase inhibitor, clade I, member 1 | 0.76 | 0.017 |
| XLOC_033875 | <i>Xist</i> | inactive X specific transcripts | 1.36 | 0.009 |
| XLOC_017222 | <i>Snhg11</i> | small nucleolar RNA host gene 11 | 1.40 | 0.009 |
| XLOC_021853 | <i>Mfsd2a</i> | major facilitator superfamily domain containing 2A | 1.43 | 0.009 |
| XLOC_023798 | <i>Miat</i> | myocardial infarction associated transcript (non-protein coding) | 1.47 | 0.009 |
| XLOC_009619 | <i>Dgkh</i> | diacylglycerol kinase, eta | 1.48 | 0.009 |
| XLOC_017497 | <i>Ptgds</i> | prostaglandin D2 synthase (brain) | 1.49 | 0.009 |
| XLOC_010672 | <i>Ly6i</i> | lymphocyte antigen 6 complex, locus I | 1.53 | 0.017 |
| XLOC_010400 | <i>Pdzd2</i> | PDZ domain containing 2 | 1.55 | 0.009 |
| XLOC_026419 | <i>Leng8</i> | leukocyte receptor cluster (LRC) member 8 | 1.57 | 0.009 |
| XLOC_001048 | <i fn1<="" i=""></i> | fibronectin 1 | 1.62 | 0.009 |
| XLOC_003748 | <i>Hba-a2</i> | hemoglobin alpha, adult chain 2 | 1.75 | 0.017 |
| XLOC_007242 | <i>Rreb1</i> | ras responsive element binding protein 1 | 1.83 | 0.009 |
| XLOC_028173 | <i>Fxyd5</i> | FXYD domain-containing ion transport regulator 5 | 1.87 | 0.017 |
| XLOC_019383 | <i>Etnppl</i> | ethanolamine phosphate phospholyase | 1.92 | 0.009 |
| XLOC_020628 | <i>Acer2</i> | alkaline ceramidase 2 | 1.93 | 0.009 |
| XLOC_029918 | <i>Fam65a</i> | family with sequence similarity 65, member A | 1.94 | 0.009 |
| XLOC_015363 | <i>Malat1</i> | metastasis associated lung adenocarcinoma transcript 1 (non-coding RNA) | 1.94 | 0.009 |
| XLOC_021100 | <i>Tnfrsf25</i> | tumor necrosis factor receptor superfamily, member 25 | 2.00 | 0.009 |
| XLOC_020851 | <i>Csf3r</i> | colony stimulating factor 3 receptor (granulocyte) | 2.04 | 0.009 |
| XLOC_025169 | <i>Vwf</i> | Von Willebrand factor homolog | 2.06 | 0.009 |
| XLOC_028803 | <i>Hbb-bs</i> | hemoglobin, beta adult s chain | 2.08 | 0.009 |
| XLOC_003397 | <i>Lyz2</i> | lysozyme 2 | 2.15 | 0.030 |
| XLOC_026272 | <i>Mgp</i> | matrix Gla protein | 2.21 | 0.009 |
| XLOC_003750 | <i>Hba-a2</i> | hemoglobin alpha, adult chain 2 | 2.28 | 0.009 |
| XLOC_002269 | <i>Apba3</i> | amyloid beta (A4) precursor protein-binding, family A, member 3 | 2.38 | 0.009 |
| XLOC_010208 | <i>Tspo</i> | translocator protein | 2.43 | 0.009 |
| XLOC_017282 | <i>Mmp9</i> | matrix metalloproteinase 9 | 2.70 | 0.009 |
| XLOC_015509 | <i>Anxa1</i> | annexin A1 | 3.20 | 0.009 |
| XLOC_010172 | <i>Tnrc6b</i> | trinucleotide repeat containing 6b | 4.00 | 0.009 |
| XLOC_008713 | <i>Gm1821</i> | predicted gene 1821 | 4.13 | 0.009 |
| XLOC_009248 | <i>Pde12</i> | phosphodiesterase 12 | 5.39 | 0.009 |
| XLOC_024662 | <i>Ubn2</i> | ubinuclein 2 | 8.01 | 0.009 |

| | | | | |
|--------------------|---------------|-------------------------------------|----------|-------|
| XLOC_013661 | <i>Lrg1</i> | leucine-rich alpha-2-glycoprotein 1 | 10.16 | 0.009 |
| XLOC_011372 | <i>Gm5483</i> | predicted gene 5483 | ∞ | 0.009 |
| XLOC_011787 | <i>Stfa2</i> | stefin A2 | ∞ | 0.009 |
| XLOC_004217 | <i>Wfdc17</i> | WAP four-disulfide core domain 17 | ∞ | 0.009 |
| XLOC_011430 | <i>Retnlg</i> | resistin like gamma | ∞ | 0.009 |
| XLOC_020241 | <i>NA</i> | not annotated | ∞ | 0.009 |
| XLOC_009720 | <i>NA</i> | not annotated | ∞ | 0.030 |
| XLOC_006983 | <i>NA</i> | not annotated | ∞ | 0.037 |

Note: Fold-changes of exactly 0.00 represent gene expression in the control and complete lack of expression in the comparator. Fold-changes of ∞ represent gene expression in the comparator and complete lack of expression in the control. q-values represent FDR-adjusted p-values.

CHAPTER 5

Summary and Future Directions

Summary

The work presented in this dissertation addresses a clinically important lack of understanding of the impact that cancer has on the development of depression. Several key findings contributed to the fundamental hypothesis that was investigated in this dissertation:

1. Clinical evidence suggests that symptoms of depression may actually precede the psychologically stressful diagnosis of cancer (Green & Austin, 1993; Jacobsson & Ottosson, 1971; Passik & Roth, 1999; Van Esch, Roukema, Ernst, Nieuwenhuijzen, & De Vries, 2012).
2. Investigations into the efficacy of antidepressants in cancer patients have produced largely mixed results (Ng, Boks, Zainal, & de Wit, 2011; Rodin et al., 2007; Williams & Dale, 2006).
3. Ketamine, an N-methyl-D-aspartate receptor (NMDAR) antagonists, possesses rapid antidepressant properties (Berman et al., 2000). The role of glutamatergic dysregulation has now been described in clinical (Ibrahim et al., 2012; Zarate et al., 2012) and preclinical studies (Banasz et al., 2010; Gourley, Espitia, Sanacora, & Taylor, 2012; Gourley & Taylor, 2009; Li et al., 2011) on depression.
4. Multiple breast and prostate cancer cell lines secrete significant amounts of glutamate into the extracellular environment through the

glutamate/cystine antiporter system x_c^- (Seidlitz et al., 2009; Sharma et al., 2010).

Therefore, I hypothesized the following:

Cancer can induce depression through defined biological mechanisms, which represent a distinct subtype of depression. Glutamatergic signalling is involved in the induction and maintenance of cancer-induced depression (CID), and is modifiable by pharmacological intervention at the tumour site.

This hypothesis was investigated through 3 distinct objectives, which will be discussed in the context of the papers presented in the previous chapters.

Objective 1: To develop a validated behavioural mouse model of CID.

This objective addressed a major impediment to the progress of CID research: the lack of a useful and validated animal model. Establishing this model was met with several challenges. Appendix 1 presents unpublished data from early experiments, providing context for the development of the CID model outlined in Chapter 2.

Preclinical data have suggested that tumour burden is associated with depressive-like behaviours, with a particular focus on the role of inflammation (Lamkin et al., 2011; Norden et al., 2015; Pyter et al., 2009; Yang et al., 2014).

However, the study outlined in Chapter 2 was the first to validate a CID model by first establishing behavioural assay sensitivity using a stress model of depressive-like behaviours. Chronic treatment with corticosterone (CORT) was used to induce this positive control model. Reversal of depressive-like behaviours with chronic fluoxetine (FLX) treatment further established that the assays were sensitive to the detection of an antidepressant. The CID model, which was induced by subcutaneous inoculation with 4T1 mammary carcinoma cells, produced very similar behavioural modifications to those observed in the CORT model. Interestingly, although anhedonia was detectable using the sucrose preference test (SPT) and behavioural despair was detectable using the forced swim test (FST), the tail suspension test (TST) did not detect depressive-like behaviours in any model. Power of movement (PM) was a perhaps more sensitive measure on the TST, but only non-significant trends were observed, which showed decreased PM for both the CORT and the CID model. As discussed in Chapter 2, it is possible that the FST and TST are sensitive to different pathophysiological mechanisms, with the former being more sensitive to glutamatergic dysregulation (Chatterjee, Jaiswal, & Palit, 2012).

In addition to the behavioural assays, we sought to validate our CID model at the neurostructural level using Sholl analyses on Golgi-Cox stained pyramidal neurons from the medial prefrontal cortex (mPFC). Again, this assay was validated using the CORT model and reversal with FLX. CORT mice exhibited atrophied apical and basilar dendritic branching, and this deficit was partially

reversed by FLX treatment. Tumour-bearing mice also had atrophied apical and basilar dendritic branching compared to control animals. These findings were particularly interesting since previous reports on murine stress models only detected deficits in apical, but not basilar, dendrites (Cook & Wellman, 2004; Wellman, 2001). The functional integration between apical and basilar dendritic domains is not well understood. However, connectionist models suggest that pyramidal cells in the cortex receive apical and basilar input from axons originating in different cortical areas (Spratling, 2002). It is therefore plausible that deficits in each dendritic domain contribute to distinct phenotypic features of depression.

Objective 2: To investigate the antidepressant efficacy of pharmacologically inhibiting system x_c^- glutamate release at the tumour site.

This objective expanded on the development of the CID model from Chapter 2. The study outlined in Chapter 3 investigated the possible antidepressant effects of sulfasalazine (SSZ), a known system x_c^- inhibitor. If the large amounts of glutamate being released by cancer cells peripherally are involved in the induction of depression, then it is reasonable to expect a system x_c^- inhibitor to prevent the development of depressive-like behaviours in the CID model.

First, *in vitro* experiments were performed to investigate whether 4T1 cells released large amounts of glutamate through system x_c^- , as we had demonstrated in human breast and prostate cancer cell lines (Seidlitz et al., 2009; Sharma et al., 2010). Previously, we had used AMPLEX Red glutamic acid assay kit (Invitrogen/Molecular Probes, Eugene, OR, USA) to quantify glutamate output by cells. One of the limitations of the AMPLEX Red assay is that it measures glutamate indirectly. Glutamate is oxidized by glutamate oxidase, which produces hydrogen peroxide. The hydrogen peroxide then reacts with the AMPLEX Red reagent to produce fluorescent resorufin. In our experience, the multiple enzymatic steps in this assay are occasionally vulnerable to interference and may produce inaccuracies. An alternative method of quantifying glutamate release by cells is by utilizing radioactive ^{14}C -cystine. This method quantifies the amount of cystine that cells uptake, which is directly proportional to the amount of glutamate released from cells through system x_c^- (Seidlitz, Sharma, & Singh, 2010). Therefore, this assay is more specific to system x_c^- activity and does not include enzymatic steps, allowing for a more direct method of quantification. Using this technique, we showed that 4T1 cells released much higher levels of glutamate compared to TM40A cells, which are non-tumorigenic breast epithelial cells derived from the same mouse strain: BALB/c. By incubating cells in the presence or absence of SSZ, we were also able to establish that system x_c^- was largely responsible glutamate release in both 4T1 and TM40 cells.

Results from Chapter 2 were replicated in Chapter 3 by showing that the CID mice experienced anhedonia and behavioural despair compared to sham control mice. A group of CID mice were treated with oral FLX to establish a benchmark antidepressant effect with a standard clinical antidepressant. FLX was in fact effective at preventing anhedonia and behavioural despair. Similarly, CID mice that were treated with oral SSZ did not develop anhedonia or behavioural despair. Orally ingested SSZ is predominantly cleaved into 5-aminosalicylic acid (5-ASA) and sulfapyridine (SP) in the gut (National Center for Biotechnology Information, 2005; Sontheimer & Bridges, 2012). Since 5-ASA has known anti-inflammatory properties (Kruis et al., 2001), and some depressed patients have high levels of systemic cytokines (Young, Bruno, & Pomara, 2014), a group of CID animals were also treated with 5-ASA/SP. The SSZ metabolites were effective at preventing anhedonia, but not behavioural despair. Serum cytokine analysis revealed that among the cytokines known to be elevated in depression, interleukin 6 (IL-6) and possibly IL-1 β were elevated in CID mice. Neither treatment with SSZ nor 5-ASA/SP were effective at preventing the elevations in cytokines. Taken together, these data suggested that intact SSZ was predominantly responsible for the observed anti-depressant effect on the behavioural assays, and this effect was primarily due to system x_c^- inhibition, rather than anti-inflammatory action.

The study in Chapter 3 also included a secondary analysis of the behavioural data. Since 4T1 cells are known to metastasize to the brain in

approximately 30% of animals (Pulaski & Ostrand-Rosenberg, 2001), it was important to address how brain metastasis might be affecting behavioural results. Regression analyses revealed that brain metastasis did not predict outcomes for the SPT. On the FST, brain metastasis was predictive of higher immobility for SSZ-treated mice. This was despite the observation that SSZ-treated mice had overall lower FST immobility compared to untreated mice, and suggests that SSZ may be less effective in mice that develop brain metastases. On the TST, brain metastasis predicted lower immobility and higher PM for untreated tumour-bearing mice. This observation was counterintuitive. However, it may help explain why the TST has been consistently ineffective at detecting behavioural despair in the CID model. It is possible that brain metastases affect locomotion on this test and confound the results. It would be interesting to further explore this possibility in a more controlled experiment using a 4T1 brain tumour model.

Objective 3: To investigate the CID model at the level of gene expression in comparison to a stress model of depressive-like behaviours.

This objective investigated the differential impact of a CORT-induced depressive state vs. a tumour-induced depressive state on hippocampal gene expression. Clinical and post-mortem studies on patients with major depressive disorder (MDD) have demonstrated abnormal function and decreased volume of the hippocampus (Fitzgerald et al., 2008; Koolschijn et al., 2009). In the study

outlined in Chapter 4, hippocampi were excised from mice used to establish the CID model in Chapter 2. RNA was extracted from the hippocampi and analyzed by RNA-sequencing (RNA-seq).

Analysis revealed that most differentially expressed genes (DEGs) that were associated with the CORT model were also associated with the CID model. This observation alone suggests a significant overlap in hippocampal alterations at the level of gene expression between the two models. However, the CID model was also associated with many additional DEGs that were not identified in the CORT model. Therefore, despite significant overlap, it appeared that some hippocampal alterations were specific to the CID model.

Quantitative real-time RT-PCR (qRT-PCR) was performed on a subset of DEGs to validate the results obtained through RNA-seq. Following validation, the DEGs were further explored using enrichment analyses. Kyoto Encyclopedia of Genes and Genomes (KEGG) pathway enrichment analysis identified calcium signalling and neuroactive ligand-receptor interaction in both models. In addition, MAPK signalling, longer-term potentiation (LTP), long-term depression (LTD), phosphatidylinositol signalling, and Alzheimer's disease pathways were identified for the CID model. Analysis of biological process gene ontologies (GO:BP) identified terms for both models relating to ion transport, chemical homeostasis, cellular communication and neurotransmission. In addition, terms were identified for the CID model relating to neuronal development and ensheathment,

intracellular signalling cascade, and locomotion. Taken together, these data suggest that alternations in neuronal signalling and communication are common between CORT and CID animals. In addition, alternations relating to learning and memory may be specific CID animals.

This study was the first of its kind to investigate and suggest a possibly distinct underlying pathophysiology associated with CID. However, caution should be taken in interpreting the results. This study was confined to changes in hippocampal gene expression. Several other brain regions are important in the study of depression, including the mPFC, amygdala, anterior cingulate cortex (ACC), and striatum. In addition, although alterations in hippocampal structure and function are associated with depression, it is possible that not all DEGs identified in this study are relevant to depression. It would be interesting to investigate the behavioural effects of pharmacologically or genetically interfering with the changes identified here. Future studies should exploit these findings to further delineate the specific mechanisms that lead to CID.

Future Directions

The development of a validated preclinical CID model represents a milestone in understanding the underlying pathophysiology of the disease. However, it is important to address some of the limitations inherent in animal models of complex disease states, and discuss possible methods of mitigating

them. The model discussed in Chapter 2 uses a specific mouse strain, BALB/c, and a specific murine cell line, 4T1. Based on early experimental data (Appendix 1), it may not be feasible to run behavioural tests on immunodeficient mouse strains inoculated with human cancer cells. Nonetheless, more models should be explored using different strains and cell lines. Chronic stress has been shown to induce different behavioural and physiological alterations in different mouse strains (Ibarguen-Vargas, Surget, Touma, Palme, & Belzung, 2008). Additionally, investigating alternate cell lines with varied characteristics would be useful in delineating the relationship between glutamate output and the induction of depressive features. For instance, it would be useful to know whether cancer cell lines that do not release large amounts of glutamate still induce depressive-like behaviours, and whether these models respond to the same treatment strategies as the model developed in Chapter 2.

As discussed in Chapter 3, the additive antidepressant effect of system x_c^- inhibition with standard antidepressants, such as FLX, would be particularly interesting to investigate. These treatment strategies are not likely to overlap at the physiological level, and yet both were shown to successfully prevent anhedonia and behavioural despair in CID mice. It is therefore plausible that the combination of both treatments would be more efficacious than either strategy alone. It may also be valuable to investigate other modes of drug administration for SSZ. Intraperitoneal administration using osmotic pumps would eliminate the confounding effect of intestinal cleavage of SSZ. However, it may introduce an

additional confound of depressive behaviours relating to invasive surgery. Future studies should also investigate the effects of S-4-carboxy-phenylglycine (S-4-CPG), a more specific system x_c^- inhibitor. To my knowledge S-4-CPG has not previously been administered orally, and would therefore require exploration of the safety and bioavailability to establish an appropriate dosage. As discussed in Chapter 3, modifying cancer cell strains to produce xCT knockdown cells with impaired system x_c^- function would be a more direct method of investigating the consequences of peripheral glutamate inhibition on the development of a depressive-like state. However, this method might introduce additional confounds relating to altered cell physiology, which might affect *in vivo* cellular growth, ability to metastasize, etc. Nevertheless, this model would be useful in determining whether cancer cell-derived glutamate is etiologically necessary in the development of CID. On the other hand, subcutaneously implanted glutamate pellets would be useful in determining whether cancer-cell derived glutamate is sufficient in inducing a depressive-like state. These pellets would mimic glutamate release by cancer cells and eliminate all other cancer-related modifications, such as stress and inflammatory responses. A major challenge with developing this model would be to determine an appropriate concentration and rate of glutamate release that reflects *in vivo* tumour growth over time. If this can be reasonable determined and glutamate pellets do not induce a depressive-like state, we may conclude that glutamate is not sufficient to induce CID. If the xCT knockdown model also does not induce a depressive-like state, we may conclude

that glutamate is likely necessary in the etiology of CID. This can be further confirmed if the combination of glutamate pellets in the xCT knockdown model restores a depressive-like state.

As discussed multiple times throughout this dissertation, peripheral glutamate is not able to cross the BBB into the brain under normal physiological conditions. In Chapter 3, I discussed the possibility that the weakening of the BBB by cancer cells might allow for bidirectional glutamate transport. Furthermore, the CID model was shown to be associated with increased IL-6 and possibly IL-1 β , both of which are known to reduce BBB integrity (Rochfort & Cummins, 2015; Wang et al., 2014). To further explore this possibility, a detailed assessment of BBB integrity should be conducted on CID mice. This could be done using tracers injected systemically and quantified in capillary depleted brain homogenate (On et al., 2013). Radiolabeled ^3H -mannitol is used as a low molecular weight marker and analyzed with a scintillation counter. Evan's Blue is used as a high molecular weight marker and analyzed spectrophotometrically.

The work presented in this dissertation did not investigate the possible contributing role of cancer therapies on the development of depression in cancer patients. This may be particularly relevant for chemotherapies that increase oxidative stress, and might therefore contribute to neuroinflammation and dendritic atrophy. It would be interesting to investigate whether the antidepressant

strategy presented in Chapter 3 remains efficacious in conjunction with common cancer treatments, such as chemotherapy, radiotherapy, and hormone therapy.

In Chapter 4, RNA-sequencing identified hippocampal gene alterations associated with both the CID model and the CORT model, some of which overlapped. As cautioned earlier, these alterations are not necessarily related to depression. To validate and further explore these alterations, intervention studies should be conducted to investigate whether the changes in mRNA levels of genes of interest correspond with altered protein activity. Most of the identified DEGs in the CID model were downregulated. Therefore, investigating the behavioural effects of inhibiting target proteins in healthy mice or creating knockdown models would help validate the DEGs identified in Chapter 4. It may also be interesting to investigate the vast amount of data produced from RNA-sequencing in more detail. Transcripts that were not detected as differentially expressed had a total abundance that was not significantly different from control. However, it is possible that for some of these transcripts, the relative abundance of different isoforms was in fact different between conditions. Since different isoforms of a transcript might lead to modified protein function, investigating alternative splicing events may be particularly important to consider.

Conclusions

The work presented in this dissertation encompasses the initial steps in determining the pathophysiology of CID. To accomplish this, a preclinical model of CID was developed and investigated. Behavioural and neuroanatomical data were used in conjunction with positive and negative control models to validate the CID model. Pharmacologically inhibiting the glutamate/cystine antiporter system x_c^- using SSZ prevented the development of anhedonia and behavioural despair in tumour-bearing mice. RNA-seq of hippocampal RNA derived from CID and control animals revealed a significant overlap of DEGs between CID mice and CORT mice. In addition, transcriptional changes relating learning and memory were specific to CID mice. This dissertation represents a fundamental shift in how depression is conceptualized in cancer. Investigating CID as a distinct form of depression will lead to a better understanding of this complex disease state, and propagate the development of better treatment strategies.

References

- Banasr, M., Chowdhury, G. M., Terwilliger, R., Newton, S. S., Duman, R. S., Behar, K. L., et al. (2010). Glial pathology in an animal model of depression: reversal of stress-induced cellular, metabolic and behavioral deficits by the glutamate-modulating drug riluzole. *Mol Psychiatry*, *15*(5), 501-511.
- Berman, R. M., Cappiello, A., Anand, A., Oren, D. A., Heninger, G. R., Charney, D. S., et al. (2000). Antidepressant effects of ketamine in depressed patients. *Biol Psychiatry*, *47*(4), 351-354.
- Chatterjee, M., Jaiswal, M., & Palit, G. (2012). Comparative evaluation of forced swim test and tail suspension test as models of negative symptom of schizophrenia in rodents. *ISRN Psychiatry*, *2012*, 595141.
- Cook, S. C., & Wellman, C. L. (2004). Chronic stress alters dendritic morphology in rat medial prefrontal cortex. *J Neurobiol*, *60*(2), 236-248.
- Fitzgerald, P. B., Laird, A. R., Maller, J., & Daskalakis, Z. J. (2008). A meta-analytic study of changes in brain activation in depression. *Hum Brain Mapp*, *29*(6), 683-695.
- Gourley, S. L., Espitia, J. W., Sanacora, G., & Taylor, J. R. (2012). Antidepressant-like properties of oral riluzole and utility of incentive disengagement models of depression in mice. *Psychopharmacology (Berl)*, *219*(3), 805-814.

Gourley, S. L., & Taylor, J. R. (2009). Recapitulation and reversal of a persistent depression-like syndrome in rodents. *Curr Protoc Neurosci, Chapter 9*, Unit 9 32.

Green, A. I., & Austin, C. P. (1993). Psychopathology of pancreatic cancer. A psychobiologic probe. *Psychosomatics, 34*(3), 208-221.

Ibarguen-Vargas, Y., Surget, A., Touma, C., Palme, R., & Belzung, C. (2008). Multifaceted strain-specific effects in a mouse model of depression and of antidepressant reversal. *Psychoneuroendocrinology, 33*(10), 1357-1368.

Ibrahim, L., Diazgranados, N., Franco-Chaves, J., Brutsche, N., Henter, I. D., Kronstein, P., et al. (2012). Course of improvement in depressive symptoms to a single intravenous infusion of ketamine vs add-on riluzole: results from a 4-week, double-blind, placebo-controlled study. *Neuropsychopharmacology, 37*(6), 1526-1533.

Jacobsson, L., & Ottosson, J. O. (1971). Initial mental disorders in carcinoma of pancreas and stomach. *Acta Psychiatr Scand Suppl, 221*, 120-127.

Kempton, M. J., Salvador, Z., Munafo, M. R., Geddes, J. R., Simmons, A., Frangou, S., et al. (2011). Structural neuroimaging studies in major depressive disorder. Meta-analysis and comparison with bipolar disorder. *Arch Gen Psychiatry, 68*(7), 675-690.

Koolschijn, P. C., van Haren, N. E., Lensvelt-Mulders, G. J., Hulshoff Pol, H. E., & Kahn, R. S. (2009). Brain volume abnormalities in major depressive

disorder: a meta-analysis of magnetic resonance imaging studies. *Hum Brain Mapp*, 30(11), 3719-3735.

Krackow, S., Vannoni, E., Codita, A., Mohammed, A. H., Cirulli, F., Branchi, I., et al. (2010). Consistent behavioral phenotype differences between inbred mouse strains in the IntelliCage. *Genes Brain Behav*, 9(7), 722-731.

Kruis, W., Schreiber, S., Theuer, D., Brandes, J. W., Schutz, E., Howaldt, S., et al. (2001). Low dose balsalazide (1.5 g twice daily) and mesalazine (0.5 g three times daily) maintained remission of ulcerative colitis but high dose balsalazide (3.0 g twice daily) was superior in preventing relapses. *Gut*, 49(6), 783-789.

Lamkin, D. M., Lutgendorf, S. K., Lubaroff, D., Sood, A. K., Beltz, T. G., & Johnson, A. K. (2011). Cancer induces inflammation and depressive-like behavior in the mouse: modulation by social housing. *Brain Behav Immun*, 25(3), 555-564.

Li, N., Liu, R. J., Dwyer, J. M., Banasr, M., Lee, B., Son, H., et al. (2011).

Glutamate N-methyl-D-aspartate receptor antagonists rapidly reverse behavioral and synaptic deficits caused by chronic stress exposure. *Biol Psychiatry*, 69(8), 754-761.

National Center for Biotechnology Information. (2005). PubChem Compound Database; CID=5384001. Retrieved November 19, 2015:
<https://pubchem.ncbi.nlm.nih.gov/compound/5384001>

- Ng, C. G., Boks, M. P., Zainal, N. Z., & de Wit, N. J. (2011). The prevalence and pharmacotherapy of depression in cancer patients. *J Affect Disord*, *131*(1-3), 1-7.
- Norden, D. M., Bicer, S., Clark, Y., Jing, R., Henry, C. J., Wold, L. E., et al. (2015). Tumor growth increases neuroinflammation, fatigue and depressive-like behavior prior to alterations in muscle function. *Brain Behav Immun*, *43*, 76-85.
- On, N. H., Mitchell, R., Savant, S. D., Bachmeier, C. J., Hatch, G. M., & Miller, D. W. (2013). Examination of blood-brain barrier (BBB) integrity in a mouse brain tumor model. *J Neurooncol*, *111*(2), 133-143.
- Passik, S. D., & Roth, A. J. (1999). Anxiety symptoms and panic attacks preceding pancreatic cancer diagnosis. *Psychooncology*, *8*(3), 268-272.
- Pulaski, B. A., & Ostrand-Rosenberg, S. (2001). Mouse 4T1 breast tumor model. *Curr Protoc Immunol*, Chapter 20, Unit 20.22.
- Pyter, L. M., Pineros, V., Galang, J. A., McClintock, M. K., & Prendergast, B. J. (2009). Peripheral tumors induce depressive-like behaviors and cytokine production and alter hypothalamic-pituitary-adrenal axis regulation. *Proc Natl Acad Sci U S A*, *106*(22), 9069-9074.
- Rochfort, K. D., & Cummins, P. M. (2015). The blood-brain barrier endothelium: a target for pro-inflammatory cytokines. *Biochem Soc Trans*, *43*(4), 702-706.

- Rodin, G., Lloyd, N., Katz, M., Green, E., Mackay, J. A., Wong, R. K., et al. (2007). The treatment of depression in cancer patients: a systematic review. *Support Care Cancer*, *15*(2), 123-136.
- Seidlitz, E. P., Sharma, M. K., Saikali, Z., Ghert, M., & Singh, G. (2009). Cancer cell lines release glutamate into the extracellular environment. *Clin Exp Metastasis*, *26*(7), 781-787.
- Seidlitz, E. P., Sharma, M. K., & Singh, G. (2010). A by-product of glutathione production in cancer cells may cause disruption in bone metabolic processes. *Can J Physiol Pharmacol*, *88*(3), 197-203.
- Sharma, M. K., Seidlitz, E. P., & Singh, G. (2010). Cancer cells release glutamate via the cystine/glutamate antiporter. *Biochem Biophys Res Commun*, *391*(1), 91-95.
- Sontheimer, H., & Bridges, R. J. (2012). Sulfasalazine for brain cancer fits. *Expert Opin Investig Drugs*, *21*(5), 575-578.
- Spratling, M. W. (2002). Cortical region interactions and the functional role of apical dendrites. *Behav Cogn Neurosci Rev*, *1*(3), 219-228.
- Van Esch, L., Roukema, J. A., Ernst, M. F., Nieuwenhuijzen, G. A., & De Vries, J. (2012). Combined anxiety and depressive symptoms before diagnosis of breast cancer. *J Affect Disord*, *136*(3), 895-901.
- Wang, Y., Jin, S., Sonobe, Y., Cheng, Y., Horiuchi, H., Parajuli, B., et al. (2014). Interleukin-1beta induces blood-brain barrier disruption by downregulating Sonic hedgehog in astrocytes. *PLoS One*, *9*(10), e110024.

- Wellman, C. L. (2001). Dendritic reorganization in pyramidal neurons in medial prefrontal cortex after chronic corticosterone administration. *J Neurobiol*, 49(3), 245-253.
- Williams, S., & Dale, J. (2006). The effectiveness of treatment for depression/depressive symptoms in adults with cancer: a systematic review. *Br J Cancer*, 94(3), 372-390.
- Yang, M., Kim, J., Kim, J. S., Kim, S. H., Kim, J. C., Kang, M. J., et al. (2014). Hippocampal dysfunctions in tumor-bearing mice. *Brain Behav Immun*, 36, 147-155.
- Young, J. J., Bruno, D., & Pomara, N. (2014). A review of the relationship between proinflammatory cytokines and major depressive disorder. *J Affect Disord*, 169c, 15-20.
- Zarate, C. A., Jr., Brutsche, N. E., Ibrahim, L., Franco-Chaves, J., Diazgranados, N., Cravchik, A., et al. (2012). Replication of ketamine's antidepressant efficacy in bipolar depression: a randomized controlled add-on trial. *Biol Psychiatry*, 71(11), 939-946.

APPENDIX 1

Optimization Data for Establishing Cancer-Induced Depression

Model

Preface

This section summarizes animal experiments leading up to the development of the cancer-induced depression (CID) model that was described in Chapter 2. The primary purpose of presenting this data is to clarify the rationale for the details of this model. Obstacles encountered during this work are highlighted, which may also be useful for the development of additional CID models and animal models of disease in general. I performed all experimental procedures described in this section. Statistical analyses were not performed for preliminary experiments due to the low numbers of animals. Rather, the purpose of these experiments was to optimize methodology and animal models. Dr. Eric Seidlitz provided technical training and input on experimental designs. Dr. Gurmit Singh, Dr. Benicio Frey, and Dr. Laurie Doering provided intellectual direction and guidance.

Experiment 1

Background Information

This study was a preliminary study to optimize the behavioural tests and experimental models. I attempted to adapt a model of cancer-induced bone pain to study depressive-behaviours. Our team had successfully developed this model in immunodeficient BALB/c nu/nu mice inoculated with human MDA-MB-231 breast cancer cells. These cells had been shown to release high levels of glutamate, primarily through the pharmacologically targetable system x_c^- antiporter. The immunodeficient model allowed for xenotransplantation of human cancer cells to an animal model. Cells were injected into the right distal femur of mice and allowed to develop for 4 weeks.

To induce a positive control model of a depressive-like state, mice were chronically administered corticosterone (CORT). *Ad libitum* oral administration was chosen, as this method is particularly non-invasive and would, therefore, avoid the additional stress of injections or gavage feeding.

Experimental Design

Behavioural Assays

The sucrose preference test (SPT) was chosen as a proxy for anhedonia. To avoid interfering with cancer cell glucose metabolism, saccharin was chosen

as a substitute for sucrose. Prior to baseline testing, BALB/c nu/nu preference for saccharin was investigated to determine an optimal concentration for the SPT. To perform the saccharin preference curve for varying concentrations of saccharin solution, animals were single housed and each animal was presented with a 2-bottle choice of water and one of the saccharin concentrations for a 24h period. Bottles were weighed after a 24h exposure period and preference was calculated as the percentage of saccharin solution consumed relative to total fluid consumption. Tests took place every other day over a 14-day period. By the end of this period, each mouse had been exposed to each saccharin concentration in random order. Typically, a concentration is used for which animals display ~70-80% preference. Significantly higher or lower baseline preferences render the test insensitive due to insufficient changes in preference post-treatment. Based on the results from this preference curve (**Figure 1.1**), a saccharin concentration of 0.2% was chosen for baseline and post-treatment testing.

The tails suspension test (TST) and forced swim test (FST) were used to assess behavioural despair. Automated testing was not available at this stage. Therefore, the TST and FST were executed manually. For both tests, mice were rated for immobility for a total of 6 minutes. Immobility was defined as the absence of active, escape-oriented behaviours. Every 30 seconds for the duration of the test, mice were observed for ~10 s and immobility recorded as being present or absent. This yielded a non-parametric 12-point data set for each test, where a low score indicated more time spent immobile.

Positive Control Model

For the positive control model, CORT hemisuccinate was dissolved in Milli-Q water to attain a concentration of 25 µg/ml. Average CORT dose was determined over a 14 day period by weighing the bottles daily and dividing consumption values by the total body weight of the animals in the cage.

Cancer Model

10⁶ MDA-MB-231 cells were injected in the distal femur of mice in the cancer group. Sham inoculations with sterile PBS were used for mice in the positive control group. Tumours were allowed to develop for 4 weeks prior to post-treatment testing.

Experimental Groups

Ten BALB/c nu/nu mice, group-housed in 2 cages, were designated to receive either chronic CORT administration (n = 5) or cancer cell inoculation (n = 5). Behavioural testing was performed at baseline and post-treatment.

Results & Discussion

Positive control mice consumed a mean CORT dose of 4.61 mg/kg/day, which was slightly below the reported effective range of 5.7 – 6.9 mg/kg/day. In the SPT, positive control mice did not exhibit a change in preference for saccharin between baseline and post-treatment (**Figure 1.2**). By contrast, cancer mice exhibited a reduction in preference for saccharin between baseline and post-

treatment. During the TST, several mice were completely immobile due to a behaviour that the mice adapt whereby they were able to grab on to their hind legs. While this behaviour persists, the animals do not struggle, but are also unable to show the characteristic immobility associated with despair, rendering a large portion of the test invalid. Therefore, all TST data was excluded. During FST testing, poor swimming ability was observed in this strain of mice. FST testing was terminated due to risk of drowning.

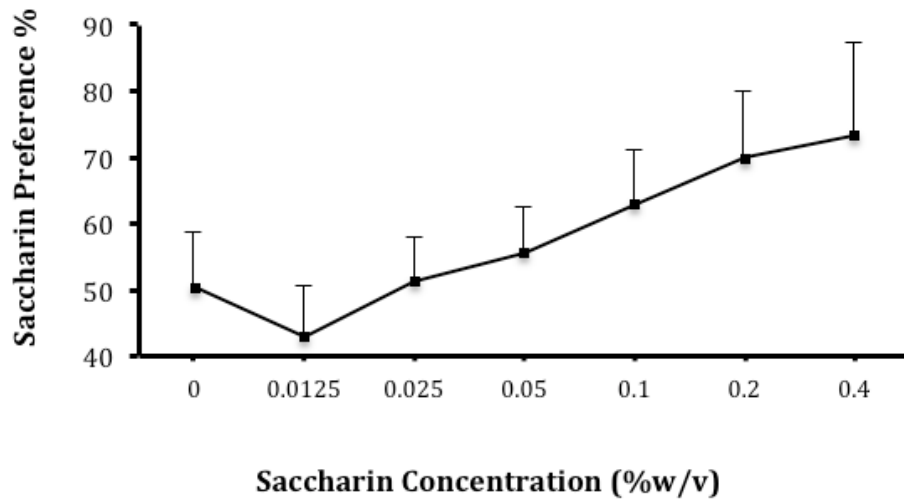
Figures

Figure 1.1. Saccharin preference curve for BALB/c nu/nu mice. Results show that the concentration of 0.2% saccharin should be utilized for this strain. 50% saccharin preference represents equal consumption of regular water compared to saccharin solution, and therefore no preference for saccharin. Data are expressed as the mean of n=10 animals \pm the standard error of the mean (SEM).

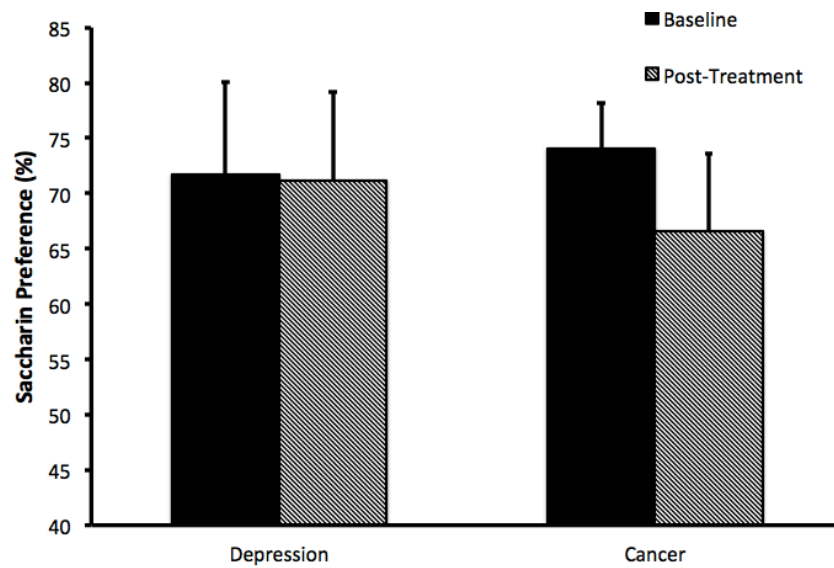


Figure 1.2. Saccharin preference test. Depression group was subjected to chronic CORT administration. This group did not show a reduction in preference for saccharin. The cancer group was injected intrafemorally with 10^6 MDA-MB-231 breast cancer cells. Post-treatment testing occurred 4 weeks after inoculations. This group showed a reduction in preference for saccharin ($\sim 7.5\%$) post-treatment. Data are expressed as the mean \pm the standard error of the mean (SEM).

Experiment 2

Background Information

To mitigate the problems encountered with BALB/c nu/nu mice in Experiment 1, Fox Chase SCID mice were obtained for this experiment. SCID mice are also immunocompromised (severe combined immunodeficiency affecting B and T lymphocytes). This model allowed for continued investigation of intrafemorally injected MDA-MB-231 cells.

Experimental Design

Behavioural Assays

The sucrose/saccharin preference test (SPT) was carried out as described in Experiment 1. A new preference curve was established for SCID mice (**Figure 2.1**), and a concentration of 0.2% saccharin solution was chosen for baseline and post-treatment testing.

The tails suspension test (TST) and forced swim test (FST) were performed manually as described in Experiment 1.

Positive Control Model

For the positive control model, CORT hemisuccinate was dissolved in Milli-Q water to attain a concentration of 35 µg/ml. A higher concentration of CORT was chosen for this experiment due to mice drinking less water than

expected in the previous experiment, and consequently achieving a suboptimal dose.

Cancer Model

10⁶ MDA-MB-231 cells were injected in the distal femur of mice in the cancer group. Sham inoculations with sterile PBS were used for mice in the positive control group. Tumours were allowed to develop for 4 weeks prior to post-treatment testing.

Experimental Groups

Nine Fox Chase SCID mice, group-housed in 3 cages, were designated to receive either chronic CORT administration (n = 3), cancer cell inoculation (n = 3), or sham inoculation (n = 3). Behavioural testing was performed at baseline and post-treatment.

Results & Discussion

Fox Chase SCID mice did not show the same confounding behaviours on the TST as BALB/c nu/nu mice, and were adept at swimming in the FST. Positive control mice consumed a mean CORT dose of 5.39 mg/kg/day, which is within the reported effective range. Despite this, positive control mice did not exhibit depressive-like behaviours on any of the 3 behavioural tests (data not shown). Mice in the cancer group exhibited increased immobility on the FST and TST, as well as reduced preference for saccharin on the SPT (**Figure 2.2**).

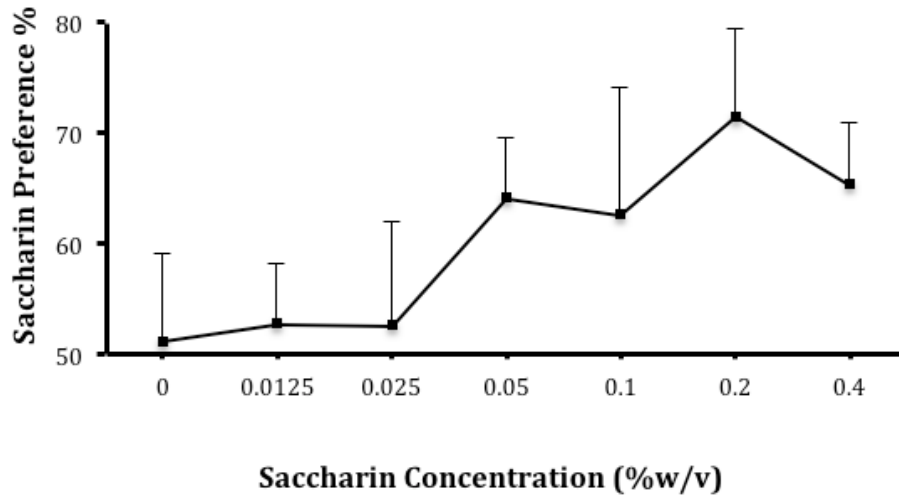
Figures

Figure 2.1. Saccharin preference curve for Fox Chase SCID mice. Results show that the concentration of 0.2% saccharin should be utilized for this strain. 50% saccharin preference represents equal consumption of regular water compared to saccharin solution, and therefore no preference for saccharin. Data are expressed as the mean of n=9 animals \pm the standard error of the mean (SEM).

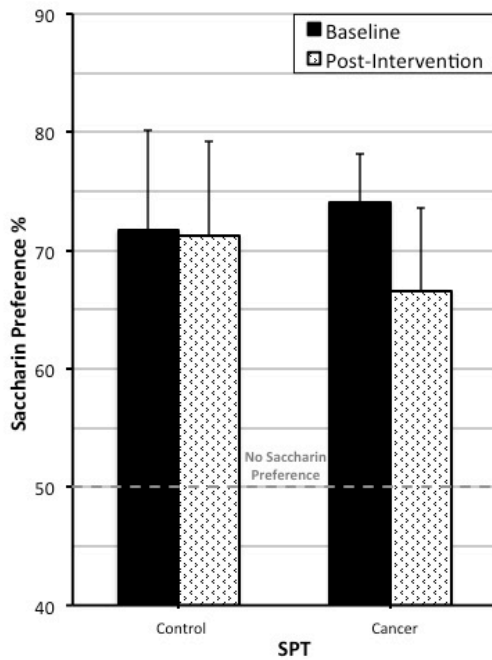
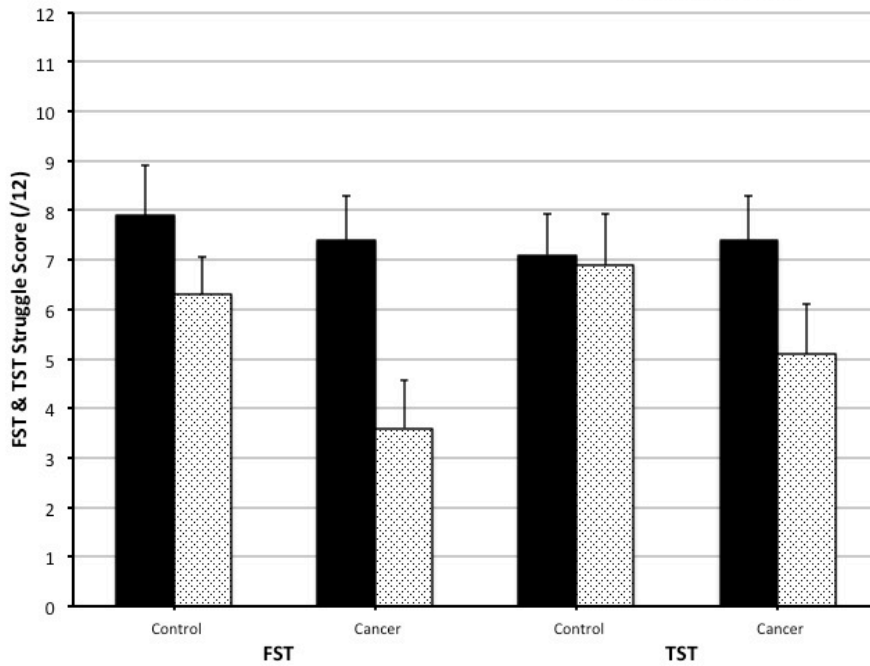


Figure 2.2. Behaviour results.

Control group was sham injected with sterile PBS. Cancer mice were intrafemorally inoculated with 10^6 MDA-MB-231 breast cancer cells. Decreased FST and TST scores for the cancer group indicate behavioural despair. Decreased preference for saccharin indicates anhedonia. Post-treatment

testing occurred 4 weeks after inoculations. Data are expressed as the mean \pm the standard error of the mean (SEM).

Experiment 3

Background Information

In Experiment 2, Fox Chase SCID mice proved to be much more amiable to behavioural testing than the BALB/c nu/nu mice in Experiment 1. However, the positive mice in Experiment 2 did not show depressive-like behaviours despite achieving a reportedly effective dose of oral CORT. This experiment focused on troubleshooting the positive control model and was designed to investigate several possible reasons for the lack of depressive-like behaviours in this model:

- 1) Low number of animals failed to detect depressive-like behaviours.
- 2) Manual scoring of TST and FST introduced scoring inaccuracies.
- 3) SCID mice (and possibly immunodeficient mice in general) are not susceptible to stress via oral administration of CORT.
- 4) Oral CORT was not properly prepared/administered.

Experimental Design

Experimental Groups

Three experimental groups were included in this experiment:

- SCID mice; subcutaneous (s.c.) CORT injections (n = 9)
- SCID mice; oral CORT administration (n = 9)
- C57BL/6 mice, oral CORT administration (n = 9)

Mice were housed 3 per cage. Increasing the number of animals per group to 9 addresses the possibility of low numbers failing to detect depressive-like symptoms. In addition, the SCID group receiving s.c. injections of CORT was introduced to investigate the possibility that the SCID mice are simply not susceptible to oral administration of CORT. Finally, the C57BL/6 group was included to test the possibility that the oral CORT is not being prepared/administered properly since this strain is known to be susceptible to oral CORT. The use of automated systems for the FST and TST, as apposed to manual scoring, eliminates the possibility of scoring bias.

CORT Administration

S.c. CORT was suspended in 0.9% saline and Tween-80, and injected in volumes corresponding to 20mg/kg/day over a period of 21 days. Based on water consumption in the preliminary results for the SCID mice and literature for the C57 mice, orally administered CORT was dissolved in water at 35 ug/ml for SCID and 25 ug/ml for C57 mice and presented ad libitum over 21 days. The average calculated dose was 5.66 mg/kg/day for SCID mice and 3.78 mg/kg/day for C57 mice. In this experiment, C57 mice did not reached the desired dosing of CORT. However, using a slightly higher concentration, SCID mice were in the appropriate dosing range.

Sucrose/Saccharin Preference Test

The SPT was carried out at baseline prior to CORT exposure, and again post-treatment starting 5 days after CORT cessation. At each time point, 3 individual SPTs were performed, the first of which was excluded from analysis as it merely served to habituate the mice to saccharin and overcome novelty anxiety. For the remaining 2 tests at each time point, saccharin and water position were counterbalanced in the cage to avoid confound of side preference. Preference was calculated as percentage of saccharin solution consumed of the total fluid consumption.

In addition to variable levels of water consumption, different strains of mice exhibit different baseline preference for sucrose/saccharin solution. Based on preliminary testing, SCID mice were administered a 0.2% saccharin solution, while C57 mice were administered a 0.1% solution. Despite this correction, it is worth noting that baseline saccharin preference for C57 mice was very high (nearly 90%), whereas SCID mice in both groups exhibited more moderate baseline saccharin preference (70-80%).

Tail Suspension Test

Automated TST was performed using the EB Instruments system. In addition to immobility time, this system is able to report energy and power of movement. Testing was performed 3 times prior to depression induction to establish a stable baseline for each experimental group. The test was performed an additional 3 times after cessation of CORT administration. Each test lasted for 6

minutes, with the first minute excluded from analysis. In addition to immobility, the energy of movement was also analyzed.

Forced Swim Test

Automated FST was performed using the EB Instruments system. Testing was performed 3 times prior to depression induction to establish a stable baseline for each experimental group. The test was performed an additional 3 times after cessation of CORT administration. Each test lasted for 6 minutes, with the first minute excluded from analysis. Water was warmed to 28-30°C to avoid hypothermia and mice were dried off using sterile surgical towels.

CORT Enzyme-Linked Immunosorbent Assay

A corticosterone ELISA (Enzo Life Sciences) was used to detect levels of CORT in the serum of animals. Orbital blood samples were collected at baseline prior to testing, and at midpoint (1 day after CORT cessation). Blood was collected intracardially at endpoint during sacrifice (3 weeks after CORT cessation). Blood was collected at the same time of day to avoid confounding fluctuations of CORT levels during different times of the day. Normal CORT levels for mice are reported in the kit manual to be 49 to 159 ng/ml. Samples for each animal were run in duplicates.

Results & Discussion

Post-treatment results for the SPT revealed no behavioural changes for any of the 3 experimental groups (**Figure 3.1**). While this was expected for the SCID mice based on preliminary results, CORT was expected to induce anhedonia in C57 mice. One possibility for the lack of anhedonic response by the C57 mice is that initial saccharin preference was simply too high to overcome. It is possible that a more dilute concentration of saccharin would produce a more sensitive SPT for the C57 strain.

Results from the TST analysis revealed a statistically significant increase in immobility time for the oral SCID group and the oral C57 group (**Figure 3.2**). Energy of motion was also significantly reduced in both of these groups. Therefore, the TST detected despair with oral administration of CORT, but not s.c. injections of CORT, for SCID and C57 mice.

Results from the FST analysis revealed a statistically significant increase in immobility time for the oral C57 group (**Figure 3.3**). Therefore, the FST only detected despair with oral administration of CORT to C57 mice. It should be noted that due to software and hardware problems with the FST during this experiment, automated testing was performed using the video data only, and does not integrate vibration sensor data.

Chronic CORT treatment severely inhibits the adrenal glands from releasing endogenous CORT. Weeks after the end of treatment, adrenal function recovers and overcompensates, becoming chronically overactive due to the

enduring effects of CORT treatment. In this experiment, both s.c. and oral CORT appear to have successfully inhibited adrenal function in both strains of mice at midpoint (**Figure 3.4**). Endpoint serum indicates that adrenal function has begun to recover in the s.c. group, but not in the 2 oral groups. If endpoint was delayed by a couple of weeks, it is likely that all groups would show elevated CORT levels compared to baseline. However, these results reveal that under the parameters of this experiment, oral CORT causes more prolonged initial inhibition of the adrenal glands. This model may, therefore, be more robust in inducing chronic depressive like behaviours.

All groups in this experiment responded physiologically similarly to chronic CORT administration, irrespective of method of delivery or mouse strain. However, behavioural responses were varied. SCID mice chronically injected s.c. with CORT did not show depressive behaviours on any of the 3 behavioural tests. SCID mice administered chronic CORT orally did not show signs of anhedonia and presented mixed results for behavioural despair. In contrast, C57 mice consistently showed signs of behavioural despair following oral CORT administration. Lack of anhedonic response may be attributed a very high baseline saccharin preference. In addition, lack of robust results for the C57 group may be attributed to failure to reach desired CORT dosing due to unexpectedly low levels of water consumption. Despite this, C57 mice displayed more depressive-like behaviours than SCID mice. Therefore, SCID mice, and other immunodeficient strains, should be avoided in behavioural studies of depression due to

complications on behavioural tests as well as difficulty in depression induction using the existing validated methodology.

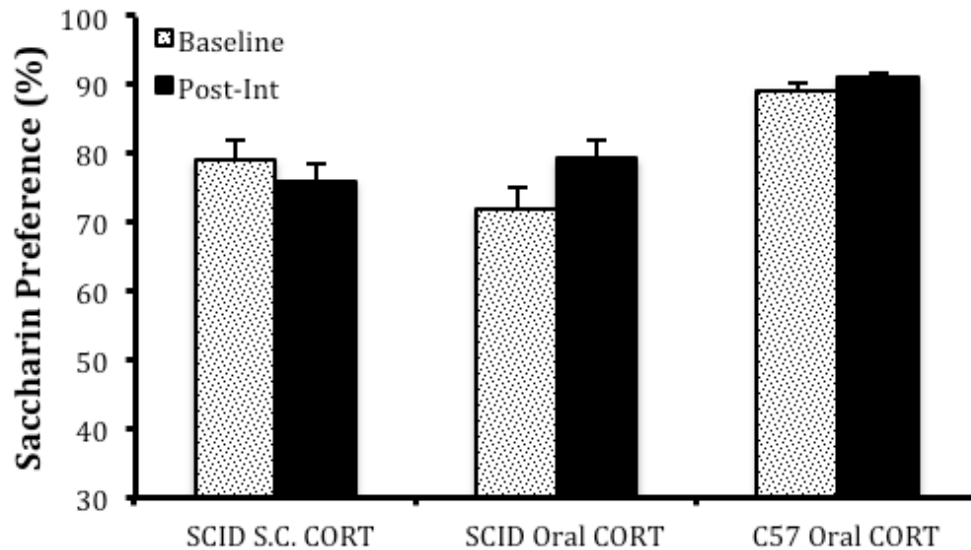
Figures

Figure 3.1. Saccharin preference test. SCID S.C. CORT group was administered subcutaneous CORT at 20mg/kg/day for 21 days. SCID Oral CORT group was administered 35ug/mL CORT *ad libitum*. C57 Oral CORT group was administered 25ug/mL CORT *ad libitum*. No behavioural indications of anhedonia were observed for any of the 3 groups. Data are expressed as the mean \pm the standard error of the mean (SEM). Statistical significance was assessed through 1-tailed pairwise student t-tests.

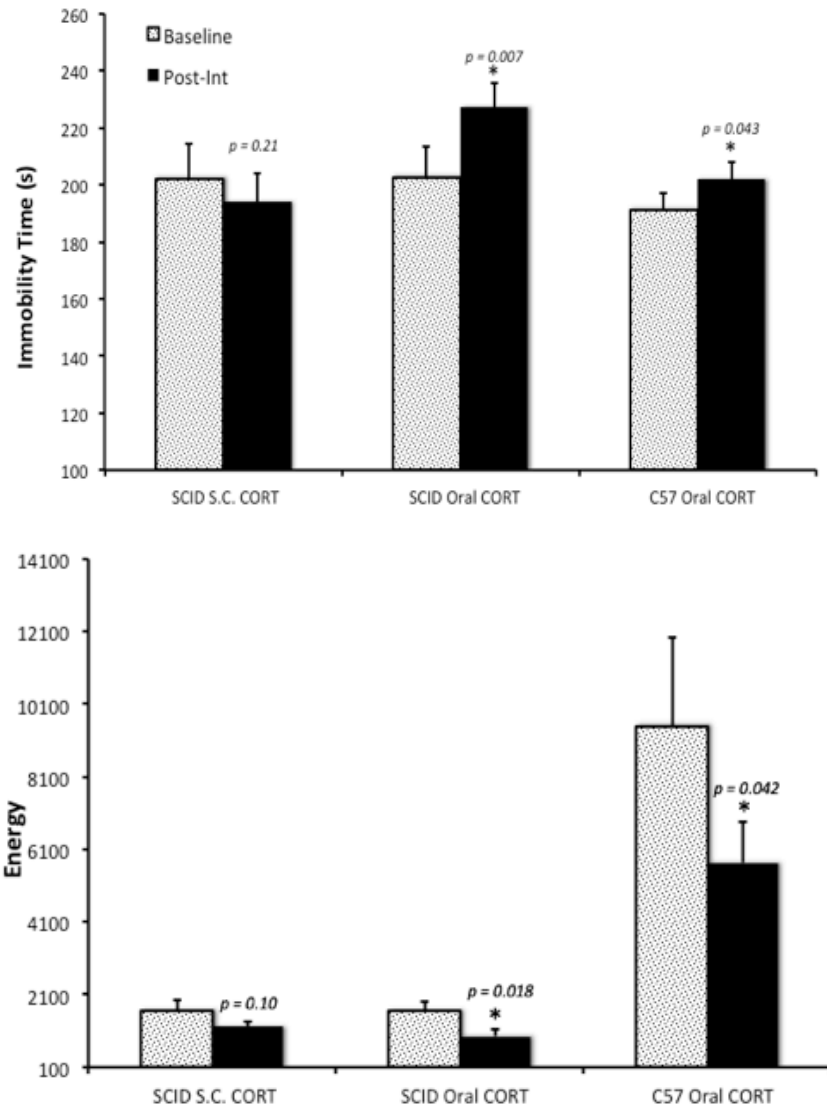


Figure 3.2. Tail suspension test. Bars represent average scores for 3 baseline tests and 3 post-treatment tests. Mice were suspended for 6 minutes, with the first minute excluded from analysis. Both strains of mice under oral CORT administration exhibited behavioural despair. Data are expressed as the mean \pm the standard error of the mean (SEM). Statistical significance was assessed through 1-tailed pairwise student t-tests. * $P < 0.05$.

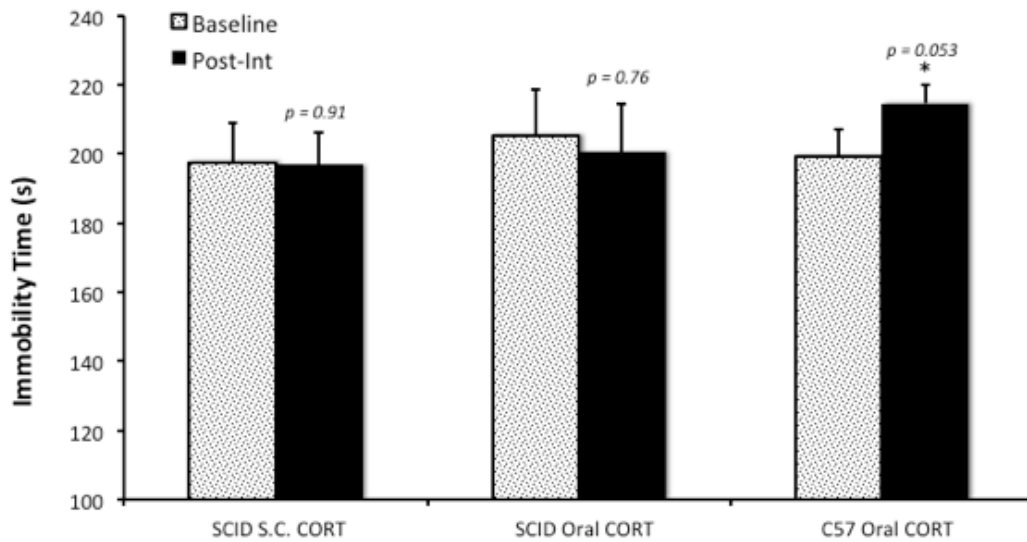


Figure 3.3. Forced swim test. Bars represent average scores for 3 baseline tests and 3 post treatment tests. Mice were placed in beakers for 6 minutes, with the first minute excluded from analysis. Only C57 mice under oral CORT administration exhibited behavioural despair. Data are expressed as the mean \pm the standard error of the mean (SEM). Statistical significance was assessed through 1-tailed pairwise student t-tests. * $P < 0.05$.

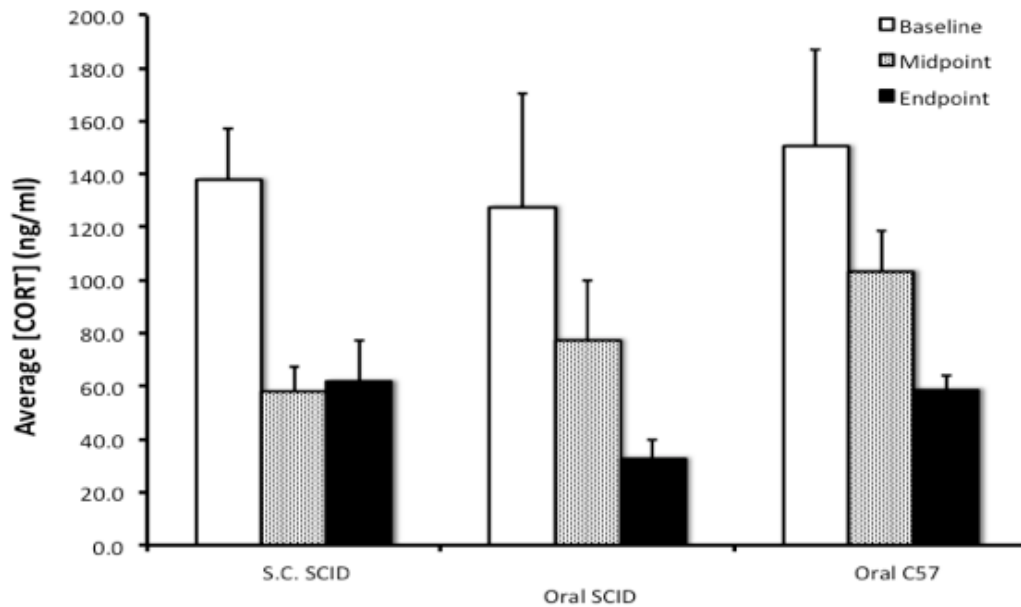


Figure 3.4. CORT ELISA. Baseline and midpoint blood was collected orbitally and serum was separated for analysis. Endpoint blood was collected intracardially. Analysis indicates inhibited adrenal function at midpoint following CORT cessation for all groups. At endpoint, the subcutaneous group shows signs of recovering adrenal function, while the oral groups show a continued decline in adrenal function 3 weeks after CORT cessation. All samples were run in duplicates.

Experiment 4

Background Information

Results from the previous experiments clearly indicate that immunodeficient mice are unsuitable for behavioural studies on depression. Therefore, a new model must be chosen that satisfies 2 criteria: 1) the mouse strain must be suitable for behavioural testing and depression induction by chronic stress, and 2) a suitable cancer cell line must be compatible with the chosen mouse strain. This cell line should be a close analogue to aggressive human breast cancers that lead to metastatic disease.

Immunocompetent BALB/c mice are a highly emotional strain and are susceptible to depression induction by chronic mild stress. Murine 4T1 mammary carcinoma, derived from a spontaneously arising mammary tumour in BALB/c mice, are highly invasive, and can spontaneously metastasize to various organs. They are, therefore, a good analogue to human stage IV breast cancer. Therefore, BALB/c mice with subcutaneous 4T1 cancer cell injections were chosen as the new model for cancer induced depression.

The primary objective of this experiment was to test the BALB/c model with 4T1 cancer cells as a potential cancer-induced depression (CID) model. In addition to the positive control using chronic oral CORT administration, this experiment also introduces a reversal group in which fluoxetine (FLX) is administered chronically to reverse the depressive-like behaviours induced by

CORT. An additional small group is included as a “double negative” control, which will not undergo any behavioural tests at baseline. This group will serve as a control for the CORT ELISA analysis and will serve to eliminate any confounding effects of behavioural testing exposure on serum CORT levels.

Experimental Design

Experimental Groups

Five experimental groups were included in this experiment, with mice housed 3 per cage:

- Negative Control (sham cancer cell injections; n = 6)
- CORT positive control (sham cancer cell injections; n = 6)
- Cancer, 20x10⁵ cells injected orthotopically (n = 6)
- Reversal, Co-admin of CORT and FLX (sham cancer cell injections; n = 6)
- Double negative control (no sham injections, no behavioural tests)

CORT & FLX Administration

In light of previous difficulty ensuring that mice reach the desired CORT dosing and exhibit behavioural changes, CORT was administered at a concentration of 50 ug/ml. CORT water was presented *ad libitum* in the cages

over a period of 21 days. The average calculated dose was 7.74 mg/kg/day for the positive control CORT group and 7.00 mg/kg/day for the reversal group.

FLX was dissolved in the CORT water at a concentration of 60 ug/ml and administered for the same 21-day period in the reversal group. The average calculated dose of FLX was 8.40 mg/kg/day, which is slightly lower than the reported effective chronic low dose of 10 to 18 mg/kg/day.

Behavioural Assays

Mice were first habituated to sucrose, as well as the TST and FST. The SPT was performed 4 times at baseline and 4 times post-treatment and bottles were counterbalanced in the cages to avoid side bias. Automated TST and FST were performed 2 times at baseline and 2 times post-treatment.

The SPT was performed as previously described in Experiment 3, with the exception of using sucrose in place of previously used saccharin. For the current experiment, a 3% sucrose solution was used, which provided baseline preference levels of about 65-70%. The TST and FST were performed as previously described in Experiment 3

CORT Enzyme-Linked Immunosorbent Assay

Blood collection was performed as described in Experiment 3, except for one alteration. Rather than collecting blood at endpoint during sacrifice, blood was collected orbitally 1 day prior to sacrifice in order to ensure consistency in blood collection method and timing.

Results & Discussion

Results for the SPT revealed a reduction in preference, and therefore an anhedonic response, for the positive control CORT group and the reversal group (**Figure 4.1**). Thus, reversal of the anhedonic response to CORT was not achieved with the current dosing of CORT and FLX in the reversal group. The cancer group did not show an anhedonic response on the SPT. This may be due to a protective effect of group-housing.

Results for the TST reveal no differences in time of immobility for any of the groups. However, energy of movement was decreased for both the CORT and reversal group, although the results are not statistically significant (**Figure 4.2**). Therefore, it is possible that the CORT and reversal groups exhibited behavioural despair on the TST in addition to anhedonia on the SPT, but further investigation is needed to establish robust response on the TST. Additionally, the energy of movement for the cancer group was markedly increased. This was due to a confounding behaviour that was observed during testing. Due to the orthotopic location of the tumour growth on the lower abdomen, mice were able to grab and hold on to their growths and avoid freely hanging. Often unsuccessful due to the tumour sizes, the mice would then release their hold abruptly, registering increased energy of movement on the TST system.

Results for the FST did not reveal any increase in immobility for the CORT group, and therefore a lack of behavioural despair (**Figure 4.3**). The control, cancer, and reversal groups showed slight decreases in immobility, which

indicates absence of behavioural despair in the cancer model, but also possible reversal of depressive behaviours for the reversal group in this paradigm.

Results for the CORT ELISA were standardized to serum CORT levels of the double negative control group at each time point (baseline, midpoint, and endpoint) (**Figure 4.4**). The control group had elevated CORT at baseline and midpoint. This was somewhat surprising and may be due to handling. The CORT group exhibits the pattern that was expected- baseline CORT is close to 100% of control, followed by a marked drop in CORT at midpoint due to adrenal inhibition, and finally an increase in CORT at endpoint that surpasses control level due to overactivity of adrenal glands. Although FLX dosing was likely too low to observe significant behavioural changes, it is evident from this serum analysis that FLX co-administration had an effect as all 3 time points show similar levels of serum CORT. FLX normalizes HPA activity when co-administered by inhibiting CORT transport across the blood-brain barrier, which increases CORT in the brain and activates glucocorticoid receptors. This in turn increases negative feedback on the HPA axis. The cancer group showed increased CORT at midpoint due to tumour group, and another very steep increase at endpoint. This may be attributable to the pro-inflammatory state of cancer, which activates the HPA axis to release CORT in order to negatively feedback on the inflammatory response.

In this experiment, results from the positive control CORT model were promising. CORT mice showed an anhedonic response the SPT as well as behavioural despair on the energy of movement measure of the TST. Several

adjustments to the current experimental design should be implemented for future investigations:

- FLX solution concentration should be increased to achieve desired dosing. To investigate reversal rather than prevention of depressive-behaviours, FLX administrations should follow CORT administration, rather than being co-administered.
- Group-housing may be inducing a protective effect. Therefore, future experiments should be performed using individually-housed mice.
- The location of cancer cell inoculation needs to be changed in order to avoid the confounding effect of tumour grabbing on the TST. For future experiments, cancer cells should be subcutaneously injected above the flank of the animal, but positioned carefully to avoid interfering with joint movement.
- Prolonged exposure to sucrose solution prior to baseline SPT may better ensure absence of novelty-related anxiety. This could be accomplished with a 72h sucrose habituation period.
- It is possible that repeated exposure to the TST and FST are reducing the sensitivity of these assays. Future investigations should apply these tests only once at endpoint.

The implementation of these changes led to the development of the CID model discussed in Chapter 2 of this dissertation.

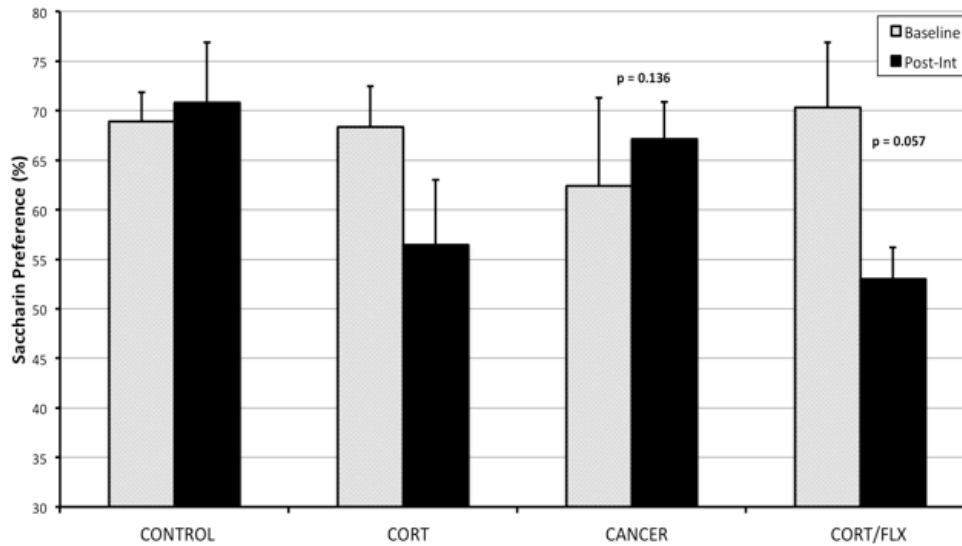
Figures

Figure 4.1. Sucrose preference test. CORT and reversal (CORT/FLX) groups exhibited anhedonic behaviours on the SPT. The cancer group did not show an anhedonic response. Data are expressed as the mean \pm the standard error of the mean (SEM). Statistical significance was assessed through 1-tailed pairwise student t-tests.

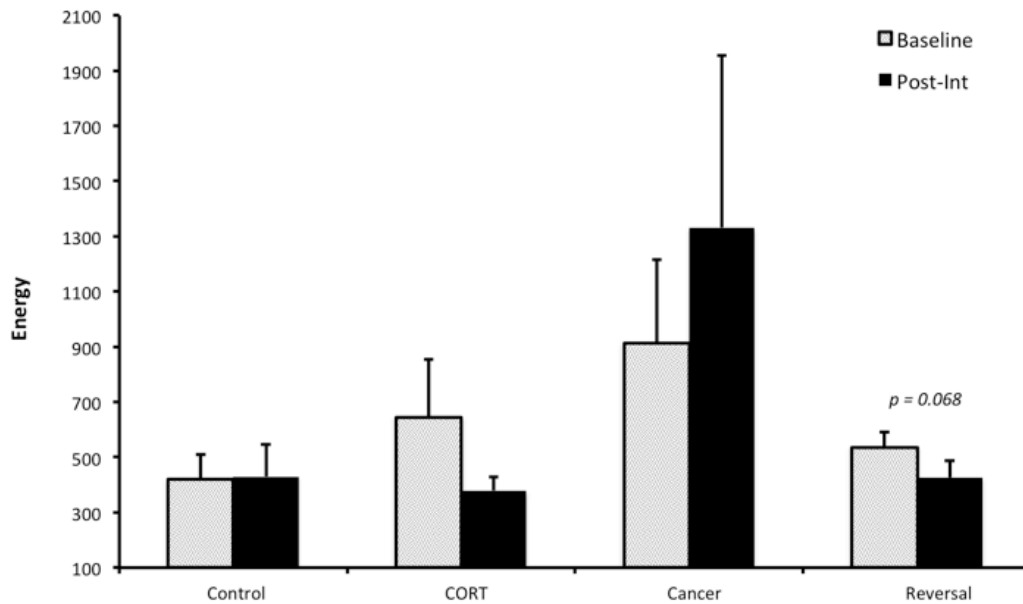


Figure 4.2. Tail suspension test (energy of movement). Bars represent average scores for 2 baseline tests and 2 post-treatment tests. Mice were suspended for 6, with the first minute excluded from analysis. None of the experimental groups showed any changes in immobility (not shown). Both the CORT and reversal group exhibited some reduced energy of movement, but this was not statistically significant. Data are expressed as the mean \pm the standard error of the mean (SEM). Statistical significance was assessed through 1-tailed pairwise student t-tests.

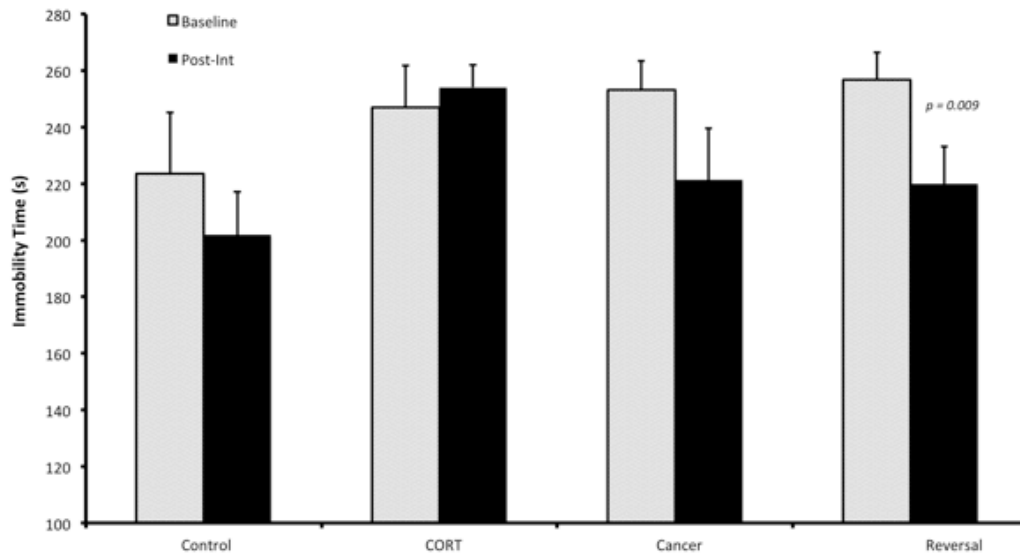


Figure 4.3. Forced swim test. Bars represent average scores for 2 baseline tests and 2 post treatment tests. Mice were placed in beakers for 6 minutes, with the first minute excluded from analysis. No statistically significant changes were observed. The reversal group showed a trend toward reversed behavioural despair response. Data are expressed as the mean \pm the standard error of the mean (SEM). Statistical significance was assessed through 1-tailed pairwise student t-tests. * $P < 0.05$.

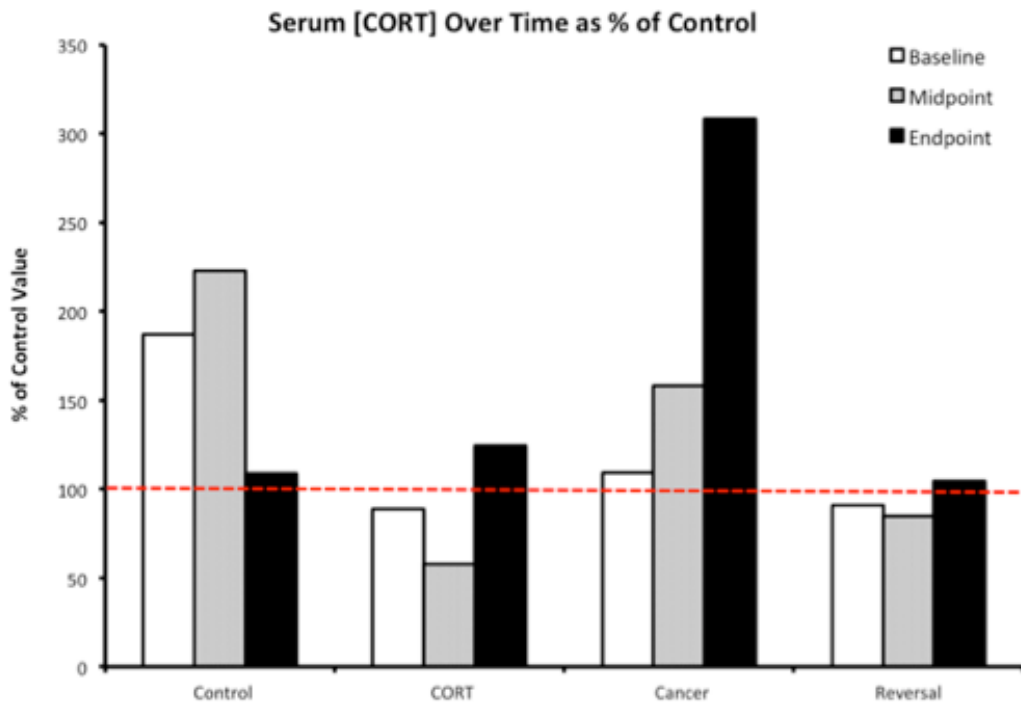


Figure 4.4. CORT ELISA. Blood was collected orbitally and serum was separated for analysis. CORT group shows inhibited adrenal function at midpoint and overactivity at endpoint. Reversal group shows normalized CORT levels via FLX. Cancer group shows elevated CORT due to inflammatory state of cancer. All samples were run in duplicates.

APPENDIX 2

Details for Methodologies

Preface

The purpose of this section is to provide additional details for central methodologies. Journal article length restrictions did not allow for these details to be presented in the original articles. Details are not provided for methods that directly followed manufacturer manuals, such as Golgi-Cox staining, RNA isolation, and mouse serum CORT ELISA. In addition, details are not provided for methods that directly followed previously published protocols. For example, the metastatic clonogenic assay is outlined in step-by-step detail by Pulaski and Ostrand-Rosenberg in their 2001 article “Mouse 4T1 breast tumor model” published in *Current Protocols in Immunology*.

Cell Culture Technique

Murine 4T1 mammary carcinoma cells were grown and maintained in T-flasks with their recommended base medium according to the American Tissue Culture Collection (ATCC) recommendations. Roswell Park Memorial Institute medium (RPMI-1640) media was supplemented with 10% fetal bovine serum (FBS) and 1% antibiotic/antimycotic. Murine TM40A mammary epithelial cells were maintained in Dulbecco's Modified Eagle Medium: Nutrient Mixture F-12 (DMEM:F12) supplemented with 10% FBS, 10 µg/mL insulin, 1% antibiotic/antimycotic, and 20 ng/mL mouse Epidermal Growth Factor (mEGF).

Cells were grown in incubators with 5% CO₂ at 37°C, and were regularly subcultured once they became confluent. To subculture, cells were first washed with 1-2 mL of 1XPBS followed by trypsinization with approximately 1-2 mL of 2x 0.1% EDTA-trypsin. Cells were placed into the incubator for ~5 minutes to allow cells to disconnect from the flask. Fresh culture media was then added to the flask to de-activate the trypsin. Excess cells were then removed, and a fraction of cells added to a new flask with fresh culture medium.

Tail Suspension Test

Mice should be moved to the behavioural room at least 1 hour prior to testing. This helps the mice acclimate to the new setting and avoids confounding novelty stress on the test.

1. Plug the TST USB connection into the laptop. Plug the software USB key into the laptop.
2. Open Instacal (on Desktop) to allow the detection of the TST system. A window may appear confirming that a new USB connection was detected. Click OK and close Instacal.
3. Open the TST software (shortcut icon on Desktop).
4. To create a new experiment, click on File > Create an experiment. There are also options to continue a halted experiment, use parameters from other experiments, and replay an experiment with different parameters.
5. Enter a name for the new experiment and set the parameters. For “Threshold for taking motion into account”, a value of 6 is standard and should be used unless there is rationale for increasing or decreasing the threshold. A 360 second experiment (6 minutes) is standard, with 60 seconds of latency time.
6. To name the groups, select the group from the dropdown menu and input the desired name in the panel to the right of the dropdown menu. NOTE: accidentally clicking outside the dropdown menu or naming panel during this process will reset all the names to default. Repeat this step for mouse names.
7. Click “Start the Randomization” to randomize the mice into suspensions.

8. Calibrate the system by clicking on Calibration > Check the calibration. A window will appear that allows you to perform a “calibration test” on to check the accuracy of each of the 3 channels. This test should read 0 when no weight is attached to the channel. A 20g calibration falcon tube was constructed, and can be used to check the accuracy of the channels with a weight attached.
9. If any of the channels are inaccurate by more than 2g, a calibration must be performed. To do this, click on the “Calibrate” button. A window will prompt you to enter a password. Enter “TsT” (case sensitive) and click Ok.
10. Select “Channel 1” and with no weights attached, click “Calibration on the first level”. Attach the 20g weight and click “Calibration on the second level”. Repeat this for Channel 2 and Channel 3. Note: a 20g weight was used because adult female BALB/c mice weigh approximately 20g. For other mice, calibration weights should be used to closely match their mean weight.
11. Attach a small piece of masking tape (~4 cm) to the tale of the mice in the first suspension. Tape should be attached so that it forms a “flag” with the tail acting as the flag post. Tape should be approximately 3 cm below the tip of the tail. To prevent tail grabbing, insert cylindrical plastic piece (made from a 1 mL syringe) around the tail with the flange toward the tape end, distal to the base of the tail to avoid grabbing onto it.
12. Back at the main test screen, click “Start” to begin the first suspension. A window will appear with a summary of the current suspension. Once you click “Ok” you will have 2 minutes to suspend the fist mouse.

13. Suspend each mouse by puncturing the tape attached to the tail through the hook of the TST system. Once a mouse is attached, begin their channel recording by clicking F1, F2, or F3 for channel 1, channel 2, or channel 3, respectively.
14. During the recording of a suspension, prepare the next set of mice by attaching tape to their tails.
15. Once all the recordings of a suspension are complete, remove mice from the hooks and place them back into their cage. To remove the tape, hold the base of the tail securely with your left hand. Grab the tape with the right hand and pull it parallel to the tail, toward the tip and away from the mouse.
16. Repeat steps 13-15 until all suspensions are complete.
17. To save the results, click Edit > Export the results and export as an excel document. The excel document will include recorded immobility, energy, and power of movement for each mouse in each group.

Forced Swim Test

Mice should be moved to the behavioural room at least 1 hour prior to testing. This helps the mice acclimate to the new setting and avoids confounding novelty stress on the test.

1. Plug the 2 FST USB connections into the laptop (one is for the vibration sensors and one is for the camera). Plug the software USB key into the laptop.
2. Open Instacal (on Desktop) to allow the detection of the FST system. A window may appear confirming that a new USB connection was detected. Click OK and close Instacal.
3. Open the FST software (shortcut icon on Desktop).
4. Under Settings in the Video Detection Setting tab, click “Start settings”. Select the video source (should be set to the correct source by default). Compression Codecs should also be left at default settings. Under “Working Areas Definition”, adjust the blue boxes on the video screen so that each box fits just around each beaker. Make sure that beakers are not touching and of the barriers around them to avoid transfer of motion. Calibrate distance using the on-screen red line—the diameter of any beaker is 20 cm. Finally, set the video detection configuration. To do this, first click “reference” to take a reference picture. Then click “start detection” and place the foam mouse in each beaker and adjust the threshold of each channel such that the green outline correctly detects the mouse. Remove the foam mouse, click on “stop detection” and click “valid settings” to finish the configuration. NOTE: for

- white mice, use the blue side of the beaker matt and the white side of the foam mouse for calibration. For black mice, use the white side of the beaker matt and the black side of the foam mice for calibration.
5. Under the General tab, make sure the time parameters are set correctly. For a 6-minute test with 1-minute latency, the acquisition time should be 300 seconds and latency time should be 60 seconds.
 6. Under the Sensors Checking tab, click “noise detection test” and run the test to make sure the vibration sensors are not detecting too much noise. NOTE: The laptop must be unplugged from the power supply during this test and all of the actual forced swim tests because the interference causes the sensors to pick up noise.
 7. Run a “peak detection test” to make sure the vibration sensors are able to pick up movement in the beakers.
 8. Check that a green box appears next to the acquisition card.
 9. For a new experiment, select 4 naïve mice that will be used for calibration. Click on the Calibration box and select “Complete calibration from a new experiment”. Create a name for the calibration and mice and begin the acquisition. For the first acquisition of any experiment (the calibration acquisition in most cases), place all mice into their beakers first before beginning. This gives you an opportunity to further adjust the video thresholds, as the foam mice used earlier are not always accurate. Begin the acquisition for each channel. Once complete, you may choose to calibrate prior to further

- acquisition, or calibrate at a later time and use an older calibration file tentatively for the remaining acquisitions. It is only important to use the proper calibration file during analysis. The calibration file used during acquisition will not have an impact on the analysis.
10. To perform the calibration, select a 2 state scoring mode (mobile vs. immobile). Click on a channel to be calibrated, click new scoring and follow the instructions to perform a manual scoring of the test. Do this for each of the 4 channels. More than one scoring for each channel can be done and you may select the one you feel was most accurate for calibration. Once the scoring is done, click on “auto-calibration: calibration file from 4 channels” under “Calibration”. Then select the Channel 1 and scoring session you want to use and click “Calibrate”. Repeat this for Channels 2, 3 and 4 then click “Save Calibration.
 11. Click on the acquisition box to start the experiment.
 12. Create a subject list by defining the number of groups and subjects per group. You can click “modify” to rename groups or subjects. You may also export the subject list you created or import subject lists from previous experiments.
 13. Select the desired randomization mode and click “apply” to generate the list of runs. Note that full runs can be deleted if necessary.
 14. In the experiment interface, click “Acquisition” to start. A window will appear with a summary of the current acquisition. Click “Start Acquisition” and being

- placing mice in beakers. As each mouse is placed, click “start” for that channel to begin.
15. Once acquisitions for all channels are completed, remove the mice one at a time and dry them with a heated surgical towel to avoid hypothermia. Towels are heated on the heating pad next to the FST system.
 16. Once all acquisitions are made for the experiment, you can close the experiment and analyze at a later time.
 17. When ready for analysis, open the experiment in the Analysis tab. You will be prompted to select a calibration file. At this point, the appropriate calibration file that was created earlier should be selected. This file can also be selected under “Analysis Mode”. Select the “analysis period” (usually the entire 5 minutes” and click “Analyse Selection”. Results will display with graphics. The important thing is to export the excel file from this results interface. This file will contain immobility times for each mouse in each group.

Dendritic Analysis

Mouse brains were stained using the Golgi-Cox method. Neurons in layer II–III of the mPFC were identified using the aid of a mouse brain atlas. Z-stacked images were captured for each neuron in 2 μm increments using OpenLab 5. Prior to saving images, a scale was calibrated and displayed for each image, which was later used in Fiji. Folders were create for each animal and image stacks saved as .tif files with file names identifying the neuron—e.g. “Mouse23_Bregma 1.45_Neuron 2”. Neurons were then digitally reconstructed using the Simple Neurite Tracer plugin for the open source software Fiji, and Sholl analyses were performed as follows:

1. Open Fiji software
2. Open image stack to be analyzed. The image will be loaded in a window that allows you to scroll left-to-right to view all the images in the stack.
3. So calibrate the image scale, zoom on the scale displayed on the image (created in OpenLab). Use the rectangular selection tool to select the width of the scale. Make note of the width (in pixels) in the top panel. Go to Analyze > Set Scale. Input the width of the scale bar in pixels for “Distance in pixels” and the known length of the bar (in μm) for “Known distance”. For “Unit of length” type “um”. Click Ok.
4. Under Plugins, go to Segmentation and choose Simple Neurite Tracer.
5. Start the neuronal reconstruction by identifying the center of the neuron’s soma. Click to start a path. By scrolling side to side through the stack, find an

- arbour to be traced, select the next point along the arbour and click again. This will prompt the software to scan through the image layers and create a path between the two points along the arbour. This process requires some practice to discern how far apart points should be for the software to identify the correct path.
6. When two points are joined by the software, a line segment is created in blue and the instructions prompt you to either accept or cancel this segment. If the segment was correctly identified by the software, click yes to accept it. The line segment now turns red and instructions prompt you to complete or cancel the path. If the arbour is not yet completely traced, click on the next point along the arbour and a new segment will be created. Repeat this until the entire arbour is traced, then click “complete path”. The completed path now turns purple.
 7. To create a branching path from an existing path, select the path from the screen listing the paths. The selected path will turn green. Holding Alt (Mac) or Ctrl (Windows) will now lock your cursor to the selected path. Choose the spot of bifurcation and click to create a new point. Select another point along the branching arbour to begin tracing it as described before.
 8. Once all the arbours have been traced, they can be grouped by category. Select all the arbours in one category (e.g. apical dendrite), right click, scroll down to “set SWC type” and select the appropriate category.
 9. To save, go to File > Save traces file. Files can also be exported as SWC.

10. Select all paths in one category to be analyzed by Sholl analysis. With all the tracings selected, go to the image window, and press and hold the Shift key and Alt (Mac) or Ctrl (Windows). Using the cursor, find the center of the soma, and while continuing to hold Shift + Alt/Ctrl, press “A”. The Sholl analysis interface should now appear.
11. In the Sholl analysis interface, specify that only the selected paths should be analyzed. Next to “Circle/sphere separation” type “10” if the desired separation between concentric rings is 10 μm . Then click on “Export detailed results as CSV”.
12. Repeat step 10-11 for all categories of traced arbours you wish to analyze by Sholl analysis (e.g. apical and basilar arbours).
13. The CSV files can be opened in Excel and combined for analysis.

¹⁴C-Cystine Uptake Assay

This protocol was adapted by Jennifer Fazzari and Natalie Zacal from the following papers:

Lutgen et al, 2013, *Psychopharmacology*, 226:531-540.

Shih et al, 2006, *The Journal of Neuroscience*, 26(41):10514-10523.

1. Seed 250,000 cells per well in a 6-well plate and let the cells adhere overnight.
2. Drug-treat the cells in 300ul of HBSS for 20 minutes in 37°C incubator.
3. DO NOT ASPIRATE DRUG AND HBSS. Instead, add the cystine directly to the HBSS and drug on the cells. Make a master mix using 0.45ul of stock radioactive ¹⁴C-cystine per well plus 4.55ul HBSS per well to bump the volume of radioactive cystine up to 5ul per well. Multiply these volumes by the number of samples or wells (plus one extra volume) you have to make your master mix.
4. Add 5ul of the master mix to each well and incubate for 20 minutes in 37°C incubator.

Stock radioactive ¹⁴C-L-Cystine is 10uCi in 500ul or 20uCi/ml

Perkin Elmer Catalog number: NEC845010UC

5. Quickly wash each well 3x in ice cold HBSS (2ml per well).
6. Lyse cells in 220ul of lysis buffer (0.1N NaOH containing 0.1% Triton-X) for 30 minutes.
7. Collect cell lysates into 1.5ml microtubes.
8. Put 100ul of each cell lysate into 1ml of Ecoscint-H solution in a 5ml plastic scintillation vial.

Make a blank using 100ul of lysis buffer in 1ml of Ecoscint-H solution.

9. Go to the High Throughput Screening Facility to do a scintillation count of your samples using the Beckman LS6500 scintillation counter. Put the scintillation vials into the blue plastic holder (Put the blank in the first position, leave a space, and then load your samples) and load the racks in the machine starting closest to you on the right hand side in the following order: first the blue holder with the “HALT” card facing you, then another blue holder that you have put your samples into. Hit the 3sec button on the printer until the “Pause” light goes off and make sure the printer is loaded with paper. Using the control buttons on the Beckman counter, select: “Main Menu”, “Count Single Rack”, Select “User Program”, Enter “15” for ^{14}C with 3 minute reads, hit Select, Select again, and hit Start.
10. Do a Bio-Rad assay of the cell lysate to determine protein concentration for normalizing CPM per mg of protein. Perform a Bio-Rad assay using the cell lysate (or a 1:2 or a 1:3 dilution if appropriate) in a 10ul volume in duplicate or triplicates of a 96 well plate.

Bio-Rad Protein Assay

This protocol was developed by Dr. Eric Seidlitz.

1. Label eppendorf tubes for BSA standards and sample dilutions
2. Prepare the BSA standard by making a stock of ~10 mg/mL BSA powder with Milli-Q water
3. Make BSA standard dilutions:
 - a. 2.0 mg/mL
 - b. 1.0 mg/mL
 - c. 0.5 mg/mL
 - d. 0.250 mg/mL
 - e. 0.125 mg/mL
 - f. 0.0625 mg/mL
 - g. 0.0313 mg/mL
4. Prepare BioRad solution in a 1:4 dilution with Milli-Q water (e.g. 3 + 12 mL; 2+8 mL; 2.5+10 mL, etc.)
5. Using a 96-well plate, add 10 μ L of each BSA standard (in triplicate) with 3 wells of Milli-Q water as a blank (rows A, B, and C will therefore have 3 blanks plus the 7 different BSA concentrations from wells 4-10)
6. Add 10 μ L of each test sample and each dilution (1:10 and 1:100 are usually sufficient) in triplicate to the plate
7. Add 240 μ L of BioRad 1:4 solution to each well
8. Remove unwanted bubbles from the wells
9. Read plate in BioTek PowerWave XL plate reader at 570 nm (using *Eric – BioRad protein* protocol)
10. Export data file to Excel then save this file on a 3.5” floppy disc

11. Using Excel, *copy* the raw absorbance values then *Paste Special...Values* into the protein measurement template file (v.3) at the appropriate location – the standard curves and equations will be automatically generated
12. Select the appropriate dilution for each sample that falls within the linear range of the standard curve and perform the final protein concentration calculation using the equation $y=mx+b$ where x is the average absorbance of the triplicate sample and both m and b are derived from the linear equation generated by Excel from the standard curve

| | 1 | 2 | 3 | 4 | 5 | 6 | 7 | 8 | 9 | 10 | 11 | 12 |
|---|-------|--------|--------|--------|--------|--------|--------|--------|--------|--------|----|----|
| A | 0.000 | 0.0000 | 0.0000 | 0.0313 | 0.0625 | 0.1250 | 0.2500 | 0.5000 | 1.0000 | 2.0000 | | |
| B | 0.000 | 0.0000 | 0.0000 | 0.0313 | 0.0625 | 0.1250 | 0.2500 | 0.5000 | 1.0000 | 2.0000 | | |
| C | 0.000 | 0.0000 | 0.0000 | 0.0313 | 0.0625 | 0.1250 | 0.2500 | 0.5000 | 1.0000 | 2.0000 | | |
| D | | | | | | | | | | | | |
| E | | | | | | | | | | | | |
| F | | | | | | | | | | | | |
| G | | | | | | | | | | | | |
| H | | | | | | | | | | | | |

Quantitative Real-Time RT-PCR

In Chapter 4, total RNA was isolated from each sample using the Qiagen RNAeasy Kit. 400 ng of total RNA was reverse transcribed into cDNA using the SuperScript III kit. Briefly, RNA in the presence of 1 μL of 50 μM oligo(dT)20 and 1 μL of 10 mM dNTP mix (final volume of 13 μL) was incubated on a thermocycler at 65°C for 5 min. Reactions were placed on ice prior to adding 4 μL of 5X first strand buffer, 1 μL of 0.1 M DTT, 1 μL RNaseOUT Recombinant RNase Inhibitor, and 1 μL SuperScript III reverse transcriptase for a final volume of 20 μL . Reactions were then incubated at 50°C for 50 min and 70°C for 15 min. The resulting cDNA was diluted to a final volume of 60 μL through addition of nuclease-free water and stored at -20°C.

Relative mRNA levels were evaluated by qRT-PCR. Each 12.5 μL reaction contained 2 μL of diluted cDNA, 6.25 μL of SYBR Green premix, and 0.5 μL of 10 μM forward (FOR) and reverse (REV) primer. All target and housekeeping gene primers based on sequences specific for *Mus Musculus* were derived from PrimerBank, with annealing temperatures of 60°C. Official gene symbols, primer sequences, product sizes, and specific melting peaks for each target gene product are listed in Table S1 of Chapter 4. The specifications of the three housekeeping genes used in this study are summarized in Table S2 of Chapter 4. A MiniOpticon 48-well Real-Time PCR System linked to CFX Manager software was programmed with the following cycling parameters: 95°C for 1 min, 40 cycles of 95°C for 10 sec and 60°C for 25 sec, and a final melting

peak determination (95°C for 15 sec, followed by incremental 0.5°C increases of 5 sec from 65°C to 95°C). Reactions for target genes were run in duplicate for each cDNA sample. Parallel duplicate reactions for the appropriate housekeeping gene were carried out to calculate relative mRNA levels using the $2^{-\Delta\Delta C_T}$ method. Fold changes relative to a given treatment were subsequently calculated to validate results derived from the analysis of RNA-seq results. For each of 9 selected target genes, a specific housekeeping gene was chosen based on efficiency testing of primer pairs. Efficiency testing was achieved by evaluating the slopes derived from plotting the log of a 2-fold serial dilution of murine brain cDNA (template) versus the C_T of each target gene compared to three different possible housekeepers at each template dilution. This test resulted in parallel lines, with slopes of well-matched targets and housekeepers being equivalent and optimally >3 . A further test was carried out by plotting ΔC_T values (target C_T at each template dilution minus housekeeper C_T at the equivalent dilution) across the dilution series, which yielded a straight line with a slope close to 0 (< 0.1). Amplification efficiencies were tested for each primer pair, with efficiency (E) = $[10^{\text{raised to } (-1/S)}] - 1$ (E should be close to 1), and the integrity of each product was verified by gel electrophoresis to validate expected product sizes.

RNA-seq Analysis

Galaxy—Tuxedo Protocol Up To CuffDiff

This protocol describes how to perform a basic analysis of differential gene expression using RNA-seq results. The platform used here is the Galaxy Project, which is free online software. The final steps to visualize results require RStudio. This analysis follows the Tuxedo protocol. Note that for this project, each biological sample (RNA from 1 mouse) was split between 2 lanes during sequencing, and therefore files from each lane needed to be merged. In addition, each lane produced multiple files (due to size) that needed to be merged in a different way.

1. Create account on usegalaxy.org.
2. Under “Get Data”, upload all FASTQ files, specifying type as "fastqsanger" and genome as "mouse mm10".
3. For each mouse, merge multiple files representing one lane into one FASTQ file using Text Manipulation > Concatenate datasets tail-to-head.
4. Remove possible new/empty lines created between files by using Filter and Sort > Select > "that: NOT Matching" and "the pattern: ^\$".
5. Rename newest merged file appropriately, ex. "Balbc 9 L1" and repeat for both lanes of each mouse sample.
6. Run FastQC (under NGS: QC and manipulation) on all samples to generate a quality control report. Note: Looking at overrepresented sequences gives you

an idea if there are any sequences (such as 3' adapters/indices) that need to be cut from the file. If there are any, consult the Clip tool). If there are issues with low quality reads, you can "Filter by quality".

- Example—Index format for my data:

```
GATCGGAAGAGCACACGTCTGAACTCCAGTCACXXXXXXXXAT
CTCGTATGCCGTCTTCTGCTTGAAAAAAA
```

Where **XXXXXXXX** represents the specific index used for that specific sample (Ex. for Balbc2 9 (both lanes) it's ATCACG). The index sequences are found on the quality report spreadsheet. If **SOME** of the files show overrepresentation of index sequences, it might be best to just filter indices out from **ALL** files.

7. For Tophat parameters: I had 70bp reads so changes allowed mismatches to 3 instead of default 2. Change max realign edit distance to 0 instead of default 1000. Select to use gene annotation model. Use gene annotation gft file downloaded from UCSC (see below). If you keep "only look for supplied junctions" on "no" then new splice variants will still be picked up. Introducing the annotation file at this stage will help guide reads to alignment but may slightly bias reads towards known alignments. Probably not good to do if main purpose is to look for splice variants, but for a study primarily looking at differential gene expression, it's best to do it this way.

- To get annotation file, Get Data > UCSC Main, select the appropriate genome (mm10 in my case) and for group choose "genes and gene

prediction tracks", for track select "UCSC" in my case (this is what matches the mm10 genome used by Galaxy), select entire genome (not chromosome location), make output format GFT and select "send to galaxy".

8. Once alignments are done, Galaxy will output multiple files for each replicate, one of which is the accepted hits BAM file. Use NGS: BAM Tools > Convert, Merge, Randomize to merge the technical replicates from the two lanes for each biological replicate and rename appropriately, e.x. "Balbc2 9 Aligned".
9. Assemble transcripts for each biological replicate using Cufflinks. In most cases, it is desirable to keep the ability to detect novel splicing events and genes. If we choose to supply an annotation file, Cufflinks will ONLY report reads that map to known/annotated genes. If we do not supply annotation file, it might be prone to false positives in terms of novel genes. So we will choose "use reference annotation as a guide" which essentially biases reads towards known genes, but still takes into consideration reads that don't map to known coding areas.
 - Other customized parameters: under "perform bias correction", select "yes". Under "use multi-read correct" select "yes".
10. Use Cuffmerge to create a merged transcriptome assembly. Here, select all the GTF files produced by cufflinks to be merged. Make sure to use "insert additional GTF input file" to insert each GTF assembly—do not use the batch option where you select all at the same time; this does individual merges for

each file instead of merging them together. Under "use reference annotation" select "yes" and use the mm10 annotation that was downloaded from UCSC. Under "use sequence data" select "yes" and keep it selected at "locally cached".

11. Use Cuffdiff to analyze differential gene expression (can also be used to analyze novel splicing events). Change the following default parameters:

- Generate SQLite: yes
- Library normalization method: quartile
- Use multi-read correct: yes
- Perform bias correction: yes
- Reference sequence data: Locally cached [Mouse (Mus Musculus): mm10]

RStudio—Tuxedo Protocol: CummeRbund

At this point, the analysis is technically completed, but still needs to be visualized. CummeRbund is not on the main Galaxy server, so CuffDiff output files must be saved to local computer.

- In working directory with all the downloaded CuffDiff files, remove cuffData.db and the SQLite file, and rename the following:

```
...splicing_differential_expression_testing].tabular → splicing.diff  
...promoters_differential_expression_testing].tabular → promoters.diff  
...CDS_overloading_differential_expression_testing].tabular → CDS.diff  
...CDS.FPKM_differential_expression_testing].tabular → cds_exp.diff
```

```
..._CDS_FPKM_tracking].tabular → cds.fpkm_tracking  
..._TSS_groups_differential_expression_testing].tabular → tss_group_exp.diff  
..._TSS_groups_FPKM_tracking].tabular → tss_groups.fpkm_tracking  
..._gene_differential_expression_testing].tabular → gene_exp.diff  
..._gene_FPKM_tracking].tabular → genes.fpkm_tracking  
..._transcript_differential_expression_testing].tabular → isoforms_exp.diff  
..._transcript_FPKM_tracking].tabular → isoforms.fpkm_tracking
```

On the local computer, download and install R and RStudio, and install the Bioconductor package. There are many resources available online for RStudio and scripts available for many different visualizations and analyses. It is recommended that users unfamiliar with R programming language watch a couple of online video tutorials prior to starting.

- Use the command `biocLite("BiocUpgrade")` to make sure BioConductor is updated
- Use the command `biocLite("cummeRbund")` to get CummeRbund and `biocLite("RSQLite")` to get SQLite
- In the bottom right console under “Packages”, users can select any of the available packages (e.g. all the BioConductor packages) to be loaded into the current session. Under “Help” users can also see examples of each package and how to customize the parameters in each one.

The following script was created and run to produce the graphics presented in Chapter 4. These are standard graphics for analysis of differential gene expression. Note, some of the code presented here also relates to specific formatting of these figures. For more detail, consult the “Help” section associated with the packages.

```
# Load CummeRbund Library
library('cummeRbund')

# Set working directory with all the CuffDiff files (after re-naming and deleting db file)
setwd("~/Desktop/MEDICAL SCIENCE/THESIS/EXPERIMENTS/NGS")

# Create CummeRbund database from the CuffDiff output
cuff_data<- readCufflinks('CuffDiff')

# Note: when you save and exit, then re-open, you should set the directory again. This time set to actual folder with newly created cuffData.db file instead of folder leading to this folder. To set directory, go to the console on the bottom right corner, select the Files tab and navigate to the directory containing the cuffData.db file. Click More > Set as Working Directory.
cuff_data <- readCufflinks(dbFile = "cuffData.db")

# Density Plot: distribution of expression levels for each sample
den <- csDensity(genes(cuff_data))
den <- den + labs(title = "Genes", x = "log10(FPKM)", y = "Density")
den <- den + theme(title=element_text(size=20),
plot.title=element_text(colour='black'), axis.title.x=element_text(hjust=0.5,
vjust=0), axis.title.y=element_text(hjust=0.5, vjust=1),
axis.text.x=element_text(size=20,
colour='black'),axis.text.y=element_text(size=20,
colour='black'),legend.text=element_text(size=14),legend.title=element_text(colour='white'), panel.background=element_rect(fill='white', colour='grey'),
panel.border=element_rect(fill=NA, colour='black',size=1.5))
den # View plot

# Scatterplot (matrix): compares expression of each gene between all conditions
scatter <- csScatterMatrix(genes(cuff_data))
scatter # View plot

# Scatterplot for Control vs. CORT
sca_Cont_CORT <- csScatter(genes(cuff_data), 'CORT', 'Control')
sca_Cont_CORT <- sca_Cont_CORT + labs(title = "Genes")
sca_Cont_CORT <- sca_Cont_CORT + theme(title=element_text(size=20),
axis.title.x=element_text(hjust=0.5, vjust=0), axis.title.y=element_text(hjust=0.5,
vjust=1), axis.text.x=element_text(size=16, colour='black'),
axis.text.y=element_text(size=16, colour='black'),
panel.border=element_rect(fill=NA, colour='black',size=1.5))
sca_Cont_CORT # View plot
```

```
# Scatterplot for Control vs. CID
```

```
sca_Cont_CID <- csScatter(genes(cuff_data), 'CID', 'Control')  
sca_Cont_CID <- sca_Cont_CID + labs(title = "Genes")  
sca_Cont_CID <- sca_Cont_CID + theme(title=element_text(size=20),  
axis.title.x=element_text(hjust=0.5, vjust=0), axis.title.y=element_text(hjust=0.5,  
vjust=1), axis.text.x=element_text(size=16, colour='black'),  
axis.text.y=element_text(size=16, colour='black'),  
panel.border=element_rect(fill=NA, colour='black',size=1.5))  
sca_Cont_CID # View plot
```

```
# Scatterplot for CORT vs. CID
```

```
sca_CORT_CID <- csScatter(genes(cuff_data), 'CID', 'CORT')  
sca_CORT_CID <- sca_CORT_CID + labs(title = "Genes")  
sca_CORT_CID <- sca_CORT_CID + theme(title=element_text(size=20),  
axis.title.x=element_text(hjust=0.5, vjust=0), axis.title.y=element_text(hjust=0.5,  
vjust=1), axis.text.x=element_text(size=16, colour='black'),  
axis.text.y=element_text(size=16, colour='black'),  
panel.border=element_rect(fill=NA, colour='black',size=1.5))  
sca_CORT_CID # View plot
```

```
# Volcano Plot (matrix): identify differentially expressed genes
```

```
volcano <- csVolcanoMatrix(genes(cuff_data), alpha=0.05, xlimits=c(-20,20))  
volcano # View plot
```

```
# Volcano Plot for Control vs. CORT
```

```
vol_Cont_CORT <- csVolcano(genes(cuff_data), 'Control', 'CORT', alpha=0.05,  
showSignificant=TRUE,features=FALSE, xlimits = c(-20, 20))  
vol_Cont_CORT <- vol_Cont_CORT + labs(title = "Genes:Control/CORT")  
vol_Cont_CORT <- vol_Cont_CORT + theme(title=element_text(size=20),  
axis.title.x=element_text(hjust=0.5, vjust=0), axis.title.y=element_text(hjust=0.5,  
vjust=1), axis.text.x=element_text(size=16, colour='black'),  
axis.text.y=element_text(size=16,  
colour='black'),legend.text=element_text(size=16),  
panel.border=element_rect(fill=NA, colour='black',size=1.5))  
vol_Cont_CORT # View plot
```

```
# Volcano Plot for Control vs. CID
```

```
vol_Cont_CID <- csVolcano(genes(cuff_data), 'Control', 'CID', alpha=0.05,  
showSignificant=TRUE,features=FALSE, xlimits = c(-20, 20))  
vol_Cont_CID <- vol_Cont_CID + labs(title = "Genes:Control/CID")  
vol_Cont_CID <- vol_Cont_CID + theme(title=element_text(size=20),  
axis.title.x=element_text(hjust=0.5, vjust=0), axis.title.y=element_text(hjust=0.5,  
vjust=1), axis.text.x=element_text(size=16, colour='black'),  
axis.text.y=element_text(size=16,
```

```
colour='black'),legend.text=element_text(size=16),
panel.border=element_rect(fill=NA, colour='black',size=1.5))
vol_Cont_CID # View plot
```

```
# Volcano Plot for CORT vs. CID
```

```
vol_CORT_CID <- csVolcano(genes(cuff_data), 'CORT', 'CID', alpha=0.05,
showSignificant=TRUE,features=FALSE, xlimits = c(-20, 20))
vol_CORT_CID <- vol_CORT_CID + labs(title = "Genes:CORT/CID")
vol_CORT_CID <- vol_CORT_CID + theme(title=element_text(size=20),
axis.title.x=element_text(hjust=0.5, vjust=0), axis.title.y=element_text(hjust=0.5,
vjust=1), axis.text.x=element_text(size=16, colour='black'),
axis.text.y=element_text(size=16,
colour='black'),legend.text=element_text(size=16),
panel.border=element_rect(fill=NA, colour='black',size=1.5))
vol_CORT_CID # View plot
```

In RStudio, you can extract corresponding UCSC gene names to match the XLOC names, but you can't directly get gene symbols. Therefore, before proceeding below, you must import list with UCSC names and corresponding gene symbols. To acquire list: UCSC -> Table -> clade(Mammal) -> genome(Mouse) -> assembly(GRCm38/mm10) -> group(Genes and Gene Prediction Tracks) -> track(RefSeq Genes) -> table(kgXref) -> output format(selected fields from primary and related tables) -> get output -> select "kgID" and "geneSymbol", then get output (send to Galaxy, download from Galaxy). Rename this list to a .txt file, open it and rename the UCSC gene column to "gene_short_name".

```
# Tools > Import Dataset > From Text File
```

To extract list of significantly different genes in pairwise comparison and have corresponding UCSC names, do the following:

```
# Identify differentially expressed genes (XLOC names): Control vs. CORT
SigGenesData_ContCORT <- getSig(cuff_data, level = "genes", 'Control', 'CORT',
alpha = 0.05)
# Use returned identifiers to create a CuffGeneSet object with all relevant info for
given genes
DiffGenes_ContCORT <- getGenes(cuff_data, SigGenesData_ContCORT)
# UCSC names and corresponding XLOC names can be retrieved from the
CuffGeneSet by using:
GeneIDs_ContCORT <- featureNames(DiffGenes_ContCORT)
# Export table
write.csv(GeneIDs_ContCORT, file = 'GeneIDs_ContCORT.csv', quote = FALSE,
row.names = FALSE)
```

```
# Open the csv file in excel. You'll notice that some loci have multiple UCSC gene names pasted in adjacent cells. Delete all but the first column of gene names. Save the new file and import the new csv file using tools > import dataset > from text file. Import back in using the same name to update the old data set.
# Merge data set containing UCSC and XLOC names with imported gene symbol list from UCSC website
ContCORT <- merge(GeneIDs_ContCORT, Gene_Symbols, all.x=TRUE)
# Export new merged table with gene symbols
write.csv(ContCORT, file = 'ContCORT.csv', quote = FALSE, row.names = FALSE)

# Identify differentially expressed genes (XLOC names): Control vs. CID
SigGenesData_ContCID <- getSig(cuff_data, level = "genes", 'Control', 'CID', alpha = 0.05)
# Use returned identifiers to create a CuffGeneSet object with all relevant info for given genes
DiffGenes_ContCID <- getGenes(cuff_data, SigGenesData_ContCID)
# UCSC names and corresponding XLOC names can be retrieved from the CuffGeneSet by using:
GeneIDs_ContCID <- featureNames(DiffGenes_ContCID)
# Export table
write.csv(GeneIDs_ContCID, file = 'GeneIDs_ContCID.csv', quote = FALSE, row.names = FALSE)
# Open the csv file in excel. Delete all but the first column of gene names. Import back in using the same name to update the old data set.
# Merge data set containing UCSC and XLOC names with imported gene symbol list from UCSC website
ContCID <- merge(GeneIDs_ContCID, Gene_Symbols, all.x=TRUE)
# Export new merged table with gene symbols
write.csv(ContCID, file = 'ContCID.csv', quote = FALSE, row.names = FALSE)

# Identify differentially expressed genes (XLOC names): CORT vs. CID
SigGenesData_CORTCID <- getSig(cuff_data, level = "genes", 'CORT', 'CID', alpha = 0.05)
# Use returned identifiers to create a CuffGeneSet object with all relevant info for given genes
DiffGenes_CORTCID <- getGenes(cuff_data, SigGenesData_CORTCID)
# UCSC names and corresponding XLOC names can be retrieved from the CuffGeneSet by using:
GeneIDs_CORTCID <- featureNames(DiffGenes_CORTCID)
# Export table
write.csv(GeneIDs_CORTCID, file = 'GeneIDs_CORTCID.csv', quote = FALSE, row.names = FALSE)
```

```
# Open the csv file in excel. Delete all but the first column of gene names. Import  
back in using the same name to update the old data set.  
# Merge data set containing UCSC and XLOC names with imported gene symbol  
list from UCSC website  
CORTCID <- merge(GeneIDs_CORTCID, Gene_Symbols, all.x=TRUE)  
# Export new merged table with gene symbols  
write.csv(CORTCID, file = 'CORTCID.csv', quote = FALSE, row.names =  
FALSE)  
  
# Create table of differentially expressed genes common to [Control vs. CORT]  
AND [Control vs. CID]  
ContCORT_ContCID <- merge(ContCORT, ContCID, all = FALSE)  
# Export table  
write.csv(ContCORT_ContCID, file = 'ContCORT_ContCID.csv', quote =  
FALSE, row.names = FALSE)  
  
# Create table of differentially expressed genes common to [Control vs. CORT]  
AND [CORT vs. CID]  
ContCORT_CORTCID <- merge(ContCORT, CORTCID, all = FALSE)  
# Export table  
write.csv(ContCORT_CORTCID, file = 'ContCORT_CORTCID.csv', quote =  
FALSE, row.names = FALSE)  
  
# Create table of differentially expressed genes common to [Control vs. CID]  
AND [CORT vs. CID]  
ContCID_CORTCID <- merge(ContCID, CORTCID, all = FALSE)  
# Export table  
write.csv(ContCID_CORTCID, file = 'ContCID_CORTCID.csv', quote = FALSE,  
row.names = FALSE)  
  
# Extract specific fold-changes:  
# Using the master excel file created with all the differentially expressed genes,  
create a simple txt list of any gene (using XLOC name) that is differentially  
expressed. To create a simple tab delimited txt file of this list, use "save as" in  
Excel, don't copy/paste into TextEdit. Read txt file in RStudio and follow these  
steps to derive FPKM values for those specific genes:  
  
# Extract specific fpkm levels for differentially expressed genes.  
# Load gplots  
library(gplots)  
# Read text gene list  
alldiff <- read.delim("alldiff.txt", header=FALSE, sep = "\t")  
# Extract expression level associated with list of genes  
fpkm_values <- fpkmMatrix(getGenes(cuff_data, t(alldiff)))
```

```
# Export this table and manually import fpkm values into master Excel file
write.csv(fpkm_values, file = "fpkm_values.csv", quote = FALSE, row.names =
TRUE)

# Extract specific stats info regarding differentially expressed genes (i.e. p and q
values)
gene_diff_data <- diffData(genes(cuff_data))
sig_gene_data <- subset(gene_diff_data, (significant == 'yes'))
write.csv(sig_gene_data, file = "sig_gene_data.csv", quote = FALSE, row.names
= TRUE)

# In Excel, calculate fold-changes for each pairwise comparison and then use the
vlookup function to match the fold-changes to the gene list using XLOC names

# Create Heatmap of significantly different genes
DEG <- diffData(genes(cuff_data))
DEG_significant <- subset(DEG, significant == 'yes')
DEG_sign_IDs <- DEG_significant$gene_id
DEG_genes <- getGenes(cuff_data, DEG_sign_IDs)
heatmap2 <- csHeatmap(DEG_genes, clustering='row', labRow=F, LabCol=T,
logMode=T, pseudocount=1.0,
heatscale=c(low='lightyellow', mid='orange', high='darkred'), heatMidpoint=NULL,
replicates=FALSE, method='none')
heatmap2 <- heatmap2 + theme(axis.text.x=element_text(size=14, colour='black',
angle=0, hjust=0.5))
heatmap2 # View heatmap

# To clear any plot that is displayed:
dev.off()
```

APPENDIX 3

Springer Copyright Licence

**SPRINGER LICENSE
TERMS AND CONDITIONS**

Jan 26, 2016

This is a License Agreement between Mina Nashed ("You") and Springer ("Springer") provided by Copyright Clearance Center ("CCC"). The license consists of your order details, the terms and conditions provided by Springer, and the payment terms and conditions.

All payments must be made in full to CCC. For payment instructions, please see information listed at the bottom of this form.

License Number

3796310276405

License date

Jan 26, 2016

Licensed content publisher

Springer

Licensed content publication

Springer eBook

Licensed content title

Oncodynamic Effect of Cancer on Depression

Licensed content author

Mina G. Nashed

Licensed content date

Jan 1, 2016

Type of Use

Thesis/Dissertation

Portion

Full text

Number of copies

100

Author of this Springer article

Yes and you are a contributor of the new work

Order reference number

None

Title of your thesis / dissertation

STUDIES ON THE PATHOPHYSIOLOGY OF CANCER-INDUCED
DEPRESSION

Expected completion date

Mar 2016

Estimated size (pages)

300

Total

0.00 CAD

Terms and Conditions

Introduction

The publisher for this copyrighted material is Springer. By clicking "accept" in connection with completing this licensing transaction, you agree that the following terms and conditions apply to this transaction (along with the Billing and Payment terms and conditions established by Copyright Clearance Center, Inc. ("CCC"), at the time that you opened your Rightslink account and that are available at any time at <http://myaccount.copyright.com>).

Limited License

With reference to your request to reuse material on which Springer controls the copyright, permission is granted for the use indicated in your enquiry under the following conditions:

- Licenses are for one-time use only with a maximum distribution equal to the number stated in your request.
- Springer material represents original material which does not carry references to other sources. If the material in question appears with a credit to another source, this permission is not valid and authorization has to be obtained from the original copyright holder.
- This permission
 - is non-exclusive
 - is only valid if no personal rights, trademarks, or competitive products are infringed.
 - explicitly excludes the right for derivatives.
- Springer does not supply original artwork or content.
- According to the format which you have selected, the following conditions apply accordingly:
 - Print and Electronic: This License include use in electronic form provided it is password protected, on intranet, or CD-Rom/DVD or E-book/E-journal. It may not be republished in electronic open access.
 - Print: This License excludes use in electronic form.
 - Electronic: This License only pertains to use in electronic form provided it is password protected, on intranet, or CD-Rom/DVD or E-book/E-journal. It may not be republished in electronic open access.

For any electronic use not mentioned, please contact Springer at permissions.springer@spi-global.com.

- Although Springer controls the copyright to the material and is entitled to negotiate on rights, this license is only valid subject to courtesy information to the author (address is given in the article/chapter).
- If you are an STM Signatory or your work will be published by an STM Signatory and you are requesting to reuse figures/tables/illustrations or single text extracts, permission is granted according to STM Permissions Guidelines: <http://www.stm-assoc.org/permissions-guidelines/>

For any electronic use not mentioned in the Guidelines, please contact Springer at permissions.springer@spi-global.com. If you request to reuse more content than

stipulated in the STM Permissions Guidelines, you will be charged a permission fee for the excess content.

Permission is valid upon payment of the fee as indicated in the licensing process. If permission is granted free of charge on this occasion, that does not prejudice any rights we might have to charge for reproduction of our copyrighted material in the future.

-If your request is for reuse in a Thesis, permission is granted free of charge under the following conditions:

This license is valid for one-time use only for the purpose of defending your thesis and with a maximum of 100 extra copies in paper. If the thesis is going to be published, permission needs to be reobtained.

- includes use in an electronic form, provided it is an author-created version of the thesis on his/her own website and his/her university's repository, including UMI (according to the definition on the Sherpa website: <http://www.sherpa.ac.uk/romeo/>);

- is subject to courtesy information to the co-author or corresponding author.

Geographic Rights: Scope

Licenses may be exercised anywhere in the world.

Altering/Modifying Material: Not Permitted

Figures, tables, and illustrations may be altered minimally to serve your work. You may not alter or modify text in any manner. Abbreviations, additions, deletions and/or any other alterations shall be made only with prior written authorization of the author(s).

Reservation of Rights

Springer reserves all rights not specifically granted in the combination of (i) the license details provided by you and accepted in the course of this licensing transaction and (ii) these terms and conditions and (iii) CCC's Billing and Payment terms and conditions.

License Contingent on Payment

While you may exercise the rights licensed immediately upon issuance of the license at the end of the licensing process for the transaction, provided that you have disclosed complete and accurate details of your proposed use, no license is finally effective unless and until full payment is received from you (either by

Springer or by CCC) as provided in CCC's Billing and Payment terms and conditions. If full payment is not received by the date due, then any license preliminarily granted shall be deemed automatically revoked and shall be void as if never granted. Further, in the event that you breach any of these terms and conditions or any of CCC's Billing and Payment terms and conditions, the license is automatically revoked and shall be void as if never granted. Use of materials as described in a revoked license, as well as any use of the materials beyond the scope of an unrevoked license, may constitute copyright infringement and Springer reserves the right to take any and all action to protect its copyright in the materials.

Copyright Notice: Disclaimer

You must include the following copyright and permission notice in connection with any reproduction of the licensed material:

"Springer book/journal title, chapter/article title, volume, year of publication, page, name(s) of author(s), (original copyright notice as given in the publication in which the material was originally published) "With permission of Springer"

In case of use of a graph or illustration, the caption of the graph or illustration must be included, as it is indicated in the original publication.

Warranties: None

Springer makes no representations or warranties with respect to the licensed material and adopts on its own behalf the limitations and disclaimers established by CCC on its behalf in its Billing and Payment terms and conditions for this licensing transaction.

Indemnity

You hereby indemnify and agree to hold harmless Springer and CCC, and their respective officers, directors, employees and agents, from and against any and all claims arising out of your use of the licensed material other than as specifically authorized pursuant to this license.

No Transfer of License

This license is personal to you and may not be sublicensed, assigned, or transferred by you without Springer's written permission.

No Amendment Except in Writing

This license may not be amended except in a writing signed by both parties (or, in the case of Springer, by CCC on Springer's behalf).

Objection to Contrary Terms

Springer hereby objects to any terms contained in any purchase order, acknowledgment, check endorsement or other writing prepared by you, which terms are inconsistent with these terms and conditions or CCC's Billing and Payment terms and conditions. These terms and conditions, together with CCC's Billing and Payment terms and conditions (which are incorporated herein), comprise the entire agreement between you and Springer (and CCC) concerning this licensing transaction. In the event of any conflict between your obligations established by these terms and conditions and those established by CCC's Billing and Payment terms and conditions, these terms and conditions shall control.

Jurisdiction

All disputes that may arise in connection with this present License, or the breach thereof, shall be settled exclusively by arbitration, to be held in the Federal Republic of Germany, in accordance with German law.

V 12AUG2015

Questions? customercare@copyright.com or +1-855-239-3415 (toll free in the US) or +1-978-646-2777.